Wavelet Packet Transform and Direct-Quadrature Axis-based Hybrid Technique for Differential protection of Power Transformers

By

© Adel Aktaibi

A Thesis submitted to the school of Graduate studies

in partial fulfillment of the requirements for the award of the degree of

Doctor of Philosophy in Electrical Engineering

Electrical and Computer Engineering Department

Faculty of Engineering and Applied Science

Memorial University of Newfoundland

St. John's, NL, Canada

May 2015

Abstract:

Detecting and identifying the disturbances in power transformers have always been challenging tasks for accurate and reliable protection of power transformers. Several approaches have been tested for designing protective devices such as DFT, ANN, fuzzy logic and wavelets etc. The modern power system is highly polluted with harmonics, and the transient disturbances usually are non-stationary and non-periodic. Thus, these techniques may not be adequate for protection of newer power transformers. Current research indicates that the wavelet packet transform (WPT) provides fast and accurate distinguishing criteria for this purpose, because WPT do not suffer from such problem. However, such wavelet based relay requires a certain sampling frequency for its analysis, which may have some impact on the new trend of interconnected protection system. According to IEEE standards (C57.116) and (1547), the requirement of 6 cycles of fault duration is valid for conventional and newer interconnected power transformer protection system.

This research introduces a new dqWPT-based hybrid technique for the protection of power transformers to be integrated with the operation and control circuits without affecting their performance. The dq axis components and the WPT are combined to provide a new hybrid technique. It is defined as the dqWPT hybrid protection system for power transformers. This hybrid technique is tested by off-line simulation and verified experimentally for two laboratory power transformers. The tests show good results for all types of faults and inrushes including CT saturation, mismatches, external faults, and over-excitation, etc. The proposed hybrid technique yields smart discrimination between faults and inrush currents, including transient phenomena in power transformers.

Acknowledgements

I would like to express my deep gratitude and thanks to my supervisor Dr. M. A. Rahman for his guidance and constructive criticism of my work throughout my study program, as well as his support in terms of providing the required equipment in the laboratory to conduct this work. I would also like to acknowledge all the members of my Ph.D. supervisory committee, Dr. Glyn George, and Dr. B. Jeyasurya, for their useful comments, and suggestions throughout my program of study.

I would like to express my thanks and appreciation to the School of Graduate Studies and the Faculty of Engineering and Applied Science as well as the Associate Dean of the Graduate studies at the Faculty of Engineering and Applied Science and all the members in his office, for providing me with all the facilities needed to successfully pursue my studies smoothly throughout my program.

My thanks also to the Almergib University and ministry of higher education in my country for providing me with the financial support to pursue my Ph.D. study at Memorial University of Newfoundland.

I would like to thank all my friends, especially Dr. Ibrahim Bedeer, and my lab mates for their support and help. Special thanks to my wife for her continuous moral support and help.

Finally, I would like to dedicate this work to the soul of my dear father and my beloved mother, who died in March 19, 2013 and February 4, 2015, while I was here in Canada. Also, I dedicate this work to my lovely wife and children and to all my precious family members, brothers and sisters.

Table of Contents:

Abstract ..... *i*

Acknowledgements ..... *ii*

Table of Contents: ..... *iii*

List of Figures: ..... *v*

List of tables: ..... *xv*

Nomenclature and Abbreviations: ..... *xvi*

Chapter 1 ..... *1*

Introduction 1

1.1 Preface 1

1.2 Power Transformer Malfunction, Protection 5

1.3 Research Objectives 6

1.4 Outlines of the Thesis 8

Chapter 2 ..... *10*

Literature Review of Differential Protection of Power Transformers 10

2.1 Preface 10

2.2 Conventional Electromechanical and Solid-State Relays 12

2.3 Digital Protective Relays 20

2.4 State-of-The-Art of The Wavelet Transform Based Digital Relays: 33

Chapter 3 ..... *39*

Differential Protection of Power Transformers:

Fundamentals and Theory 39

3.1 Preface 39

3.2 Conventional Differential Protection 41

3.3 Basic Problems of Differential Protection: 48

3.4 Conventional Solutions for Differential Protection 59

3.5 Digital Percentage Differential Protection 60

Chapter 4 ..... *73*

Mathematical Framework: Basic Principles and Analysis 73

4.1 Preface 73

4.2 Wavelet Analysis....74
4.3 Wavelet Transforms....82
4.4 The Synchronously Rotating (dq0) Reference Frame....90
Chapter 5....*93*
Development, Implementation and Off-Line Testing of the *dqWPT* Based Hybrid Technique for Power Transformer Protection.... **93**
5.1 Preface....93
5.2 Development of the dqWPT Based Algorithm for Digital Differential Protection of Power Transformers....93
5.3 Implementation of the *dqWPT* Based Algorithm for the Digital Differential Protection of Power Transformers....96
5.4 Off-Line Testing of the *dqWPT* Based Algorithm for the Digital Differential Protection of Power Transformers....98
5.5 The Laboratory Experimental Setup and Data collection....99
5.6 Off-Line Simulation results and Signature Evaluation for the Proposed Technique....101
Chapter 6....*112*
Experimental Testing of the dqWPT Based Hybrid Technique for the Digital Differential Protection of Power Transformers.... **112**
6.1 Preface....112
6.2 Experimental Testing of the Proposed Technique:....112
Chapter 7....*185*
Conclusions and Future Work.... **185**
7.1 Conclusions....185
7.2 Future Work:....188
Bibliography:....*189*
Appendices....*204*
Appendix A: The Matlab Code and the Simulink Model....204
Appendix B: Circuit Breaker Control Circuit....205
Appendix C: The Experimental Setup Photographs....207

List of Figures:

Figure Number	*Figure Citation*	*Page Number*
Figure 1-1	*The first few models of the transformers that were designed in the late 19th century [2]*	*3*
Figure 2-1	*Some samples of the first generation of the differential relay [54]*	*12*
Figure 2-2	*Different types of real digital differential protection relays [15], [16]*	*22*
Figure 3-1	*Transformer faults statistics [3], [146]*	*40*
Figure 3-2	*Differential relay for 1Φ two winding transformer*	*42*
Figure 3-3	*Output currents of the CTs are equal in magnitude and opposite in direction*	*44*
Figure 3-4	*Output currents of the CTs are not equal in magnitude and not opposite in direction*	*44*
Figure 3-5	*Schematic diagram of the 3ϕ differential current protection*	*46*
Figure 3-6	*Relationship between line to line voltage and the phase to neutral voltage and the phase shift between them which reflects the phase shift in Y-Δ or Δ-Y connected transformers*	*47*
Figure 3-7	*CTs connection for a Δ-Y power transformer [5]*	*48*
Figure 3-8	*Voltage, flux, and current during a magnetizing inrush when the transformer is energized at zero crossing on the voltage wave*	*53*
Figure 3-9	*Derivation of inrush current wave from excitation [36]*	*53*
Figure 3-10	*The typical magnetizing inrush current waveform with the primary voltage waveform. The orange (T), sign on the top of the figure, and the blue Arrow, on the right, are the horizontal and the vertical triggering limits.*	*54*
Figure 3-11	*Sample of inrush currents in a three-phase Y-Δ connected*	*54*
Figure 3-12	*Relationship between the voltage and the magnetizing inrush current [148]*	*56*
Figure 3-13	*Differential relay-operating characteristic*	*61*
Figure 3-14	*The general structure of the FFNN*	*68*
Figure 3-15	*The neuron model*	*68*
Figure 4-1	*The schematic diagram of the quadrature mirror filter (QMF)*	*78*
Figure 4-2	*Scaling function and wavelet spaces*	*80*
Figure 4-6	*The frequency response and the zero pole representation of g and h*	*82*

Figure 4-7 Some types of the non-orthogonal wavelet functions *83*
Figure 4-8 Some types of the orthogonal wavelet functions *85*
Figure 4-9 DWT Decomposition of the signal f(n) *87*
Figure 4-10 WPT Decomposition of the signal f(n) *89*
Figure 4-11 The dq synchronously rotating reference frame is rotating with an angular velocity equal to ω_s. *The three- phase currents* I_{abc} *are separated by 120 electrical degrees, and* I_d, I_q *are dc quantities* *92*
Figure 5-1 The flowchart of the differential relay-operating characteristic *98*
Figure 5-2 The circuit diagram for the purpose of data collection *99*
Figure 5-3 Off-line simulation testing for three-phase currents and their coefficients of the high frequency sub-bands for the case of inrush phenomenon *102*
Figure 5-4 Off-line simulation testing for three-phase currents and their coefficients of the high frequency sub-bands for the case of sudden change in the load currents *103*
Figure 5-5 Off-line simulation testing for three-phase currents and their coefficients of the high frequency sub-bands for the case of three-phase fault *103*
Figure 5-6 Off-line simulation testing for three-phase currents and their coefficients of the high frequency sub-bands for the case of single phase C to ground fault *104*
Figure 5-7 Simulation of three-phase inrush currents at no load: the trip signal is still high which means that no trip signal is issued. *107*
Figure 5-8 Simulation of three-phase magnetizing inrush current at non-linear load at the time of energization: the trip signal is still high, which means no trip signal is issued. *108*
Figure 5-9 Simulation of three-phase currents representing the CTs mismatches at non-linear load: the trip signal is still high, which means no trip signal is issued. *108*
Figure 5-10 Simulation of three-phase inrush currents at the CT saturation case: the trip signal is still high, which means no trip signal is issued. *109*
Figure 5-11 Simulation of three-phase currents for unloaded line A to line B fault occurring on the secondary side: the trip signal is low which means that a trip signal is issued. *109*
Figure 5-12 Simulation of three-phase currents for loaded phase B to ground fault occurring on the primary side: the trip signal is low which means that a trip signal

is issued. *110*

Figure 5-13 Simulation of three-phase currents for loaded phase A to phase C fault occurring on the secondary side: the trip signal is low which means a trip signal is issued. *110*

Figure 5-14 Simulation of three-phase currents for non-linear loaded 3φ-to-ground fault occurring on the secondary side: the trip signal is still low which means a trip signal is issued. *111*

Figure 6-1 The circuit diagram of the experimental setup for the 5kVA transformer using ds-1102 ..... *115*

Figure 6-2 The experimental setup for 5kVA laboratory power transformer using ds-1102 . *116*

Figure 6-3 The experimental test case of the magnetizing inrush current with phase A has positive peak and phase C has negative peak a) the three-phase unloaded magnetizing inrush currents and the 1st level high frequency sub-band, b) dq current components and the 1st level high frequency sub-band: the trip signal is still high. It means that no trip signal is issued. *119*

Figure 6-4 The experimental test case of the unloaded magnetizing inrush current with phase C has positive peak and phase B has negative peak a) the three-phase magnetizing inrush currents and the 1st level high frequency sub-band b) $I_n = I_d^2+I_q^2$ *current component and the 1st level high frequency sub-band: the trip signal is still high, means no trip signal is issued.* *120*

Figure 6-5 The experimental test case of the unloaded magnetizing inrush current with phase B has positive peak and phases A and C have negative peak, a) the three-phase magnetizing inrush currents and the 1st level high frequency sub-band b) $I_n = I_d^2+I_q^2$ *current components and the 1st level high frequency sub-band: the trip signal is still high, means no trip signal is issued.* *121*

Figure 6-6 The experimental test case of the unloaded magnetizing inrush current with phase A has positive peak and phase B has negative peak, a) the three-phase magnetizing inrush currents and the 1st level high frequency sub-band b) $I_n = I_d^2+I_q^2$ *current components and the 1st level high frequency sub-band: the trip signal is still high, means no trip signal is issued.* *122*

Figure 6-7 The experimental test case of the magnetizing inrush current at balanced

resistive-inductive load a) the three-phase magnetizing inrush currents and the 1st level high frequency sub-band, b) dq current components and the 1st level high frequency sub-band: the trip signal is still high, means no trip signal is issued. 123

Figure 6-8 The experimental test case of the magnetizing inrush current at unbalanced R-L load, a) the three-phase magnetizing inrush currents and the 1st level high frequency sub-band b) $I_n = I_d^2+I_q^2$ current components and the 1st level high frequency sub-band: the trip signal is still high, means no trip signal is issued. 124

Figure 6-9 The experimental test case of the magnetizing inrush current at nonlinear loa,d a) the three-phase magnetizing inrush currents and the 1st level high frequency sub-band b) $I_n = I_d^2+I_q^2$ current components and the 1st level high frequency sub-band: the trip signal is still high, means no trip signal is issued. 125

Figure 6-10 The experimental test case of the primary side magnetizing inrush current at induction motor load a) the three-phase magnetizing inrush currents and the 1st level high frequency sub-ban,d b) $I_n = I_d^2+I_q^2$ current components the 1st level high frequency sub-band: the trip signal is still high, means no trip signal is issued. 126

Figure 6-11 The experimental testing case of primary single line B to ground fault at non-linear load a) the three-phase transformer currents the 1st level high frequency sub-band b) $I_n = I_d^2+I_q^2$ current components and the 1^{st} level high frequency sub-band: the trip signal becomes low means the trip signal is issued. 131

Figure 6-12 The experimental testing case of unloaded primary single line A to ground fault a) the three-phase transformer currents the 1st level high frequency sub-band b) dq current components and the 1^{st} level high frequency sub-band: the trip signal becomes low means the trip signal is issued. 132

Figure 6-13 The experimental testing case of unloaded primary single line B to ground fault a) the three-phase transformer currents the 1st level high frequency sub-band b) $I_n = I_d^2+I_q^2$ current components and the 1^{st} level high frequency sub-band: the trip signal becomes low means the trip signal is issued. 133

Figure 6-14 The experimental testing case of unloaded primary single line C to ground fault a) the three-phase transformer currents the 1st level high frequency sub-band b) $I_n = I_d^2+I_q^2$ current components and the 1^{st} level high frequency sub-band: the trip signal becomes low means the trip signal is issued. 134

Figure 6-15 The experimental testing case of unloaded secondary phase C to B fault a) the three-phase unloaded transformer currents and the 1st level high sub-band frequencies b) dq current components and the 1st level high sub-band frequencies (high value): the trip signal becomes low means the trip signal is issued.....135

Figure 6-16 The experimental testing case of unloaded secondary phase B to C to ground fault a) the three-phase transformer currents the 1st level high frequency sub-band b) $I_n = I_d^2+I_q^2$ current components and the 1^{st} level high frequency sub-band: the trip signal becomes low means the trip signal is issued. 136

Figure 6-17 The experimental testing case of unloaded secondary phase C to A to ground fault a) the three-phase transformer currents the 1st level high frequency sub-band b) $I_n = I_d^2+I_q^2$ current components and the 1^{st} level high frequency sub-band: the trip signal becomes low means the trip signal is issued. 137

Figure 6-18 The experimental testing case of secondary phase C to B to ground fault at unbalanced R-L load a) the three-phase transformer currents the 1st level high frequency sub-band b) $I_n = I_d^2+I_q^2$ current components and the 1^{st} level high frequency sub-band: the trip signal becomes low means the trip signal is issued. 138

Figure 6-19 The experimental testing case of secondary three-phase fault at balanced load a) the three-phase unloaded transformer currents and the 1st level high frequency sub-band b) dq current components and the 1st level high frequency sub-band: the trip signal went low, means the trip signal is issued.....139

Figure 6-20 The experimental testing case of the secondary side three-phase Fault at non-linear load a) the three-phase transformer currents the 1st level high frequency sub-band b) $I_n = I_d^2+I_q^2$ current components and the 1^{st} level high frequency sub-band: the trip signal becomes low means the trip signal is issued. 140

Figure 6-21 The experimental testing case of the secondary side three-phase Fault at induction motor load a) the three-phase transformer currents the 1st level high frequency sub-band b) $I_n = I_d^2+I_q^2$ current components and the 1^{st} level high frequency sub-band: the trip signal becomes low means the trip signal is issued. 141

Figure 6-22 The experimental testing case of secondary Single Line A to Ground Fault at unbalanced load a) the three-phase transformer currents the 1st level high frequency sub-band b) $I_n = I_d^2+I_q^2$ current components and the 1^{st} level high

frequency sub-band: the trip signal becomes low means the trip signal is issued. 142

Figure 6-23 The experimental testing case of secondary Single Line B to ground fault at non-linear load a) the three-phase transformer currents the 1st level high frequency sub-band b) $I_n = I_d^2+I_q^2$ current components and the 1^{st} level high frequency sub-band: the trip signal becomes low means the trip signal is issued. 143

Figure 6-24 The experimental testing case of secondary single line C to ground fault at induction motor load a) the three-phase transformer currents the 1st level high frequency sub-band b) $I_n = I_d^2+I_q^2$ current components and the 1^{st} level high frequency sub-band: the trip signal becomes low means the trip signal is issued. 144

Figure 6-25 The experimental testing case of unloaded secondary single line A to ground fault a) the three-phase transformer currents the 1st level high frequency sub-band b) dq current components and the 1^{st} level high frequency sub-band: the trip signal becomes low means the trip signal is issued. 145

Figure 6-26 The experimental testing case of unloaded secondary single line B to ground fault a) the three-phase transformer currents the 1st level high frequency sub-band b) $I_n = I_d^2+I_q^2$ current components and the 1^{st} level high frequency sub-band: the trip signal becomes low means the trip signal is issued. 146

Figure 6-27 The experimental testing case of unloaded secondary single line C to ground fault a) the three-phase transformer currents the 1st level high frequency sub-band b) $I_n = I_d^2+I_q^2$ current components and the 1^{st} level high frequency sub-band: the trip signal becomes low means the trip signal is issued. 147

Figure 6-28 The experimental testing case of secondary phase A turn to turn fault a) the three-phase transformer currents the 1st level high frequency sub-band b) $I_n = I_d^2+I_q^2$ current components and the 1^{st} level high frequency sub-band: the trip signal becomes low means the trip signal is issued. 148

Figure 6-29 The experimental testing case of secondary phase B turn to turn Fault a) the three-phase transformer currents the 1st level high frequency sub-band b) $I_n = I_d^2+I_q^2$ current components and the 1^{st} level high frequency sub-band: the trip signal becomes low means the trip signal is issued. 149

Figure 6-30 The experimental testing case of the CT mismatches at balanced load a) the three-phase loaded transformer currents and the 1st level high frequency sub-band

b) dq current components and the 1st level high frequency sub-band and the trip signal is still high, means no trip signal is issued.....152

Figure 6-31 The experimental testing case of the CT mismatches at unbalanced load a) the three-phase loaded transformer currents and the 1st level high sub-band frequencies b) dq current components and the 1st level high sub-band frequencies (zero value): the trip signal is still high, means no trip signal is issued.....153

Figure 6-32 The experimental testing case of the CT Saturation a) the three-phase loaded transformer currents and the 1st level high sub-band frequencies b) $I_n = I_d^2+I_q^2$ current components and the 1st level high sub-band frequencies (zero value): the trip signal is still high, means no trip signal is issued.....154

Figure 6-33 The experimental testing case of the over excitation at unbalanced load a) the three-phase loaded transformer currents and the 1st level high sub-band frequencies b) $I_n = I_d^2+I_q^2$ current components and the 1st level high sub-band frequencies (zero value): the trip signal is still high, means no trip signal is issued. 155

Figure 6-34 The experimental testing case of the external fault at unbalanced load a) the three-phase loaded transformer currents and the 1st level high sub-band frequencies b) $I_n = I_d^2+I_q^2$ current components and the 1st level high sub-band frequencies (zero value): the trip signal is still high, means no trip signal is issued. 156

Figure 6-35 The circuit diagram of the experimental setup for the 2kVA transformer using ds-1104.....159

Figure 6-36 The experimental setup for 2kVA laboratory power transformer using ds-1104159

Figure 6-37 The experimental testing case of the unloaded magnetizing inrush current with phase A has positive peak and phase B has negative peak, a) the three-phase unloaded magnetizing inrush currents and the 1^{st} level high frequency sub-band, b) dq current components and the 1^{st} level high frequency sub-band: the trip signal is still high, means no trip signal is issued. 160

Figure 6-38 The experimental testing case of the unloaded magnetizing inrush current with phase C has positive peak and phases A& B have negative peaks, a) the three-phase magnetizing inrush currents and the 1^{st} level high frequency sub-band, b) $I_n = I_d^2+I_q^2$ current component and the 1^{st} level high frequency sub-band: the trip signal is still high, means no trip signal is issued.....161

Figure 6-39 The experimental testing case of the unloaded magnetizing inrush current with phase B has positive peak and phases A has negative peak, a) the three-phase magnetizing inrush currents and the 1st level high frequency sub-band, b) $I_n = I_d^2+I_q^2$ current components and the 1st level high frequency sub-band: the trip signal is still high, means no trip signal is issued.....162

Figure 6-40 The experimental testing case of the magnetizing inrush current at unbalanced resistive-inductive load a) the three-phase magnetizing inrush currents and the 1st level high frequency sub-band b) $I_n = I_d^2+I_q^2$ current components and the 1st level high frequency sub-band: the trip signal is still high, means no trip signal is issued.163

Figure 6-41 The experimental testing case of the magnetizing inrush current at induction motor load a) the three-phase magnetizing inrush currents and the 1st level high frequency sub-band b) $I_n = I_d^2+I_q^2$ current components the 1st level high frequency sub-band: the trip signal is still high, means no trip signal is issued.....164

Figure 6-42 The experimental testing case of primary single line A to ground fault at unbalanced R-L load a) the three-phase transformer currents the 1st level high frequency sub-band b) $I_n = I_d^2+I_q^2$ current components the 1st level high frequency sub-band: the trip signal becomes low, means a trip signal is issued. 167

Figure 6-43 The experimental testing case of primary single line C to ground fault at induction motor load a) the three-phase transformer currents the 1st level high frequency sub-band b) $I_n = I_d^2+I_q^2$ current components and the 1st level high frequency sub-band: the trip signal becomes low, means a trip signal is issued. 168

Figure 6-44 The experimental testing case of unloaded primary single line B to ground fault a) the three-phase transformer currents the 1st level high frequency sub-band b) $I_n = I_d^2+I_q^2$ current components and the 1st level high frequency sub-band: the trip signal becomes low, means a trip signal is issued. 169

Figure 6-45 Another experimental testing case of unloaded primary single line B to ground fault a) the three-phase transformer currents the 1st level high frequency sub-band b) $I_n = I_d^2+I_q^2$ current components and the 1st level high frequency sub-band: the trip signal becomes low, means a trip signal is issued. 170

Figure 6-46 The experimental testing case of secondary phase B to C fault at balanced R-L load a) the three-phase transformer currents the 1st level high frequency sub-band

b) $I_n = I_d^2+I_q^2$ current components and the 1st level high frequency sub-band: the trip signal becomes low, means a trip signal is issued. 171

Figure 6-47 The experimental testing case of primary three-phase fault at balanced R-L load a) the three-phase unloaded transformer currents and the 1st level high frequency sub-band b) dq current components and the 1st level high frequency sub-band: the trip signal went low, means the trip signal is issued. 172

Figure 6-48 The experimental testing case of secondary side three-phase to ground fault at balanced R-L load a) the three-phase fault currents and the 1st level high frequency sub-band b) dq current components and the 1st level high frequency sub-band: the trip signal went low, means the trip signal is issued.....173

Figure 6-49 The experimental testing case of the secondary side three-phase fault at non-linear load a) the three-phase transformer currents the 1st level high frequency sub-band b) $I_n = I_d^2+I_q^2$ current components and the 1st level high frequency sub-band: the trip signal becomes low, means a trip signal is issued. 174

Figure 6-50 The experimental testing case of secondary single line B to ground fault at unbalanced load a) the three-phase transformer currents the 1st level high frequency sub-band b) $I_n = I_d^2+I_q^2$ current components and the 1st level high frequency sub-band: the trip signal becomes low, means a trip signal is issued. 175

Figure 6-51 The experimental testing case of primary phase A to B fault at induction motor load a) the three-phase transformer currents the 1st level high frequency sub-band b) dq current components and the 1st level high frequency sub-band: the trip signal becomes low, means a trip signal is issued.....176

Figure 6-52 The experimental testing case of primary phase A to C fault at balanced R-L load a) the three-phase transformer currents the 1st level high frequency sub-band b) $I_n = I_d^2+I_q^2$ current components and the 1st level high frequency sub-band: the trip signal becomes low, means a trip signal is issued. 177

Figure 6-53 The experimental testing case of the CT mismatches at balanced load a) the three-phase loaded transformer currents and the 1st level high frequency sub-band b) dq current components and the 1st level high frequency sub-band and the trip signal is still high, means no trip signal is issued.....180

Figure 6-54 The experimental testing case of the CT Saturation a) the three-phase loaded

transformer currents and the 1st level high sub-band frequencies b) $I_n = I_d^2+I_q^2$ current components and the 1st level high sub-band frequencies (zero value): the trip signal is still high, means no trip signal is issued. *181*

Figure 6-55 The experimental testing case of the over excitation at unbalanced load a) the three-phase loaded transformer currents and the 1st level high sub-band frequencies b) $I_n = I_d^2+I_q^2$ current components and the 1st level high sub-band frequencies (zero value): the trip signal is still high, means no trip signal is issued. 182

Figure 6-56 The experimental testing case of the external phase B to C fault at non-linear load a) the three-phase loaded transformer currents and the 1st level high frequency sub-band b) $I_n = I_d^2+I_q^2$ current components and the 1st level high frequency sub-band (zero value): the trip signal is still high, means no trip signal is issued. *183*

Figure A-1 the Matlab/Simulink model of the proposed algorithm *204*

Figure B-1 The experimental control circuit layout *206*

List of tables:

Table 2-1 A comparative study of various digital differential protection [79] 24

Table 3-1 Major transformer faults and their protection methods [3], [146].....40

Table 3-2 Harmonic content in the magnetizing inrush current [3], [5] 57

Nomenclature and Abbreviations:

FFT	Fast Fourier transform
DFT	Discrete Fourier transform
DWT	Discrete wavelet transform
DTFT	Discrete time Fourier transform
WPT	Wavelet packet transform
CWT	Continuous wavelet transform
dq	Direct and quadrature axis rotating reference frames components
$\circledast$	Circular convolution
N	The circular window length
ω_s	The angular frequency in rad/sec
$\psi(t)$	Mother wavelet
db4	Daubechies 4 mother wavelet
g(l)	The low pass filter wavelet db4 coefficients
h(l)	The high pass filter wavelet db4 coefficients
DAC	Digital to analog converter
ADC	Analog to digital converter
HVDC	High voltage dc transmission line
ANN	artificial neural network
FACTS	Flexible AC transmission system
FIR	finite impulse response filter
FIRANN	finite impulse response combined with artificial neural network
EMTP	Electro-magnetic transients program
$\phi(t)$	Scaling function
$\emptyset$	Flux
mmf	magneto-motive-force
QMF	Quadrature mirror filter
MRA	Multiresolution Analysis
$L^2(R)$	Hilbert space
$\oplus$	Direct orthogonal summation operation of the spaces

Chapter 1

Introduction

1.1 Preface

Over the past few years, industry has been adapting the deregulated generation, transmission and distribution structures in modern power systems. Such a trend has placed considerable stresses on electric utilities to improve the reliability of generation, transmission and distribution systems. In order to accomplish such objectives, proper detection and classification of transients is required. This mandate is required due to its role in establishing accurate and reliable protection for all elements of the power system. The protection of power system elements like transformers is vital for ensuring the stability of power systems. Proper installation of the protection system can extend the life of the protected elements in the power system. The main task of the protection system is to take prompt action to isolate the three-phase power transformer whenever faults take place, not only to minimize the damage that may happen to the equipment but also to avoid blackout. At fault time, the protection system sends a trip signal to certain circuit breakers to isolate the faulted equipment to minimize the damage that could happen due to faults. Every protection system has to have high levels of characteristics to perform its function perfectly such as speed, reliability, selectivity, accuracy, simplicity, etc.

According to the history of the protective relaying technology that has been used for power system protection, this technology has passed through three generations, namely, the electromechanical relays, the solid-state relays and the computer-based digital relays. These relays solved some of the problems that were the shortcomings of the electromechanical protective relays for power transformers. The main advantage of the solid state over the

electromechanical relays is the lack of mechanical parts that need maintenance from time to time. Moreover, there was a major improvement in terms of the sensitivity, reliability and speed of operation. In addition, the size of the relay and the implementation cost were significantly reduced. After the invention of the microprocessor in the early 1970s, digital technology started to show up slowly until the digital protective relay was introduced in the early 1980s. After that, rapid improvement and development of the digital protective relaying took place. The main idea of the digital relaying is that the analog signal is sampled to a digital signal and a pre-filtration process takes place to purify the signal and avoid the aliasing problem by using anti-aliasing filters. These computer-based relays have required advantages and overcome all the disadvantages that were reducing the perfect functionality of the older relays such as flexibility, reliability, performance, size, cost and lower burden to the current transformers.

According to Natural Resources Canada, the electric power demand is increasing every year, where, the electricity generation was about 467 billion kilowatt hours in 1990 and then increased gradually to reach 589 billion-kilowatt hours in 2010 [1]. The increase in the power demand has resulted in the increase of the number of the elements and devices in the power system such as transformers, generators and transmission lines. Every element in the power system has to be protected by modern protection systems to ensure the continuity of power delivery to the consumers without interruption.

Power transformers are one of the most vital and essential elements in power system. The first transformer was invented in the early 1880s by Ottó Bláthy, Miksa Déri, and Károly Zipernowsky [2]. After that, the design was enhanced by Sebastian Ferranti and William Stanley [2] in the same decade. Then, the technology of the power transformer improved rapidly during the 20^{th} century. Nowadays, power transformers are manufactured by almost

all the countries around the world using the most modern technology. Figure ***1-1*** shows early few models of the transformers that were designed in the late 19th century [2].

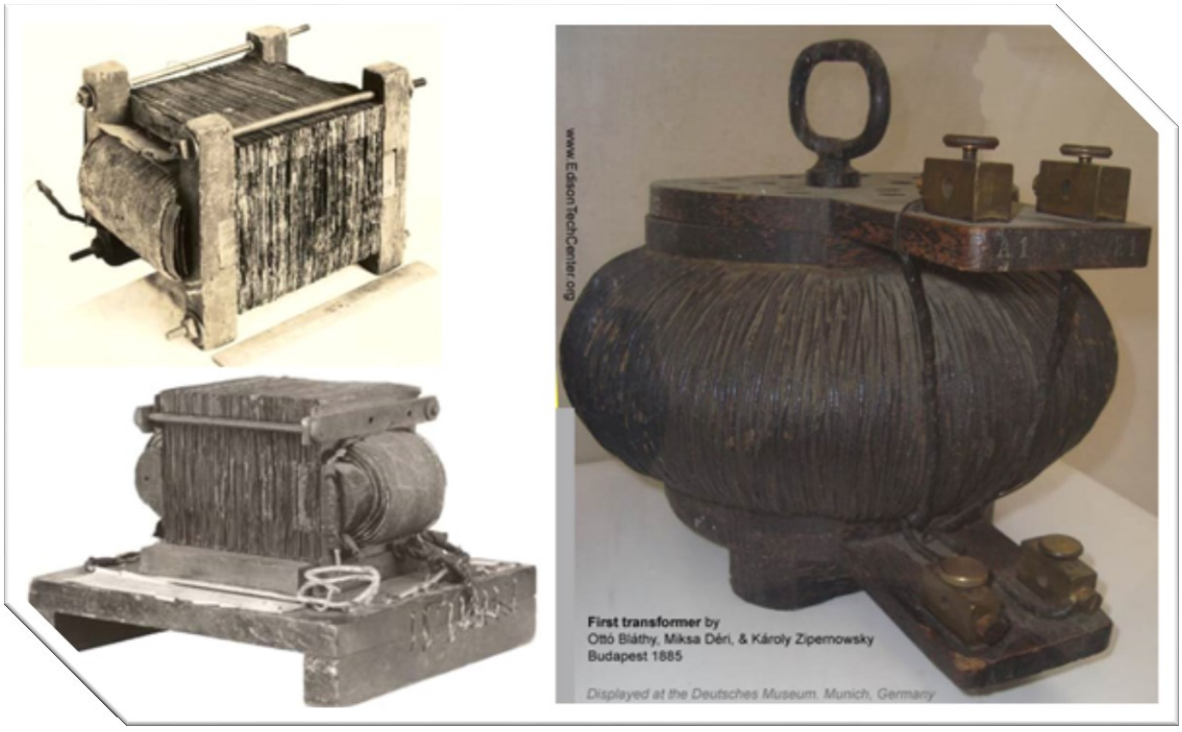

Figure 1-1 The first few models of the transformers that were designed in the late 19th century **[2]**

When the transformer failures occur, the cost associated with repairing it could be high and it results in long outage. The unplanned outage of the power transformer may cause some important loads to shut down and that costs the utility a lot of money. In addition, the failure of the power transformer may create shutdown of the whole power system. These issues are important considerations in terms of providing high quality protection for power transformers. For these reasons, if the power transformer is experiencing any fault conditions, the transformer must be isolated to reduce the consequences. Power transformers play the role of connecting different zones operating at different voltage levels to the grid.

There are many types of failures, which prevent the power transformer from optimal operation. These failures can be classified into internal faults, open circuit faults and short

circuit faults. Incipient faults are the faults that build up slowly inside the power transformer sometimes due to the gradual deterioration of the winding insulation. Winding failure usually occurs due to many reasons such as heating, vibration, mechanical stress, moisture, chemical effects, etc. Early detection of these causes of the incipient faults may provide some information that can be used to overcome the power transformer failures before they take place. Such conditions create partial electrical discharges in the coolant oil, which lead to the oil dissolving and creating some gases that accumulate at the top of the transformer tank. As a result, the online monitoring of such faulted conditions may provide an early warning of faults before they occur. Since the incipient faults are not instantaneous and they require a long time to take place, the classical relays are not useful for protecting the power transformer against such incipient faults. These types of faults require protection devices that provide continuous monitoring and testing of the coolant oil for power transformers. One of these protection systems that is used to protect against such faults is the Buchholz relay. Although this relay is an old technology, it is still used even with modern power transformers. It is mounted on the top of the transformer before the oil reservoir. There are some other complementary protection methods such as daily visual monitoring, thermal imaging, insulation resistance testing, turns ratio testing, magnetic balance testing, oil break down testing, etc. [3], [4].

The percentage differential protection scheme is widely used for such types of faults. It is considered as the most effective method to protect the power transformer against faults that may occur in the protection zone. However, this method in its simplest form suffers from some problems such as magnetizing inrush currents, tap changing ratios and current transformers (CT) mismatches, saturation, over-excitation, etc. Modern power transformers use amorphous metal type core materials in transformer laminations to reduce the core losses due to high resistivity of such materials. This significantly affects the harmonic contents in

the inrush current. Harmonic-based techniques are not suitable to perform the required job for such power transformers and due to the fact that some faults may contain values of harmonic contents. The solution to these difficulties is becoming easier with the digital relays. These relays are developed ideas of the conventional differential relays, and they have provided satisfactory solutions to these problems. The advances in the art of the relay technologies and the protection schemes used have involved many compromises. Literature reviews are given in chapter two to provide a clear vision about what researchers have done.

1.2 Power Transformer Malfunction and Protection

Power transformer reliability and security can be improved by limiting the failures that may disturb the perfect operation of the transformer and thereby reduce the total cost of the delivered energy to the consumers. In addition to the proper insulation design of the power transformer, the proper protective systems have to be utilized to limit the damage that may occur in the power transformer due to the failure of the insulation. Moreover, limiting the damage may reduce the maintenance and operation costs. Power transformers suffer from several types of failures such as short circuits, open circuits, flashovers, overheating, insulation failure, and others. All these types of failures may cause a long downtime for the power transformer, which costs electric utilities millions of dollars.

The failure of operation of the power transformer may occur due to internal or external conditions. The internal conditions could be the accumulation of defects due to the age of the power transformer. The external condition could be due to short circuits between the phases or between one phase and the ground. In addition, insulation flashovers could cause huge transients in power transformers. Periodic and proper maintenance could play a large role in reducing the downtime of the power transformer operation [3], [5], [6], [7].

1.3 Research Objectives

Engineers started using protection systems when the number of failures increased with the increase of the size of power systems in the late 19th century [8]. They started to develop the protection techniques when they realized that the power system could not be reliable without protection. Since then, many protection algorithms have been developed depending on the facilities that were available at that time. The protection of power transformers has received special attention by researchers due to its importance. Several approaches have been tested for digital relays such as DFT, ANN, fuzzy logic and wavelets etc. However, most of the existing differential protection algorithms, that are used in the industry nowadays, are harmonic-based analysis techniques [9], [10], [11], [12] [13], [14] [15], [16]. Such techniques may not be able to provide the proper protection when fault currents are highly distorted due to harmonics especially the second harmonic [17]. Modern transformers use amorphous core material that has high resistivity and high reluctance that makes the inrush current hard to discriminate from fault currents [7], [18], [19]. Moreover, due the increased use of non-linear loads, modern power systems are highly polluted with harmonics and the transient disturbances usually are non-stationary and non-periodic, which lead to confuse these kinds of differential relays that are based on harmonic analysis [20], [21]. This makes the inrush currents having less second harmonic content. Because of these reasons and due to the improvement of power transformers, the older designs of protection systems may not be suitable to protect them.

Hence, the recent research in this field is deviating from the harmonic analysis techniques. Current research also indicates that the wavelet packet transform (WPT) provides fast and accurate distinguishing criteria for this purpose, because WPT do not suffer from such problem. However, such wavelet based relay requires a certain sampling frequency for its

analysis, which may have some impact on the new trend of interconnected protection system for the distributed generation units. According to IEEE 1547 standard for Interconnecting Distributed Generation, dq transformation is always embedded with the current controllers for grid connections. For these reasons, new protection technique is required for interconnected power transformer protection.

This work presents a *WPT*-based hybrid technique for the protection of power transformers including transient analysis to be integrated with the operation and control circuits without affecting their performance and functionality. In this research, two mathematical tools were used. The synchronously rotating reference frame (dq) is combined with the *WPT* to provide the $dqWPT$ powerful hybrid technique, which is the main contribution of this research. The hybrid technique is primarily tested by off-line simulation tests and then verified in real-time experimental testing for laboratory power transformers. For testing purposes, different types of faults and transients are observed and included in chapter six of this thesis to show the efficacy of the proposed technique. The results show that the proposed technique provided a fast and accurate response in clearing faults. Moreover, it has provided good selectivity against the natural phenomena that resemble faults in power transformers such as magnetizing inrush currents. The results are found to be satisfactory and provided clear evidence about the successful work that has been done in this thesis. Wavelet Packet Transform (WPT) analysis has been proposed previously in many papers such as [22], [23], [24], [25], [26]; however, the combination of the (dq) axis components with the WPT and its application in the real time protection of power transformers is a new contribution.

1.4 Outlines of the Thesis

The contents of this thesis are divided into six chapters and sorted logically in a way to simplify the understanding of the work that has been carried out.

Chapter One:

This chapter is the introduction of the thesis. It includes a brief description about the malfunction issues in power transformers. A brief historical background of faults, transients diagnosing, and analysis techniques that are used in the area of transformer protection is provided. Some important principles and definitions that are often used in power system protection are provided to simplify the understanding of the explanations and the comparisons provided in the research matters. In addition, the circuit breaker control circuit is illustrated. Finally, the research objectives and outlines of the thesis are provided.

Chapter Two:

The literature review of this work is provided in this chapter. It is classified into three sections, the conventional electromechanical and solid-state relays, the digital relays and the state-of-the-art of the wavelet transform based digital relays. It is classified in this way to show the different types of technologies used in this regard.

Chapter Three:

This chapter provides a brief description of the fundamentals and the theory of the differential protection algorithm of power transformers and its operating principles. In addition, the difficulties that face the perfect operation of this algorithm are provided to give a clear understanding of the research challenges. Equations and figures are provided to explain the principles and the problems. Finally, some significant contributions in digital protection that have been used for transformer protection are summarized.

Chapter Four:

In this chapter, the basic principles and an analysis of the mathematical framework that is utilized in this work are studied. It explains the types of mathematical tools used in this research and wavelet analysis, quadrature mirror filter, multiresolution analysis, selection of the best mother wavelet, Daubechies (db4) wavelet filter parameters analysis, wavelet transforms and the synchronously rotating (dq0) reference frame are presented.

Chapter Five:

In this chapter, the development, implementation and off-line testing of the proposed technique of the algorithm used in this thesis are provided. The laboratory experimental setup and circuit topology of the data collection for off line testing and explanations are provided. In addition, the combination of these mathematical algorithms is explained to illustrate the development of the new algorithm to solve the proposed problem in this research area. These analytical tools are confined to the wavelet analysis techniques and the synchronously rotating (dq) reference frames. Finally, the implementation of the proposed technique model is explained.

Chapter Six:

This chapter is the backbone and the significant contribution of the thesis. The evaluation and testing of the proposed technique for digital differential protection of power transformers are explained with the support of the results and analysis. Different types of results are provided with figures for experimental testing. Different types of tests using two different transformers are provided to show the performance of the algorithm.

*Chapter S*even*:*

This last chapter gives the conclusions and the future work. The references and appendices are provided at the end of the thesis.

Chapter 2

Literature Review of Differential Protection of Power Transformers

2.1 Preface

The history of the protective relaying for power system protection has shown a rapid improvement in this technology. It has been improved many times within the same century, in which, this technology has passed through three main generations: electromechanical relays, solid-state relays and computerized digital relays. Current differential relays are one of the protective relays that have been improving since they were first introduced in the early 1900s as electromechanical devices. They have been introduced in many different forms such as magnetic induction relay, magnetic attraction relay, thermal relay and D'Arsonval movement coil relay. The protective relays significantly improved in the early 1940s after semiconductor devices, which were invented in the early 1930s, became available to the market. After the invention of the first microprocessor in the early 1970s, the first microprocessor based relay was introduced in the early 1980s. The invention of the microprocessor gave researchers an easier way to develop new algorithms without the need to go over the complexity of building the hardware circuits. Since then, digital protection has been the trend. Such digital relays have given better performance than the conventional relays. Since that time, researchers have introduced many ideas to improve the performance of these relays [8], [27], [28].

The differential relay for power transformer should be designed to detect all the faults in the protected zone. In addition, it should discriminate inrush currents from fault currents, and its performance should not be affected by the over-excitations of the power transformer, CTs

mismatch and saturations and through-faults. The main concern of differential protection is the natural phenomenon known as magnetizing inrush current. This current is generated at the primary side only of the power transformer whenever the transformer is energized. The problem is that, if the differential relay is not properly designed to overcome this problem, this current may trip the power transformer. Therefore, the protective relay has to be properly designed so that it can discriminate between inrush currents and fault currents. [29], [30], [31], [32].

To design a good protection system for power transformers, many factors have to be considered in order to get an efficient protection system. Among these factors are the nonlinearities of the power transformer core, the core losses, leakage and mutual inductances. A lot of work has been done on this subject matter such as [33], [34], [35], [36], [37], [38], [39]. Each one of them has covered part of these factors, however, few of them has covered them all. The nonlinearity of the transformer core leads to the magnetizing inrush current [3], [40]. The inrush current characterizes with special content of some major harmonics such as the second and fifth harmonics. This characteristic is used as the ratio of the second harmonic component to the fundamental frequency component. Many papers [9], [13], [41], [42], [43] used harmonic restraint and harmonic blocking to design transformer protection systems. Discrepancies among the results of these papers show the shortcomings of this concept in some cases of transformer protection. Usually, the ratio between the second harmonic and the fundamental component is quite high between (0.3-0.7) of the fundamental [3], [5], [40]. However, sometimes this ratio falls below this range due to the severity of the inrush current or the type of the transformer core material. Moreover, fault currents sometimes have a high ratio of the second harmonic. Despite this problem, these relays have served transformer protection for a long time until the digital relays were introduced.

2.2 Conventional Electromechanical and Solid-State Relays

According to Walter Schossig [44] the first proposed idea about electromechanical differential protection was in 1896, which got the German Patent DRP 92442. This relay was based on the comparison of voltages and currents using a balanced beam relay in one and two phases with the neutral. However, the first real differential protection relay was born in 1904, in which the designed differential relay compares the currents of both sides of the protected device. This design was patented by Charles Hestermann Merz and Bernhard Price, which got the UK patent 3896 in February 1904, and the German patent DRP 166224 in May 1904. Figure ***2-1*** depicts some samples of the first generation of the differential relays that were used in the early years of the 20th century.

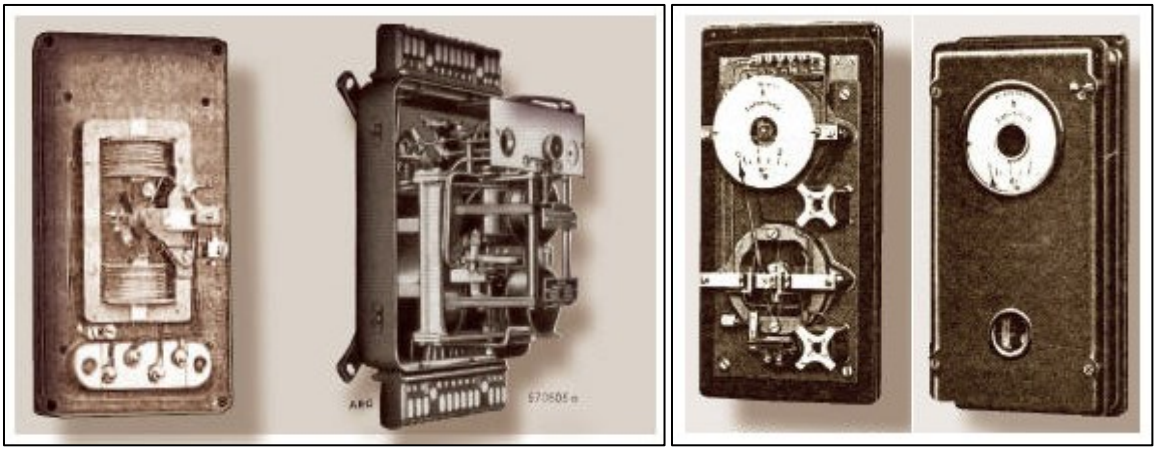

Figure 2-1 Some samples of the first generation of the differential relay **[44]**

Electromechanical protective relays were the basic model and they form the foundation of the power system protection devices. The unbiased differential relay was the simplest model of the differential relays, which did not have restraining coils. In this relay, under normal conditions, the differential current was equal to zero if the current transformers were well selected according to the specification of the power transformer. These balanced conditions do not continue for long if any fault occurs in the protected zone. Moreover, there were

some other cases which were not faults but still can cause unbalanced conditions such as CTs mismatches. There were some differences in their characteristics if the CTs were not well selected or if they were saturated. In these cases, the differential current have a significant value, which is enough to activate the relay and release a trip signal as soon as it senses this as a faulted condition in order to isolate the transformer. The lack of having restraining coils in the unbiased differential relay caused false tripping without the existence of real faults, which makes it unreliable for such non-faulted conditions. This problem was avoided by using the modified unbiased relay that had restraining coils in addition to operating coils. It was known as the percentage differential relay. Despite this modification, the percentage differential relay still produced false trips due to the problem of the inrush currents. Many solutions was proposed to solve these problems such as delaying the operation of the relay until the inrush period finishes, which was used with the induction disk relay. However, this time delay put the transformer at absolute risk of fault occurrence [3], [5].

The improvement of the differential relay increased rapidly because the first generation faced many difficulties in working properly. The need to have high-speed differential relays became compulsory in order to provide more reliable protective relays. For this, new techniques were proposed to provide high-speed protective relays such as harmonic restraint relays, which were based on the existence of high values of the second and fifth harmonics in the inrush current. The main idea of this method was that the relays utilize two analog filters: a low pass filter and a band pass filter. The low pass filter was used to extract the fundamental component of the differential current and the band pass filter was used to extract the second harmonic component of the differential current. The fundamental component was made to flow through the operating coils; however, the second harmonic component was made to flow in the restraining coils [3], [4], [5].

Based on these principles, researchers began to propose other solutions to these problems and the transformer producing companies started to recognize some of these solutions in order to provide relays that were more reliable. In 1924, Fitzgerald [45] presented the differential protection systems that were used with neutral earthing resistance in the system. It was about a discussion on how the existing algorithms can be simplified and how to increase their reliability. In 1931, Cordray [46] described the difficulties that protection engineers face in providing the proper protection for a three-phase three-winding power transformer. He also mentioned the effect of the inrush current on the performance of the differential protection especially with the three-windings. In 1932, Lipman [47] presented some of the recent advances in the design of protective relays for the protection of alternating current systems. The requirements of the proper relay functionality were described and discussed to provide the ideal relay. Moreover, some novel designs of the protective relays were studied and a comparison among them was presented as well.

The protective relaying technology saw some changes with the invention of the grid controlled gas-filled (mercury-vapor-filled) hot cathode electronic tube, which was called the Thyratron. In 1938, Kennedy and Hayward [13] proposed a paper about Harmonic-Current-Restrained Relays for Differential Protection. They provided a comprehensive study about the harmonic contents of the fault currents and the inrush currents. In addition, the reasons for the false tripping of the differential relay due to false differential currents were studied. He presented a new method for preventing the false tripping of the differential relay, which was called the harmonic current restraint. They tried to develop a harmonic restraint relay through their study of the spectral characteristics of both the inrush current and the fault currents. In their design, they suggested using all the harmonics for restraining rather than using the second harmonic only. The reason was that the relays designed for second

harmonic restraint were good for typical inrush currents only, this might not be useful for inrush currents if the power transformer or the CTs were saturated. In 1940, Wentz and Sonnemann [48] presented a paper discussing the CTs performance with the relays for high-speed differential protection. In addition, they studied the mechanism of the CT saturation with particular reference to offset transient currents. Some mathematical analysis of the CTs was carried out based on the equivalent circuit of the CT.

In 1941, Hayward [9] presented a new high-speed relay using the same principle of harmonic restraint, which was able to distinguish between the internal fault and the inrush currents by their difference in waveform. However, this method was characterized by complicated circuits and it consisted of mechanical parts. Hayward also studied [42] the prolonged inrush currents in the case of parallel transformers and their effect on differential relaying. In this study, two types of two parallel transformers connections were considered, the case of transformers with equal sizes and the other case with two transformers in parallel with different sizes. The result from this study was that the harmonic restraint relay was found to be the best suited to the protection of transformers connected in parallel. This relay was found to give high speed and sensitive operation on internal faults and reliably restrained from false operating in cases with long-duration magnetizing inrush currents. However, there was a condition with this operation which was that only one transformer was included within the differential zone. The harmonic-current-restraint percentage-differential relay was shown in [9]. The relay received the current through two auxiliary current-transformers, which were the relay differential current operating transformer (DCOT) and the relay through current restraining transformer (TCRT). The DCOT had only one primary coil and is connected to the differential circuit. The TCRT had two primary coils; each one was connected to the differential circuit from the inner terminals and to the main current-

transformers from the outer terminals. The two coils were wound in such a way so that their magnetizing effects were additive in the case of through fault currents. Both transformers were tapped and connected to each other through these taps to allow matching to the main current transformer ratios. Across the secondary side of the DCOT, two filter circuits were connected in parallel to supply the relay contacts. The first circuit includes the relay operating coil and a low pass filter to allow only the fundamental component to pass to the relay operating coil. The second circuit includes the relay restraining coil and a high pass filter to allow all the harmonic frequencies to pass to the relay restraining coil except the fundamental component. The second circuit contains also a rectifier to smooth the restraint magnet pull. The resistor R2 was used to adjust the proportion of the harmonic current required to pass. The DCOT was equipped with an air-gap core to block the dc current component present in the differential current because it saturates the reactors L1 and L2. A Thyrite is a resistor connected across the DCOT secondary terminals, and was used to limit the voltage surges that occur due to shock current excitation of the tuned circuits, which may damage the rectifiers or capacitors. The secondary of the TCRT also supplies current to the restraining coil through a second rectifier, which also had an air gap core to block the d-c component. The multi-tap shunt resistor R1 was used to adjust the percent slope of the through-current restraint characteristic. One of the highly accepted high-speed relays at that time in the 1940s was the Westinghouse relay type HDD [4] that did not require potential transformers or any auxiliary means. The main idea of this percentage differential relay was harmonic restraining by using two filter circuits to achieve this restraint. However, this type of relay was not able to functional properly in the case of CT saturation.

In 1944, Blume, *et. al.* [49] presented in their paper a discussion about the mechanism on how the inrush currents were detected. An experimental testing was used to model the inrush

current depending on the flux densities and the physical dimensions of the power transformer. In addition, methods for mitigating the effect of the inrush current on the power system operation and reducing it were discussed. In 1951, Finzi and Mutschler [50] presented a simple formula, which was derived to express the first and the subsequent peaks of the inrush currents in terms of line-to-line voltage. Some approximations were used which led to low accuracy of the solution of the time integral equations used in their model. In 1945, Michelson [51] came up with a new different concept of differential protection for power transformers using rectification. This concept was based on the fact that the inrush current was a sinusoidal current signal but a pulsating dc current of positive or negative polarity. In this design, there were two relays connected in series with dry-type rectifiers, so that one of them works in the positive pulse and the other one works with the negative pulse. The main idea for this relay depended on the equality of the area of the positive current pulse and the negative current pulse. If the area was equal that, implied that a faulted condition was taking place and both the relays was energized and a trip signal was issued. If the areas were not equal that, implied that an inrush current was passing through, only one relay was energized, and no trip signal was issued. In order to avoid tripping due to the CT saturation, another time delay auxiliary relay was added.

In 1950, McKenna [52] wrote a paper about the theory and application of transformer differential protection. General remarks about the fundamentals of the transformer protection using the percentage current differential protection were raised in this paper as well as some selected applications of this relay. A discussion about the problems of the transformer protection for a wide variety of transformer connections and types was presented. However, the main problem, which was the magnetizing inrush current, was not within the scope of this study. In addition, Specht in 1951, [53] developed some formulas and curves for calculating

the inrush current approximately in a power transformer. A comprehensive mathematical analysis was provided in this paper for developing the inrush current model. He mentioned that this information was required not only for the differential protection relay design, but even for the power transformers that were protected with fuses. In order to protect a transformer with fuses it is necessary to know the peak current values so that the proper fuses are selected. The calculation method made it possible to calculate the maximum and RMS values for any cycle of the inrush current by using the curves. In 1954, Mathews [54] came up with an improved modified version of the Westinghouse one with a smaller size and less CT burden, which was called a BDD relay. This differential relay was also based on harmonic restraining and it was designed for two winding and three winding transformers, in which the operating time was less than three cycles (50 msec). In 1954, Neupauer [55] presented a paper about the drawbacks of the occurrence of simultaneous single-line-to-ground faults on opposite sides of Δ-Y transformer banks. The occurrence of simultaneous faults was not common but it did occur. This paper discussed the voltage dynamic behaviour on the other two un-faulted phases. A derivation of simple equations was provided for the fault currents and the voltages at the faulted points supported with general curves. Sharp and Glassburn [56] developed a new relay in 1958 describing a high-speed variable percentage differential relay for two and three winding power transformer protection. They mentioned that this relay was reliable in terms of internal faults and secure for external faults and inrush currents as well as providing a good response during under frequency conditions. This design was based also on harmonic restraining, as it uses the second harmonic to restrain the relay in case of inrush currents. It also retains the principle of the variable percentage differential relay. The relay was provided with tuning taps to compensate the relay for any

CTs mismatches. During this time the mid-1970s, the new generation of the protective relays started to show up in the market. However, researchers continued to propose new papers for the static relays. Sonnemann*, et. al.* in 1958 [57] provided a detailed study about the inrush current in single-phase and three-phase transformers. In this study, they came up with some results such as the second harmonic was the predominant harmonic in the inrush current with a minimum amount of 16% to 17% of the fundamental component. However, in the case of fault currents, the second harmonic was much less than that. Nevertheless, the effect of the mutual coupling was not considered in this paper.

In 1961, Holcomb [58] discussed the magnetizing inrush current in distribution transformer. This paper presented a new method of calculating the peak of the inrush current for many cycles. The sum of the current squared-time integral was also discussed in this paper, which was more useful for selecting the required fuse characteristics for distribution transformer protection. Again, in 1969, Specht [59] described another method to determine the inrush current for a single-phase transformer supplied through a resistance and reactance in series. Formulae were developed to generate the magnetizing inrush current data for a single-phase transformer and curves for the calculated inrush current were provided. In this paper, assumptions were made that the transformer has no excitation current under saturation level and constant inductance over saturation. In addition, Hegazy [11] proposed an idea in 1969 describing a new principle for the differential protection of transformers using full-wave rectifiers. The proposed principle was based on blocking the differential relay during the inrush current period. The differential current was rectified first and then a filtration process takes place to extract the fundamental component. According to his description of the idea, if the rectified signal has a fundamental component that meant a faulted condition was occurring, otherwise an inrush current was flowing. .

2.3 Digital Protective Relays

Digital relays are considered as the third generation of the protective relays. Because of the shortcomings of the conventional relays, digital relays are widespread and accepted worldwide to overcome these shortcomings. They use a microprocessor in their hardware circuit programmed with software based protection methods. These software programs analyze the applied current and voltage signals for the purpose of the detection of any abnormalities in the input signals. Digital computer principles were first introduced in the mid-1940s [60]. Researchers contemplated the use of digital computers for digital protective relaying in the late 1960s. Since then, much research has been carried out on digital protective relays for power transformers protection based on digital computers. Yet, Rochfeller in 1969 [61] was one the first to introduce a detailed model of a protective relay based on digital computers and suggested that every element in the power system could be protected by digital protective relays. In his digital relay, the development of some fundamental basics was introduced for the use of a time-shared and stored program of digital computer to perform many functions of the protective relays. Some logic circuits were used to detect and locate the faults and isolate certain circuit breakers as soon as any fault occurs. The paper included some interesting subtitles such as the philosophy behind the use of digital relaying and the main structure of the digital relays circuits supported with flow charts.

The invention of the microprocessor in the early 1970s created a new revolution in the world of digital industry applications [62]. It simplified the development of digital protective relay technologies. In 1972, Sykes and Morrison [63] proposed a paper using the same principle of the static relay, which was the harmonic restraint for transformers differential protection. The fundamental component and the second harmonics of the differential current were extracted using two infinite impulse response (IIR) recursive filters. These two

components were used to discriminate the inrush current from the fault current. Off-line simulated data for the inrush current were processed by a Fortran IV program. However, the data was developed for a 1Φ transformer and that might not work properly for 3Φ transformers. In 1977 Schweitzer et. al. [64] proposed a finite impulse response (FIR) which required only additions and subtractions. In the algorithm, four Fourier coefficients were calculated off-line for the fundamental and second harmonic components for discrete data of differential current using Fortran IV. It was found that the response time of the algorithm was about one cycle based on 60 Hz frequency. Based on this paper, Larson et. al. [65] designed, in 1979, a digital relay for transformer protection and tested it experimentally on a 500VA laboratory transformer on a Motorola MC6800 microprocessor. After that, the source code became input for the cross-assembler resident in an IBM-360 computer. The speed of the response of the relay was 19.1 msec for fault current without involving the inrush current.

After this rapid improvement in the protective relays, digital protective relays began to replace the conventional relays in the early 1980s. Thorp and Phadke [66] were among the earlier researchers who considered the harmonic restraint-based analysis for implementing digital differential relays. Their paper, in 1982, presented a simple recursive algorithm for digital protection of a three-phase, three-winding power transformer. These recursive expressions were used to obtain certain harmonics up to the fifth one using a sampling rate of 12 samples per cycle. This analysis was carried out using the discrete Fourier transform (DFT). The responses of the DFT calculations were designed to restrain the relay for approximately one cycle to make a secure decision. The algorithm was performed and tested for off-line based analysis on data obtained from a laboratory model transformer for 19 cases of energization and faults. In the 1990s, more advanced digital relaying algorithms were

introduced [62], [67], [68]. Nowadays, the digital protection of all power system elements has become a vigorous and vital research area [62], [67]. Artificial intelligence techniques, such as fuzzy logic, artificial neural network (ANN), genetic algorithm and hybrid techniques blending some of the above-mentioned techniques were applied in digital protective relays for power system protection [69], [70]. Also, digital techniques have become more advanced in the last two decades because of the availability of the modern computers [62], [67], [68].

There are many relay manufacturing companies still using the harmonic restraint and blocking principles in their design for differential protection of power transformers. For instance, Bickwith Electric mentioned, in their M-3311A transformer protection relay specification manual [15], that their design for discriminating between inrush current is based on the harmonic restraining and blocking principles. They use the second harmonic for inrush discrimination and the fifth harmonic for over-excitation. It is mentioned in the report that Trip response, if the time delay set to 1 cycle, is less than 1.5 cycles, which is about 24 msec. Another example is the Schweitzer Engineering Laboratories, Inc. (SEL), transformer differential protection relay [16], [71]. It is mentioned in the specification manual of the relay that the waveform-based inrush detection method is used to augment the harmonic restraint and blocking functions to prevent differential element operation during an inrush condition with low second harmonic content. Figure ***2-2*** shows some types of digital differential protection relays for different companies.

Figure 2-2 Different types of real digital differential protection relays **[15], [16]**

Rahman and Dash [14] developed a new method in 1982 for power transformer protection using a rectangular transform. This method was based on generating the Fourier coefficients by using the simplest mathematical operations, addition and subtraction only. Involving only the simple mathematical operations provided a reasonably fast response. Both simulation and real-time experimental testing were carried out in the laboratory. A PDP-11/60 computer was used for off-line testing of the simulated inrush current and fault currents waveforms. However, the real-time experimental testing was carried out using an Intel 8085 microprocessor for a three-phase 400V, 60Hz transformer. The sampling rate was chosen to be 12 samples per cycle compared to 16 and 4 samples per cycle that were also used to test the algorithm. It was found that it was impossible to get good results below 12 samples per cycle. The results were quite satisfactory with the old microprocessor as the time range for releasing a trip signal was between one-half and three quarters of a cycle, based on 60Hz. In 1985, Jeyasurya and Rahman [12] presented a paper about the application of Walsh functions for power transformer protection using microprocessors. This algorithm was based on extracting the fundamental and second harmonic components in terms of Walsh coefficients, which uses only additions and subtractions. This makes it an easier and faster algorithm than the discrete Fourier transform. Real-time experimental testing was carried out using an Intel 8088 microprocessor with a sampling frequency of 960 Hz. The speed of the response of the proposed algorithm was about 9-14 msec, which was less than one cycle based on 60 Hz. Again, in 1988, Rahman and Jeyasurya [72] presented a comparative study and a state-of-the-art review of many digital algorithms for transformer protection as illustrated in Table ***2-1***. This kind of comprehensive study was the first study in the literature that provided a complete summary of all digital protection algorithms. In this study, a brief description was provided for all digital algorithms that were known at that time. The comparison was based

on many major factors such as simplicity, speed of response, security of distinguishing inrushes from fault currents and computational burden. All the algorithms were able to discriminate inrushes from fault currents, and they provided reasonable speeds within one cycle for tripping the transformer in faulted cases.

Table 2-1 A comparative study of various digital differential protection schemes **[72]**

Algorithm	Sampling interval (μs)	Number of Arithmetic operations			Time for arithmetic computation	Percentage of sampling interval %
		+/-	×/÷	$\sqrt{}$		
Fourier	1042	51	14	2	380	36
Rectangular	1042	106	8	2	410	39
Walsh	1042	116	14	2	426	50
Haar	1042	96	16	2	512	49
FIR	1042	84	4	2	298	29
Curve	1389	46	19	2	447	32

In 1988, Murty and Smolinski [73] designed and implemented a digital differential relay based on a five-state Kalman filter for three-phase power transformers. The relay response time was less than a half cycle of 60 Hz and restrained during inrush current efficiently. Real-time experimental testing was carried out using a TMS320 processor for three-phase transformer. The authors suggested some extensions to their algorithm to provide restraining during over-excitation by employing higher order harmonics. Also, Habib and Marin, in 1988, [74] prepared a comparative study of many differential protection techniques for power transformers. In this study, two performance keys were defined; the first one was used to evaluate the performance in time and the other one used to evaluate the performance in frequency. After a review of the fundamentals and the problems of transformer differential protection, the existing solutions were addressed. According to this paper, the best algorithm for digital protection was the DFT.

In 1989, Sachdev et al. [17] presented a new digital algorithm to detect faults in single-phase and three-phase transformers. This algorithm was based on the differential equations of the transformer. Unlike the other previous algorithms, the proposed algorithm did not use the harmonic restraint principle. The authors mentioned that the transformer differential equations were only valid at non-faulted conditions such as the inrush currents or normal operation. This algorithm calculated the primary voltage for the quantized measured voltage samples at the primary side as well as for the current. With the aid of the transformer parameters such as the leakage inductances and the mutual flux linkage of the primary and secondary windings, the measured voltage signal was compared with the estimated voltage signal. A trip signal was issued only if the difference between them lies in the faulted region of the characteristic curve and exceeds the pre-specified threshold value. The computational time for this algorithm was acceptable and it was applicable for digital relays for either two or three winding power transformers. A detailed mathematical calculation of the proposed algorithm was provided in [17] with the support of the flow chart.

To avoid the false tripping due to inrush currents, second harmonic restraining and blocking techniques were commonly used in digital protective relaying for power transformer protection. However, the second and fifth harmonic levels were increased significantly in modern power systems. This significant increase was due to many reasons, including the series and parallel capacitances in the transmissions lines. There were some other reasons such high voltage underground cables and the increased use of power rectifiers, power inverters and FACTS technology to control the power flow and improve the power quality in many applications such as EHV transmission lines and HVDC transmission. In 1990, Murty and Smolinski [75] proposed a modified version of their digital differential relay that was designed in 1988 [73]. This version of their design improved the speed of the

response of the relay during internal faults. The new design utilized a set of eleven- state Kalman filters to estimate the magnitudes of the fundamental components and the harmonic components of the differential current signals. The percentage differential relay was used in collaboration with the Kalman filters to provide efficient restraining capabilities during inrush, over-excitation, and external faults conditions. The operation time of the relay was about half a cycle of 60 Hz. Real time experimental testing was carried out using a TMS320 processor for the protection of a three-phase laboratory transformer.

In 1991, Hermanto et. al. [76] presented a complete design of a stand-alone digital protective relay for power transformers using DFT. The major work in this paper was the emphasis on the description of both the hardware and the software of the prototype relay in detail. The same principles of the second and fifth harmonic restraint and the percentage differential protection concept were used in this paper. The relay design was an open model that accepts any protection algorithm by replacing the software of the relay. Experimental testing was carried out using a TMS320E15 processor for three-phase transformer protection.

In 1992, Chaudhary et. al. [77], [78] presented a development of a differential protection relay for power transformers using the Electromagnetic Transients Program (EMTP) for the General Electric (GE) differential relay (BDD15B). This model was designed with the ability to set the relay using the percentage and harmonic restraint principles, which was the main feature of the model. This feature permits the user to use the model in a wide range of simulations for transformer differential problems such as CT ratio mismatches and saturation, transformer remnant flux, and inrush current. This model relay was validated using test data obtained from the power system simulator at the American Electric Power Company (AEP). Liu et. al. [79] used the restraining technique of the second harmonic to study the possibility of non-operation for internal faults in transformer differential protection. This idea was tested

for faults and energization cases on a laboratory transformer using three methods: the least-squares curve-fitting algorithm, Fourier analysis, and rectangular transform. Real-time experimental tests of a laboratory transformer were carried out to collect the data used for this analysis. The experimental setup contained a three-phase transformer bank, which consists of three 2kVA, 462V:200V, 50Hz single-phase transformers. The percentage of the second harmonic to the fundamental one was provided up to the 5^{th} cycles of the input differential current signals. The restraining time of the three algorithms with the original signal was provided in terms of cycles, and a comparison between them was explained.

In 1997, Yabe [43] described a new method for discriminating the inrush currents from fault currents by the sum of the active power flowing into the transformer. This technique did not use second harmonic restraining or blocking. Under normal operating conditions, the average power flowing into the transformer was almost zero, which was not the case for internal faults where it consumes a large amount of power. It combined the information from the current and voltage signals to provide more sensitivity. This voltage and current information was used in four analysing techniques. 1- the logical increase of voltage at the instant of energization, 2-impedance and admittance calculation, 3-the comparison of the measured and calculated current and voltage signals, 4- the calculation of the instantaneous power by the multiplication of the voltages and currents. However, there were some problems with the first three compared methods. The first one had a time delay in case of failure. The second one had a problem in the calculation with the division by zero and it does not use the accurate transformer equivalent circuit in case of saturation of the core. These problems were avoided in the proposed fourth technique, by observing the energy directly in relation to any physical damage that could happen to the transformer due to arcing. The performance of this technique was proved by a real-time data and simulation of faults.

In late 1990s, the research trend started to take a move away from harmonic restraining techniques. Intelligent techniques such as the neural network and fuzzy logic became a trend in power transformer protection. Many papers were proposed during the last twenty years, some of which will be described here. In 1998, Zaman and Rahman [80] presented an artificial neural network (ANN) based technique to discriminate inrush currents from internal fault currents in transformer protection. In this paper, a back-propagation technique was used with experimental testing data to train the proposed neural network. This proposed technique was carried out in two different ways, simulation and on-line testing. These tests were carried out to evaluate the efficacy of the proposed algorithm for different types of transient conditions. Both the simulation and the experimental testing results were quite satisfactory and the speed of the response for both of them, as shown in the results, was longer than half a cycle based of 60Hz frequency. In 2001, Orille-Fernandez et. al. [81] presented a combination of two mathematical tools, the finite impulse response (FIR) filter and the neural networks (ANN) to form a FIRANN differential relay for three-phase power transformer protection. The application of a FIR filter and the ANN technique was provided as a differential relay for a three-phase power transformer. Three FIRANN models were trained and tested for transformer protection. The first FIRANN was used to identify internal faults only from all other transients. The other two FIRANNs were used to discriminate internal from external faults. However, the authors did not mention anything about the classification of the inrush current from the internal or external faults. In 2003, Myong-Chul Shin et. al. [82] presented a fuzzy logic technique for the protection of power transformers. As the authors mentioned that the frequency environment of the power system became polluted with many harmonics so that the harmonic restraining techniques may not be helpful any more. Moreover, the improvement of the transformer core steel had less second harmonic content in

the inrush current, which was the main feature of the inrush current over the fault currents. Therefore, they presented in their paper a new algorithm for a differential protection relay using fuzzy logic. The proposed technique consists of harmonic restraining, flux-differential current derivative curve, and percentage differential characteristic curve. This work was based on a simulation using the Salford EMTP program. 2005 Guzman Diaz et. al. [83], [84] provided an approach to improve the differential relay security and dependability. This approach was based on space-vector analysis of the differential current. It depended on the time characteristics of the shape of the input signals in Park's plane. That means they observed the peaks and their numbers in the space-vector difference for a sliding window of 20 msec. The response time for the algorithm of around one cycle is achieved in the laboratory tests. However, the simulated results did not show any actual response of the relay such as releasing a trip signal. The results show only an analysis of different current signals. In 2007-2010, Tripathy et. al. [85], [86], [87] presented two papers on the differential protection of power transformers using a probabilistic neural-network (PNN). They use the ratio of the voltage to the frequency and the differential current amplitude for their relay design. The two papers were based on simulation process using PSCAD/EMTDC software with the integration of MATLAB.

In 2011, Abniki et. al. [88] presented a criterion for discriminating inrush currents from internal fault currents using the difference between the outputs of two moving windows. Both of the windows were used to estimate the magnitude of differential current of the power transformer. The first window was based on a full-cycle Fourier algorithm and the second one was based on the least square error method and had five sample point input data. This technique was a simulation-based technique using PSCAD/EMTDC software. However, not enough results were shown in the paper to prove its efficacy. Zoran Gajić [89], [90] used the

universal power transformer differential protection (87T) relay for the phase-shifting transformers transformer applications to demonstrate its feasibility of advanced online phase-angle shift compensation for the phase-shifting transformer applications. This relay used the second and the fifth harmonics based analysis to discriminate inrush currents from fault currents. The analysis was based on off-line data collected from the specified relay and MATLAB simulation. Bin Zheng et. al. [91] examined the application and analysis of three different current compensation methods for transformer differential protection, 1- YΔ current phase compensation method 2- ΔY current phase compensation method 3- compensation method-adopting phase current. The study tested the ability of the three methods to identify inrush currents and their effects on protection reliability. It was based on analysing the ratio between the first and the second harmonic components contained in the differential current. Daniel Barbosa et. al. [67] presented Clarke's transform and fuzzy logic based method for the digital protection of power transformers. Their algorithm did not use harmonic analysis as a basis for the decision of the proposed algorithm. ATP software was used to simulate the tests for the proposed algorithm. A comparison between the proposed technique and commercial relay was provided. Shi et. al. [92] proposed a method based on mathematical morphology (MM) and a neural networks (ANN), for the identification of the inrush current in power transformers. The mathematical morphology was used to extract the shape features from differential currents, and then the features were fed into ANN to be identified. The testing results showed that using the MM based feature extraction was an effective method to reduce the ANN complexity and increase the identification speed. It was implemented using MATLAB and evaluated on the data obtained from PSCAD/EMTDC simulation.

In 2012, Oliveira et. al. [93] presented a paper for the extended Park's vector approach (EPVA) based differential protection for three-phase power transformers. A new method for

power transformers protection was presented in this paper based on the analysis of the harmonic content of the differential current Park's vector modulus. This method was designed to detect the low-level turn-to-turn faults and restraining for the inrush current. This method distinguished the inrush current from fault currents and detected the turn-to-turn winding insulation failures. Both simulation and experimental testing were carried out. Hooshyar et. al. [94] presented a paper on time-domain analysis of the differential power signal for detecting the inrush in power transformers. This power-based algorithm depended on some low frequency content of the differential power waveform and did not depend on the magnitude of differential power signal. In the method, during inrush conditions, the differential power signal was examined. Then it introduced the inherent characteristics of the signal to a time-domain-based wave-shape classification technique. After half one cycle the algorithm was designed to decide the type of the tested case. The testing was carried out in PSCAD/EMTDC software as well as real-time experimental testing using real fault and inrush signals. Barbosa et. al. [95] presented an intelligent systems technique based on the differential protection of power transformers. Three mathematical methods were presented, the ANN (using Shannon's entropy) for CT saturation correction, the genetic algorithms for estimating the current harmonic content of the input signal and fuzzy logic for decision-making. The ATP program was used to model a complete electrical system.

In 2013, a self-adaptive differential protection of power transformers was presented by Wenkui Zhang et. al. [96]. This method regulated the parameters of percentage differential characteristics automatically, namely the pickup current and the restraining coefficient and current at the knee point of the slope characteristic. Also, Hooshyar et. al. [97] studied the CT saturation based on the wave-shape properties of the current difference functions. Two indices were introduced of a consecutive minimum and maximum pair of the current's

second difference function and were used to detect the CT saturation. This study was based on simulation data signals using PSCAD software. Kojovic et. al. [98] presented a low-energy current sensors based differential protection method for power transformers using Rogowski coil current sensors. A review of the Rogowski coil sensors characteristics and their application in protection purposes was presented. A comparison between these sensors and the regular CTs was presented in this paper for differential protection schemes of power transformers. An analysis of transformer inrush currents and a comparison of harmonic restraint methods in transformer protection is provided by Hamilton [10], in which a review of many restraining methods was provided with a conceptual logic diagram and the inrush current with a simplified excitation curve was analyzed. Based on the residual flux and saturation flux, mathematical equations were derived to calculate the magnetizing inrush current. The study provided the advantages and disadvantages of each method. This study was based on the analysis of the simulated data and compared with data collected from a real system to investigate the efficacy of the study.

In 2014, Dashti and Sanaye-Pasand [99] presented a multi-region adaptive differential protection for power transformer. This approach discriminated between the various types of the disturbances in power transformers. Unlike the traditional dual-slope, differential characteristic, the proposed algorithm was divided into five operating regions. The new two regions were for inrush current and CT saturation detection. A new technique was added to decrease the relay operation time called the phase differential units. A three-phase, 230/63-kV power transformer was used in PSCAD/EMTDC software for testing the proposed technique. Tavares and Silva [100] used the ATP Software to evaluate the performance of transformer differential protection. A numerical relay was implemented using the MODELS language for phase, negative sequence and restricted earth fault differential protection.

2.4 State-of-The-Art of The Wavelet Transform Based Digital Relays:

The introduced modern techniques that use the ANN, Kalman filtering and Fuzzy logic techniques have some drawbacks and shortcomings. For instance, ANN is a powerful technique; however, it requires a lot of training and a large amount of memory. More memory may be required with the increase in the number of hidden layers, which may influence the simplicity of the designed relay. Training the ANN is sometimes annoying, because each case of the testing must be trained individually for a long time. Moreover, some types of sudden transients in a power system do not have any specific shape, which makes it a very hard job for ANN to be trained for. Transients that may take place in the power system usually have a short duration, impulse superimposed and non-periodic signals [101], [102]. DFT is used to decompose periodic signals in the frequency domain. However, this tool assumes the periodicity of the signal at all times, even with a non-periodic signal. This assumption creates some errors when the analysed signal is not periodic, even with the use of the modified version, STFT. The STFT uses a fixed window width in the entire frequency scale, which does not give a good resolution with the change of frequency. Moreover, the frequency analysis does provide the frequency content of the signal but cannot provide any information about the time location of the extracted frequencies spectrum. This mathematical tool has served power transformer protection for quite a long time.

Digital protection is moving towards the simplest and most efficient, powerful mathematical techniques such as the wavelet transform because of its ability to deal with both the periodic and non-periodic signals. Wavelet transform has been used for transient analysis for the last three decades; however, it did not gain any special attention in terms of transformer protection until the last decade. This powerful mathematical tool has been delegated in many sides of analysis such as disturbance analysis and classification, signal and

image processing and pattern recognition. Power system protection, analysis, detection and the classification of electromagnetic transient and power quality studies are some of the applications of the wavelet transform in the power system area.

In 2003, Youssef [103] presented a wavelet-based protection technique for discriminating inrush currents from fault currents in power transformers. The speed of the response of the proposed technique was less than half a cycle based on the 50 Hz power frequency and 5 kHz sampling frequency. The EMTP software was used to simulate a 132/11 kV power transformer and the generated data was analysed by MATLAB to test the speed, reliability and efficacy of the proposed technique. In 2003-2005, Saleh and Rahman [104], [105] introduced a method for differential protection of three-phase power transformers based on the WPT. The minimum description length (MDL) data criteria were used to find the optimal wavelet analysis. In addition, it included the selection of the optimal number of resolution levels. In this work, the WPT was used to extract certain features of the differential current, which could be used to distinguish between the inrush and different internal fault currents.

In 2006, Faiz and Lotfi-Fard [106] presented a wavelet-based technique to discriminate inrush currents from fault currents in power transformers. The criterion function was defined by the difference in magnitudes of the wavelet coefficients within a certain frequency band. This criterion signature was used to discriminate the inrush current from fault currents in power transformers. The response speed was about a quarter cycle of the system frequency. Moreover, this criterion did not depend on any threshold values. The study was based on a simulation process using PSCAD/EMTDC software. In addition, the proposed technique was tested off-line for a data collected for a laboratory three-phase power transformer.

In 2010, Saleh and Rahman [107] presented a real-time testing of a wavelet packet transform based algorithm for 3Φ power transformers differential protection. A digital signal

processor (DSP board) was used in a host computer to test two different 3Φ power transformers (5kVA and 2kVA) with their neutral grounded through a resistance. Different tests were carried out to test this algorithm including the inrush and internal fault currents for different cases of CT saturation and different loading conditions, including neutral resistance-grounded and capacitive loads. Daubechies (db4) was the mother wavelet used in this paper and the number of resolutions was two levels. Gaouda and Salama [108] presented a digital signal processing technique for transformer inrush currents and internal faults monitoring using a wavelet transform. A small number of coefficients of the local maxima were used by the proposed method. In this paper, measurement of the magnitude of the variation of the signal was carried out using only one coefficient at each level of resolution. The ratio of the signal magnitude at the fourth resolution level to the signal magnitude at a reference resolution is used to overcome the false tripping due to normal disturbances. A sliding Kaiser window of data was used in this technique in simulated data and in a real laboratory testing.

In 2011, Jamali et. al. [109] developed a wavelet-based technique for discriminating inrush currents from fault currents in power transformers coupled with a finite element analysis method. This algorithm has characterized different behaviours of inrush and fault currents by using the wavelet coefficients over a specific frequency range. This algorithm was based on analysing the slope of the start of the inrush current waveform and the fault current waveform. They supported their results by using a finite element analysis method based simulation, using MAXWEL software, to simulate the three-phase power transformer. Their results showed that the proposed methodology could classify and discriminate inrush currents from fault currents. Saleh et al. [110] presented an implementation of WPT using Butterworth passive filters for differential protection of power transformers. This work was based on two cascaded stages of third order Butterworth high-pass filters. The high-pass

filters were designed in such a way to extract the second level high frequency components that exist in the three-phase differential currents, which were supplied to the filters from the current transformers. The extraction of the second level high frequency components was required to detect the transients that may occur in three-phase power transformers. The high-pass filters cut-off frequencies were identical to the cut-off frequencies of WPT associated digital quadrature mirror filters. Then, the output was used to classify the type of the transient, which only release trip signals in the case of internal faults. Maofa Gong et. al. [111] proposed many aspects in this paper such as analysing the transient mechanism, establishing a mathematical model, and studying inrush current. PSCAD/EMTDC simulation software was used to perform this study. The wavelet toolbox in MATLAB was adopted to implement the wavelet multi-resolution analysis. The Daubechies (db5) was used to extract the wavelet transform energy characteristic values of inrush currents and fault currents. Then, a neural network-pattern recognition algorithm was used to distinguish inrush current and short circuit current. The computation time of the proposed protection algorithm was presented as approximately 14msec. Yang Long and Ning Jingdong [112], [113] described a few methods for discriminating inrushes from internal faults in power transformers using the wavelet transform. This study was based on a simulation using MATLAB, in which the wavelet analysis was carried out for three levels of resolution. However, the paper did not show any tripping decisions made based on the simulated results. Abniki et. al. [114] presented a new technique for detecting the inrush current in power transformers based on a combined wavelet analysis and the Prony analysis method. DWT of power system frequency was used to discriminate the inrush currents from fault currents. The power system frequency was estimated using the Prony analysis method with three consecutive samples rapidly. Then, the Daubechies mother wavelet was used to investigate the unbalanced conditions in the

power system by analysing the estimated frequency. The changes of the estimated power system frequency were used in this criterion to discriminate internal fault currents from inrush currents. This simulation was carried out using PSCAD/EMTDC software. Munir and Smit [115] evaluated several methods in order to determine the best method for the transformer conditions. Vibration signals were taken sequentially to conduct this evaluation. The utilized algorithms were the FFT, DFT, Hilbert Huang transform (HHT) and WPT with HHT. This work led to the use of the WPT with the HHT as the best algorithm for this purpose. It was used to decompose the vibration signal into a set of narrow bands before being screened to select the greatest energy signal only. Finally, the evaluation result showed that the main frequency signal was the key signature to this analysis.

In 2013, Gomez-Luna et. al. [116] proposed an on-line theoretical analysis of the application of the wavelet transform in power transformer transient signals. This on-line analysis was carried out to obtain the frequency response curve from the transient signals by using the CWT. The proposed study was validated by simulating the transient signals in an ATP program. The Morlet wavelet and the modifier Morlet wavelet were used in this study. Rahman et. al. [117] developed a finite impulse wavelet filter for localising partial discharges inside a transformer winding. It was based on a linear combination of the wavelet decomposition filter for which the transfer functions of the filters were estimated using the Yule-walk equation for IIR filter approximation. A discussion of the data mining theory with the experimental testing in the Tony Davies High Voltage Laboratory was provided in this paper. Principal component analysis (PCA) was used to aid in the visualization process.

Recently, in 2014, Ghunem et. al. [118] presented an algorithm for selecting a wavelet-based transformer differential protection. The selection of the optimal mother wavelet and the optimal level of resolution were carried out using MDL with entropy criteria. The

stepwise regression (STWR) was used to get the best feature. Acceptable classification accuracy can be maintained by the selected features and offer the minimum dimensionality possible. A neuro-wavelet- based classifier was used to validate the proposed technique for inrush current and internal faults. Many wavelet functions were employed in the analysis and they were found to be useful using the MDL results for testing the inrush currents. In addition, the study was done for several resolution levels, and the best results were found at the fourth resolution level. Gonzales and Mombello [119] presented a methodology for transformer failure detection in order to overcome some limitations using DWT and frequency-response analysis (FRA). The proposed technique was based on decomposing the input signal into several levels of resolution using DWT. The correlation and differences between original and smoothed FRA traces at low-frequency ranges were deployed to choose an adequate number of decomposition levels. The Daubechies mother wavelet and the Symlets mother wavelet gave the same results, but the analysis in this paper was carried out using the Daubechies mother wavelet.

Several approaches have been reviewed for digital relays in this chapter. Many relay producing company are still using the harmonic-based analysis techniques, may be because of economic reasons or they do not trust the new developed techniques yet. These techniques may not be adequate for newer special power transformers protection. The literature indicates that the WPT provides fast and accurate distinguishing criteria for transformer protection. However, such techniques require a certain sampling frequency for its analysis, which may have some impact on the new trend of interconnected special protection systems. For these reasons, new protection technique is required for interconnected power transformer protection.

Chapter 3

Differential Protection of Power Transformers: Fundamentals and Theory

3.1 Preface

The differential protection of power transformers has become an important consideration for researchers, because of the huge financial losses that may occur due to faulted power transformers. When power transformer failure takes place, the costs associated with repairing the damaged power transformer and the long outage time could be very high. The unplanned outage of the power transformer may cause some important loads to shut down, costing the utility a lot of money. In addition, the failure of the power transformer may create a shutdown of the whole power system. These issues are important considerations in terms of providing high quality protection for power transformers. For these reasons, if the power transformer is experiencing any faulted conditions, the transformer must be isolated from the grid so that the consequences can be limited. One of the most effective protection methodologies of power transformers is the differential current protection algorithm. Current differential relays are one of the protective relays that have been improving since they were first introduced in the early 1900s as electromechanical devices. The history of this methodology has been discussed in detail in chapter two.

Typically, differential protection is focused on the discrimination of magnetizing inrush currents from fault currents in power transformers as well as over-excitation and current transformer saturation. Many techniques have been developed for the differential protection of power transformers based on harmonic restraining or on modern digital techniques. The

principle of operation of some of these techniques is briefly discussed later in this chapter, and the proposed technique is described in detail in the following chapters. There are many types of power transformer failures, which cause the power transformer to be isolated from the power system grid. These failures can be classified into two types of faults, internal faults and external faults [3], [5], [62], [120].

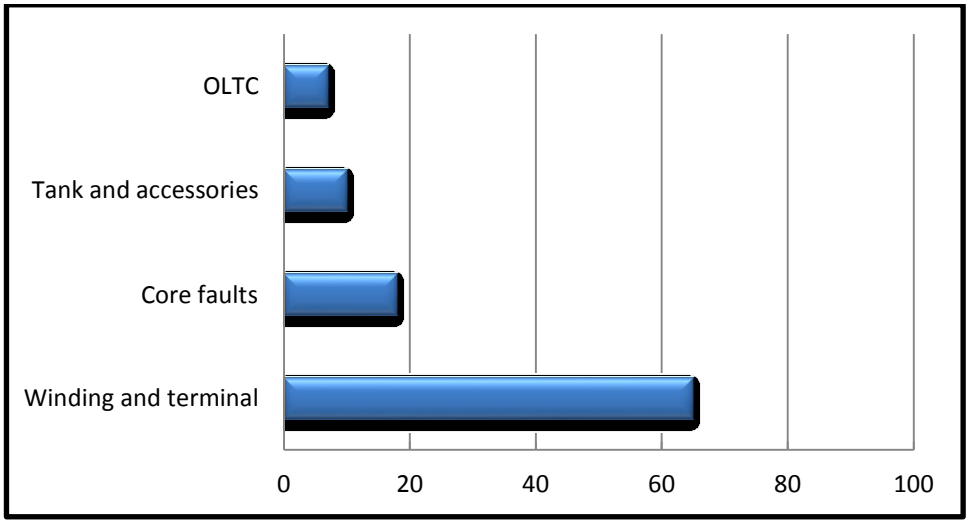

Figure 3-1 Transformer faults statistics **[3]**, **[120]**

Table 3-1 Major transformer faults and their protection methods **[3]**, **[120]**

Fault Type	***Protection Method Used***
Primary winding phase to phase fault	Differential; Over current
Primary winding phase to ground fault	Differential; Over current
secondary winding phase to phase fault	Differential
secondary winding phase to ground fault for Δ-Y connection	Differential; Restricted Earth fault
Inter-turn fault	Differential; Buchholz
Core & tank fault	Differential; Buchholz; Tank-Earth
Overheating	Thermal
Over fluxing	Over fluxing, Over excitation

Power transformer internal faults, or faults that originate inside the power transformer, can be classified into five main categories: winding faults, thermal faults, iron core faults, tank and transformer accessory faults, and On-Load Tap Changer (OLTC) faults. The approximate proportion of the different types of faults due to each of the causes listed above is shown in Figure ***3-1*** [3], [5], [41], [72], [120], [121].

3.2 Conventional Differential Protection

A conventional differential scheme is based on the principle that the input power to the power transformer under normal conditions is equal to the output power. Under normal conditions, no current will flow into the differential relay current coil shown in Figure ***3-2***. Whenever any type of internal fault occurs, within the power transformer protected zone, the current balance will no longer exist, and the differential relay contacts will close and release a trip signal to cause certain circuit breakers (CBs) to open in order to disconnect the faulted power transformer from the power system grid, so that the consequences are minimized. Figure ***3-2*** shows the differential relay in its simplest form and explains its principle of operation. In the differential relay circuit, the differential relay compares the primary and secondary side currents per phase of the power transformer. The difference between the primary side current and the secondary side current is called the differential current. Current transformers (*CTs*) are utilized to reduce the amount of the power transformer currents in such a way that their secondary side currents will be equal. Two *CTs* are required for single-phase power transformer protection, but in a three-phase power transformer, six *CTs* are needed which are divided into two *CTs* per phase. In addition, the polarity of *CTs* is chosen in such a way that the currents in the differential circuit flow normally without going through the differential relay during normal load conditions and external faults [3], [5], [121].

The turns ratio of a transformer is defined as the ratio between the number of turns in the primary side to the number of turns in the secondary side. For the differential protection of power transformers, the current transformer ratings are selected carefully in order to be matched with the power transformer ratings, to which they are connected, so that the *CTs* secondary side currents are equal. However, the problem is that the *CTs* that are available in the market have standard ratio ratings. They are not available exactly as the desired ratio ratings. Therefore, the primary ratings of the *CTs* are usually limited to those of the available standard *CTs* ratios. In this case, the closest current transformers ratios to the required turn ratios are selected to minimize the discrepancies between the selected *CTs*. Commonly, the primary side of the current transformer has only one turn (1 turn) and the secondary side has many turns (n) depending on the transformation ratio of the *CTs*, which is selected to match the ratings of the power transformer. For the protection system of the power transformer shown in Figure ***3-2***, if the turn ratio of the primary side CT_1 is $\frac{n}{n_1}$ and the secondary side CT_2 is $\frac{n}{n_2}$, where ($n = one\ turn$), then the turn ratio of the primary current transformer is $\frac{1}{n_1}$ and the turn ratio of the secondary side current transformer is $\frac{1}{n_2}$.

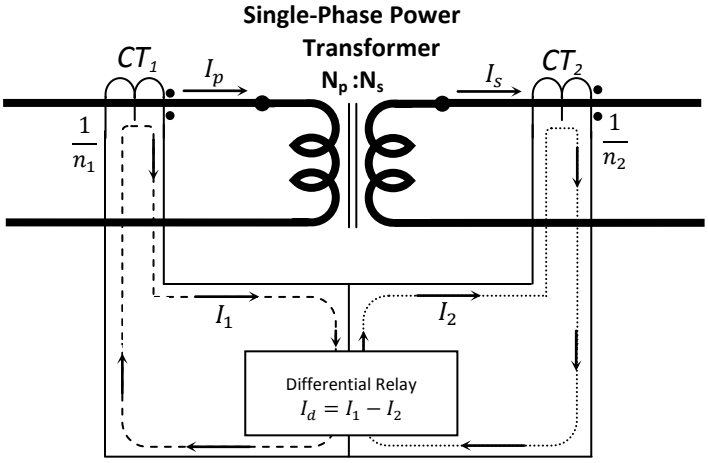

Figure 3-2 Differential relay for 1Φ two winding transformer

Therefore, the secondary current I_1 of the CT_1 located in the primary side of the power transformer is [3], [5], [8], [41], [72], [121];

$$\frac{I_1}{I_p} = \frac{n}{n_1} = \frac{1}{n_1}$$

$$I_1 = \frac{I_p}{n_1} \tag{3.1}$$

where

I_p : primary side current of the power transformer.

I_1 : secondary side current of CT_1.

n_1 : number of turns in the secondary side of CT_1

n : number of turns in the primary side of CT_1 and equal to one turn [3].

In the same manner for the power transformer secondary side CT_2, the CT_2 secondary current I_2 is [3], [5], [8]:

$$\frac{I_2}{I_s} = \frac{n}{n_2} = \frac{1}{n_2}$$

$$I_2 = \frac{I_s}{n_2} \tag{3.2}$$

where

I_s : secondary side current of the power transformer,

I_2 : secondary side current of CT_2.

n_2 : number of turns in the secondary side of CT_2

n : number of turns in the primary side of CT_2 and equal to one turn.

Since the differential current is: $I = I_1 - I_2$, then, from equations (3.1) and (3.2), the differential current flowing in the relay operating coil current I_d can be calculated as;

$$I_d = I_1 - I_2 = \left(\frac{I_p}{n_1} - \frac{I_s}{n_2}\right) \tag{3.3}$$

If there is no internal fault occurring in the power transformer protected zone between the current transformers, ideally the currents I_1 & I_2 are equal in magnitude and opposite in

direction, i.e. the differential current $I_d = 0$ as shown in Figure 3-3. The primary side current I_p and secondary side current I_s of the power transformer are related to each other by the equation (3.4);

$$\frac{I_p}{I_s} = \frac{N_s}{N_p} \tag{3.4}$$

where: N_p and N_s : number of turns of the primary and secondary sides of the power transformer respectively.

$\frac{N_p}{N_s}$: power transformer transformation ratio.

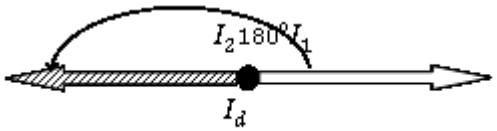

Figure 3-3 Output currents of the CTs are equal in magnitude and opposite in direction

If there were any faults in the power transformer protected zone, the currents I_1 & I_2 would no longer be equal in magnitude or opposite in direction. That means the differential current $\mathrm{I_d} = \mathrm{I_d}\angle\theta$ has a significant value as shown in Figure 3-4.

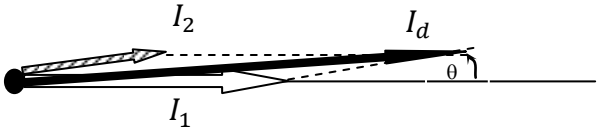

Figure 3-4 Output currents of the CTs are not equal in magnitude and not opposite in direction

The amount of current $I_d = I_d\angle\theta$ induces the relay operating coil to operate in order to send a trip signal to the circuit breakers to isolate the power transformer. From equation (3.4) the secondary current with respect to the primary current of the power transformer is:

$$I_s = \frac{I_p \times N_p}{N_s} \tag{3.5}$$

Therefore, by substituting equation (3.5) in (3.3) and manipulating we get,

$$I_d = \frac{I_p}{n_1} - \frac{I_p \times (N_p/N_s)}{n_2}$$

or, $$I_d = \frac{I_p}{n_1} \times \lambda \tag{3.6}$$

where $$\lambda = \left(1 - \frac{N_p/N_s}{n_2/n_1}\right)$$

From the equation (3.6) it is obvious that if the term $\lambda = 0$ then $I_d = 0$

for $I_d = 0$, $\frac{N_p/N_s}{n_2/n_1} = 1$

$$\frac{n_2}{n_1} = \frac{N_p}{N_s} \tag{3.7}$$

Equation (3.7) gives the condition for the security of the differential protection relay, which means that the ratio of the number of turns of the secondary side CT_2 to the number of turns of the primary side CT_1 should be equal to the turn ratio of the power transformer. If this condition is satisfied, then there will be no *CTs* mismatches and the differential current is equal to zero. However, if this condition is not satisfied then the differential current caused by the *CTs* mismatches may cause the differential relay to trip, depending on whether the differential relay used is designed to mitigate such a case or not.

Typically, in power transformers, the input power is equal to the output power. However, the voltages and the currents in both the primary and secondary sides are different with different levels depending on whether the transformer is step up or step down. For instance, if the transformer is step up that means, the input voltage of the power transformer is low and the current is high, in the meantime, the voltage in the secondary side is high and the current is low. This action makes both the input power and output power equal. Due to this nature, the *CTs* in the primary and the secondary sides of the power transformer do not have a similar turn ratio. Therefore, they must be carefully selected, in terms of their turn ratios and their magnetizing characteristics, so that they give the same output current at normal conditions of operations. If identical *CTs* are not available, the closer ones have to be

chosen and then the mismatch between them is compensated for by using the interposing *CTs*. The interposing *CTs* may fix the mismatch in the *CTs*; however, they add their own burden to the output of the main current transformers, which creates another problem. The same principles are applied for three-phase (3Φ) power transformers, except some extra considerations are added to the above-mentioned difficulties that face single-phase power transformers. Figure 3-5 shows the schematic diagram of the three-phase differential protection. In some cases of three-phase power transformer connections, a 30^{o} phase shift between primary and secondary currents takes place. This phase shift occurs in the Y-Δ or Δ-Y connected power transformers due to the transformation of the currents from the primary to secondary side. This phase shift can be easily corrected by connecting the CTs` secondary circuits in the opposite way to how the power transformer phases are connected, in both the primary and the secondary sides. For instance, if the transformer windings are connected in Y-Δ, the CTs windings should be connected in Δ-Y and vice versa, as illustrated in Figure 3-5 [3], [5], [8], [72], [121].

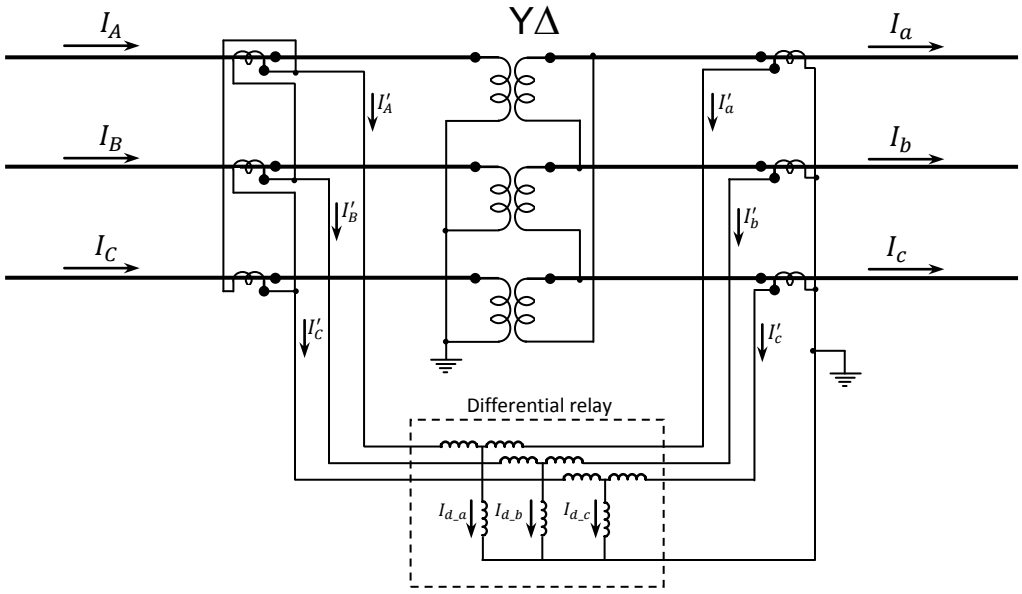

Figure 3-5 Schematic diagram of the 3ϕ differential current protection

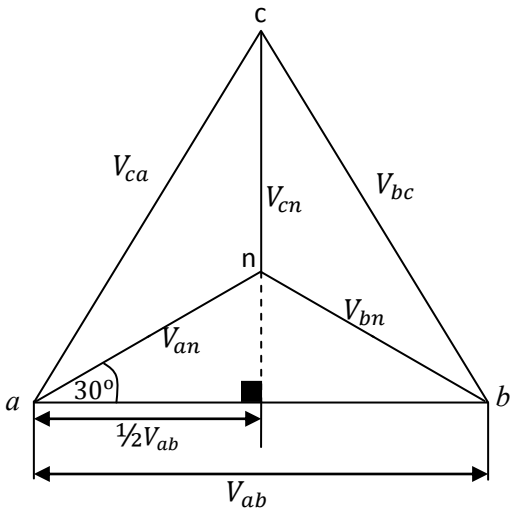

Figure 3-6 Relationship between line to line voltage and the phase to neutral voltage and the phase shift between them which reflects the phase shift in Y-Δ or Δ-Y connected transformers

Figure 3-6 is provided to depict how the 30^o phase shift is created in a Δ-Y transformer connection. As shown in Figure 3-6 the relation between the line-to-line voltage (V_{LL}) and the phase voltage (V_{ph}) can explain the phase shift between the Δ-Y transformer connection. Moreover, the relation is obvious in equation (3.8). The following equation demonstrates the relationship between the line-to-line voltage (V_{LL}) and phase voltage (V_{ph}):

$$\frac{V_{ab}}{2} = V_{an} \cos(30^o) \tag{3.8}$$

so that

$$\frac{V_{ab}}{2} = V_{an} \frac{\sqrt{3}}{2}$$

or

$$V_{ab} = \sqrt{3} V_{an}$$

There is another problem associated with this type of three-phase power transformer connection. For Δ-Y connected power transformers, if the utilized CTs are connected in Y -Y in both sides of the power transformer, there will be a zero sequence current flowing in the differential circuit operating-coil, which could result in exciting the relay and releasing a

trip signal as shown in Figure 3-7-a. However, if the CTs are connected in an opposite way to the power transformer connection as shown in Figure 3-7-b, the zero sequence will be prevented from flowing through the differential circuit operating-coil.

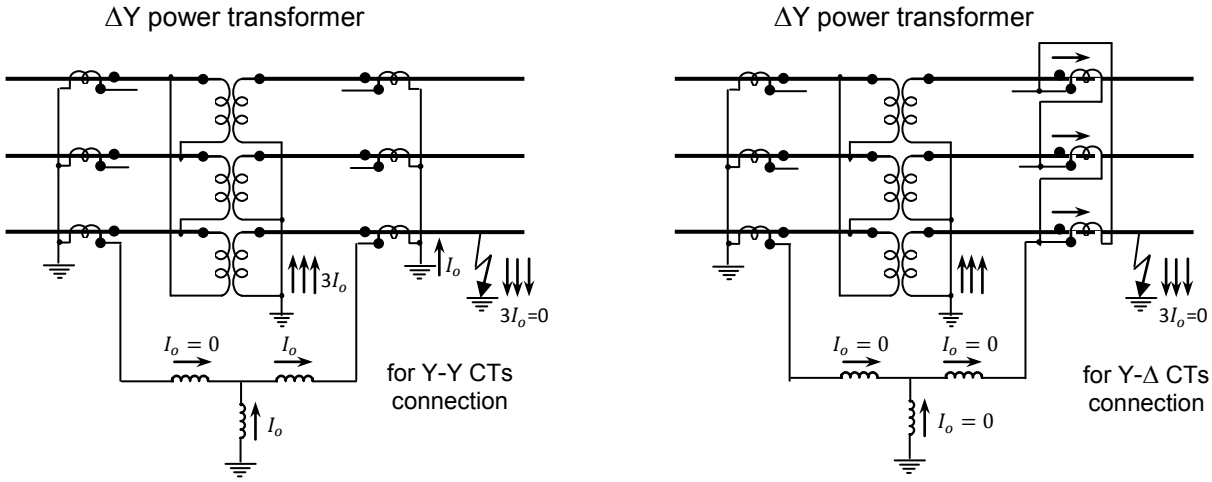

Figure 3-7 CTs connection for a Δ-Y power transformer [5]

(a) CTs are connected in Y-Y (b) CTs are connected in Y-Δ

3.3 Basic Problems of Differential Protection:

Generally, there are four main difficulties and problems, confronting the conventional differential protection scheme:

- Magnetizing inrush current during initial energization,
- Over-excitation,
- CTs mismatch and saturation,
- Transformation ratio changes due to tap changer.

3.3.1 Magnetizing Inrush Current

This phenomenon, of the magnetizing inrush current or the exciting current, occurs in the primary side of the transformer whenever the transformer is switched on (energized) and the instantaneous value of the voltage is not at 90^o. At this instant of time, the first peak of the flux wave is higher than the peak of the flux at the steady state condition. Because this

current is flowing in the primary side of the power transformer only, this current is flowing in the differential operating coil and it is sensed as an internal fault by the differential relay. The value of the first peak of the magnetizing current may be as high as several times the peak of the full load current. The effect of the inrush current on the differential relay is the false tripping of the transformer without any existing type of faults. From the principle of operation of the differential relay, the relay compares the currents coming from both sides of the power transformer through the current transformers as explained above. However, the inrush current is flowing only in the primary side of the power transformer. Therefore, the differential current will have a significant value due to the existence of current in only one side. For this reason, the relay has to be designed to recognize this current as a normal phenomenon, and not trip due to this current. The magnitude and duration of the inrush current is influenced by many factors; some of these factors are [3], [5], [8]:

- *Instantaneous factors:*
    - The instantaneous value of the voltage waveform at the moment of closing *CB*,
    - The value of the residual (remnant) magnetizing flux in the transformer core,
    - The sign of the residual magnetizing flux,
- *Permanent factors:*
    - The type of iron laminations used in the transformer core,
    - The saturation flux density of the transformer core
    - The total impedance of the supply circuit,
    - The physical size of the transformer,
    - The maximum flux-carrying capability of the iron core laminations,
    - The input supply voltage level,

On top of that, these factors change from single-phase to three-phase transformers, and the number of windings in the transformer affects that as well. As a result, the inrush current is studied separately in the following two sections in order to simplify and clarify the principle of generation of the inrush current in single-phase and three-phase transformers.

a) Magnetizing inrush phenomenon in single-phase power transformers

When the secondary side winding of the power transformer is open, the transformer can be represented by the following differential equation:

$$e = Ri + n_1 \frac{d\emptyset}{dt} \tag{3.9}$$

where, e the instantaneous value of the power supply,

i the instantaneous value of the current

R the winding resistance

$\emptyset$ the instantaneous flux threading primary winding

n_1 the number of primary turns

At no load and the secondary side winding open, the exciting current i is very small, and normally the winding resistance R has a very small value as well. Consequently, the term Ri in equation (3.9) is very small so it can be neglected. Therefore, the equation (3-9) will be:

$$e = n_1 \frac{d\emptyset}{dt} \tag{3.10}$$

This means that the voltage is proportional to the derivative of the flux. Assume a sine wave voltage of the power supply $e = \sqrt{2}\, E \sin(\omega t + \lambda)$, in which E is the RMS value of the supply voltage and $\omega = 2\pi f$. By substituting in equation (3.10), we get:

$$\sqrt{2}\, E \sin(\omega t + \lambda) = n_1 \frac{d\emptyset}{dt} \tag{3.11}$$

By solving this differential equation, we get the flux

$$\emptyset = -\frac{\sqrt{2}\,E}{\omega\, n_1}\cos(\omega t + \lambda) + \emptyset_t \tag{3.12}$$

The first term represents the normal steady state flux and the second term represents the transient component of the flux, which depends on the instant of the transformer energization. This equation shows that, under normal conditions of power transformer operation, the voltage waveform leads the flux waveform by 90°. The flux $\emptyset$ in a power transformer core changes in a rate proportional to the voltage drop across the primary side winding. The flux is proportional to the magneto-motive-force (mmf) in the transformer core and the mmf in the transformer core is proportional to the primary side current. As a result, the current waveform of the primary side will be in-phase with the flux waveform in the transformer core, and both of them are lagging the voltage waveform of the primary side by 90°. From Figure 3-8 the total flux may be viewed as consisting of two components, namely the steady state flux and the transient flux [3], [5], [57], [121].

The magnitude of the inrush current depends on many factors, as mentioned earlier. Some of these factors are permanent and do not change after manufacturing, and some of them are instantaneous. In this section, the effect of the instantaneous factors will be studied namely the residual flux and the instant of switching ON of the power transformer. If the power transformer is switched ON at a time when the instantaneous value of the voltage waveform is equal to zero and the residual flux has a significant value, then the resultant flux will start from the value of the residual flux and rise up to $2\emptyset_{\max} \pm \emptyset_{\mathrm{R}}$ in the next cycle. However if there is no residual flux $\emptyset_{\mathrm{R}}$ in the core, then the resultant flux will start from zero and following the same pattern like the first case as shown in Figure 3-8 and the total peak value of the flux will became $2\emptyset_{\max}$. Based on this, the magnetizing inrush current grows as the flux builds up. If the transformer is switched on at the peak value of the instantaneous

voltage waveform then the resultant flux will have the value of $\emptyset_{\max} \pm \emptyset_{\mathrm{R}}$, if the residual flux has a significant value; otherwise, it will be $\emptyset_{\max}$ if there is no residual flux in the transformer core. If the magnetic characteristics of the transformer core iron were linear, the current would have the same waveform like the flux waveform as illustrated by the equation (3.11). However, as illustrated in Figure 3-9, due to the nonlinearity of the magnetic characteristics of the transformer iron core, the current rises significantly when the core saturation takes place.

$$i = \frac{1}{L}\int V \sin \omega t \; dt = \frac{-V}{\omega L} \cos \omega t \tag{3.13}$$

Because the transformer, under normal operating conditions, is usually designed to operate near the knee point of the saturation curve for economic reasons, the maximum inrush may be expected whenever the residual flux is maximum. Figure 3-9 depicts an excitation curve which has been assumed with a small hysteresis loop, and then simplified by two lines (O – A) and (A – B) in order to simplify the calculation. The value of the excitation current could be found from the saturation curve for every point on the flux curve. The saturation curve depicts the magnetizing current needed to provide a certain level of flux. For the condition of maximum transient flux, the magnetizing inrush current I_x is determined graphically by entering the excitation curve OAB with the instantaneous flux values. When switching the transformer at angle 0° on the voltage waveform on the right hand portion of the figure, a value of $\emptyset_x$ is determined. If the actual hysteresis loop curve is used to get the magnetizing curve, an approximation of the curve may be obtained as illustrated by the dotted line in the right hand side [3], [5], [8], [57].

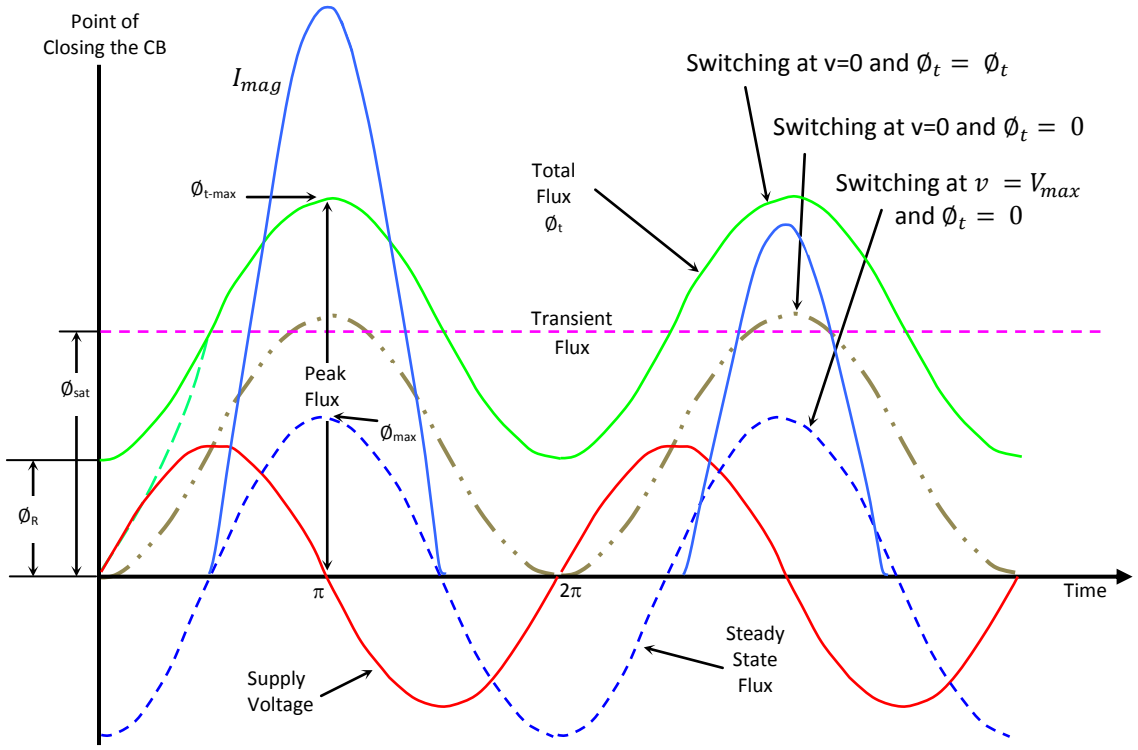

Figure 3-8 Voltage, flux, and current during a magnetizing inrush when the transformer is energized at zero crossing on the voltage wave

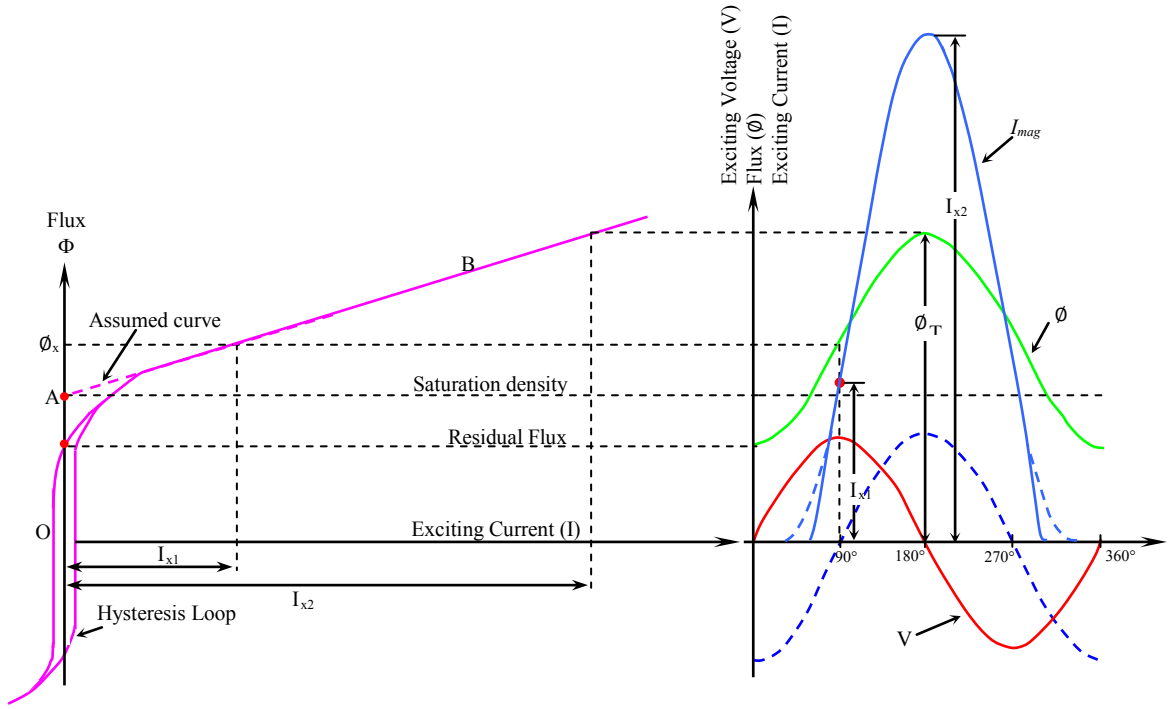

Figure 3-9 Derivation of inrush current wave from excitation [57]

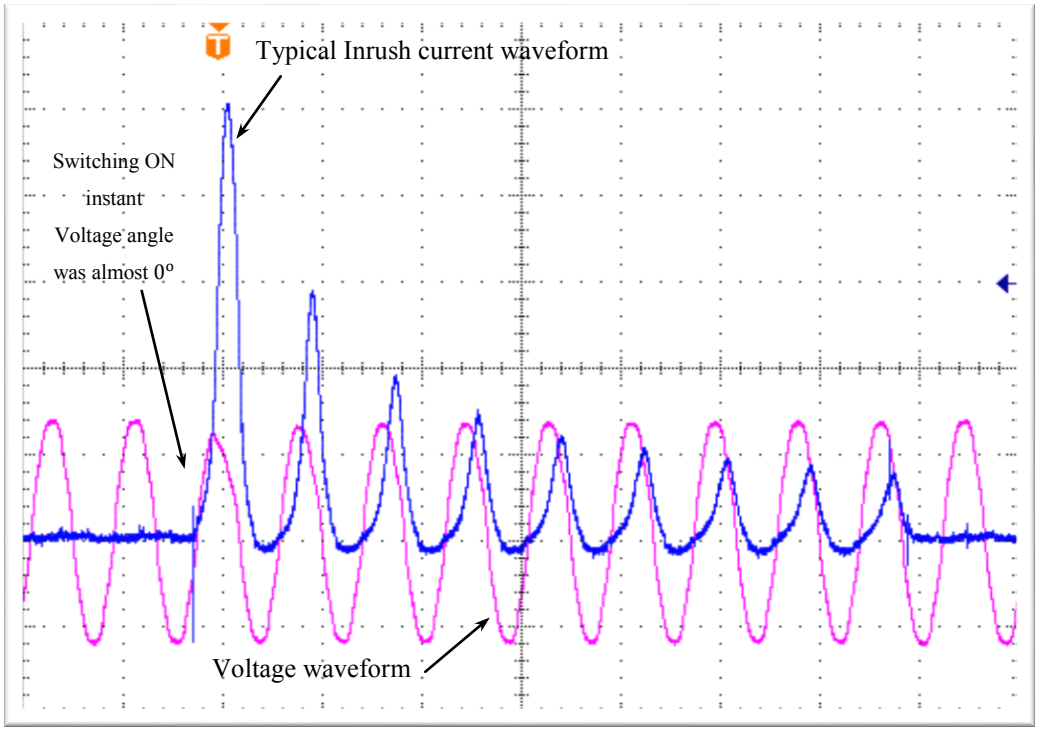

Figure 3-10 The typical magnetizing inrush current waveform with the primary voltage waveform. The orange (T), sign on the top of the figure, and the blue Arrow, on the right, are the horizontal and the vertical triggering limits.

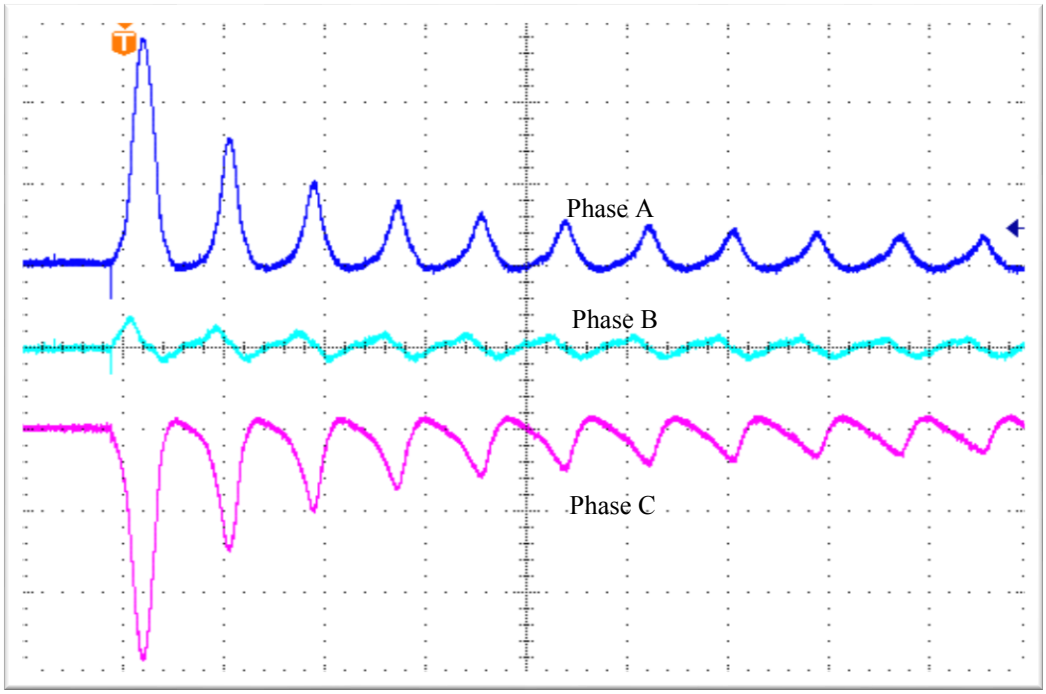

Figure 3-11 Sample of inrush currents in a three-phase Y-Δ connected

Figure ***3-10*** shows a typical inrush current waveform together with the voltage waveform. As mentioned above, the flux lags the voltage waveform by 90o; the resultant magnetizing inrush current will be lagging the voltage with the same angle as shown in the figure. It is obvious that the magnetizing inrush current waveform decays gradually in successive cycles due to the resistance of the transformer winding (R) in the energizing circuit and the reluctance of the transformer core ($\mathcal{R}$). The rate of the decay of the inrush current is large for the first few cycles because of the short time constant ($\tau = L/R$) of the circuit [3], [5].

b) Magnetizing inrush phenomenon in three-phase power transformers

The magnetizing inrush phenomenon in 3Φ power transformers may happen in more than one phase with different levels. The electrical connection and magnetic coupling between the phases may affect these inrush currents. Figure 3-11 shows typical magnetizing inrush currents for a three-phase $Y-\Delta$ connected power transformer. Therefore, beyond the above-mentioned factors affecting the inrush current in three-phase transformers, extra factors may be considered:

- The angle of the energizing voltages is different in different phases.
- Transformer with primary windings connected in delta or Star.
- The current in any given phase is a vector sum of two-phase currents.

In Figure 3-11, phases A and C have significant inrush currents, but phase B does not. That means the angle of switching was close to the angle 90° on the voltage waveform of phase B. In addition, the peak of the transient flux of the phase B core is below saturation level, and then the magnetizing current demanded by the coil could be negligible. In the meantime, it can be observed that the inrush currents in phases A and C are of opposite polarities, which can show the effect of the sign of the residual flux [3], [5], [121].

As mentioned above, for economic design aspects, the power transformer is designed to operate at a point closer to the knee point at the normal operating voltage level. Any increase of the terminal voltage above the normal value will greatly increase the magnetizing inrush current. In Figure 3-12, the relationship between the exciting current and the voltage applied to the transformer terminals is displayed. It is obvious from the figure that the current increases far more rapidly than the increase of the applied voltage [122].

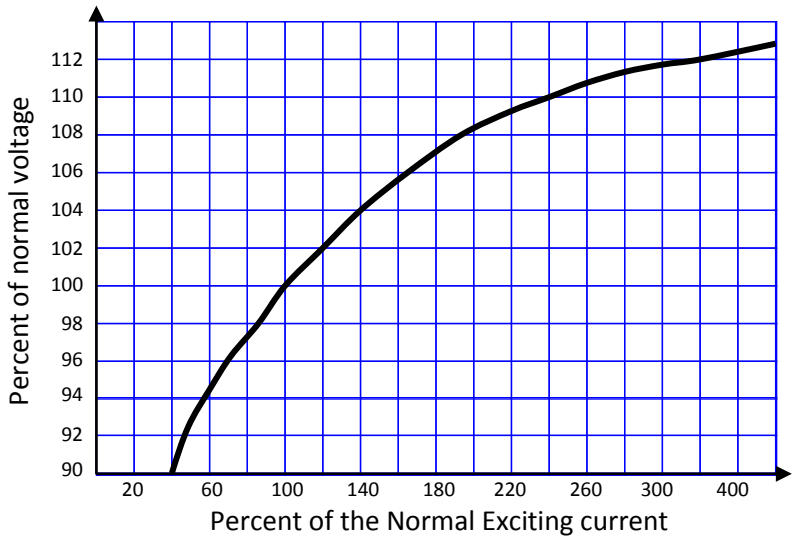

Figure 3-12 Relationship between the voltage and the magnetizing inrush current [122]

Generally, since the inrush current exists only in the primary side of the power transformer, the inrush current appears in the differential relay as an internal fault current. Therefore, a magnetizing inrush current resembles a fault current, which trips the transformer without the occurrence of any real fault. Tripping due to inrush current when a transformer is energized is not acceptable, because it delays connecting the power transformer to the grid. If we go back to the last two figures, it is obvious that the magnetizing inrush current has a distorted waveform not a sinusoidal waveform even though the flux does. In the analysis of the harmonic content of the inrush current, it was found that it has considerable amounts of the low order harmonics such as the second, the third, and the fifth and smaller amounts of

the higher order harmonics. Table ***2-1*** show these amounts of harmonics in terms of frequency with the fundamental component frequency of 60Hz [3], [4], [5].

Table 3-2 Harmonic content in the magnetizing inrush current [3], [5]

Component	***dc component***	***2nd Harmonic***	***3rd Harmonic***	***5th Harmonic***
Typical value	up to 55%	(17 – 65) %	up to 28 %	up to 5%

3.3.2 Power Transformer Over-Excitation

Over-excitation is considered one of the main difficulties that cause false tripping of the differential relay even without a real fault in the protected zone. There are many reasons why the power transformer can become over-excited such as inrush current, large external faults, decrease in the supply frequency and excessive applied voltage. The power transformer is said to be over-excited when the peak flux density of the transformer core iron exceeds the highest range of the flux density of the transformer core iron. Typically, the peak flux density of the most available transformers is within the range of 1.6T to 1.8T. With the flowing of high current through the power transformer, the flux density reaches 2T and then the transformer core saturates. The magnetic flux circulates in the core of the transformer directly proportional to the primary side voltage and inversely proportional to the frequency of the primary side voltage. If the primary side voltage is increased beyond the rated value, or the frequency of the primary side voltage is decreased significantly, then the transformer core will experience excessive flux that increases the magnetizing (exciting) current, heat, and vibrations. Over-excitation conditions are detected using a per-unit-ratio of voltage to frequency (V/f). If the value exceeds 1.05 p.u. at full-load or 1.10 p.u. at no-load, then over-excitation is declared. High-level over-excitation causes the transformer to

overheat and may cause serious damage to the power transformer's windings insulation and core. Many algorithms have been used to protect power transformers from over-excitation problems. Fuses are one of the methods used to protect small size power transformers against over-excitation; however, poor selection of the optimal fuse could cause damage to the protected power transformer. In fact, the over-excitation current is rich in the third harmonic and fifth harmonic, which gives a good opportunity to discriminate the over-excitation current from high operation load current and fault current. However, the conventional relays do not correlate well on such currents with limited characteristics of transformer over-excitation. This problem is a big concern in large transformers. Therefore, they should be equipped with the proper over-excitation protection associated with differential protection [123], [124], [125].

3.3.3 False Trip due to C.T Characteristics

The performance of the differential relays depends on the accuracy of the CTs in reproducing their primary currents in their secondary side. In many cases, the primary ratings of the CTs, located in the high voltage and low voltage sides of the power transformer, do not exactly match the power transformer rated currents. Due to this discrepancy, CTs mismatches take place, which in turn creates a small false differential current, depending on the amount of this mismatch. Sometimes, this amount of the differential current is enough to operate the differential relay. Therefore, CTs ratio correction has to be done to overcome this CTs mismatch, such as using interposing CTs of multi taps. Another problem that may face the CT is the saturation of its core. When saturation happens to one or both CTs at different levels, false differential current appears in the differential relay. This differential current could cause mal-operation of the differential

relay. The worst case of CT saturation could be produced by the dc component of the primary side current. This causes the secondary current to contain dc offset and extra harmonics [3], [5], [8], [41].

3.3.4 False Trip due to Tap Changer

An On-Load Tap-Changer (OLTC) is required wherever there are heavy fluctuations in the voltage. This device is installed on the power transformer to control the transformer output voltage automatically. The transformation ratio of the CTs can be matched with only one point of the tap-changing range. Therefore, if the OLTC is changed an unbalanced current will flow in the differential relay. This action causes CTs mismatches [3], [5], [8].

3.4 Conventional Solutions for Differential Protection

Based on the above-mentioned problems and the characteristics of the magnetizing inrush current, some signatures are extracted to help in designing the proper protection relay for power transformers to avoid tripping due to this phenomenon. Accordingly, research has been carried out since this phenomenon was first discovered. Many techniques and methodologies have been proposed for this matter, starting with electromechanical relays and then improving slightly to static relays and, finally, major improvement coming with digital relays. There are several conventional solutions for solving this problem; however, they are somewhat complex and expensive and they are not efficient for protecting modern power transformers especially in the modern power systems that are massively polluted with the harmonics, such as operating relay with time delay, harmonic current restraint, relay desensitizing or blocking, and harmonic filtration. Percentage Differential Relay based Harmonic Restraining was the most widespread effective technology until the 1960s before

the introduction of digital relays. The HU variable percentage differential relay with second harmonic restraining is shown in [4], [5]. This relay provided a good reliability of protection for power transformers at that time. It consists of three air-gap transformers to feed the restraining coils and one non-air-gap transformer to feed the operating coil in the differential circuit. In this design, the relay restraint is proportional to the maximum restraining current flowing in any restraint circuit [4], [5].

3.5 Digital Percentage Differential Protection

Percentage differential protection is the most effective protection criterion that has been used for quite some time to protect power transformers. This criterion has been improved through collaboration with modern mathematical techniques and fast digital computers. Some of them will be considered in the next sections. This collaboration gives efficient performance for modern digital differential relays for power transformer protection. Digital differential protection principles are based on the conventional differential protection that was explained in section 3.2. However, digital computers make the design of the protective relay easier and more flexible. In this, only the software of the algorithm needs to be modified and updated to improve the performance without needing to change the hardware of the relay. This makes the development of the digital differential protection relay easier and more flexible. Conventional percentage-differential relays are offered with a variety of percentage slopes, which are considered as the setting of the relay. Some of them have adjustable slopes or multi slopes. Figure ***3-13*** illustrates a typical percentage differential relay-operating characteristic, in which there is a horizontal line representing the minimum pick up current for the relay I_{min}. In addition, there is another line with one or two slopes separating the two regions of operations, namely the operating area and the restraining area.

The main function of this slope is to give some restriction to the relay to prevent tripping due to some differential relay problems such as the mismatch between the CT characteristics and the tap changer [3], [5], [57].

Many digital algorithms have been used since the invention of the computer. These algorithms do the same job with different methodology, accuracy and speed. According to IEEE standard C57.116, the acceptable speed for transformer protection is 6 cycles, (100msec for 60Hz power system) [126]. This IEEE standard time includes the time that the relay takes to respond to the fault and the time that the CB takes to fully open after receiving the trip command from the relay. Nowadays, all modern algorithms are faster than this standard, where some algorithms perform their function in less than one cycle (16.67 msec).

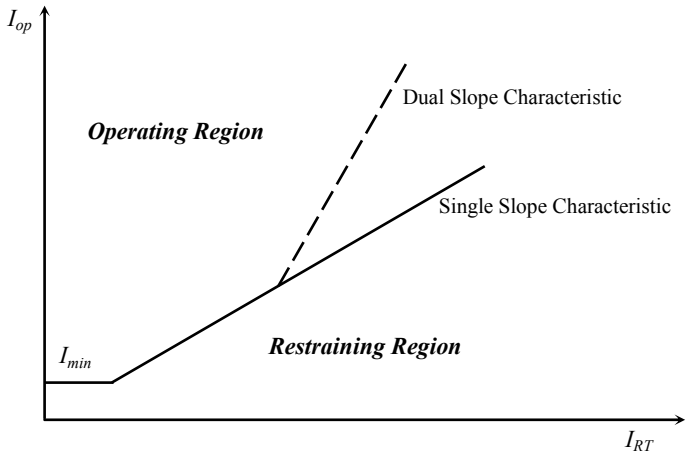

Figure 3-13 Differential relay-operating characteristic

3.5.1 Fourier transforms (FT)

The Fourier transform is a mathematical transformation was founded in the 18th century by Joseph Fourier and utilized to transform signals between the time domain and frequency domain. There are many types of Fourier transforms such as continuous Fourier transform (CFT), discrete time Fourier transform (DTFT), discrete Fourier transform (DFT), fast Fourier transform (FFT) and short time Fourier transform (STFT). The philosophy behind

the Fourier transform is the ability to break down any periodic signal into a combination of simple signals of sine and cosine functions waveforms, which is called harmonics.

This algorithm is built on the principle of harmonic-current restraint, where the magnetizing-inrush current is characterized by large harmonic components in the content that are not noticeably present in fault currents. Due to the saturated condition of the transformer iron, the waveform of the inrush current is highly distorted. The amplitude of the second harmonic, compared with the fundamental, is somewhere between 30% to 60% and the third harmonic 10% to 30%. The other harmonics are progressively less. The Discrete Fourier Transform (DFT) is used to implement this approach. In general, any periodic signal $f(t)$ having a finite number of discontinuities over the interval of (0,T) can be decomposed to its sine and cosine components as follows [5], [9], [42]:

$$f(t) = \frac{a_0}{2} + \sum_{k=1}^{\infty} [C_k \cos(k\omega t) + S_k \sin(k\omega t)] \tag{3.14}$$

Where

$$\frac{a_0}{2} = \frac{1}{T} \int_0^T f(t)dt \tag{3.15}$$

$$C_k = \frac{2}{T} \int_0^T f(t) \cos(k\omega t)\, dt \tag{3.16}$$

$$S_k = \frac{2}{T} \int_0^T f(t) \sin(k\omega t)\, dt \tag{3.17}$$

where: a_0 is the dc component of the f (t), and C_k, S_k are the cosine and sine coefficients of the frequencies present in $f(t)$, respectively. The discrete forms of the coefficients C_k, S_k with a sample rate of ΔT and total samples of $\frac{N}{T}$ per cycle, are expressed in the following equations [9], [42]:

$$C_k = \frac{2}{N} \sum_{n=1}^{N-1} x(n) \cos\left(\frac{2k\omega t}{N}\right) \tag{3.18}$$

$$S_k = \frac{2}{N}\sum_{n=1}^{N-1} x(n)\sin\left(\frac{2k\omega t}{N}\right) \tag{3.19}$$

These summation equations can be factorised and analysed to a $(N \times N)$ matrix form where N is the window width, as follows [9], [42]:

$$C_s = \begin{bmatrix} \cos\left(\frac{2\pi.1.1}{N}\right) & \cos\left(\frac{2\pi.2.1}{N}\right) & \dots & \cos\left(\frac{2\pi.N.1}{N}\right) \\ \cos\left(\frac{2\pi.1.2}{N}\right) & \cos\left(\frac{2\pi.2.2}{N}\right) & \cdots & \cos\left(\frac{2\pi.N.2}{N}\right) \\ \vdots & \vdots & \ddots & \vdots \\ \cos\left(\frac{2\pi.1.N}{N}\right) & \cos\left(\frac{2\pi.2.N}{N}\right) & \dots & \cos\left(\frac{2\pi.N.N}{N}\right) \end{bmatrix} \times x \tag{3.20}$$

$$S_s = \begin{bmatrix} \sin\left(\frac{2\pi.1.1}{N}\right) & \sin\left(\frac{2\pi.2.1}{N}\right) & \dots & \sin\left(\frac{2\pi.N.1}{N}\right) \\ \sin\left(\frac{2\pi.1.2}{N}\right) & \sin\left(\frac{2\pi.2.2}{N}\right) & \cdots & \sin\left(\frac{2\pi.N.2}{N}\right) \\ \vdots & \vdots & \ddots & \vdots \\ \sin\left(\frac{2\pi.1.N}{N}\right) & \sin\left(\frac{2\pi.2.N}{N}\right) & \dots & \sin\left(\frac{2\pi.N.N}{N}\right) \end{bmatrix} \times x \tag{3.21}$$

The Fourier harmonic coefficients can be expressed as:

$$F_k = \sqrt{S_k^2 + C_k^2} \tag{3.22}$$

where: $F_k$is the k^{th} harmonic coefficient for k = 1, 2 ... N and $x(n)$ is the signal $f(t)$ in its discrete form. The use of this technique for transformer protection is based on extracting the harmonic content of the input differential current, because the inrush, current is characterized with the second harmonic content. The DFT sine and cosine coefficients are used as discrete frequency filters for selective frequencies namely the fundamental frequency (F_1), the second harmonic frequency (F_2), and the fifth harmonic frequency (F_5). These filters extract the harmonics (F_1,F_2,F_5) in the differential current to classify the inrush current from the over-excitation and fault currents. The signature used in this classification is the ratio of the second harmonic to the fundamental F_2/F_1 for identifying the inrush current, and F_5/F_1 to identify the over-excitation. If the ratio F_2/F_1 is higher than a certain percent γ_1 that means

an inrush phenomenon is taking place. If the ratio F_5/F_1 is higher than a certain percent γ_2 that means an over-excitation is taking place. Otherwise, if the percentage is less than these two cases, that means a faulted condition is taking place. There is considerable disagreement in the literature on the values the γ_1 and γ_2 should have [9], [42], [127].

3.5.2 The rectangular transform technique

The rectangular transform technique is used to extract the fundamental harmonic component from the discrete differential input current. To implement this technique, assume that the input signal $f(t)$ is sampled at a sampling rate of Δt for time length T, so that there are $N = T/\Delta t$ samples. For this signal, the Fourier coefficients can be presented as in [14], [72], [79] and [127];

$$\hat{C}_k = \sum_{j=1}^{N-1} f(t_j) \cos\left(\frac{2\pi jk}{N}\right) \tag{3.23}$$

$$\hat{S}_k = \sum_{j=1}^{N-1} f(t_j) \sin\left(\frac{2\pi jk}{N}\right) \tag{3.24}$$

by replacing the sine and cosine terms with the equivalent rectangular function

$$\cos \gamma t\ (x) = sgn\ (\cos x) \tag{3.25}$$

$$\sin \gamma t\ (x) = sgn\ (\sin x) \tag{3.26}$$

where the rectangular function is defined as:

$$sgn(y) = \begin{cases} \dfrac{y}{|y|} & for\ \ y \neq 0 \\ 0 & for\ \ y = 0 \end{cases} \tag{3.27}$$

therefore, the equivalent rectangular transform coefficients will be as:

$$C_k = \sum_{j=1}^{N-1} f(t_j)\ \text{sgn} \cos\left(\frac{2\pi jk}{N}\right) \tag{3.28}$$

$$S_k = \sum_{j=1}^{N-1} f(t_j)\, sgn\, \sin\left(\frac{2\pi jk}{N}\right) \tag{3.29}$$

At the end of the long process [14], [72], [127] the result will be:

$$I_1 = \frac{2}{N}\left[\hat{S}_1^2 + \hat{C}_1^2\right]^{1/2} \tag{3.30}$$

$$I_2 = \frac{2}{N}\left[\hat{S}_2^2 + \hat{C}_2^2\right]^{1/2} \tag{3.31}$$

$$I_5 = \frac{2}{N}\left[\hat{S}_5^2 + \hat{C}_5^2\right]^{1/2} \tag{3.32}$$

These three components, the fundamental, the second harmonic and the fifth harmonics are used to perform the task for transformer protection. The ratio of the second harmonic to the fundamental is used to reorganize the inrush current and the fifth harmonic is used to detect the over-excitation of the transformer.

3.5.3 Walsh functions (WF)

The Walsh functions form a complete orthogonal set by [12], [14], [72], [72]and [127]:

$$Wal(k,t) = \prod_{j=0}^{m} sgn\,(\cos 2^j k_j \pi t) \tag{3.33}$$

where, k_j is the digit 0 or 1 of the binary number k. Walsh functions appear to be a squared-up version of sine and cosine functions; they take only values +1 and -1. Therefore, the Walsh expansion of $x(t)$ in the interval [0, *T*] can be defined as:

$$x(t) = \sum_{k=0}^{\infty} W_k\, wal\left(k, \frac{t}{T}\right) \tag{3.34}$$

$$W_k = \frac{1}{T}\int_0^T x(t) wal\left(k, \frac{t}{T}\right) dt \tag{3.35}$$

These Walsh coefficients form a vector in Hilbert space like the Fourier coefficients F_k. At the end [14], [72] and [127]:

$$S1 = 0.9\ W1 - 0.373\ W5 - 0.074\ W9$$
$$C1 = 0.9\ W2 + 0.373\ W6 - 0.074\ W10$$
$$S2 = 0.9\ W3 - 0.373\ W11$$
$$C2 = 0.9\ W4 + 0.373\ W12$$
$$S5 = 0.18\ W1 + 0.435\ W5 + 0.65\ W9$$
$$C5 = 0.18\ W2 - 0.435\ W6 + 0.65\ W10$$

3.5.4 Least Squares:

In this method, the inrush current is assumed to have a dc current decay and only five harmonics, so that the inrush current can be approximated for a certain time interval by [14], [72], [127], [128] and [129]:

$$i(t) = p_0\, e^{(-\lambda t)} + \sum_{k=1}^{5} p_k \sin(k\omega_0 t + \theta_k) \tag{3.36}$$

where $i(t)$ is the instantaneous sampled differential current, p_0 is the dc component, λ is the inverse time constant of the dc component, p_k is the peak value of the k^{th} harmonic, ω_0 is the fundamental frequency and θ_k is the phase angle of the k^{th} harmonic. If the time interval is small, the dc component can be approximated as:

$$p_0\, e^{(-\lambda t)} \approx p_0 - p_0\, \lambda t \tag{3.37}$$

Using a Taylor expansion the current $i(t)$ waveform can be simplified to the form:

$$i(t) = p_0 - p_0\, \lambda t + \sum_{k=1}^{5} p_k \cos\theta_k \sin(k\omega_0 t) + \sum_{k=1}^{5} p_k \sin\theta_k \cos(k\omega_0 t) \tag{3.38}$$

Equation 3.38 can be expanded in the matrix format as follows [127] and [128]:

$$\begin{bmatrix} 1 & t_1 & \sin\omega_0 t_1 & \cos\omega_0 t_1 & \dots & \sin k\omega_0 t_1 & \cos k\omega_0 t_1 \\ 1 & t_2 & \sin\omega_0 t_1 & \cos\omega_0 t_1 & \dots & \sin k\omega_0 t_2 & \cos k\omega_0 t_2 \\ \vdots & \vdots & \vdots & & \ddots & \vdots & \\ 1 & t_N & \sin\omega_0 t_1 & \cos\omega_0 t_1 & \dots & \sin k\omega_0 t_N & \cos k\omega_0 t_N \end{bmatrix} \begin{bmatrix} p_0 \\ -p_0\lambda \\ \vdots \\ p_k \sin\theta_k \end{bmatrix} = \begin{bmatrix} i(t_1) \\ i(t_2) \\ \vdots \\ i(t_N) \end{bmatrix} \tag{3.39}$$

In matrix notation

$$[\,A\,].[\,X\,] = [\,I\,]$$

and then the least squares become:

$$[\,X\,] = [(A^T A)^{-1} A^T].[\,I\,] = [B][I]$$

And

$$[B] = [\,(A^T A)^{-1} A^T\,]$$

The Fourier sine and cosine components of the fundamental, second and fifth harmonic contents can be calculated by [14], [72], [128] and [127]:

$$C_k = p_k \cos\theta_k(t_n) = \sum_{n=1}^{16} B(2k+1,n)i(t_n) \quad and \quad k = 1,2,5 \tag{3.40}$$

$$S_k = p_k \sin\theta_k(t_n) = \sum_{n=1}^{16} B(2k+2,n)i(t_n) \quad and \quad k = 1,2,5 \tag{3.41}$$

3.5.5 Artificial Neural Networks (ANN)

The first fundamentals of the neural networks were put forward in the 1940s, but the real applications for power system protection did not start until the 1980s. Pattern recognition applications are the most common application for neural networks. In the protection of power transformers, differential current pattern recognition is used to classify the different types of transients in the power transformer. This algorithm is different from the other techniques with the process of implementation, as the inputs and outputs need to be formulated and then the network needs to be trained for these inputs and outputs. The training of the network is very important and it might take a long time; failure to do so will lead to false decisions. The longer the training time of the network, the better and more accurate decisions we get. The neural network has three different layers in its construction; the input layer; the hidden layer(s), which could be one layer or more; and the output layer. Each layer consists of a number of cells called neurons connected to each other. The input layer contains the input terminals connected to the input neurons. The hidden layer(s) contains the processing units

and neurons, which receive the net summation from the input neurons. The net summation is processed within the processing unit itself with its transfer function. The output layer neurons receive the net sum of the processed data from the hidden layer(s) and transfer the net sum of each neuron to the output terminals. The general form of the neural network is called the feed forward neural network (FFNN) as shown in Figure *3-14* [80], [86], [130].

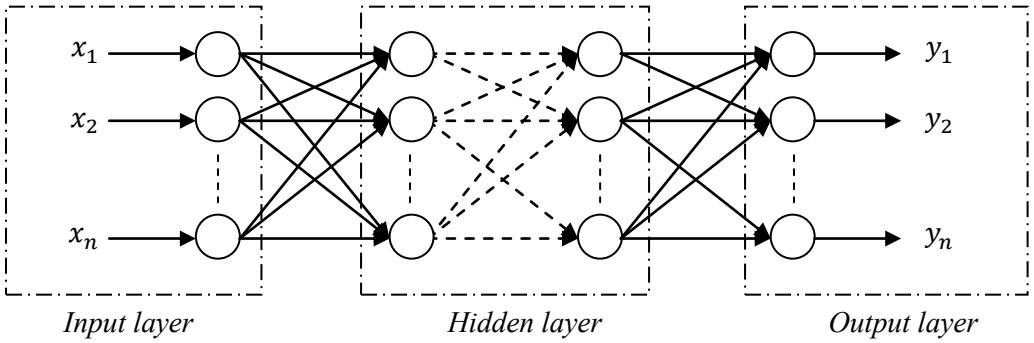

Figure 3-14 The general structure of the FFNN

Each layer contains a number of neurons depending on the design. The basic structure of the neuron model, which is the processing unit, is shown in Figure ***3-15***. Each neuron k receives n inputs I_n, and these inputs are multiplied by n weights W_{kn} and then added together through a summation unit. The result of the summation S_k is passed to the activation function or the transfer function, which works to limit the weights and is treated with the bias factor B_k [111], [130].

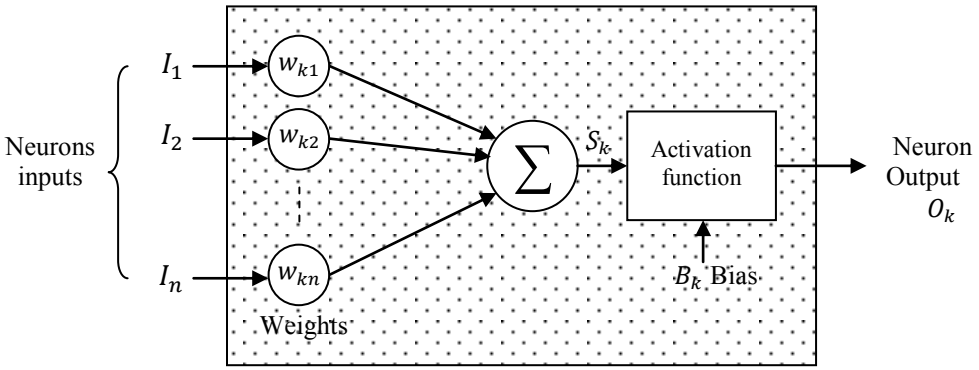

Figure 3-15 The neuron model

The general mathematical representation of the neuron k can be described as follows:

$$S_k = \sum_{n=1}^{N} W_{kn} I_n \tag{3.42}$$

$$O_k = f(S_k\ ,\ B_k) \tag{3.43}$$

The function $f(.)$ is the transfer function of the neuron, which is a function of the summation result S_k and the corresponding bias B_k and defines the output of the neuron. There are a few types of transfer functions that are utilized with ANNs [80], [130].

1- The Hard limiter: $f(v) = \begin{cases} 1 & if \quad v \geq 0 \\ 0 & if \quad v < 0 \end{cases}$

2- Piecewise-Linear function : $f(v) = \begin{cases} 1 & if \quad v \geq \frac{1}{2} \\ (v + \frac{1}{2}) & if \quad \frac{1}{2} > v > -\frac{1}{2} \\ 0 & if \quad v \leq -\frac{1}{2} \end{cases}$

3- Sigmoidal functions: $f(v) = logsig\ (v) = \frac{1}{1+ e^{-mv}}$

where, m is the slope parameter and $v = S_k + B_k$.

The calculation of the output of ANN is carried out with the following equation:

$$O_j^h = f_j^h \left(\sum_{n=1}^{N^h} W_{jn}^h x_n + B_j^h \right) \tag{3.44}$$

where h is the hidden layer quantities, W_{jn}^h is the weight of the input n to the neuron j. N^h is the number of neurons in the hidden layer. O_j^h is the neuron j output. The same process is taking place at the output layer [80], [130].

$$O_k^o = f_k^o \left(\sum_{j=1}^{N^o} W_{kj}^o\ O_j^h + B_k^o \right) \tag{3.45}$$

where o is the output layer quantities, W_{kj}^{o} is the weight of the input j to the neuron k. N^{o} is the number of neurons in the output layer. O_{k}^{o} is the neuron k output.

The weights in the entire layer are started with initial values. Then these weights are updated by training until the desired error is achieved and the final weights values are found. The error function is defined, for the k^{th} output unit for pattern *p,* as follows [80], [130]:

$$E_{pk} = (Y_{pk} - O_{pk}^{o}) \tag{3.46}$$

$$E_{p} = \frac{1}{2}\sum_{k}(Y_{pk} - O_{pk}^{o})^{2} \tag{3.47}$$

where Y_{pk} represents the goal error, O_{pk}^{o}represents the actual output from the k^{th} unit and E_{p} is the cost function of all output units for the pattern p. The aim of the training of the ANN is to minimize the value of the cost functions for all patterns. This process can be done by using the steepest descent algorithm, which states that the correction of the weights of the output layer is proportional to the negative slope of the cost function. That means:

$$\Delta W_{kj}^{o} \propto -\frac{\delta E}{\delta W_{kj}^{o}} \tag{3.48}$$

$$\Delta W_{kj}^{o} = -\beta \frac{\delta E}{\delta W_{kj}^{o}} \tag{3.49}$$

where δ the error [80] is the term of the layers and β is the learning rate parameters of the back propagation algorithm. Finally, the weights and biases on each k^{th} neuron at the output layer are updated as follows [80], [130]:

$$W_{kj}^{o}(n+1) = W_{kj}^{o}(n) + \Delta W_{kj}^{o} \tag{3.50}$$

$$B_{k}^{o}(n+1) = B_{k}^{o}(n) + \Delta B_{k}^{o} \tag{3.51}$$

The application of ANN for transformer protection requires some formulation of the differential protection problems to find the proper inputs and the outputs of the ANN. For this purpose, the differential current samples are used as an input to the ANN with a window width that compromises between the accuracy and the speed of the process. Therefore, the

input vector of the ANN structure will be equal to the window width, which then represents the number of inputs of the ANN at the input layer. The number of outputs in the differential protection using ANN will be only one output, which provides the decision of the differential relay (0 or 1) whether it is a faulted condition or not. The number of the hidden layers determines the accuracy of the results, as the more hidden layers used the better result you get. However, the higher the number of the hidden layers the more computational time it takes. Therefore, a compromise between the speed and the accuracy takes place again. Finally, the training of the ANN for transformer protection is very important, to make the ANN technique able to discriminate between all the types of the transients that may occur in the power transformer.

3.5.6 Wavelet Transform (WT)

Wavelet analysis is considered as a new and exciting mathematical technique compared with Fourier analysis. It is an improved version of analysis based on other transforms, such as the Fourier transform. The main advantage of the wavelets transforms over the Fourier transform is the ability to analyze the non-periodic signals. Some other advantages of wavelets are that they offer a simultaneous localization of the signal in time and frequency domains. The wavelet transform is computationally very fast. Small wavelets are used to localize fine details in a signal, while large wavelets are used for localizing coarse details, and it is used to de-noise or compress signals without degradation. It has many applications for solving difficult problems in different areas of the sciences such as physics, mathematics, and engineering. Some of the recent and modern applications of wavelets are signal and image processing, wave propagation, pattern recognition, computer graphics and data compression. Using wavelets, complex data can be decomposed into some basic and simple

forms in different scales and resolutions and then reconstructed back to the original one with high precision. In general, the wavelet transform can be expressed as [25], [103]:

$$F(a,b) = \int_{-\infty}^{\infty} f(t)\, \psi^{*}_{(a,b)}(t)dt \tag{3.52}$$

where " * " denotes the complex conjugate and ψ is the wavelet function. There are many types of wavelets and they can be classified according to the wavelet orthogonality. The orthogonal wavelets are used for discrete wavelet transform applications; however, the non-orthogonal wavelets are used for continuous wavelet transform (CWT) applications [131], [112]. Substantial redundant information is generated when using the CWT, because the wavelet function is dilated and translated continuously all the time. This shortcoming of the CWT leads to the introduction of the discrete wavelet transform (DWT), which uses a low pass and a high pass filter. In the discrete wavelet transform, the input signal is decomposed into different frequency bands at different resolutions by down sampling these frequency bands into coarser ones. For this purpose, scaling functions and wavelet functions are used in the discrete wavelet transform associated with low pass filter and high pass filter, respectively [105], [107]:

The next chapter studies the mathematical framework of the tools utilized in this work, which are the wavelet packet transform and the synchronously rotating reference frame (*d-q*) axis transformation. The combination of these two mathematical tools is used in this work to provide the proposed hybrid technique. This hybrid technique is used to classify the different transients and determine their characteristics for power transformer. From this analysis, the proposed hybrid algorithm is required to detect and classify the faults from inrush current.

Chapter 4

Mathematical Framework: Basic Principles and Analysis

4.1 Preface

Signal analysis is essential when it comes to studying the transients in power systems. Many mathematical tools are used for analyzing power transients. The Fourier transform (FT), short-time Fourier transform (STFT) and wavelet transform (WT) are the most common transforms that are used in this regard. The Fourier transform is useful for analyzing stationary and periodic functions, which can represent the signal in a time domain or in a frequency domain separately. The problem with the Fourier transform is that it can tell what the frequency content of the signal is but it cannot tell the time of the occurrence of those frequencies. For non-stationary signals, it is important to know the frequencies that are dominant at each specific time. Sometimes, localizing the frequencies in time is required, which cannot be accomplished using Fourier transform. The short-time Fourier transform is a modified version of the Fourier transform, in which frequency localization can be achieved to a certain degree. The short-time Fourier transform is the Fourier transform of a function at a certain period of time t of that function which uses a fixed width of a window centered on that time. The wavelet transform was built on the principle of avoiding the shortcomings of the above-mentioned transforms. The analysis of the signal using a wavelet transform is carried out through a window with a variable width to provide the time-frequency joint representations of the signal.

A combination of two mathematical techniques is used in this work, namely, the wavelet packet transform and the synchronously rotating reference frame (d-q) axis (Park's

transformation). The combination of these two mathematical concepts provides the proposed hybrid technique, which is used to analyse the differential current signal in order to determine its transient characteristics. The proposed hybrid algorithm is required to detect and classify faults and distinguish faults from inrush currents. In this chapter, a summarised review for these required mathematical tools is provided.

4.2 Wavelet Analysis

Wavelet analysis is a rapidly developing mathematical tool with increasing applications in science and engineering that has attracted the attention of many researchers because it is able to analyze any signal to investigate the rapid changes and transients in the signal. Moreover, wavelet analysis can decompose the range of frequencies of the signal into different levels of resolution. The wavelet analysis designates the degree of similarity between the input signal and the wavelet function that is called the mother wavelet, which is achieved by the dilation and translation of the mother wavelet over the signal. The main characters in the wavelet analysis are the mother wavelet $\psi(t)$ and its companion the scaling function $\phi(t)$, which is needed to produce the basis-functions required to represent the analysed signals. All the basis functions are extracted from the scaling function using elementary operations such as shifting, scaling or rotating. The mother wavelet is a function that implies some functions with different regions of support as explained in section 4.2.5. Outside of these regions of support, these functions are equal to zero. The scaling functions generate a number of polynomials of degree that is equal to or less than the vanishing points of the mother wavelet. The translation of the mother wavelet frequency-band refers to the number of levels of resolution. This translation produces another shifted and scaled version of the mother wavelet in the former level of resolution called the daughter wavelet. In equation (4.1), the scaling function at each level of resolution is responsible for generating the basis function

related to that level, in which j represents the level of resolution and k represents the dimension of the function space at the level j [103], [105].

$$\boldsymbol{\phi_{j,k}(t) = 2^{-j/2}\,\phi(2^j t - k) \qquad j,k \in \mathbb{Z}} \tag{4.1}$$

$$\boldsymbol{\psi_{j,k}(t) = 2^{-j/2}\,\psi(2^j t - k) \qquad j,k \in \mathbb{Z}} \tag{4.2}$$

4.2.1 Orthogonality and Orthonormality of the wavelet functions

There are two types of wavelet functions, orthogonal and non-orthogonal wavelet functions, depending on the applications and the method of the analysis. If the wavelet function overlaps with one next to it, this means that this function is non-orthogonal, which gives much information that is not required. In the continuous wavelet transform, the wavelet function slides along the way of the time series, in which overlapping is required to ensure the continuity of the process. Some examples of non-orthogonal wavelet functions are Morlet, Mexican Hat and others. However, in the discrete wavelet transform, overlapping is not desired at all, as the wavelet function skips along the sampled form of the time series. There are many wavelets, which provide the condition of orthogonality such as Daubechies, Symlets, Coiflets, Meyer and many more. The orthogonal wavelets have scaling functions that are able to generate basis functions orthogonal to the mother wavelet at all the levels of the resolution. These wavelet basis are generated via integer shifts and 2^j dilation. In order to get orthogonal wavelets, the following conditions in equations (4.3) and (4.4) must be verified. The inner product of the mother wavelet with any basis functions must be equal to zero, and the inner product of the mother wavelet to itself must be equal to unity as explained in appendix A [132], [133].

$$\int_{-\infty}^{\infty} \psi(t)\phi_j(t)dt = 0 \tag{4.3}$$

$$\int_{-\infty}^{\infty} \psi(t)\psi(t)dt = 1 \tag{4.4}$$

There are some other differences between the orthogonal and the non-orthogonal wavelet functions. Some of the non-orthogonal wavelet functions do not even have scaling functions. However, the big difference between them is that the non-orthogonal wavelet functions and its basis are not compactly supported. Moreover, the main properties of the orthogonal functions are the symmetry and smoothness but the non-orthogonal ones provide better balance in terms of regularity and reduced support.

The decomposition of any signal is achieved based on the compactly supported orthonormal wavelet basis. Any signal $f(t)$ can be decomposed into details and approximations considered as smoothed versions. A brief description of orthonormal, compactly supported wavelet basis of $L^2(R)$ is provided to explain how it is formulated by the dilation of the wavelet function $\psi(t)$ and how translating it over the input signal $f(t)$ designates the degree of similarity between them [103], [105], [132], [133].

$$\psi_{j,k}(t) = 2^{-j/2}\,\psi\left(\frac{t - 2^j k}{2^j}\right), \qquad j,k \in \mathbb{Z} \tag{4.5}$$

The mother wavelet $\psi(t)$ has a number of vanishing moments M up to order $M-1$, which satisfies a two-scale difference equation as follows,

$$\psi(t) = \sqrt{2}\sum_{k=0}^{L-1} g_k \phi(2t-k) \tag{4.6}$$

where $\phi(t)$ is the companion scaling function of the wavelet function $\psi(t)$, which generates a set of orthonormal and compactly supported basis functions in $L^2(R)$ as follows,

$$\phi_{j,k}(t) = 2^{-j/2}\,\phi\left(\frac{t - 2^j k}{2^j}\right), \qquad j,k \in \mathbb{Z} \tag{4.7}$$

The companion scaling function $\phi(t)$ satisfies the unity average condition over the region of support [103], [105], [132]

$$\int_{-\infty}^{\infty} \phi(t)dt = 1 \tag{4.8}$$

and also satisfies the two-scale difference equation as follow:

$$\phi(t) = \sqrt{2} \sum_{k=0}^{L-1} h_k \phi(2t - k) \tag{4.9}$$

The two scale difference equations (4.6) and (4.9) have two coefficients sets g_k and h_k, respectively, which have the same finite length L, a certain basis function, where L is related to the number of vanishing moments in the mother wavelet $\psi(t)$. These two coefficient sets g_k and h_k represent the low pass filter and the high pass filter coefficients in the wavelet analysis, where $k = 0,1,2 \ \ldots \ L-1$. These two filters are related to each other according to the relation in equation (4.10) and create a set of filters called the quadrature mirror filter (QMF) [23],

$$\boldsymbol{g_k = (-1)^k \, . \, h_{L-1-k} \quad , \quad k = 0, 1, 2 \ \ldots \ L-1} \tag{4.10}$$

4.2.2 Quadrature mirror filter (QMF)

The quadrature mirror filter (QMF) was first introduced by Esteban and Galand [134] for speech coding in 1977. At that time, the authors observed that any signal could be split by using some kind of filter and then down-sampled and up-sampled after being reconstructed without aliasing. This type of filter construction was called the conjugate quadrature filters. These conjugate quadrature filters were improved by Smith and Barnwell [135] in order to construct the perfect reconstruction filter banks. Later, the name of conjugate quadrature filters changed to the quadrature mirror filter (QMF) [136].

The quadrature mirror filter (QMF) is a composition of two filters and their magnitude responses have mirror images about $\pi/2$ of each other. There are two parts of the QMF, an analysis part and a synthesis part, and they are separated by down sampling and up sampling operations as shown in Figure *4-1*. At the analysis part, the input signal is decomposed into two frequency bands, low and high frequencies, using a low pass filter h_k and high pass

filter g_k. In wavelet analysis, QMF is used to decompose the input signal into a multilevel of resolutions to provide the multiresolution analysis of the signal. If H and G are assumed to be convolution coefficients [136], [137] of the low and high pass filters, they must satisfy the orthogonally and perfect reconstruction conditions to be perfect quadrature mirror filters which are $HG = GH = 0$ and $HH + GG = I$, where I is the identity operator [134], [136].

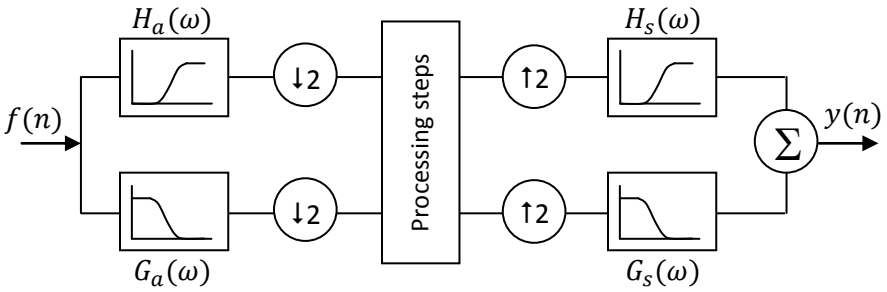

Figure 4-1 The schematic diagram of the quadrature mirror filter (QMF)

The quadrature mirror filters (*QMF*) are 2π-periodic functions satisfying the condition of orthonormality shown in the following relation,

$$|H(\omega)|^2 + |H(\omega + \pi)|^2 = 1 \qquad \omega \in \mathbb{R} \tag{4.11}$$

If $H(\omega) = \sum_k h_k\, e^{-jk\omega}$, then the sequence h_k is called the coefficients of the filter. The main use of the filter banks is in multiresolution analysis (*MRA*), which is basically a decomposition of any signal to its approximation and details using the wavelet filters.

4.2.3 Multiresolution Analysis (MRA)

Meyer [138] and Mallat [139] were the first people who introduced the concept of multiresolution analysis (MRA) in the early 1990s. *MRA* is based on the orthonormal, compactly supported wavelet basis. The multiresolution analysis in the Hilbert space $L^2(R)$ consists of a nested sequence of subspaces $\{V_j\}$ in which $V_j \subset V_{j+1}$, where, $j \in \mathbb{Z}$ and $\mathbb{Z}$ is the set of integers. For MRA, the following properties (4.12)-(4.16) must be satisfied:

- The nested property

$$\ldots \subset V_{-2} \subset V_{-1} \subset V_0 \subset V_1 \subset V_2 \subset \cdots = \mathrm{V_j} \subset \mathrm{V_{j+1}} \tag{4.12}$$

- The density property

$$\ldots \cup V_{-2} \cup V_{-1} \cup V_0 \cup V_1 \cup V_2 \cup \ldots = \overline{\cup_j V_j} = L^2(R) \tag{4.13}$$

- The separation property

$$\ldots \cap V_{-2} \cap V_{-1} \cap V_0 \cap V_1 \cap V_2 \cap \ldots = \cap_j V_j = \{0\} \tag{4.14}$$

- The scaling property

$$f(t) \in V_0 \quad \Leftrightarrow \quad f\left(2^j t\right) \in V_j \tag{4.15}$$

The orthonormal basis property is given as follows

$$\int_{-\infty}^{\infty} \phi(t-k)\overline{\phi(t-k')}\, dx = \begin{cases} 0 & k \neq k' \\ 1 & k = k' \end{cases} \; and \;\; k, k' \in \mathbb{Z} \tag{4.16}$$

The orthonormal scaling function $\phi(t)$ is part of the space V_j in which;

$$\left\{2^{\frac{j}{2}}\phi(2^j t - k)\right\} \in V_0 \tag{4.17}$$

With these conditions:

$$\int_{\mathbb{R}} \phi(t)\, dt \neq 0 \tag{4.18}$$

$$\left|\int_{\mathbb{R}} \phi(t)\, dt\right| = 1 \tag{4.19}$$

The set $\{\phi(t-k)\}_{k\in\mathbb{Z}}$ is an orthonormal basis for V_0. Therefore, multiresolution analysis provides a good approach to decompose any signal for the space $L^2(R)$. The subspaces $\{V_j\}_{j\in\mathbb{Z}}$ of MRA are considered as approximation spaces and another subspace is defined here as the detailed spaces of the $L^2(R)$, which is the $\{W_j\}_{j\in\mathbb{Z}}$. The detailed subspaces W_j are orthogonal component s of V_j in V_{j-1}, where [103], [132], [137]

$$V_{j+1} = V_j \oplus W_j = V_0 \oplus W_0 \oplus W_1 \oplus W_2 \;\; \ldots \oplus W_j \tag{4.20}$$

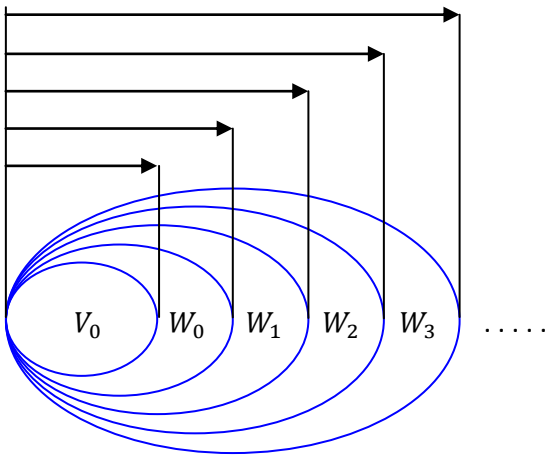

Figure 4-2 Scaling function and wavelet spaces

Figure *4-2* illustrates the scaling function and wavelet vector spaces. In general, the multiresolution can be presented in the following formula [132], [137]:

$$MRA\ (\phi, \psi) = \bigcup_{j \in \mathbb{Z}} \left(V_j(\phi) \oplus W_j(\psi) \right) \tag{4.21}$$

where, $V_j(\phi)$ is the space spanned by the basis function $\phi_{j,k}(t)$, $W_j(\psi)$ is the space spanned by the wavelet function $\psi_{j,k}(t)$ and the sign $\oplus$ is the direct orthogonal summation operation of the spaces. The wavelet function, Daubechies (*db4*), was found to be the best candidate among all the selected candidates. [103], [137].

4.2.4 Daubechies (db4) Wavelet Filter Parameters Analysis and Construction

This section considers the analysis and construction of the Daubechies scaling function and then finds the wavelet filter coefficients of Daubechies (*db4*). Wavelets have many properties such as regularity, symmetry, continuity, vanishing moments, orthonormality and compact support. The designed Daubechies scaling function must obey the main desirable properties as follows [103], [132], [137], [140]:

- Compact support:

This is done in order to make the scaling filter h have finitely nonzero entries for the

compactly supported scaling function. This means that the values of the scaling function are zero except within the interval of support $[t_1, t_2]$ of the mother wavelet.

$$\phi(t) = 0 \quad \forall \quad t \notin [t_1, t_2] \tag{4.22}$$

The dilation equation in the wavelet transform domain must take the form

$$\hat{\phi}(\omega) = H\left(\frac{\omega}{2}\right) \hat{\phi}\left(\frac{\omega}{2}\right) \tag{4.23}$$

where $H(\omega)$ is a trigonometric polynomial with degree L as in the equation (4.29).

$$H(\omega) = \frac{1}{\sqrt{2}} \sum_{k=0}^{L} h_k e^{-jk\omega} \tag{4.24}$$

- Average:

The average value of the scaling function must be equal to one over the region of support $[t_1, t_2]$ of the mother wavelet.

$$\int_{t_1}^{t_2} \phi(t)\, dt = 1 \tag{4.25}$$

- Orthogonality:

A main condition of orthogonality in wavelets is that the scaling function sequence is orthogonal to any shifts of it by an even number of coefficients:

- Orthonormality:

If the scaling function $\phi(t)$ is a function that is able to generate a multiresolution analysis $\{V_j\}_{j\in\mathbb{Z}}$ of $L^2(\mathbb{R})$, then $H(\omega)$ must satisfy for all $\omega \in \mathbb{R}$ the condition

$$|H(\omega)|^2 + |H(\omega + \pi)|^2 = 1 \quad \forall\ \omega \in \mathbb{R} \tag{4.26}$$

- Continuity:

The eight nonzero scaling coefficients of Daubechies (db4) of the low pass filter (g) and the high pass filter (h) (rounded to four decimal digits) are:

$$h[n] = [-0.2304 \quad 0.7148 \quad -0.6309 \quad -0.0280 \quad 0.1870 \quad 0.0308 \quad -0.0329 \quad -0.0106]$$

$$g[n] = [-0.0106 \quad 0.0329 \quad 0.0308 \quad -0.1870 \quad -0.0280 \quad 0.6309 \quad 0.7148 \quad 0.2304]$$

The $g(n)$ coefficients are calculated in the same manner as the $h(n)$. The frequency response and the zero pole representation of $g(n)$ and $h(n)$ is illustrated in the Figure *4-3*.

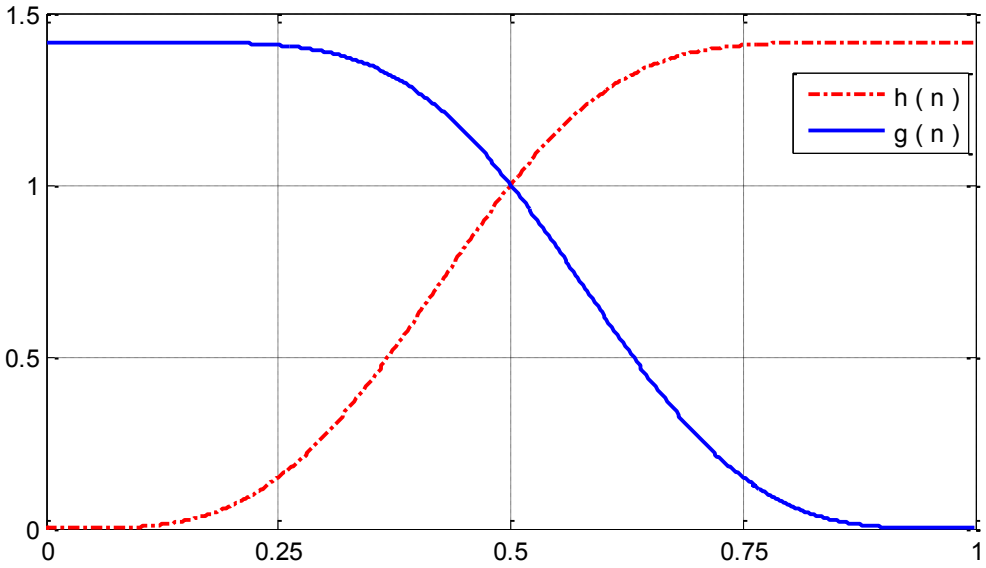

Figure 4-3 The frequency response and the zero pole representation of g and h

4.3 Wavelet Transforms

There are many different scopes of wavelet analysis techniques, which are used to study the transients in all types of signals. Wavelet transforms are considered the main tools of the wavelet analysis such as continuous wavelet analysis (CWT), discrete wavelet transform (DWT), wavelet packet transform (WPT) and others [103], [132].

4.3.1 Continuous wavelet transform (CWT)

Continuous wavelet transform is required to find the approximation and the details coefficients of a continuous signal. This type of wavelet transform deals with non-

orthogonal wavelet functions such as the Morlet wavelet function and Mexican Hat wavelet function as shown in Figure *4-4*. The continuous wavelet transform for a continuous signal $f(t)$ is given by the following formula:

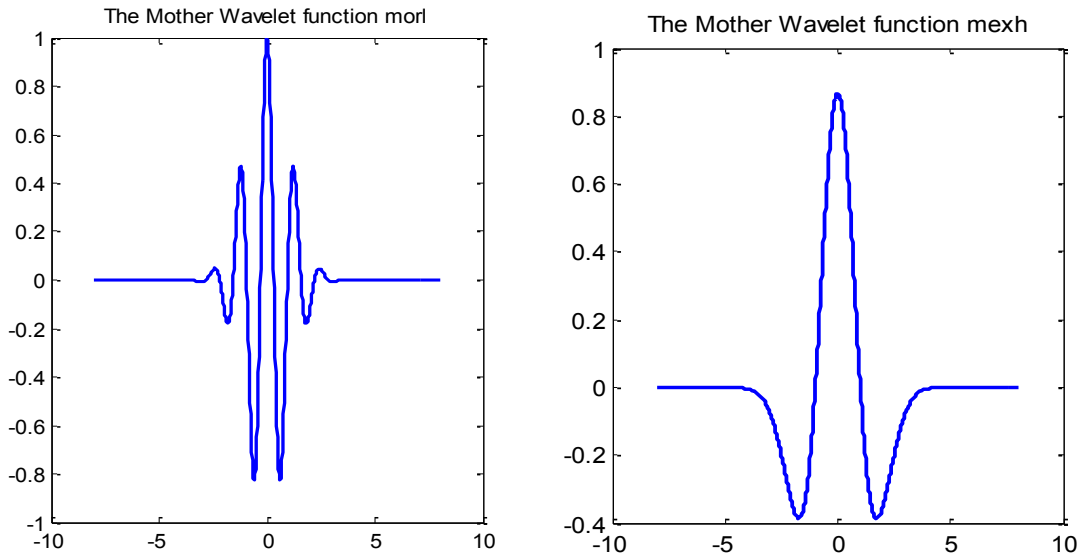

Morlet wavelet function *Mexican Hat wavelet function*

Figure 4-4 Some types of the non-orthogonal wavelet functions

$$CWT(a,b) = \frac{1}{\sqrt{|a|}} \int_{-\infty}^{\infty} f(t)\, \psi\left(\frac{t-b}{a}\right) dt \tag{4.27}$$

where (a) represents the scaling factor which is responsible for zooming in and out of the signal view, where the high scales correspond to a wide or global view and low scales correspond to a detailed view of the signal. In terms of frequency language, high scales correspond to low frequencies and low scales correspond to high frequencies. In terms of mathematical language, high scales $(a > 1)$ correspond to dilation or stretching out of the signal and low scales $(a < 1)$ correspond to the compression or squeezing of the signal. The factor (b) represents the translation factor which is responsible for the location of the window. The term $1/\sqrt{|2|}$ represents the weighting function, which ensures the identical

energy spread of the wavelet coefficients at each scale. The continuous signal is transformed by the analyzing function $\left(\frac{t-b}{a}\right)$, which is analogous to the window function $\{w(t-\tau)e^{-j2\pi ft}\}$ in the short-time Fourier transform. *CWT* is similar to the *STFT*, which is the improved version of the *DFT*. *STFT* uses a fixed width window to provide some kind of representation of time and frequency together. However, the window width of the *CWT* is changing with time and is inversely proportional to the frequency, which means that with low frequencies, the window will be wide and there will be a narrow window with the high frequencies. The wavelet function in equation (4.27) can be normalized to provide a better sense of the wavelet energy, as follows

$$\psi_{a,b}(t) = \frac{1}{\sqrt{a}}\,\psi\left(\frac{t-a}{a}\right) \tag{4.28}$$

$$CWT(a,b) = \int_{-\infty}^{\infty} f(t)\,\psi_{a,b}(t)\,dt \tag{4.29}$$

4.3.2 Discrete Wavelet Transform

Substantial redundant information is generated when using the CWT, because the wavelet function is dilated and translated continuously all the time. This shortcoming of the CWT led to the introduction of the discrete wavelet transform (DWT), which uses a low pass and a high pass filters. DWT is a powerful technique that allows for the investigation of the frequency content of any signal, regardless of whether it is a periodic or non-periodic signal. A transformation from analog to digital signal is required for this process. DWT gives a time scale representation of the digital signal. In this process, digital wavelet filters of different cut-off frequencies are utilized to analyze the input signal at different scales of resolution in multiple levels of analysis. Digital wavelet filtering is carried out by using a convolution process of the wavelet low pass filters (LPF) and high pass filters (HPF)

coefficients with the input discrete signal as in the equations (4.30), (4.31), where the convolution could be linear or circular depending on the application, which is circular in this work [25], [133], [141].

$$g[n] \circledast f[n] = \sum_{l=1}^{N} g[l] f[N-l] \tag{4.30}$$

$$h[n] \circledast f[n] = \sum_{l=1}^{N} h[l] f[N-l] \tag{4.31}$$

where, $g[n]$ is the LPF coefficients, and $h[n]$ is the HPF coefficients, $f[n]$ is a discrete time input current signal and N is the window length. The relationship between the impulse responses of $g[n]$ and t $h[n]$ was depicted in equation (4.9).

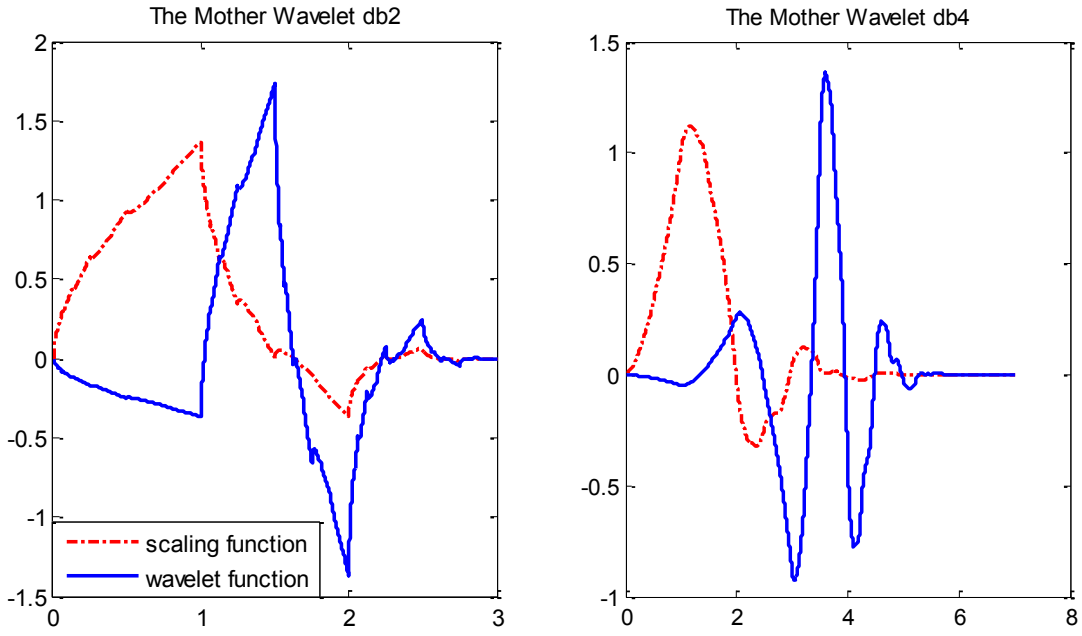

Daubechies db2 wavelet function *Daubechies db4 wavelet function*

Figure 4-5 Some types of the orthogonal wavelet functions

The decomposition using these two wavelet filters provides two frequency side bands, Approximation and details. The approximations are the low frequency band and called the scaling coefficients that are beyond the scope of this work. The details are the high frequency

band, and called the wavelet coefficients, which are the main concern in this work. The scaling coefficients are calculated using equation (4.32) which is an inner product of the input current signal with the scaling basis $\phi_{i,j}(t)$. The wavelet coefficients are calculated using equation (4.33), which is an inner product of the input current signal with the wavelet basis $\psi_{i,j}(t)$ [25], [133], [141].

$$A_{i,j} = \langle f(t), \phi_{i,j}(t) \rangle = \int_{-\infty}^{\infty} f(t) \,.\, \phi_{i,j}^{*}(t)\, dt \tag{4.32}$$

$$D_{i,j} = \langle f(t), \psi_{i,j}(t) \rangle = \int_{-\infty}^{\infty} f(t) \,.\, \psi_{i,j}^{*}(t)\, dt \tag{4.33}$$

where, $A_{i,j}$ is the approximation coefficient and $D_{i,j}$ is the detail coefficient [25], [133]. *DWT* decomposes the input signal into different frequency bands at different resolutions by down sampling these frequency bands into coarser ones. For this purpose, scaling functions and wavelet functions are used in the discrete wavelet transform associated with low pass filter $g[l]$ and high pass filter $h[l]$, respectively. Then, a down sampling by two takes place in order to eliminate half of the samples to reduce the data rate or the size of the data. In other words, down sampling is a reduction of the sampling rate. The first level of decomposition can be expressed as in equations (4.34) and (4.35), in which, $a^1[n]$ refers to the output of the low pass filter and represents the approximations of the signal and the number "1" refers to the first level of resolution. In the same manner, $d^1[n]$ refers to the output of the high pass filter and represents the details of the signal and the number "1" refers to the first level of resolution.

$$a^1[n] = \sum_{l=1}^{N} g[l] f[N - l] \tag{4.34}$$

$$d^1[n] = \sum_{l=1}^{N} h[l] f[N - l] \tag{4.35}$$

In the same manner, the second level of resolution will be produced after the down sampling of the first level decomposition is carried out. *DWT* employs only half the band of the frequencies, in which only the low frequency sub band will be decomposed again after the down sampling takes place. In the analysis of both the first and the second levels of resolution, the dominant frequencies in each sub band will have higher amplitudes than the rest of the frequencies in that sub band. The resolution of the time localization in *DWT* depends on the level that these dominant frequencies appear in it. The decomposition analysis in *DWT* provides a good frequency resolution and bad time resolution at the low frequency sub bands. On the contrary, it provides a good time resolution and bad frequency resolution at the high frequency sub bands. Figure ***4-6*** describes the decomposition tree of the discrete wavelet transform.

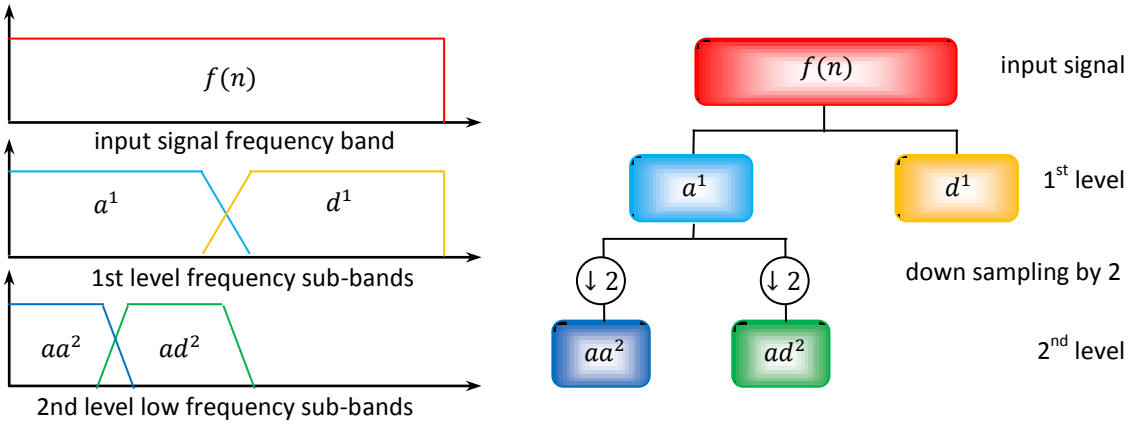

Figure 4-6 DWT Decomposition of the signal f(n)

4.3.3 Wavelet Packet Transform

The wavelet packet transform (*WPT*) is a generalized form of discrete wavelet transform (*DWT*), i.e. the *WPT* is localized in time such as *DWT*, but offers more flexibility than *DWT* in representing a wide range of different types of signals in the whole sub bands of the frequencies. *WPT* applies the same principles of *DWT* and it is performed by the analysis

of the input signal into a tree of low pass and high pass filtering operations as shown in Figure *4-7*. After each level of resolution, down sampling by '2' takes place to both the details and approximations of the first level of the discrete input signal. Then, a filtration process is carried out again by using the same filters in all levels of resolution. The wavelet packet function is a triple indices function$j$, k, n which is defined by [25], [133], [141]:

$$W_{j,k}^{n}(t) = 2^{j/2}\, W^{n}\left(2^{j}t - k\right) \tag{4.36}$$

where j represents the scaling operations and k represents the translation operations. However, the index n is defined as the modulation or the oscillation parameter. Figure *4-7* depicts that the frequency bandwidth of the levels decreases with the growing number of levels, which means that the frequency resolution becomes better and the time resolution becomes coarser with the increase of the level number. In this process, the discrete input signal $f[n]$ is decomposed into low and high frequencies, namely approximations and details. The low frequency of the first level is considered as the approximation $a^{1}[n]$ of the discrete signal and the high frequency is the details $d^{1}[n]$ of the discrete input signal. This process is repeated again in each level of resolution. The approximations and details in each level are decomposed in the same manner into another two parts of approximations and details by using the same low pass and high pass filters used in the first level of decomposition but after the down sampling by '2' is carried out. In other words, four frequency sub-bands are produced in the second level of resolution from the first two frequency sub-bands. The general form of this wavelet analysis for the input signal in a discrete $f(n)$ form can be represented as the following [25], [67], [141], [142]:

$$f[n] = \sum_{j\in\mathbb{Z}}\sum_{k\in\mathbb{Z}} a_{j,k}[n] + \sum_{j\in\mathbb{Z}}\sum_{k\in\mathbb{Z}} d_{j,k}[n] \tag{4.37}$$

where $a_{j,k}[n]$ are the approximation of $f[n]$ and represent its low frequencies at the scale j, and $d_{j,k}[n]$ are the details of $f[n]$ and represent its high frequencies at the scale j [125].

$$a_{j,k}[n] = \sum_{k\in\mathbb{Z}} \left(g[k]a_{j-1}[2n-k] + h[k]a_{j-1}[2n-k]\right) \tag{4.38}$$

$$d_{j,k}[n] = \sum_{k\in\mathbb{Z}} \left(g[k]d_{j-1}[2n-k] + h[k]d_{j-1}[2n-k]\right) \tag{4.39}$$

The first and second level frequency sub-bands are obtained by using the low pass filter (LPF) and the high pass filter (HPF) as shown in Figure *4-7*. The first level two frequency sub-bands can be expressed in equations (4.34) and (4.35) [23], [105], [110], [143],

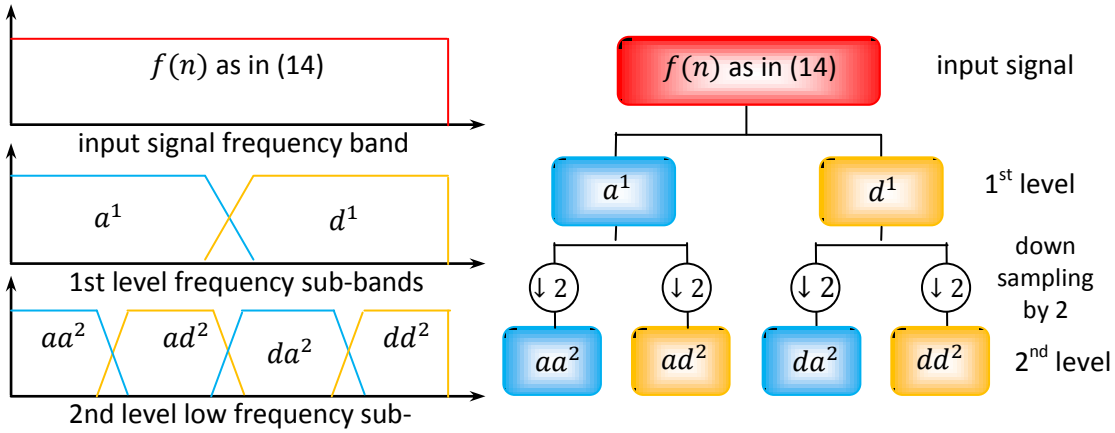

Figure 4-7 WPT Decomposition of the signal f(n)

where $g[l]$ and $h[l]$ are the low pass filter and high pass filter coefficients of the utilized wavelet function respectively and N is the length of the window. In the same manner, the second level four frequency sub-bands can be expressed in equations (4.40)-(4.43) [110], [133], [144], [145]:

$$aa^2[n] = \sum_{l=1}^{N/2} g[l]a^1\left[\frac{N}{2} - l\right] \tag{4.40}$$

$$ad^2[n] = \sum_{l=1}^{N/2} h[l]a^1\left[\frac{N}{2} - l\right] \tag{4.41}$$

$$da^2[n] = \sum_{l=1}^{N/2} g[l] d^1\left[\frac{N}{2} - l\right] \tag{4.42}$$

$$dd^2[n] = \sum_{l=1}^{N/2} h[l] d^1\left[\frac{N}{2} - l\right] \tag{4.43}$$

where, $aa^2[n]$ refers to the output of the low pass filter and represents the approximations of the signal and the number "2" refers to the second level of resolution. In the same manner, $ad^2[n]$ refers to the output of the high pass filter and represents the details of the approximations of the signal and the number "2" refers to the second level of resolution. $da^2[n]$ refers to the output of the low pass filter and represents the approximations of the details of the signal and the number "2" refers to the second level of resolution. In the same manner, $dd^2[n]$ refers to the output of the high pass filter and represents the details of the signal and the number "2" refers to the second level of resolution.

4.4 The Synchronously Rotating (dq0) Reference Frame

Direct and quadrature (dq) axis transformation can be defined as a mathematical transformation of coordinates from the three-phase stationary coordinate system (abc) to the $dq0$ rotating coordinate system. It describes the behaviour of the three-phase system at any condition of operation such as stable/unstable, balanced/unbalanced, symmetrical/unsymmetrical, sinusoidal/non-sinusoidal, and periodic/non-periodic signals. This transformation is used to simplify the analysis of the three-phase stationary system. This transformation technique reduces the three-phase components (abc) of the ac signal into two dc (dq) axis components. This transformation can be done in two different ways either to change from the three-phase (abc) ac stationary components to two stationary components $(\alpha - \beta)$ and then to two rotating components (dq) or to change from the three-

phase ac stationary components (abc) to two (dq) rotating components directly [146], [147], [148], [149]. The three-phase currents under balanced conditions can be expressed as

$$I_a = I_m \sin(\omega t) \tag{4.44}$$

$$I_b = I_m \sin\left(\omega t - \frac{2\pi}{3}\right) \tag{4.45}$$

$$I_c = I_m \sin\left(\omega t + \frac{2\pi}{3}\right) \tag{4.46}$$

The first criterion is to transfer the three-phase current to a synchronously rotating reference frame in only two stationary phases ($\alpha - \beta$) axis transformation. This can be done using equation (4.47):

$$\begin{bmatrix} I_\alpha \\ I_\beta \end{bmatrix} = \begin{bmatrix} 1 & 1/2 & -1/2 \\ 0 & \sqrt{3}/2 & -\sqrt{3}/2 \end{bmatrix} \begin{bmatrix} I_a \\ I_b \\ I_c \end{bmatrix} \tag{4.47}$$

Then, the direct and quadrature axes currents are expressed in (4.48):

$$\begin{bmatrix} I_d \\ I_q \end{bmatrix} = \begin{bmatrix} \cos\theta & \sin\theta \\ -\sin\theta & \cos\theta \end{bmatrix} \begin{bmatrix} I_\alpha \\ I_\beta \end{bmatrix} \tag{4.48}$$

The second criterion is to directly transfer the three-phase currents to a synchronously rotating reference frame with only two stationary phases (dq axis transformation). This can be done using equation (4.49) [146], [147], [148], [150].

$$\begin{bmatrix} I_d \\ I_q \\ I_0 \end{bmatrix} = \sqrt{\frac{2}{3}} \begin{bmatrix} \cos(\theta) & \cos\left(\theta - \frac{2\pi}{3}\right) & \cos\left(\theta + \frac{2\pi}{3}\right) \\ -\sin(\theta) & -\sin\left(\theta - \frac{2\pi}{3}\right) & -\sin\left(\theta + \frac{2\pi}{3}\right) \\ \sqrt{2}/2 & \sqrt{2}/2 & \sqrt{2}/2 \end{bmatrix} \begin{bmatrix} I_a \\ I_b \\ I_c \end{bmatrix} \tag{4.49}$$

where $\theta = \omega_s t$ and $\omega_s$is the system synchronous angular frequency $\omega_s = 2\pi f$ and f is the system frequency, as shown in Figure ***4-8*** [147], [150], [149]. It is to be noted that I_d and I_q components are phasor representation. I_0 is the unidirectional phasor quantity (dc component).

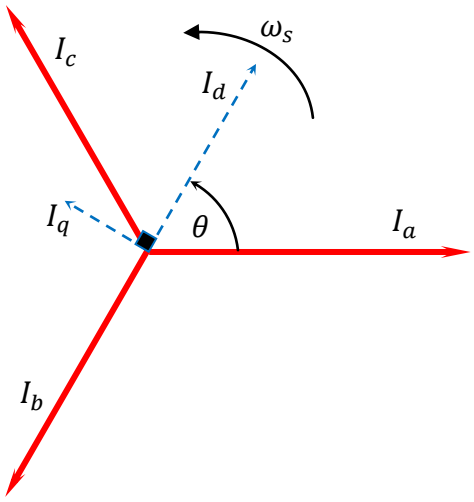

Figure 4-8 The dq synchronously rotating reference frame is rotating with an angular velocity equal to ω_s. The three- phase currents I_{abc} are separated by 120 electrical degrees, and $I_{d,}$ I_q are dc quantities

In this chapter, the reviews of the mathematical concepts required in this work are studied. The different wavelet transforms and analysis are presented in brief. The next chapter studies the development and implementation of the proposed $dqWPT$ hybrid technique for power transformer protection. The development of the $dqWPT$ based algorithm for digital differential protection of power transformers is illustrated in detail. Finally, data collection for the off-line simulation and the simulation results are provided. .

Chapter 5

Development, Implementation and Off-Line Testing of the $dqWPT$ Based Hybrid Technique for Power Transformer Protection

5.1 Preface

The previous chapter provided the mathematical derivation and the principles that are required for implementing the proposed hybrid technique for power transformer digital differential relays. In this chapter, the development and implementation of the proposed algorithm is provided using the wavelet packet transform (WPT) and the synchronously rotating reference frame dq0 axis-coordination system. These two mathematical concepts are combined together to provide the new hybrid technique $dqWPT$ for the digital differential protection of power transformers. For which the required data was collected from laboratory experimental testing and then stored in the computer to perform the off-line testing using MATLAB. Simulation data could be used; however, the data collected from real-time experiments will provide results that are more accurate.

5.2 Development of the dqWPT Based Algorithm for Digital Differential Protection of Power Transformers

In this work, a new technique for the digital differential protection of power transformers is proposed. This technique is based on extracting the high frequency sub-band contents using one level of WPT decomposition of the input signal. At this stage of analysis, the input signal is represented by the dq axis components of the differential currents. The

transformation from (abc) to (dq) axis components has many advantages, such as, it does not depend on the principle of the harmonic content of the differential current, removing the constraints on the selection of the sampling frequency of the currents, simplifying the implementation of the algorithm, as well as reducing the computational time and memory requirements. The proposed approach combines the dq axis components with the WPT mathematical tools to produce the new hybrid technique ($dqWPT$) for the digital differential protection of power transformers. This algorithm is able to ensure the security for any external fault and inrush conditions and dependability for all types of internal faults.

For the three input differential currents denoted by I_{Da}, I_{Db} and I_{Dc}, the transformation from the three-phase coordinate system to the dq0 axis reference frame is carried out as using the equation (5.1). In this transformation process, the frequencies in the three-phase current signals are relocated to different positions in the frequency domain of the dq axis frame. At this stage the advantage of this transformation, becomes obvious, which is concentrating the energy of the input signal over narrow frequency sub-bands. The low frequencies are localized at low frequency sub-bands and the high frequencies are localized at high frequency sub-bands, which simplify the classification of any frequencies in the input signal [125]. As a result of this transformation, the relocation of the frequencies can be classified into two categories, the low frequency sub-band and the high frequency sub-band. The frequencies associated with the normal system transient disturbances, which do not create any changes in the system configuration, are relocated to the low frequency sub-band. These kinds of transient frequencies are mainly amplitude disturbances, and they are represented in the magnetizing inrush currents and load disturbances. On the other hand, the frequencies associated with the abnormal system transient disturbances, which may create some changes

in the system configuration, are relocated to the high frequency sub-band. These kinds of transient frequencies are time-dependent frequencies as well as amplitude disturbances and are represented in the internal faults. Therefore, the localization of the high frequencies due to the faulted conditions is employed to be the signature for discriminating the inrush currents from the fault currents. In other words, in the case of faulted conditions, the high frequency sub-band coefficients (details) of the wavelet packet transform will have a significant value. These details can be extracted by using the high pass wavelet filter (*HPF*). The three-phase currents are converted into their direct and quadrature components $dq0$ as illustrated in the following equation [125], [143], [147];

$$\begin{bmatrix} I_{Dd}[n] \\ I_{Dq}[n] \\ I_{D0}[n] \end{bmatrix} = \sqrt{\frac{2}{3}} \begin{bmatrix} \cos(\theta) & \cos\left(\theta - \frac{2\pi}{3}\right) & \cos\left(\theta + \frac{2\pi}{3}\right) \\ -\sin(\theta) & -\sin\left(\theta - \frac{2\pi}{3}\right) & -\sin\left(\theta + \frac{2\pi}{3}\right) \\ \sqrt{2}/2 & \sqrt{2}/2 & \sqrt{2}/2 \end{bmatrix} \begin{bmatrix} I_{Da}[n] \\ I_{Db}[n] \\ I_{Dc}[n] \end{bmatrix} \tag{5.1}$$

The zero component $I_{D0}[n]$ has a very small value, which has no effect on this analysis, so it is neglected. At this stage, the synchronously rotating reference frame components I_{Dd} and I_{Dq} are representing the three-phase differential current signals. These two signals are changed again into one signal carrying the same characteristics of the original signals, using unbiased method described in equation (5.2), in which the currents I_{Dd} and I_{Dq} are squared and summed to produce one vector of samples. This method is called the unbiased method, which has the advantage of reducing the burden of calculation on the DSP and reduces the noise in the signal as well [80], [105], [125].

$$I_D[n] = (I_{Dd}[n])^2 + \left(I_{Dq}[n]\right)^2 \tag{5.2}$$

This signal now is ready to be analysed by the wavelet packet filter $d^1[n]$, [125]:

$$d^1[n] = \sum_{l=1}^{N} h[l] I_D[N-l] \tag{5.3}$$

where, $h[l]$ is the set of coefficients of the wavelet high pass filter for the Daubechies ($db4$) mother wavelet for Daubechies ($db4$) mother wavelet;

$h[\ l\ ]$ = [-0.2304 0.7148 -0.6309 -0.0280 0.1870 0.0308 -0.0329 -0.0106]

and n is the counter coefficient resulting from the circular counter that is calculated by equation (5.4), in which N is the circular window length [125];

$$n = remainder\left(\frac{n}{N}\right) \tag{5.4}$$

The output of $d^1[n]$ represents the signature of the proposed algorithm, from which the relay can determine the type of the disturbance.

5.3 Implementation of the *dqWPT* Based Algorithm for the Digital Differential Protection of Power Transformers

The host computer receives the three analog input currents through its ADC terminals and then converts them to three digital sampled signals. After these input analog signals are converted to three digital signals, the calculation and analysis of these digital signals take place inside the computer using the code of the proposed technique. Then, the sampled digital signal is windowed and stored in the memory of the *DSP* board in a circular buffer with a size of 16 bits, in which the initial value of the window is set to zeroes and then is filled by the input samples one by one. After all the zeroes in the window are replaced by the new samples, the 1st sample of the input current in the circular window (buffer) is replaced by the 17th current sample and the rest of the window stays the same. Then, the second sample is replaced with the 18th one and so on. The circular window is implemented by calculating the modulus (remainder) of the input samples using equation (5.4). The

resultant signals from the three circular buffers are considered now as the input three-phase input current signals. These input three-phase current signals are then transformed into the dq axis components as explained in equation (5.1). This transformation process produces two current signals in the direct and quadrature axes. The next step in the code is preparing the input signal to the first WPT filter stage using equation (5.2) [23], [151].

At this stage, the signal in the code is ready to be filtered by the WPT high-pass filter as in equation (5.3). This filtering process produces the details (coefficients) of the high frequency sub-band of the first level of decomposition. The amplitudes of these coefficients are compared instantaneously to the specified threshold value. Based on this comparison, the algorithm can classify and characterize the input current signal. Accordingly, a trip signal is issued in case of the occurrence of any internal fault within the protected area. Initially, the trip signal is high at a value of 10 volts. A detailed process of the control circuit is given appendix B. The algorithm is illustrated in the flowchart of Figure ***5-1***, and it can be summarized in the following steps;

1. Initialize all the variables and the counters ($n = 0$ and $i = 0$)
2. Define the wavelet filter coefficients $h[N]$, where $N = 16$ samples
3. Calculate the modulus n using equation (5.4);
4. Read the n^{th} sample of the 3Φ input currents

$$I_{Da}[n] = I_{DA}[i] \quad , \quad I_{Db}[n] = I_{DB}[i] \quad , \quad I_{Dc}[n] = I_{DC}[i]$$

5. Evaluate I_{Dd} and I_{Dq} using the equation (5.1)
6. Evaluate $I_D[n]$ using equation (5.2)
7. Evaluate $d^1[n]$ using equation (5.3)
8. If $d^1[n] > threshold\ value\ \lambda$, then a trip signal is issued

9. If $d^1[n] < threshold\ value\ \lambda$, then update ($n = n + 1$) , ($i = i + 1$) , ($t = t + \Delta t$) and repeat the steps from step 3.

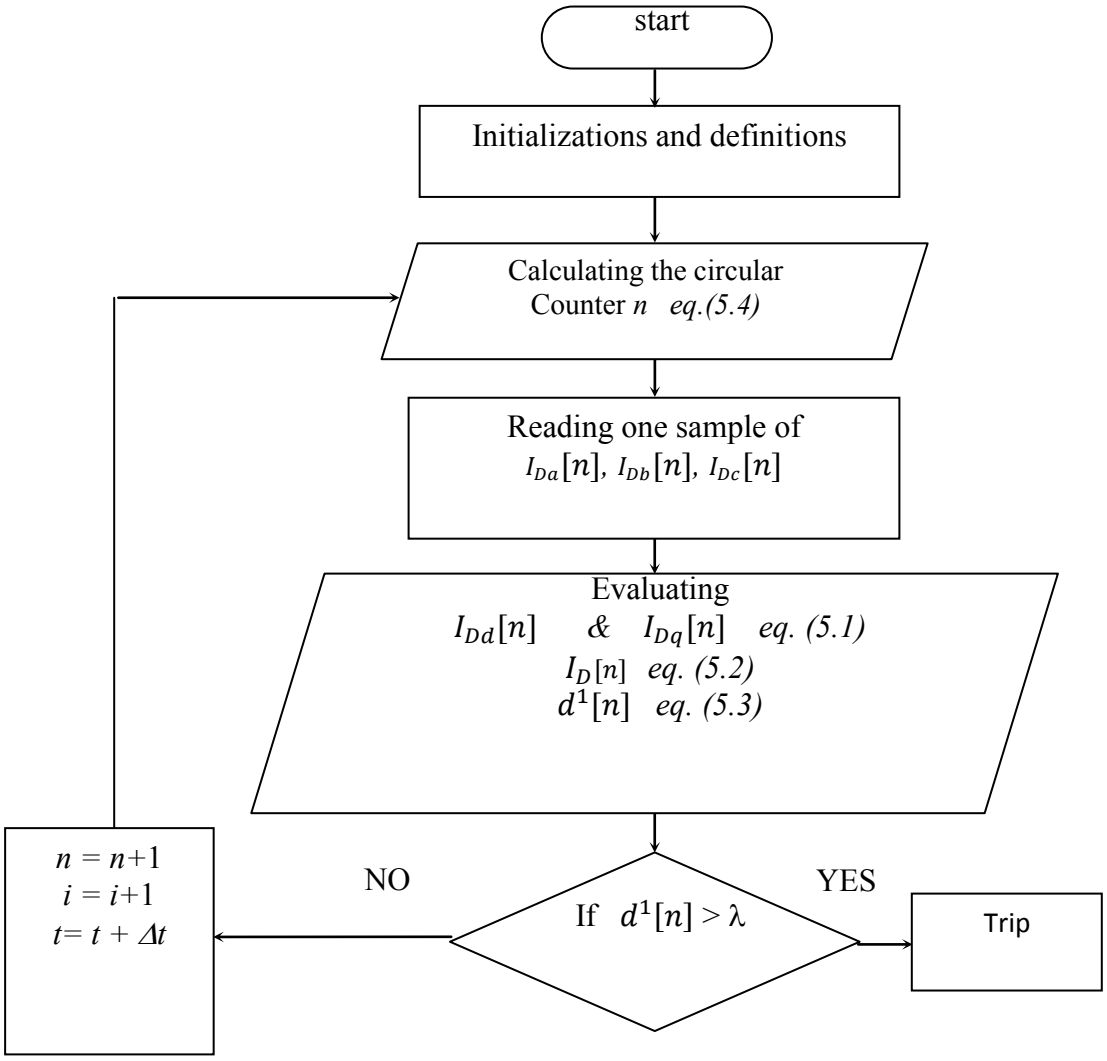

Figure 5-1 The flowchart of the differential relay-operating characteristic

5.4 Off-Line Testing of the *dqWPT* Based Algorithm for the Digital Differential Protection of Power Transformers

In order to prove the successful performance of the new hybrid technique, off-line testing has to be carried out before applying the proposed technique to real-time experiments. In this section, off-line simulation testing process and its results are provided to examine the

proposed technique before using it in real-time testing. In order to carry out this type of testing, real data has to be collected from an experimental setup for different types of disturbances. These disturbances include internal and external faults, CTs mismatch and saturation, over-excitation and magnetizing inrush currents.

5.5 The Laboratory Experimental Setup and Data collection

Experimental data collection and acquisition were carried out using the equipment available in the laboratory, namely, power transformers, dSPACE, current transformers and other peripherals. Figure ***5-2*** shows the schematic diagram of the experimental setup for data collection and the way the auxiliary devices are connected to each other, in which a 5kVA, 230/550-575-600V, Δ-Y, 60Hz, core type, multi-tap three-phase laboratory prototype power transformer is utilized to perform the tests on it.

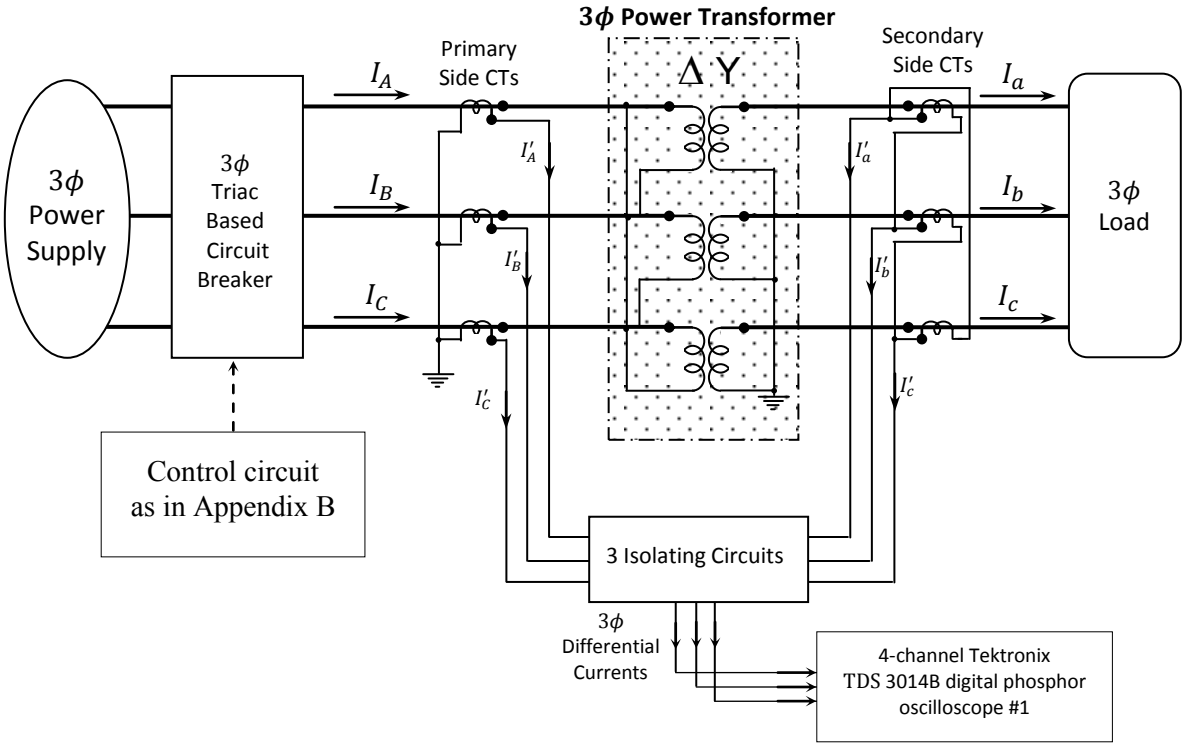

Figure 5-2 The circuit diagram for the purpose of data collection

The power transformer used in this experiment is a Δ-Y connected transformer. Current transformers were used to step down the primary and secondary currents and they were connected in Y-Δ for the reasons that were explained in chapter 3. There was a small mismatch between the CTs, which was also useful to test the proposed technique. Three Tektronix A6302 current isolating units were used to collect the data on the differential currents. These isolating units have two functions:

1- to determine the difference between the primary and the secondary currents in order to produce the differential current. If the currents are not equal, a differential current is produced.

2- to change the current signal into a voltage signal with a maximum value of *10* volts according to the input current value. This transformation is necessary because the oscilloscope can only measure voltage signals. Moreover, the DSP board can only deal with current signals at a few milli-amperes of current and voltage signals up to *10* volts. Thus the voltage signal received by the DSP board resembles the current signal with exactly the same characteristics.

The current isolating units were connected to a 4-channel Tektronix TDS 3014B digital phosphor oscilloscope. This oscilloscope sampled the input voltage waveforms at a sampling frequency of 100 MHz and then tabulated the collected waveforms into Excel files with the comma-separated values (CSV) format and then downloaded to a computer. Then, these files were converted into MATLAB data M.files format. These M.files were then used as input files for a MATLAB code that was developed for the purpose of selecting the mother wavelet and then for the off-line testing of the proposed algorithm. Many inrush currents and different types of fault currents were collected for the off-line testing.

By switching ON the power transformer using the control circuit and the three TRIAC switches, the current flows from the power supply through the power transformer to the connected load. In the meantime, the current flows through the CTs that are located on the primary and secondary sides of the power transformer. Whenever the power transformer is switched ON, the magnetizing inrush current may have different waveform shapes depending on many factors, as illustrated in chapter 3. These inrush currents were collected for different angles of switching. Faults were also created by short-circuiting the different combinations of the three phases *A*, *B* and *C* with or without the ground faults, in both the primary and the secondary sides of the power transformer. These faults were carried out at different loading conditions of the transformer.

5.6 Off-Line Simulation results and Signature Evaluation for the Proposed Technique

In this work, MATLAB simulation was carried out in two ways to analyse the collected current data. The first one was by using MATLAB code and the second was by using MATLAB/Simulink model. This code/model was designed to perform the steps described in section 5.3. Figure *5-3*, Figure ***5-4***, Figure ***5-5*** and Figure ***5-6*** show some samples of some results that were obtained from running the simulation code. Figure *5-3* and Figure ***5-4*** show the inrush currents and normal load disturbance, dq axis current components and their WPT coefficients for the highest frequency sub-bands. Figure ***5-5*** and Figure ***5-6*** show line to ground fault currents when the transformer is loaded with a nonlinear load, dq axis current components and their WPT coefficients for the high frequency sub-bands. The testing was extended to cover two levels of resolutions. This extension was provided to prove that the proposed algorithm is able to give the required decision without the need to use an extra level of resolution. These figures clearly show that the magnitude of the signature is smaller by

half than that for the first level. This decrease in the signature may lead to false decision for identifying the results of the experimental testing and may affect the efficacy of the proposed technique. For this reason, only the first level of details is chosen for the proposed technique to perform the real-time experimental verifications.

Based on the computer used, the CPU computational time was higher by increasing the number of levels of resolutions used. By using two levels of resolution for different test cases, the CPT time was in the range of 23.4 - 32.7 µsec. However, the CPU time was in the range of only 1.56 - 3.12 µsec when using only one level of resolution. Based on these results, the use of two levels of resolution may not increase the efficacy of the proposed technique. However, it may increase the CPU computational time requirement per every time step of analysis, which may affect the speed of response of the relay.

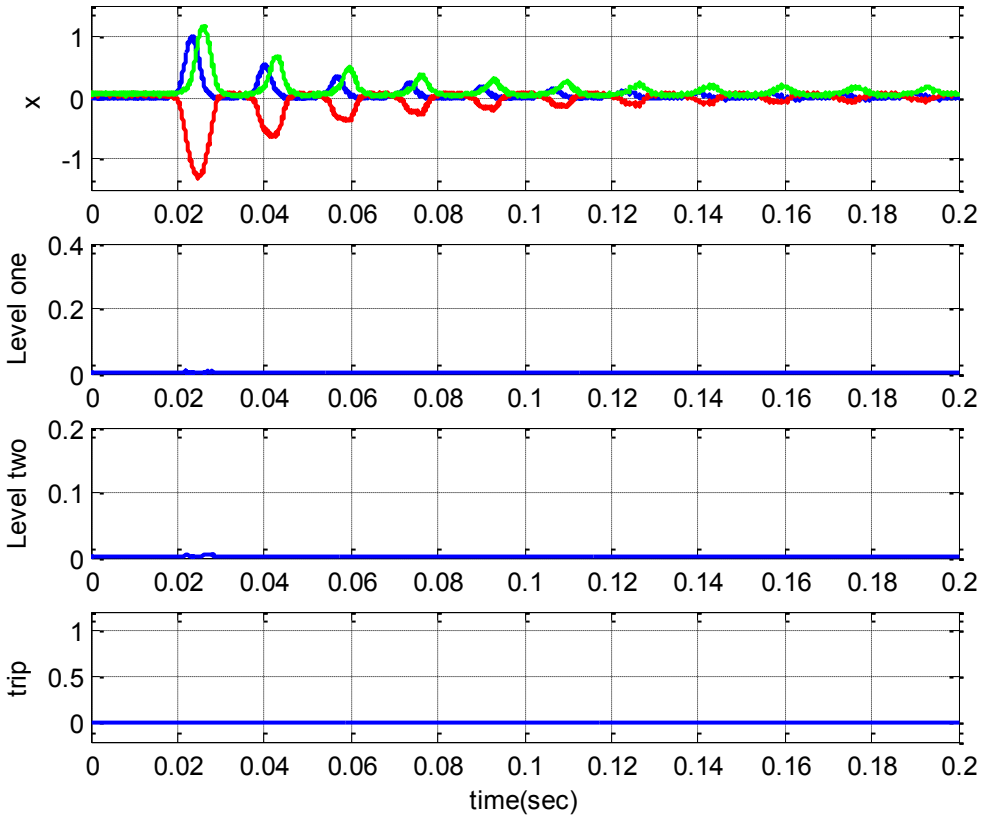

Figure 5-3 Off-line simulation testing for three-phase currents and their coefficients of the high frequency sub-bands for the case of inrush phenomenon

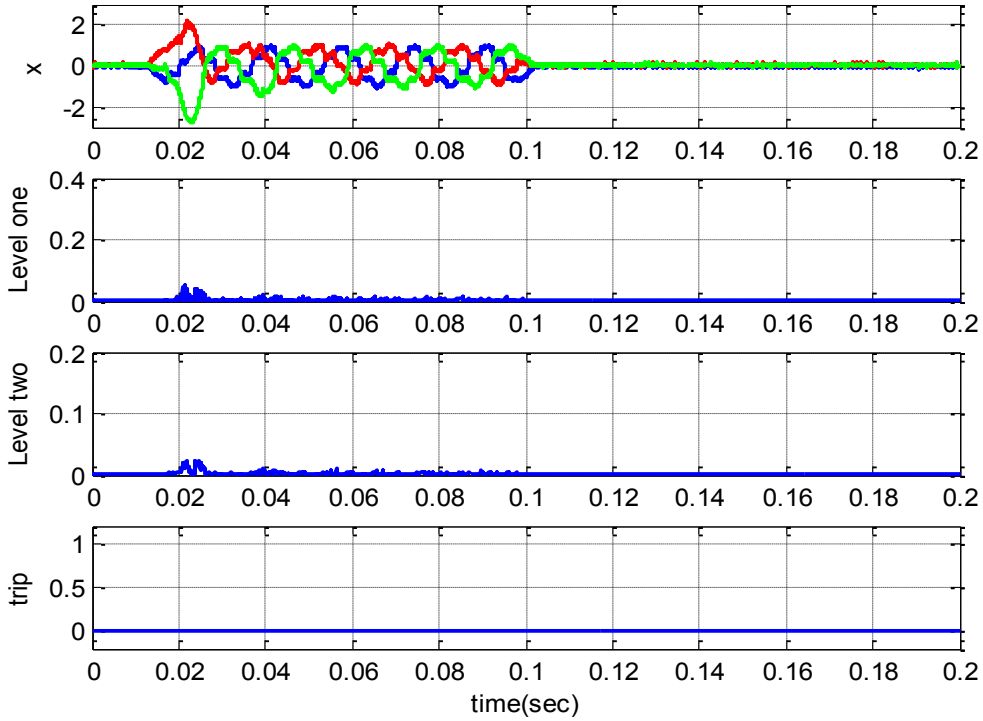

Figure 5-4 Off-line simulation testing for three-phase currents and their coefficients of the high frequency sub-bands for the case of sudden change in the load currents

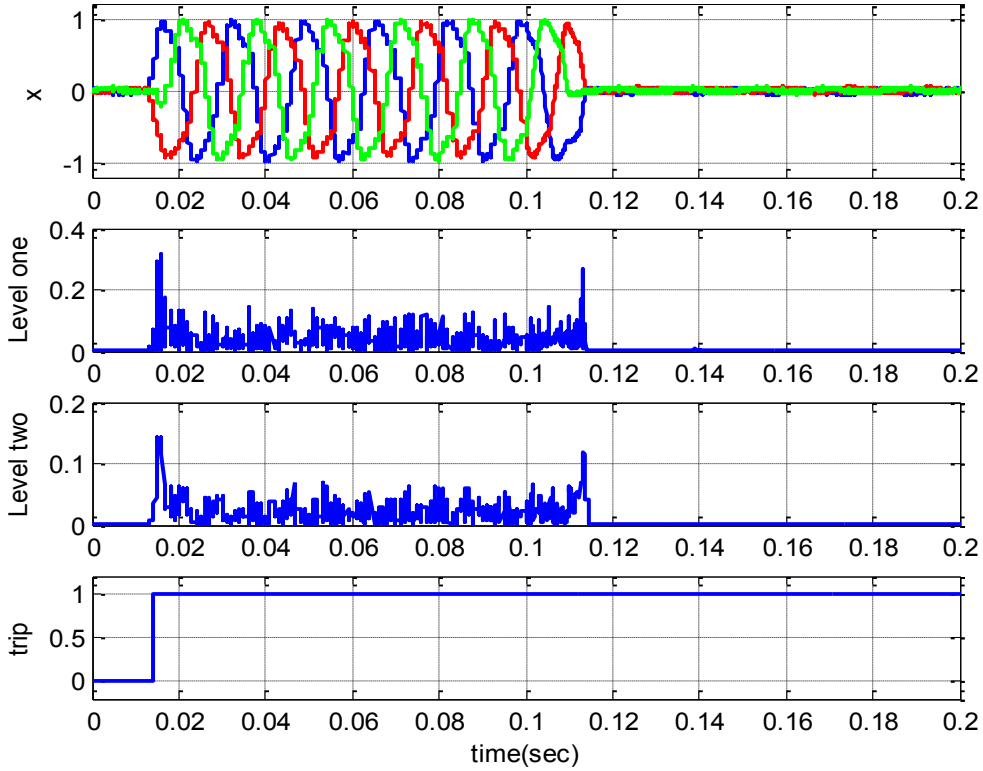

Figure 5-5 Off-line simulation testing for three-phase currents and their coefficients of the high frequency sub-bands for the case of three-phase fault

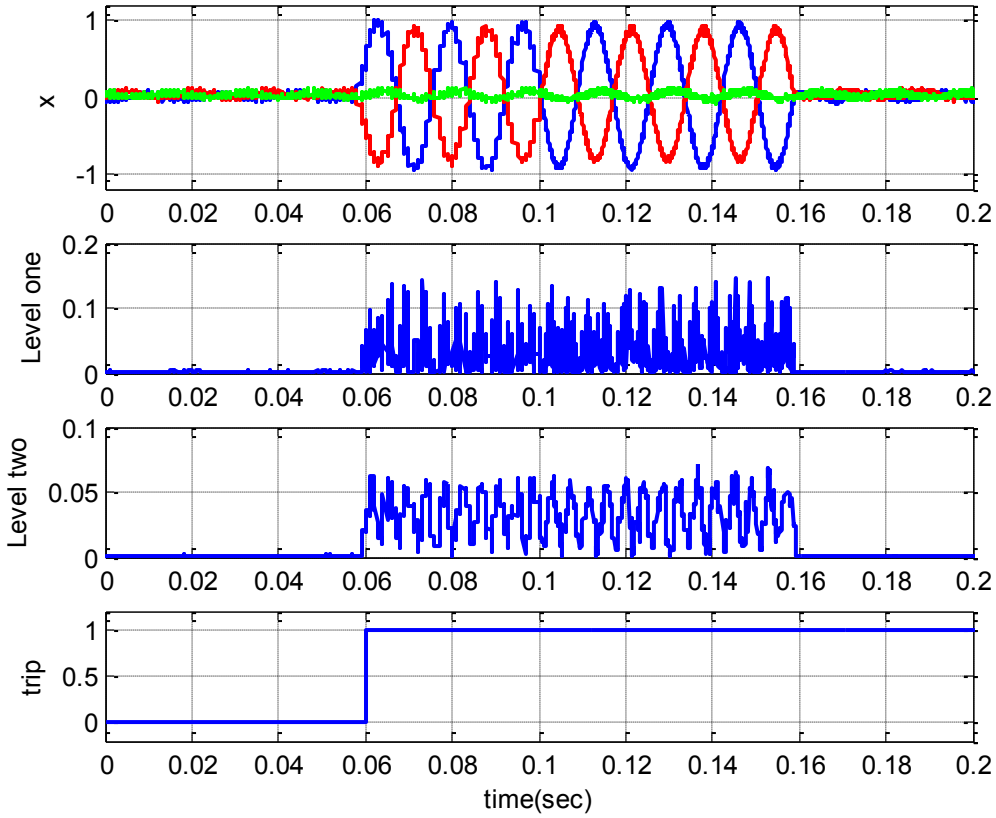

Figure 5-6 Off-line simulation testing for three-phase currents and their coefficients of the high frequency sub-bands for the case of single phase C to ground fault

Some extra simulation results were carried on the collected data for different cases of testing and loading conditions.

a) Magnetizing inrush current at no load (energization start)

For this test, the data were collected when the power transformer was unloaded. The proposed dqWPT-based protection algorithm was applied on this type of the collected data and it has never generated a trip signal for this type of tests even with high inrush current magnitudes or CT saturating cases. Figure ***5-7*** shows the simulation of the 3Φ inrush currents with no trip signal issued to trip the power transformer.

b) Magnetizing inrush current for non-linear Load (energization start)

For this test, the data were collected when the power transformer was loaded with a non-

linear rectifier load. The proposed algorithm was applied on this type of the collected data and it has never generated a trip signal for this type of test, even with high inrush current magnitudes or CT saturating cases. Figure ***5-8*** shows the simulation of the 3Φ inrush currents with no trip signal issued to trip the TRIAC circuit breaker.

c) CTs Mismatch

This simulation test was carried out to test the immunity of the algorithm against the CTs mismatch that may occur due to the dissimilarity of the three CTs used for three-phase inrush currents. The current appears only if there is a CTs mismatch among the utilized CTs in this case. Figure ***5-9*** shows no change in the trip signal, which indicates a non-fault condition. The proposed algorithm was tested for this type of disturbance in the simulation process many times and it has never generated a trip signal, even with high differential current magnitudes or saturating cases.

d) CTs saturation

Current transformers cannot reproduce the primary current correctly at the secondary side according to the transformation ratio whenever they saturate. Transformer core saturation takes place due to many reasons and the most important one is the excessive flow of current in the primary winding. This saturation will cause distortions in the output current of the CT, which leads to the disturbance of the protection relay. This simulation test is carried out to test the immunity of the algorithm against the CTs saturation of the utilized CTs that may occur due to the excessive amounts of the magnetizing inrush currents. As shown in Figure *5-10*, there is not any change in the trip signal, which indicates a non-faulted condition. The proposed algorithm was tested in off-line simulation many times for this case and it has never generated a trip signal, even with high differential current magnitudes or saturating cases.

e) Secondary single line C to ground fault at no load

This test was carried out by solidly connecting phase C to ground on the secondary side of the three-phase power transformer. Figure *5-11* shows clearly the simulation of the differential currents and the trip signal. The algorithm identified the fault currents and issued a trip signal, as is obvious in the figure. In addition, the proposed algorithm has been tested many times under faulted conditions, for which the dqWPT-based protection algorithm has never misidentified any fault.

f) Primary single line A to ground fault at no load

This test was carried out by solidly connecting phase A to ground on the primary side of the three-phase power transformer. Figure ***5-12*** depicts the simulation of the differential three-phase currents and the trip signal. The algorithm identified the fault currents and issued a trip signal as is clearly shown in the figure. In addition, the proposed algorithm has been tested many times under faulted conditions, for which the dqWPT-based protection algorithm has never misidentified any fault.

g) Loaded Secondary Phase A to Phase B Fault

In this case, the algorithm was tested by solidly short-circuiting phase A to phase B on the secondary side of the three-phase power transformer. In Figure ***5-13***, the simulation of the differential three-phase currents and the trip signal are shown. The algorithm successfully identified the fault and issued a trip signal. The proposed algorithm was tested many times to test for faulted conditions, and never failed to identify any line-to-line faults at loaded and unloaded conditions.

h) Non-linear Loaded Secondary 3ϕ Fault

In this most severe test, the three phases were solidly short-circuited on the secondary side of the three-phase power transformer. As shown in Figure ***5-14***, the simulation of the differential three-phase currents and the trip signal illustrates the amount of increase in the fault currents. The algorithm successfully identified the three-phase fault and issued a trip signal. In addition, the proposed algorithm has been tested in simulation many times under three-phase faulted conditions, for which the dqWPT-based protection algorithm has never misidentified any three-phase fault.

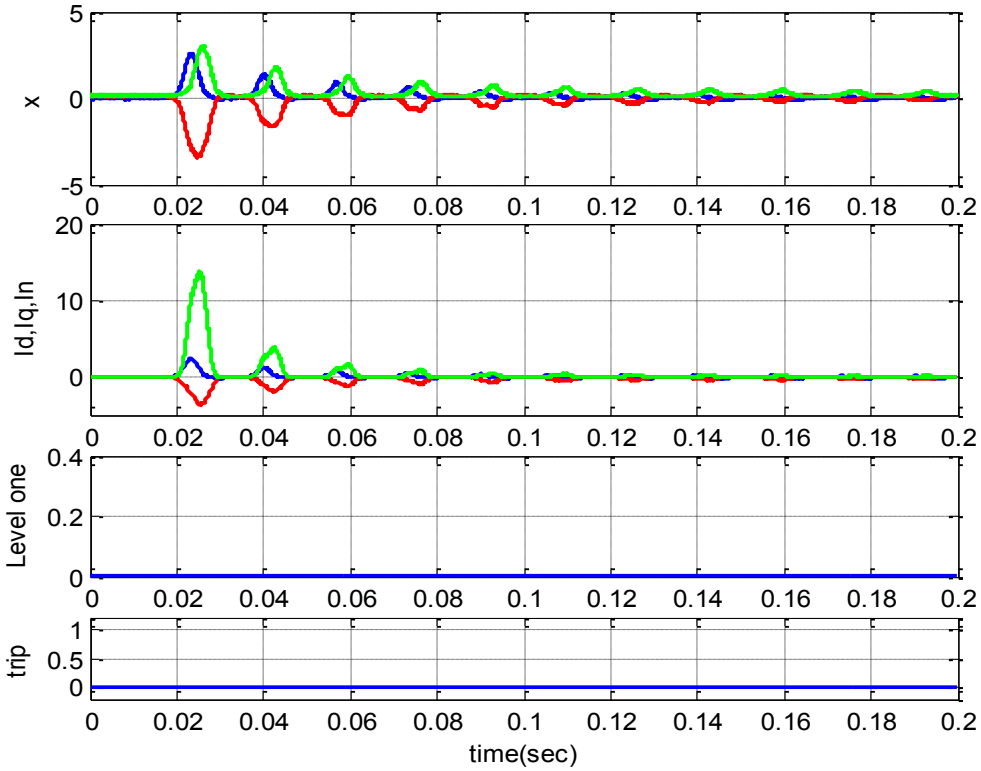

Figure 5-7 Simulation of three-phase inrush currents at no load: the trip signal is still high which means that no trip signal is issued.

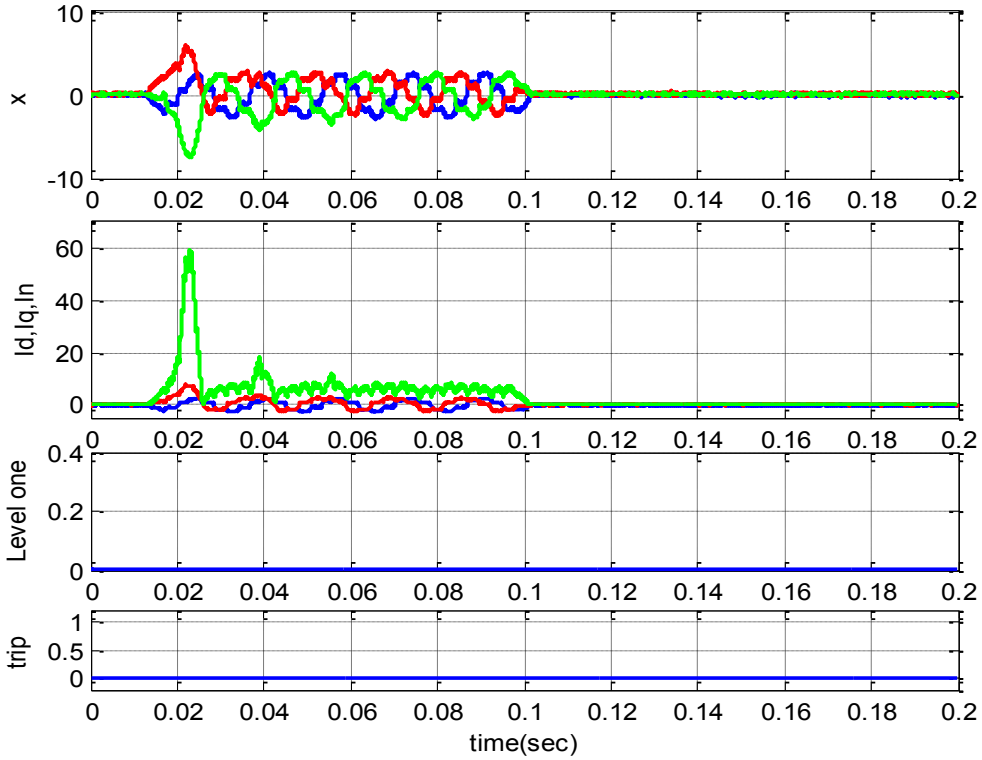

Figure 5-8 Simulation of three-phase magnetizing inrush current at non-linear load at the time of energization: the trip signal is still high, which means no trip signal is issued.

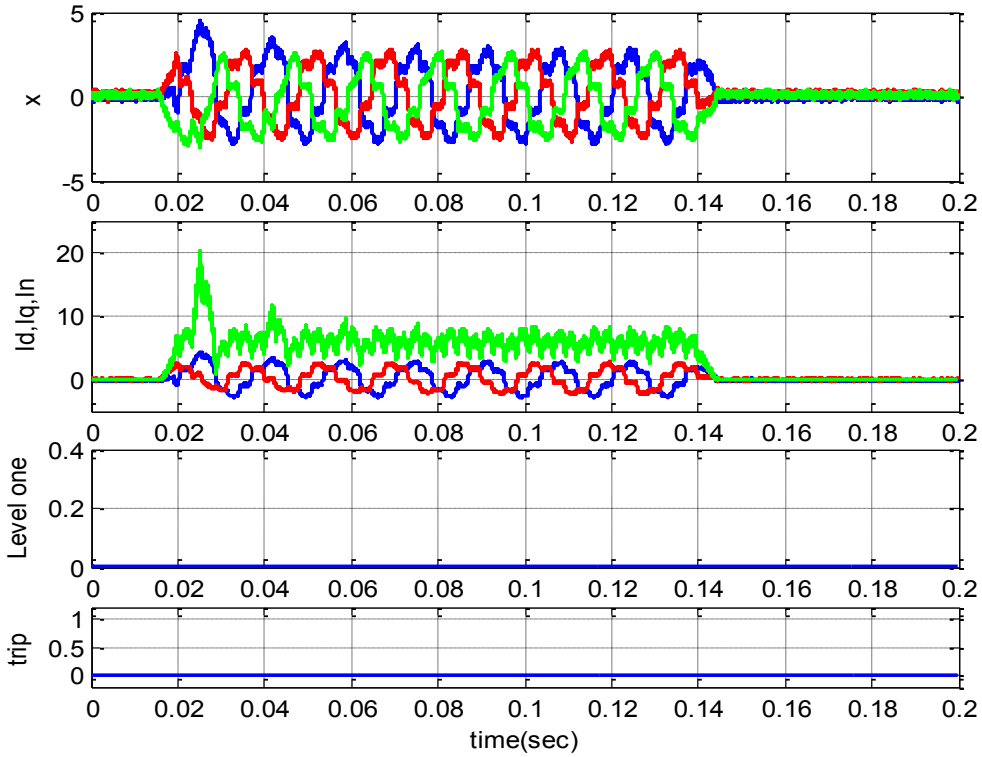

Figure 5-9 Simulation of three-phase currents representing the CTs mismatches at non-linear load: the trip signal is still high, which means no trip signal is issued.

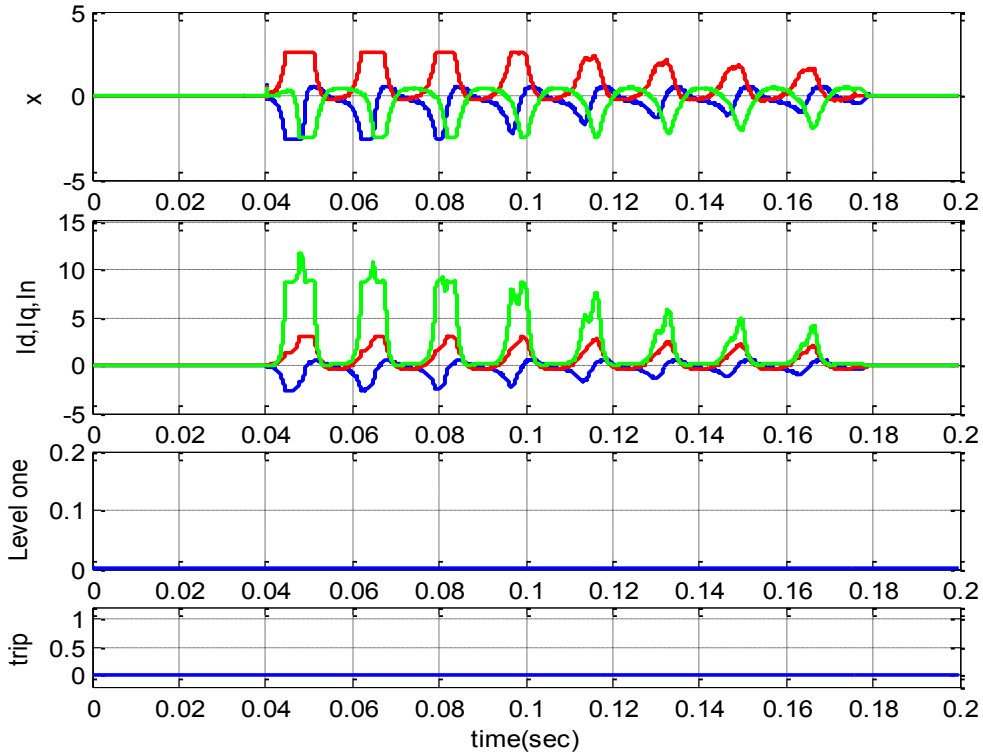

Figure 5-10 Simulation of three-phase inrush currents at the CT saturation case: the trip signal is still high, which means no trip signal is issued.

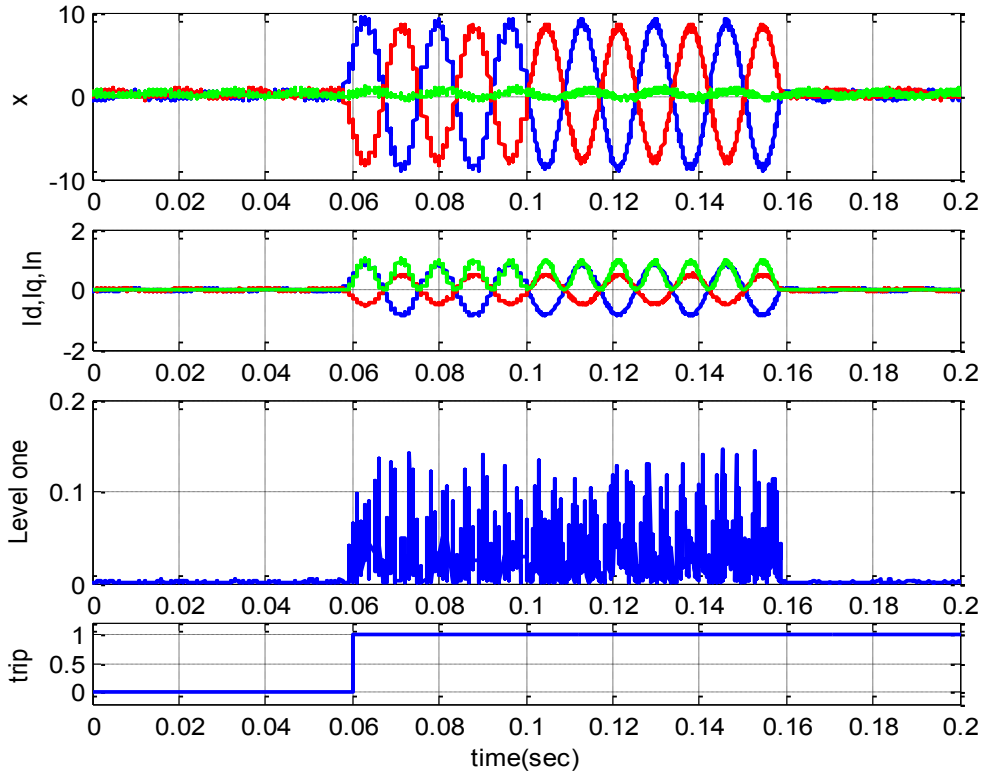

Figure 5-11 Simulation of three-phase currents for unloaded line A to line B fault occurring on the secondary side: the trip signal is low which means that a trip signal is issued.

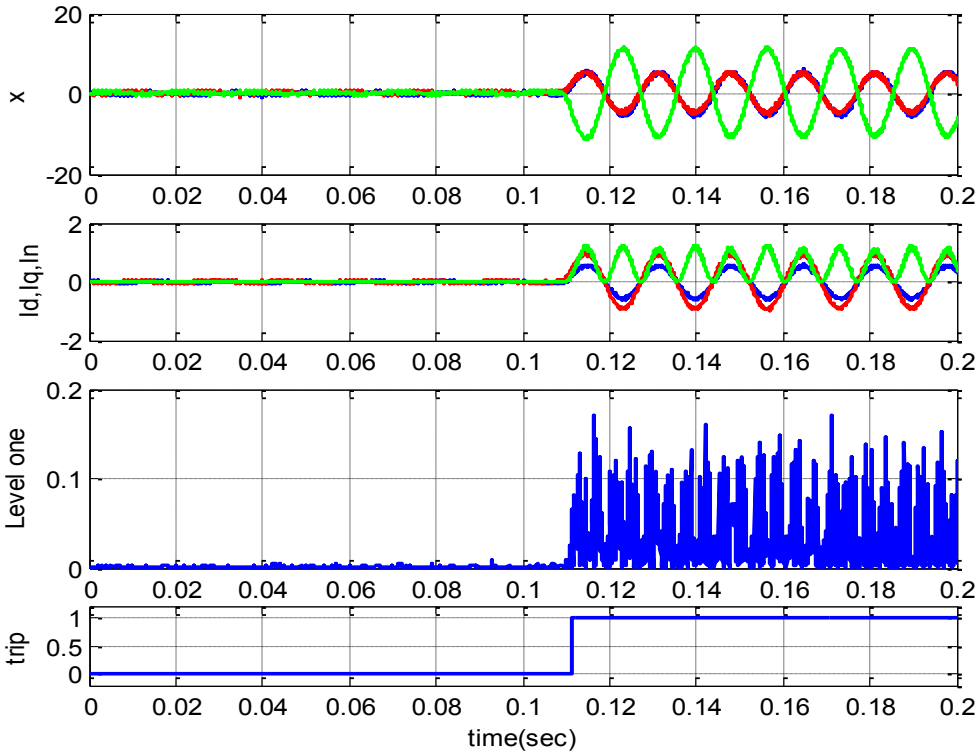

Figure 5-12 Simulation of three-phase currents for loaded phase B to ground fault occurring on the primary side: the trip signal is low which means that a trip signal is issued.

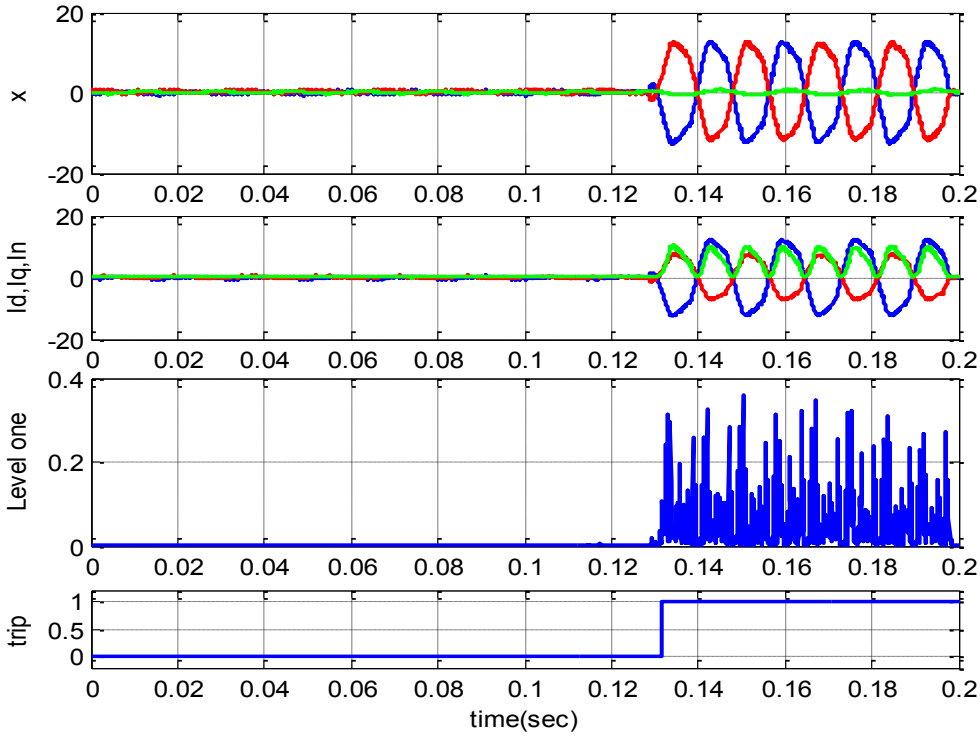

Figure 5-13 Simulation of three-phase currents for loaded phase A to phase C fault occurring on the secondary side: the trip signal is low which means a trip signal is issued.

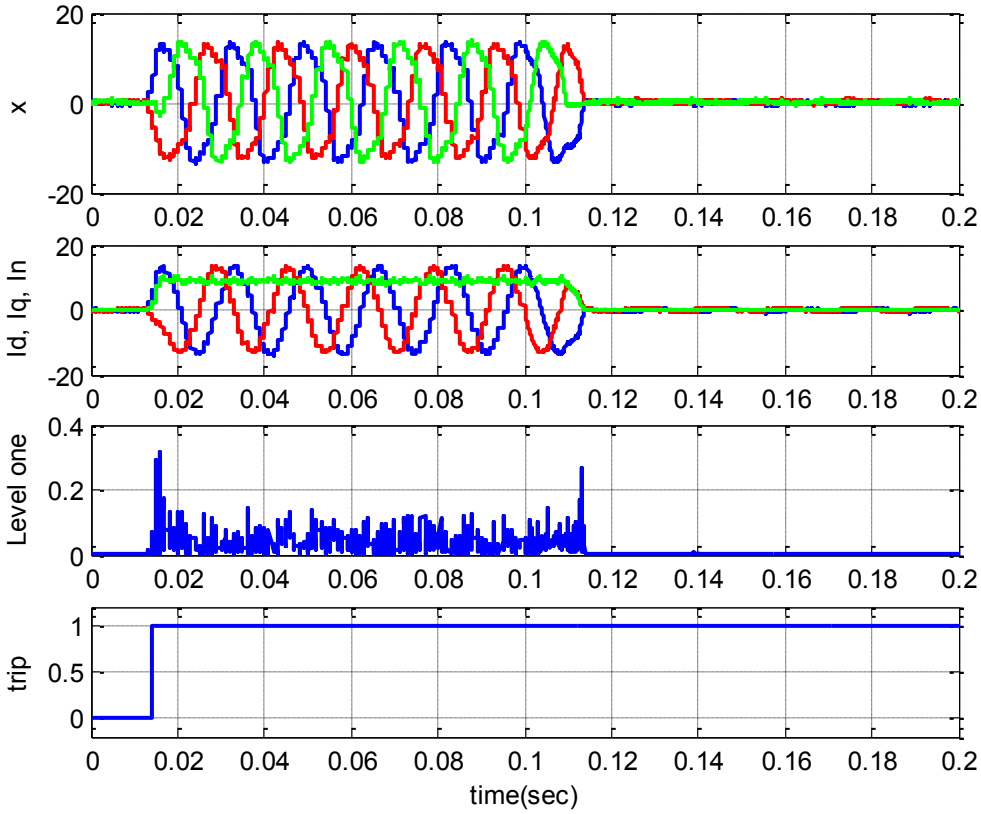

Figure 5-14 Simulation of three-phase currents for non-linear loaded 3φ-to-ground fault occurring on the secondary side: the trip signal is still low which means a trip signal is issued.

In this chapter, the development, implementation and off-line testing of the proposed $dqWPT$ hybrid technique for power transformer protection was described. the development of the *dqWPT* based algorithm for digital differential protection of power transformers was illustrated in detail. The data collection for off-line testing has been presented. At the end, off-line test results were studied for testing the proposed technique. The next chapter provides the results of the experimental testing of this work.

Chapter 6

Experimental Testing of the dqWPT Based Hybrid Technique for the Digital Differential Protection of Power Transformers

6.1 Preface

In the previous chapter, the proposed $dqWPT$ technique for transformer protection was described in detail. The signature evaluation and visualisation were provided in order to explain how the proposed technique works. After that, off-line testing using the collected data was provided to demonstrate the efficacy of the proposed technique before using a real transformer in experimental testing. In this chapter, an experimental testing is carried out to validate the efficacy of the proposed technique.

6.2 Experimental Testing of the Proposed Technique:

As an integral part of the work in this thesis, a verification of the simulation results of the proposed technique is provided experimentally. The experimental tests have been carried out for several types of testing cases for two different three-phase power transformers rated at 5kVA and 2kVA, respectively. This experimental implementation includes the software and hardware setup of the proposed technique. The experimental tests include symmetrical and asymmetrical faults, and other normal disturbances. These tests were carried out for different operational conditions of loading, with different types of loads, to perform the testing, namely, resistive load, inductive load, dynamic load and nonlinear load at different balanced and unbalanced conditions. Different samples of the test cases are listed below to prove the efficacy of this algorithm. The two power transformers were tested for different tests among

these ones in this list.

Magnetizing Inrush currents:

- Unloaded magnetizing inrush current (energization start),
- magnetizing inrush current at balanced R-L Load (energization start),
- magnetizing inrush current at unbalanced R-L Loaded (energization start),
- Non-Linear Loaded magnetizing inrush current (energization start),
- Dynamic Loaded magnetizing inrush current (energization start),

Internal faults:

- Unloaded secondary single line to ground fault,
- Unloaded secondary single line to ground fault through resistance,
- Loaded secondary side turn to turn fault,
- Loaded primary single line to ground fault,
- Unloaded secondary line to line to ground fault,
- Loaded three-phase fault at the secondary side.
- Loaded three-phase fault at the primary side.

Other disturbances:

- Unbalanced load, CTs mismatch currents,
- CTs saturation,
- Over-excitation,
- External or through faults,

A description for each of these cases is provided below in detail in two parts for the two different power transformers with the figures obtained from the experimental testing. Among all the results obtained from running these sets of testing cases, few results are presented in this chapter. The three-phase currents with their *dq* axis and/or the I_n components and the high frequency sub-band signal are shown in the figures with a specific channel scale to compare its amplitude in each case. The figures were taken directly from two synchronized 4-channel Tektronix TDS3014B digital oscilloscopes. The Y-scale of the figures represents the amplitude of the differential current. This Y-scale depends on the oscilloscope channel's scale switch (Ch). Since the input current was initially divided by 10 at the current isolating circuits, each square division in the figure of the oscilloscope screen shot equals the Ch switch multiplied by 10. The Experimental testing was carried out for two power transformers, and the results are divided into two sections, A and B.

A: Experimental Results for the Three-Phase 5kVA Laboratory Power Transformer:

The specification of this transformer are 3Φ, 5kVA, 60Hz, 230/550-575-600V, Δ-Y step-up, core-type, laboratory power transformer. Using this power transformer, the experimental tests have been carried out for different types of testing cases using the experimental setup shown in Figure ***6-1***. This setup required a C-code implementation of the proposed technique using the digital signal-processing (DSP) unit DS-1102. The power transformer is connected to a $3\Phi, 208\text{V}$ power supply through a 3Φ circuit breaker (CB), and the transformer supplies a balanced 3Φ resistive and inductive load of ($\text{Z} = 343 + \text{j}171.4\ \Omega$/phase). The primary and the secondary side three-phase CTs currents are connected to three current isolating circuits and the three outputs of the current isolating circuits represent the 3Φ differential currents. Then the 3Φ differential currents are fed to the analog input terminals of the DSP unit,

(*DS1102*). The built-in analog to digital converter (ADC) converts the continuous analog currents to discrete ones with a sampling time of *0.0001* sec and a sampling frequency equal to 10 kHz. This rate was found to be suitable because it gives a good resolution to the sampled signal within an acceptable computation time. Then the procedure of the proposed algorithm takes place in the host computer. The sampled 3Φ digital differential currents are converted into (dq) axis components. After that, the high frequency sub-band contents of the sampled (dq) axis components are extracted using the WPT through a circular convolution of a 16- bit circular window.

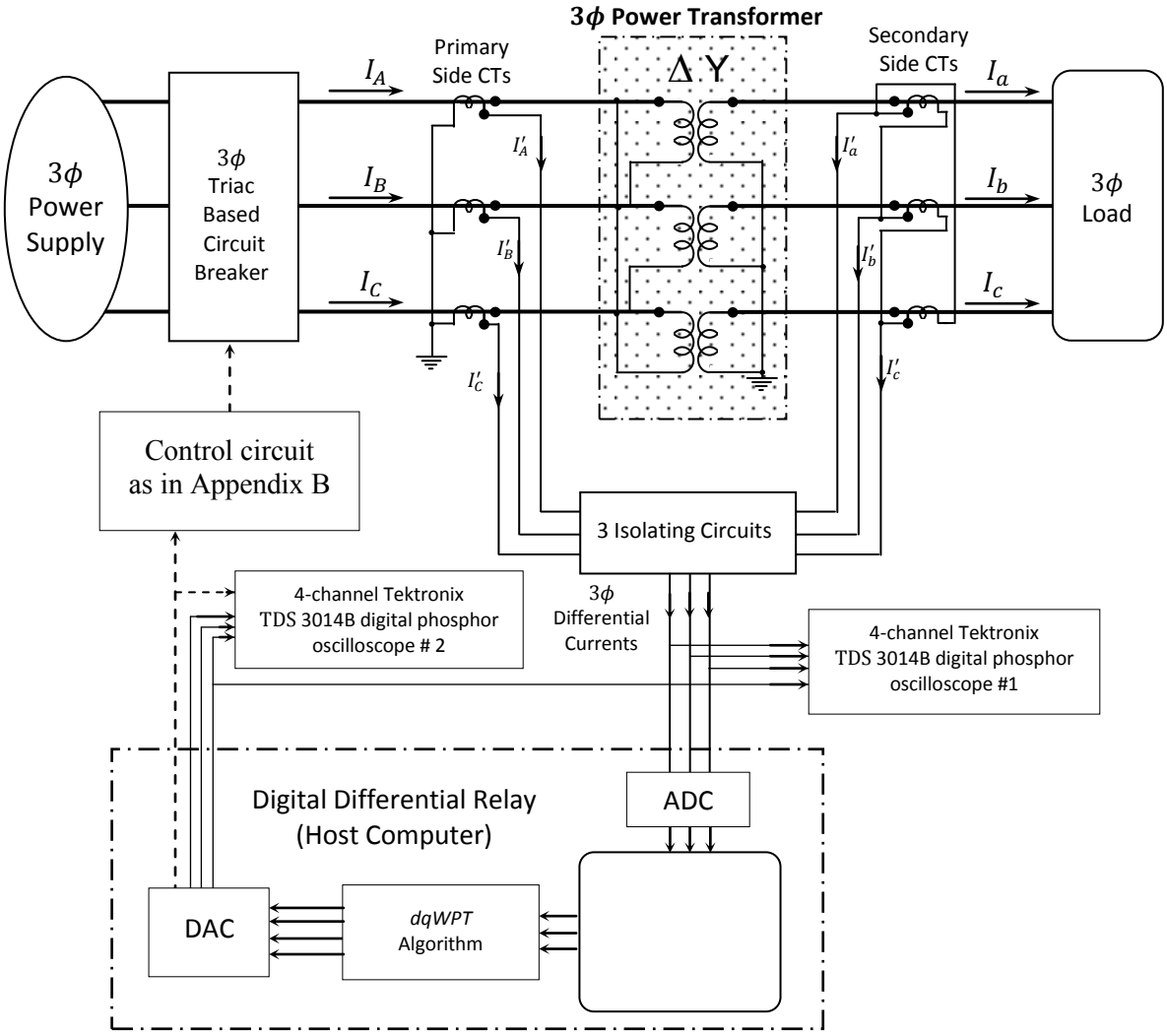

Figure 6-1 The circuit diagram of the experimental setup for the 5kVA transformer using ds-1102

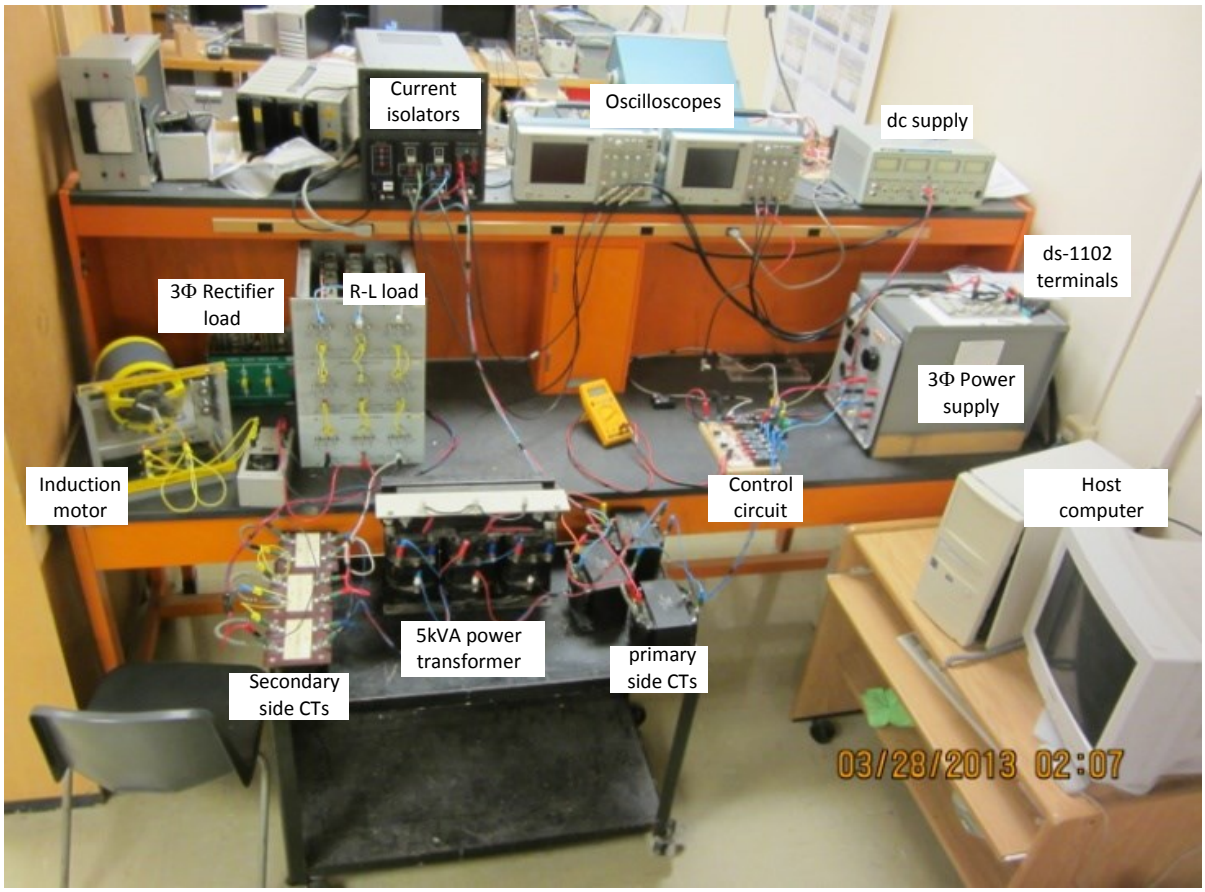

Figure 6-2 The experimental setup for 5kVA laboratory power transformer using ds-1102

Finally, a comparison to a threshold point with the high frequency sub-band coefficients of the first level takes place. The threshold in this analysis should be zero, because the normal current disturbances have no components in the high frequency sub-band. However due to some noise in the signal a small value is chosen by try and error to avoid wrong decision due to this noise. This comparison is able to determine the characteristics of the input 3Φ currents. As a result, a trip signal is issued only when there are faulted conditions. Then the digital trip signal is converted into an analog signal through a DAC and then sent to the control circuit to isolate the transformer. The main signature used in this work to identify and discriminate the inrush currents from the fault currents, is the amplitude of the coefficients of the sub-band frequencies of the first level decomposition.

- **Experimental Results for Magnetizing Inrush Currents:**

This type of test was performed by switching ON the circuit breakers located at the primary side of the power transformer in order to energize the transformer. Magnetizing inrush currents flow only if the initial conditions for the inrush currents are available at the instant of switching. Several tests were carried out by random switching and it has been observed that the proposed technique has never given a trip signal for such testing cases. These tests were performed both at loaded and unloaded conditions. Some of the sample results are provided for negative and positive inrush currents in different phases and with or without load are also demonstrated in Figures (6.3-6.10). It is obvious from the figures that, in some phases, even though the current magnitudes are relatively high, the proposed dqWPT technique is able to distinguish the inrush currents as a non-faulted condition and, hence, no trip signal output was issued. It is worth mentioning that throughout hundreds of cases of transformer energization, the magnetizing inrush currents have quite different patterns in the shape and direction in the three-phases and are unpredictable. However, the proposed dqWPT technique is able to recognize this natural phenomenon and keep the transformer energized as long as there are no faulted conditions. The proposed dqWPT technique provided a satisfactory performance both for no load and with load conditions. Some of these cases are described in detail.

a) Experimental Unloaded Magnetizing Inrush Currents

This experimental testing was carried out when the primary side of the power transformer was connected to a 3Φ supply and its secondary side was not connected to the load. The proposed algorithm has been tested many times to investigate the magnetizing inrush current.

It has never generated a trip signal to isolate the transformer due to the inrush phenomenon, even with high differential current magnitudes. Some cases with negative and positive inrush conditions without load are illustrated in Figure ***6-3***, Figure ***6-4***, Figure ***6-5*** and Figure ***6-6***, in which the 3Φ inrush currents with no trip signal are shown.

b) Experimental Magnetizing Inrush Current at different loading conditions

The loaded magnetizing inrush current test was carried out when the power transformer was switched ON while it was connected directly to a 3Φ load. The proposed algorithm has been tested experimentally several times for the magnetizing inrush currents phenomenon and it has never generated a trip signal for this case to trip the power transformer, even with high differential magnetizing inrush current magnitudes. A few cases are illustrated in the following figures in which the 3Φ inrush currents and the high frequency sub-band with no issued trip signal are shown. Figure ***6-7*** illustrate the results of this test for a balanced R-L load of $Z = 343 + j171.4\ \Omega$/phase. Figure ***6-8*** illustrates the results of this test for an unbalanced R-L load of $Z_a = 800 + j400\ \Omega$/phase, $Z_b = 480 + j240\ \Omega$/phase, $Z_c = 400 + j200\ \Omega$/phase. Figure ***6-9*** illustrates the results of this test at a non-linear rectifier load. Figure ***6-10*** illustrates the test results for 3Φ, ¼ hp induction motor. These test results confirm that the proposed algorithm operated correctly.

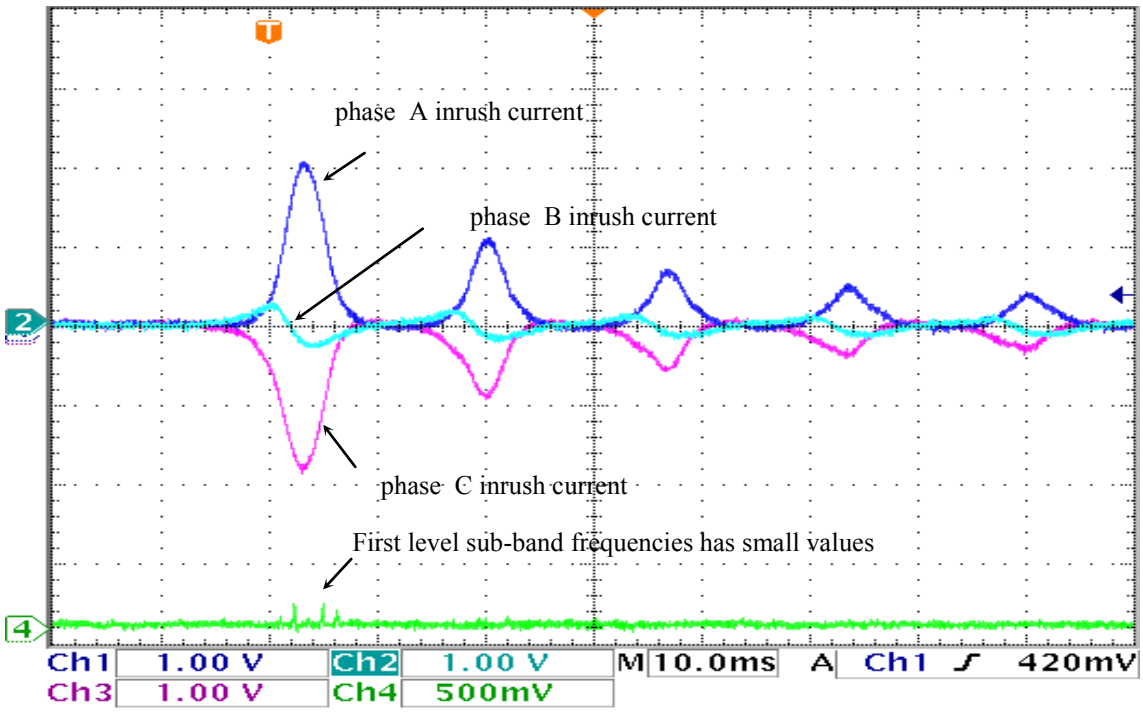

(a)

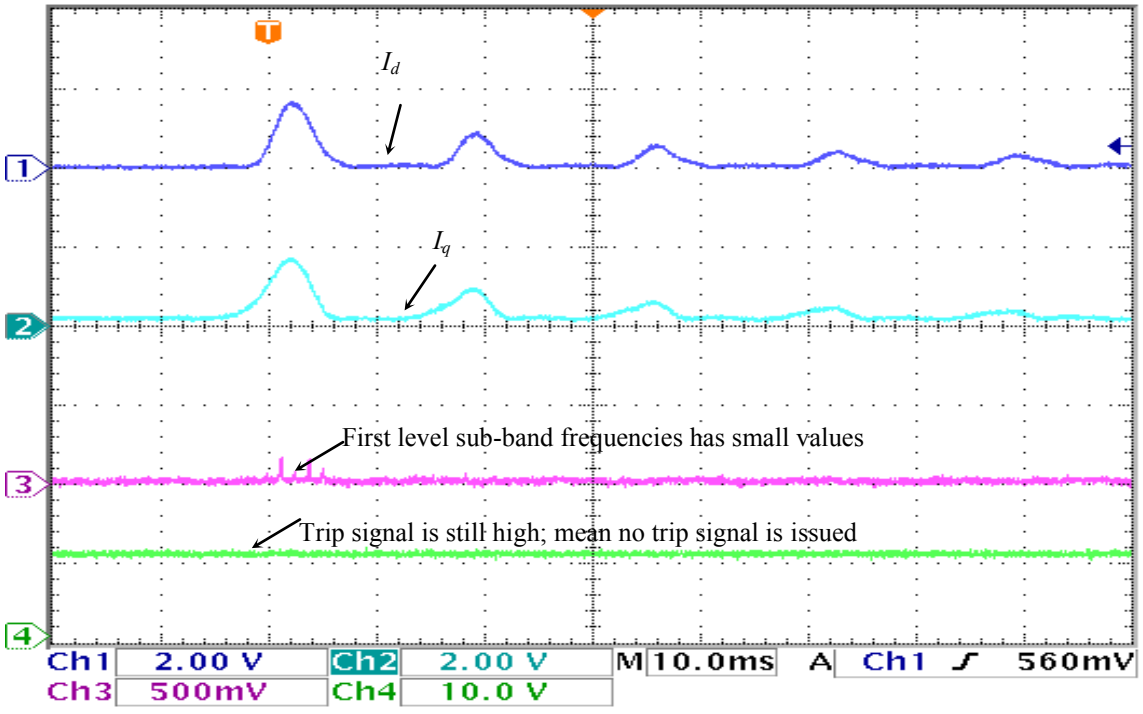

(b)

Figure 6-3 The experimental test case of the magnetizing inrush current with phase A has positive peak and phase C has negative peak a) the three-phase unloaded magnetizing inrush currents and the 1st level high frequency sub-band, b) dq current components and the 1st level high frequency sub-band: the trip signal is still high. It means that no trip signal is issued.

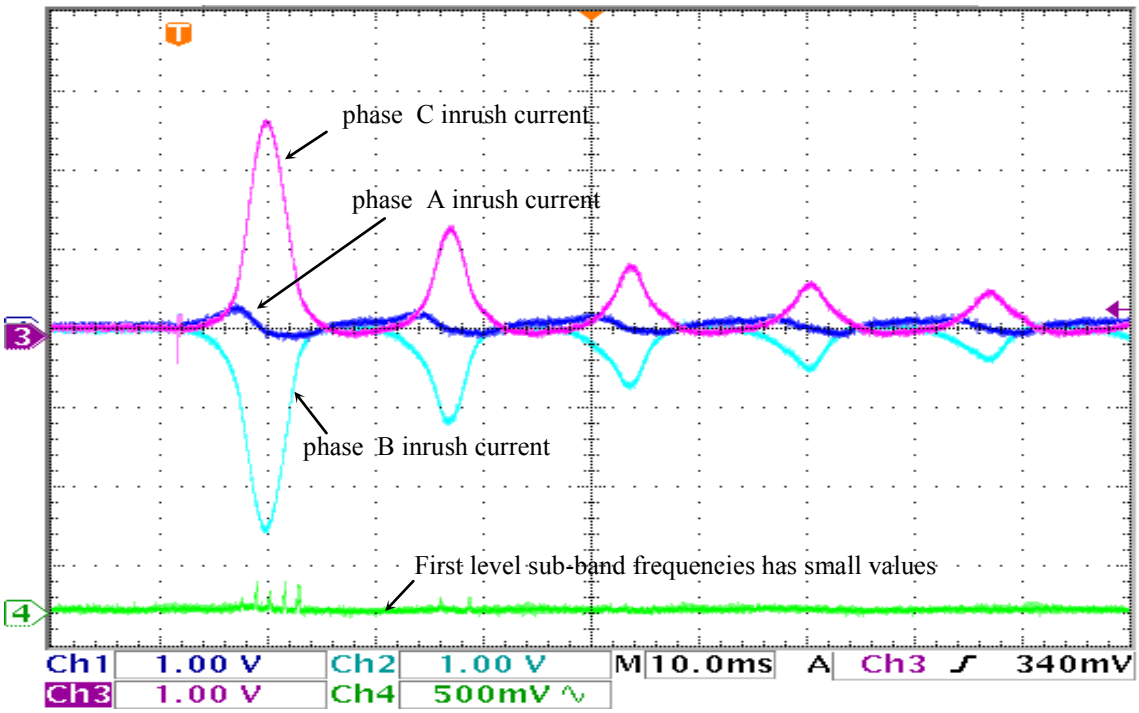

(a)

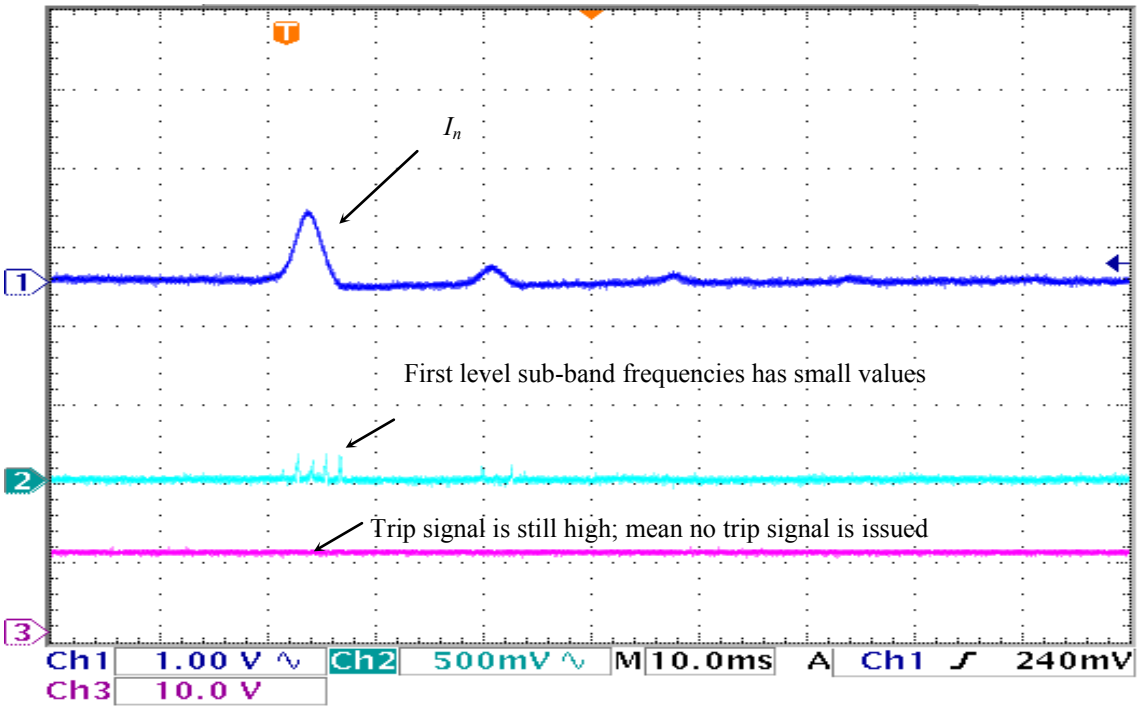

(b)

Figure 6-4 The experimental test case of the unloaded magnetizing inrush current with phase C has positive peak and phase B has negative peak a) the three-phase magnetizing inrush currents and the 1st level high frequency sub-band b) $I_n = I_d^2+I_q^2$ current component and the 1st level high frequency sub-band: the trip signal is still high, means no trip signal is issued.

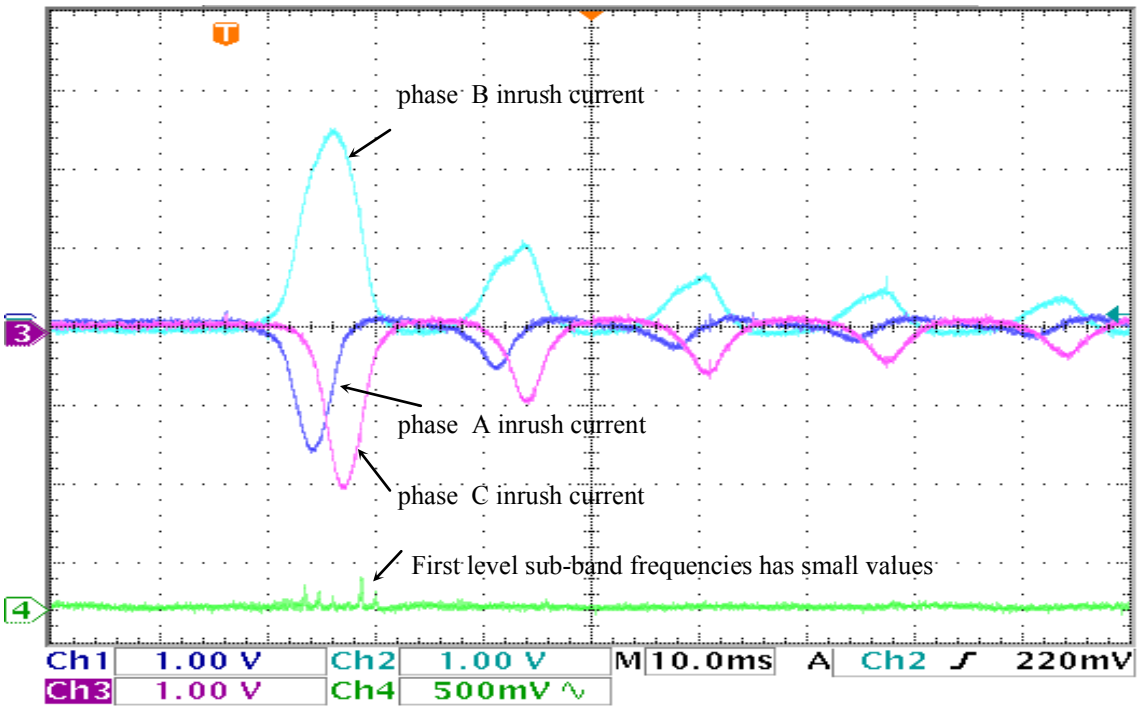

(a)

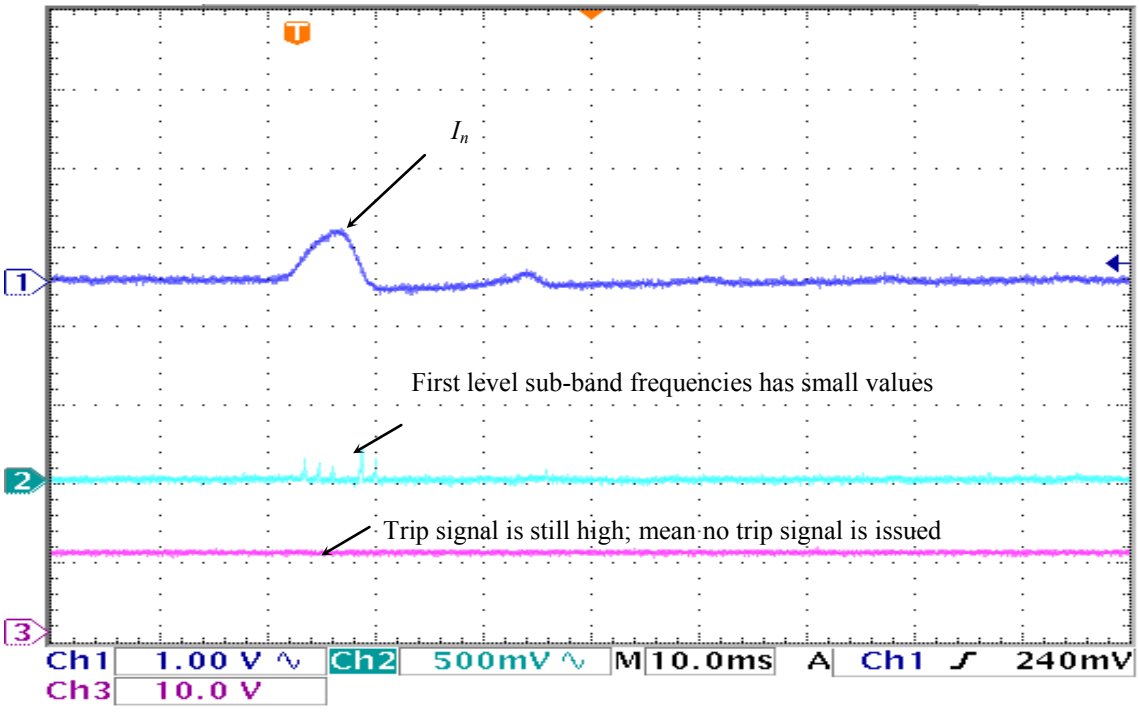

(b)

Figure 6-5 The experimental test case of the unloaded magnetizing inrush current with phase B has positive peak and phases A and C have negative peak, a) the three-phase magnetizing inrush currents and the 1st level high frequency sub-band b) $I_n = I_d^2+I_q^2$ current components and the 1st level high frequency sub-band: the trip signal is still high, means no trip signal is issued.

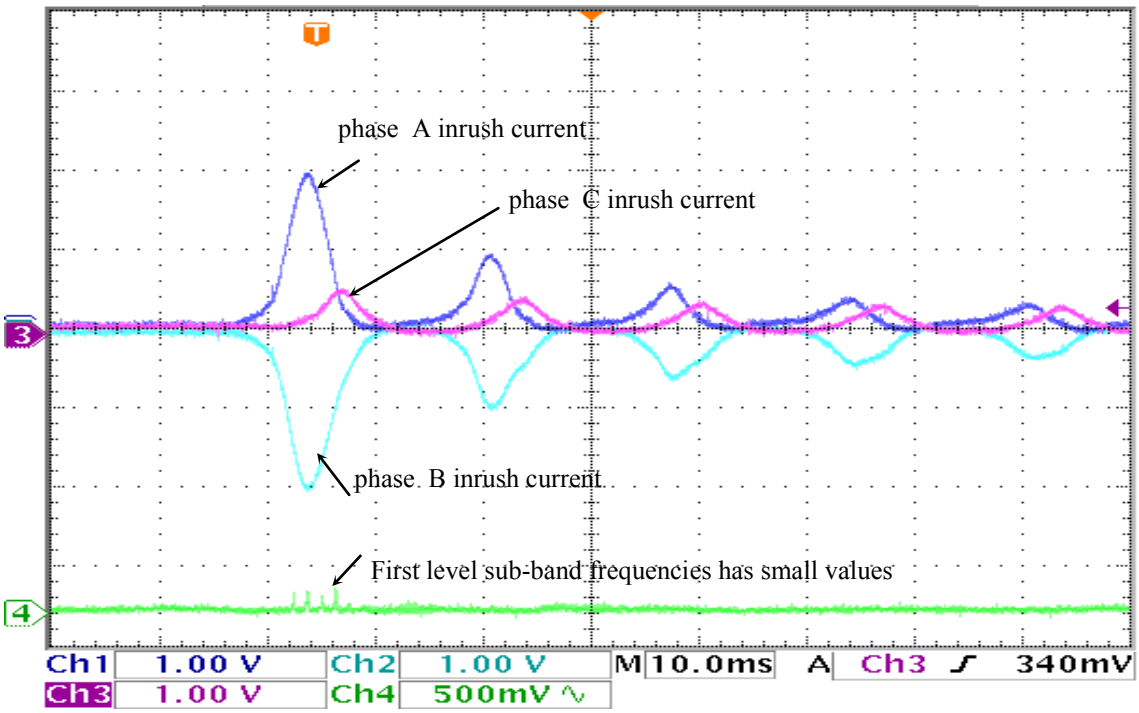

(a)

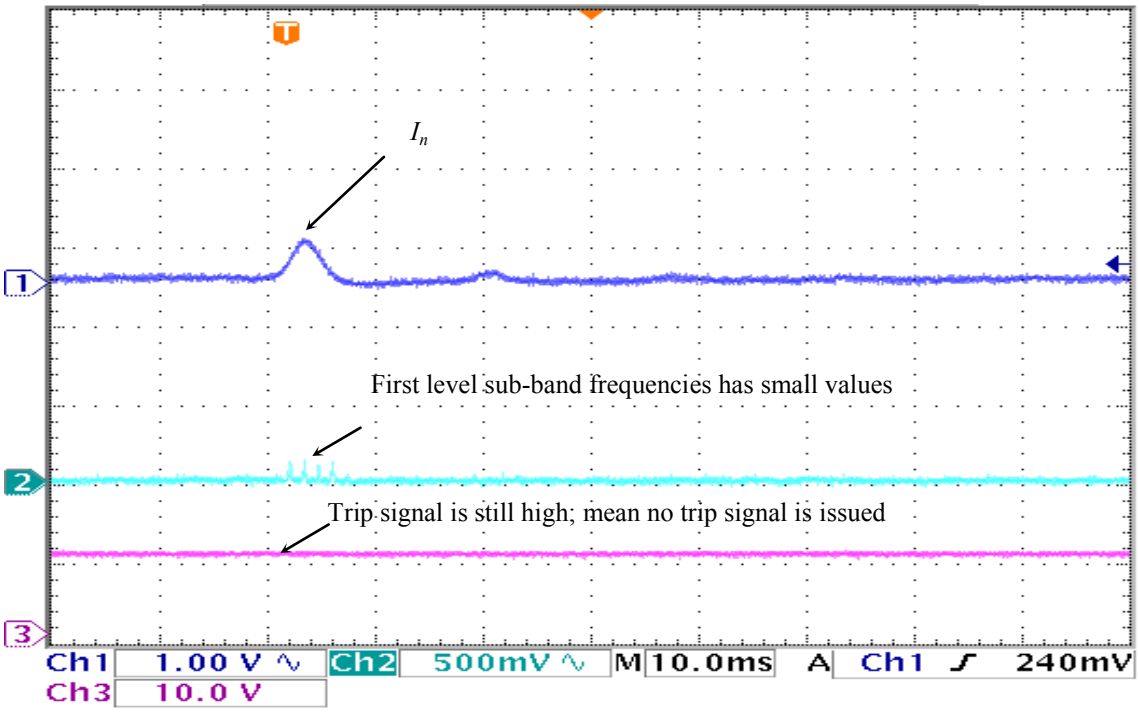

(b)

Figure 6-6 The experimental test case of the unloaded magnetizing inrush current with phase A has positive peak and phase B has negative peak, a) the three-phase magnetizing inrush currents and the 1st level high frequency sub-band b) $I_n = I_d^2+I_q^2$ current components and the 1st level high frequency sub-band: the trip signal is still high, means no trip signal is issued.

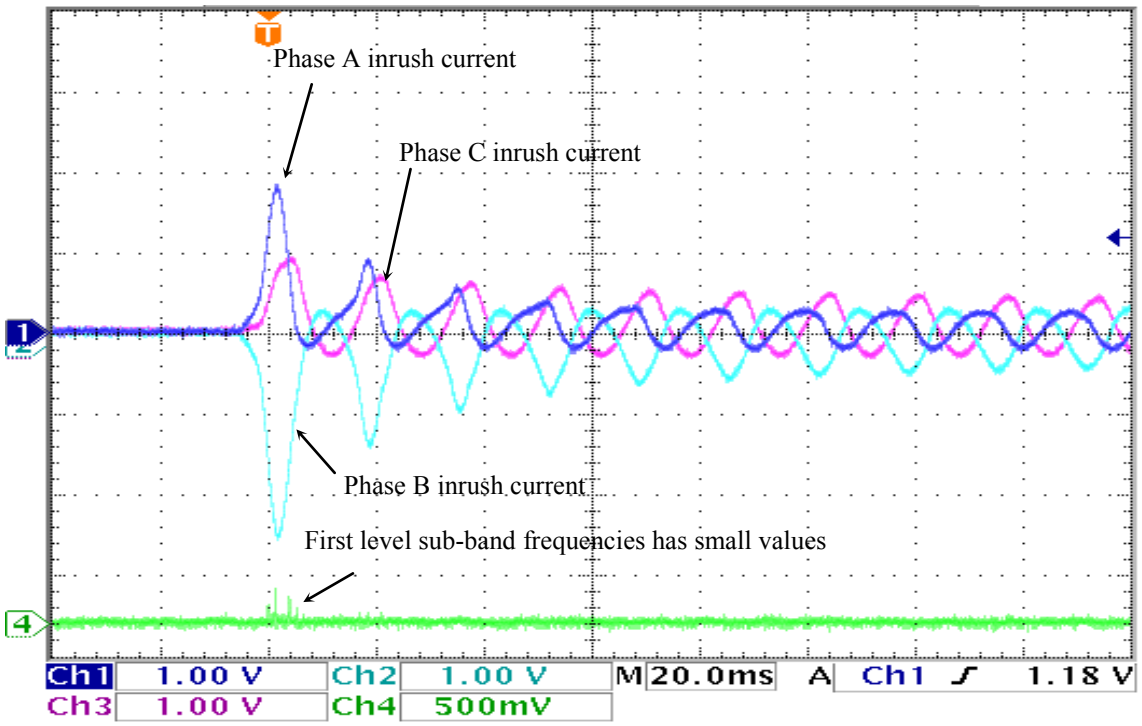

(a)

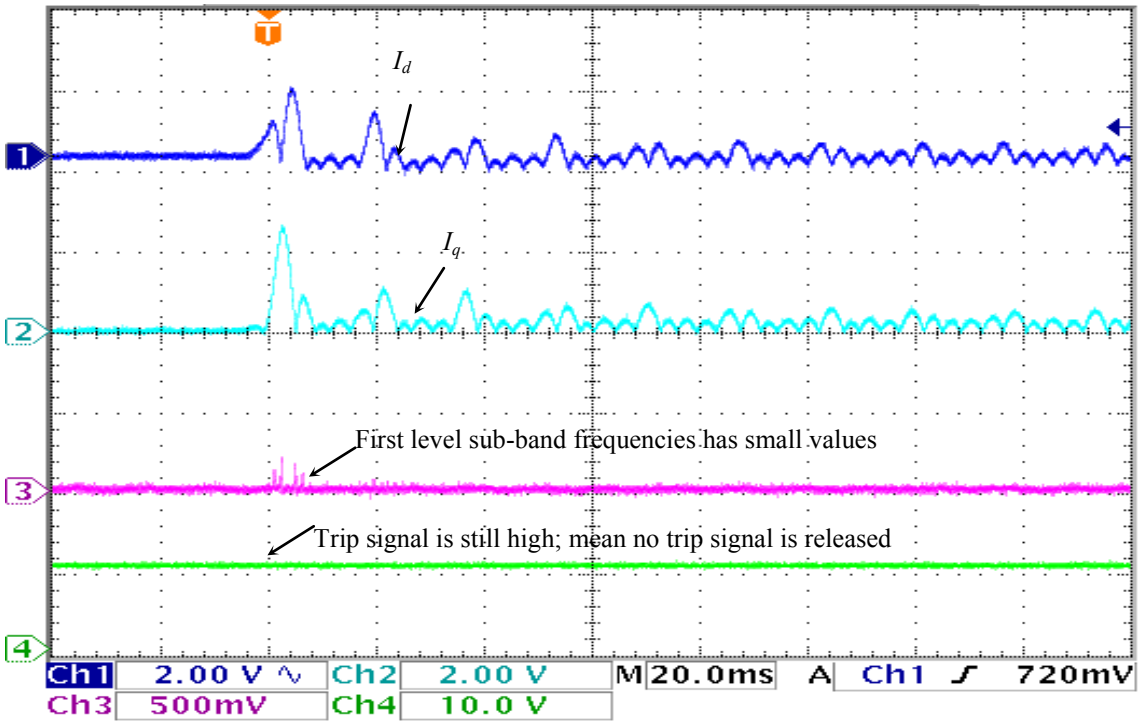

(b)

Figure 6-7 The experimental test case of the magnetizing inrush current at balanced resistive-inductive load a) the three-phase magnetizing inrush currents and the 1st level high frequency sub-band, b) dq current components and the 1st level high frequency sub-band: the trip signal is still high, means no trip signal is issued.

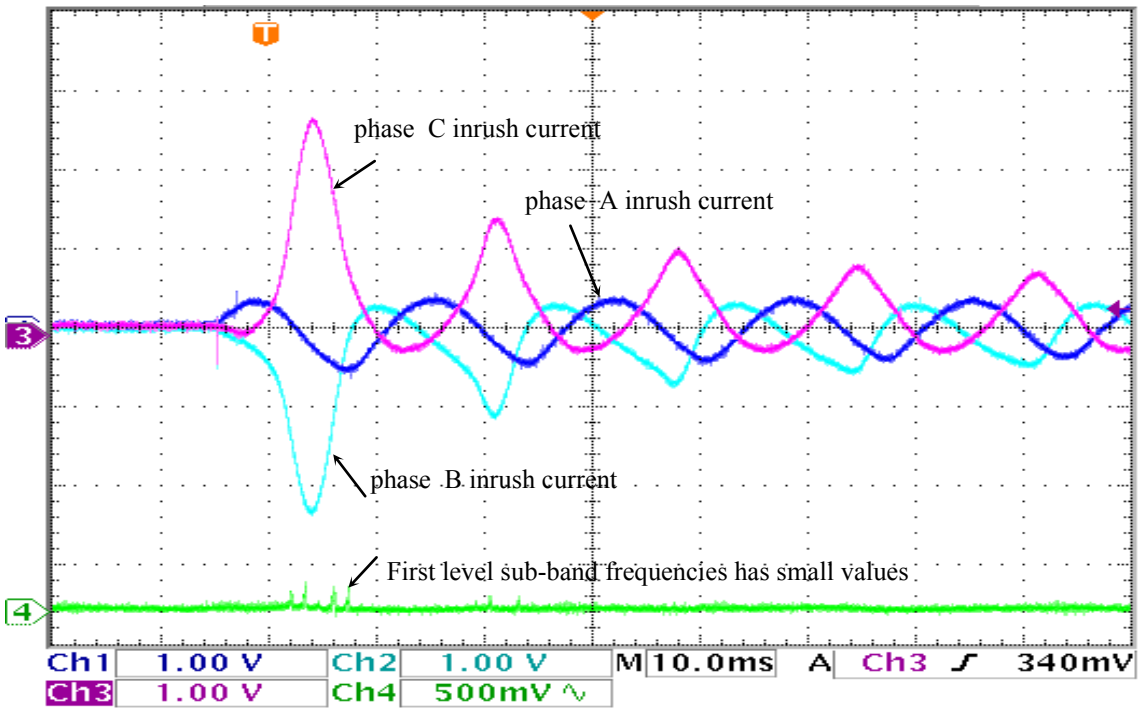

(a)

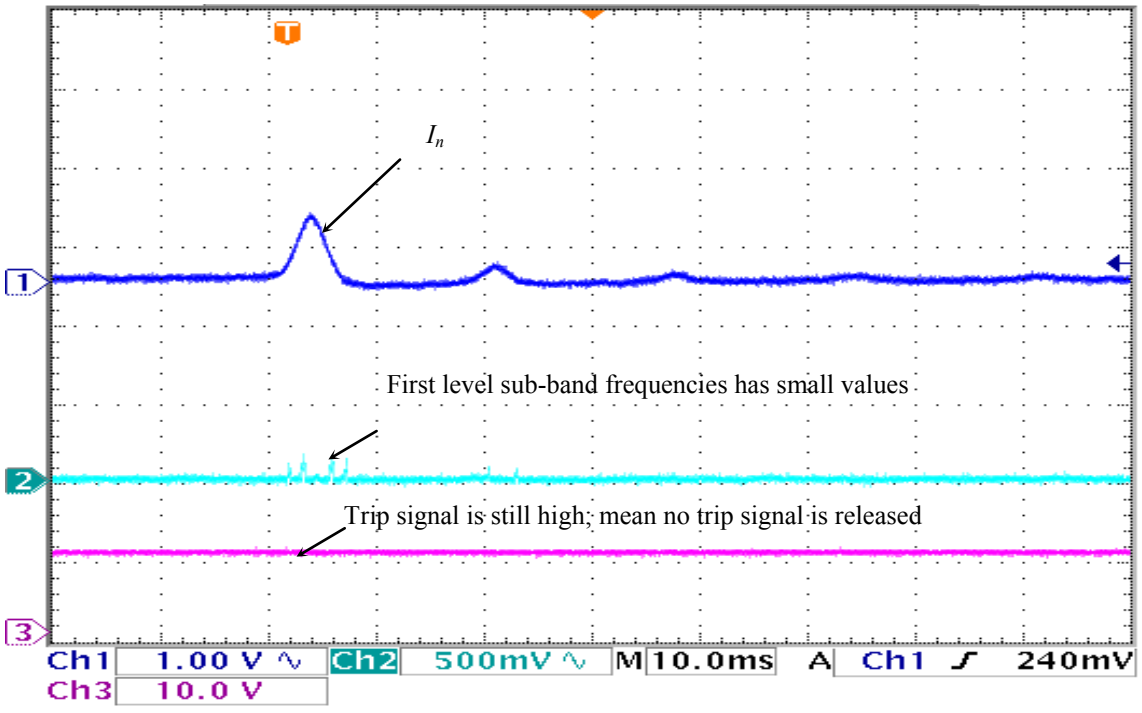

(b)

Figure 6-8 The experimental test case of the magnetizing inrush current at unbalanced R-L load, a) the three-phase magnetizing inrush currents and the 1st level high frequency sub-band b) $I_n = I_d^2+I_q^2$ current components and the 1st level high frequency sub-band: the trip signal is still high, means no trip signal is issued.

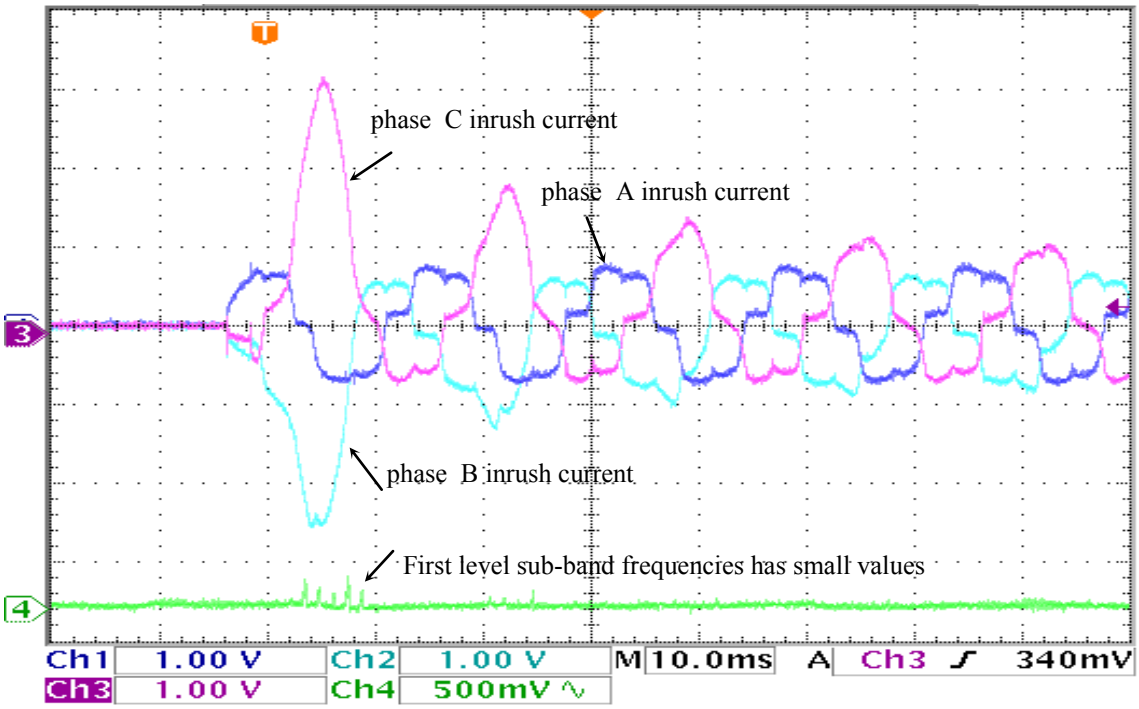

(a)

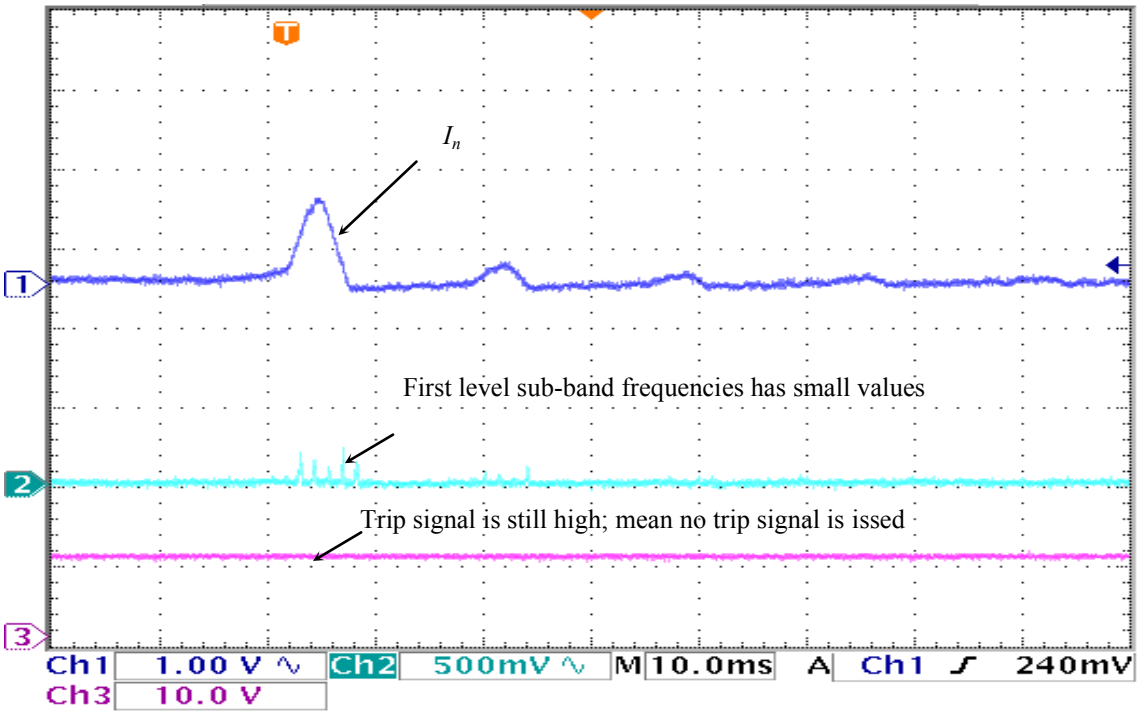

(b)

Figure 6-9 The experimental test case of the magnetizing inrush current at nonlinear loa,d a) the three-phase magnetizing inrush currents and the 1st level high frequency sub-band b) $I_n = I_d^2+I_q^2$ *current components and the 1st level high frequency sub-band: the trip signal is still high, means no trip signal is issued.*

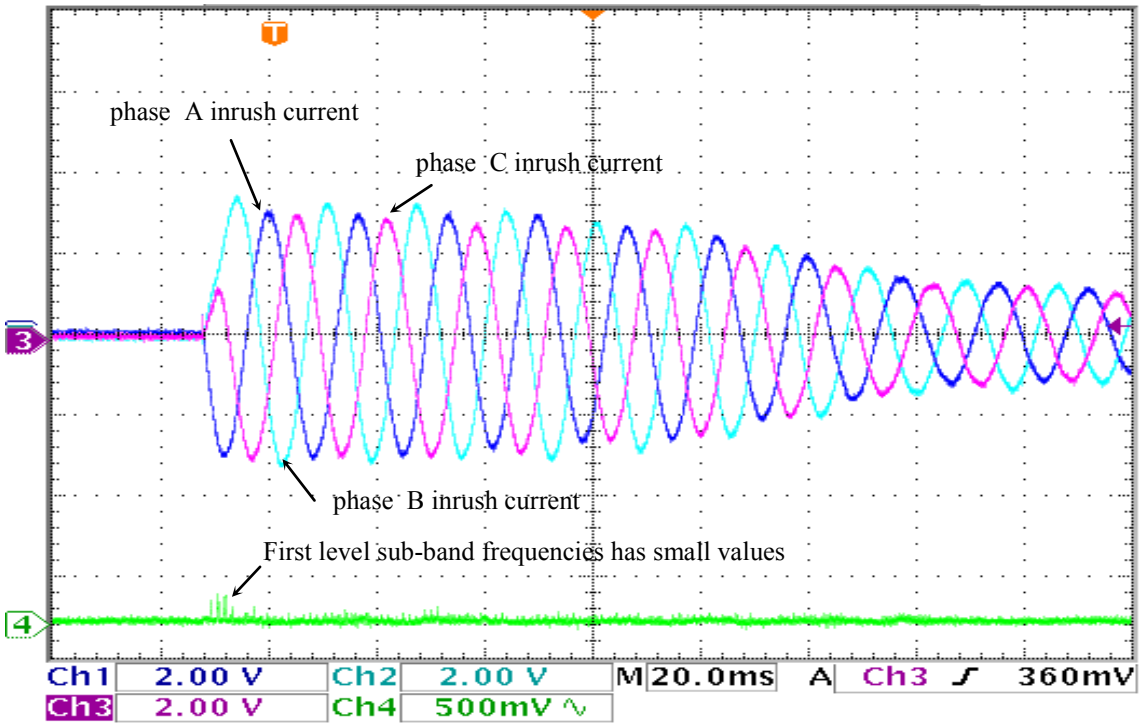

(a)

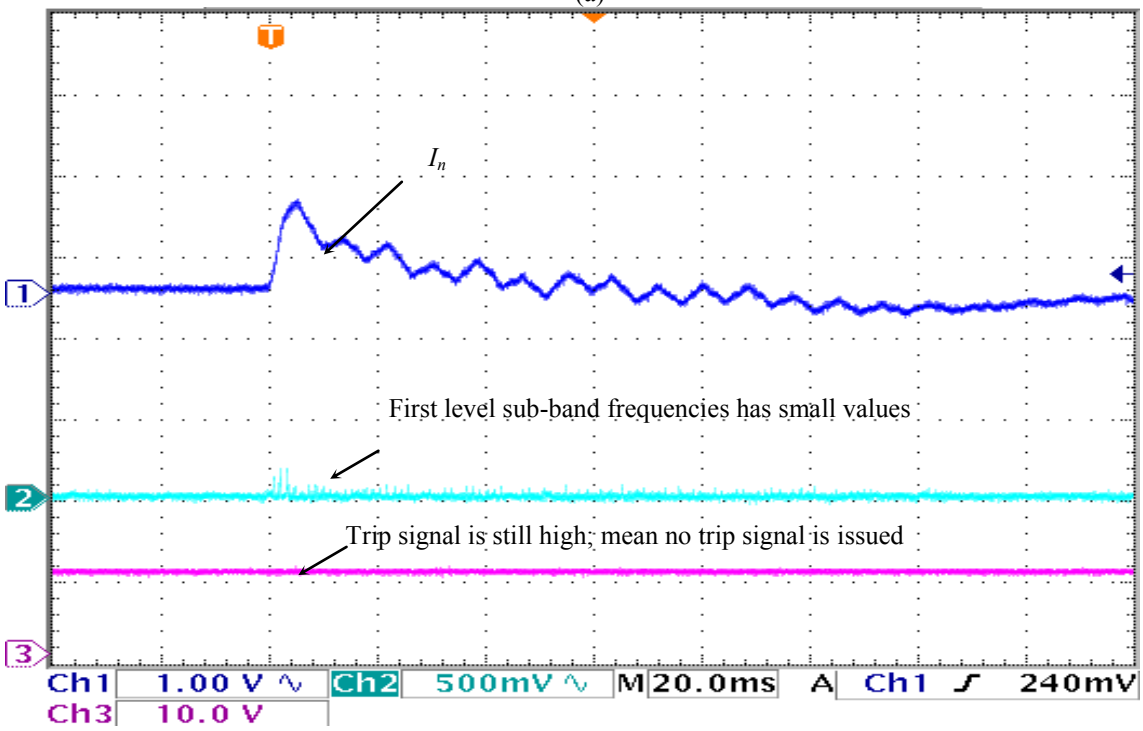

(b)

Figure 6-10 The experimental test case of the primary side magnetizing inrush current at induction motor load a) the three-phase magnetizing inrush currents and the 1st level high frequency sub-ban,d b) $I_n = I_d^2+I_q^2$ current components the 1st level high frequency sub-band: the trip signal is still high, means no trip signal is issued.

- **Experimental Test Results for Internal Faults:**

In this type of experimental test, all fault tests were performed by solidly connecting two points in the transformer that are involved in the fault, which are represented in the transformer phases and/or the ground through or without resistance. The testing results can be categorized into many different combinations of different conditions of energization and loading. This includes whether the fault has happened during or after the energizing of the power transformer at different loading conditions, in addition to the location of the fault, whether it is at the primary or secondary side of the power transformer. Several hundred tests were carried out for different types of faults and it has been observed that the proposed technique has never misrecognized any faulted condition among all the above-mentioned testing cases. A few samples of the results are provided as demonstrated in the Figures (6.11-6.29) for different types of faults at different conditions of loading and locations. It is clear from the figures that, the proposed dqWPT technique is able to detect the faulted conditions and, hence, a trip signal was issued within a few milliseconds. It is worth mentioning that throughout the hundreds of faults that were created; the proposed dqWPT technique has never misrecognized any faulted conditions. The proposed dqWPT technique provided a satisfactory performance both for load and no load conditions, and these results prove its efficacy. Some of these cases are described in detail. It should be noted, in all figures, that there is a time delay between the trip signal and the interruption of the current in the circuit. This is due to the fact that the Triac switches take some time to transition from the ON state to the OFF state, which is not a problem in practical applications, in which mechanical circuit breakers are used and sometimes they take longer for the opening time. It should be mentioned that all the faults were carried out with the source line-to-line voltages

less than 100V to avoid the high fault currents that may destroy the testing equipment or cause an excessive saturation to the current transformers.

a) *Primary Single Line to Ground Fault*

It is important to test the performance of the proposed dqWPT technique at loaded conditions. This experimental fault test was carried out by solidly short-circuiting the primary side, phase B to the ground when the transformer was connected to a balanced inductive load of $Z = 343 + j171.4\ \Omega$/phase. Figure ***6-11*** shows the three-phase differential currents, the first level high frequency sub-band and the trip signal. It is worth mentioning that, in this test, there is no inrush effect on the fault, because the fault happened long after the transformer was energized. The algorithm has successfully identified the fault and issued a trip signal in about 3 msec. The proposed algorithm has been tested experimentally several times under such conditions of different single-phase to ground faults, for which the dqWPT-based protection algorithm has correctly recognized a fault and issued a trip signal to isolate this fault. Similar results were obtained by performing this test on the other two, phases B and C, at different loading conditions. A few other samples of the results are provided in Figure ***6-12***, Figure ***6-13*** and Figure ***6-14***. The proposed dqWPT technique responded correctly again in all cases and most of them were within 5 msec of the fault inception.

b) Secondary Line to line faults

This fault test was carried out experimentally by solidly short-circuiting two phases at a time on the secondary side of the power transformer. Figure ***6-15*** depicts the three-phase differential currents of phase B to phase C to ground, the first level high frequency sub-band

and the trip signal for an unloaded faulted transformer. It is worth mentioning that, in this test, there is no inrush effect on the fault, because the fault happened long after the transformer was energized. It has been observed that the proposed dqWPT technique produced the trip signal and it went down to zero in about one msec after the beginning of the fault in order to protect the transformer against the fault. As a result, the proposed algorithm did not misidentify any line to line to ground fault. In addition, similar kinds of tests were carried out in the other two pairs of phases, namely, faults between phases B and A, and between phases C and A. These extra results are provided in Figure ***6-16***, Figure ***6-17***, and Figure ***6-18***. Finally, the performance of the proposed dqWPT technique was tested as well for the case of load existence. The proposed dqWPT technique was able to respond properly in all cases and most of them were within 3 msec of the fault inception.

c) Secondary Three-Phase Faults

This fault test is carried out by connecting the three-phases solidly to each other on the primary side of the power transformer when the transformer was connected to a balanced inductive load of $\mathrm{Z} = 343 + \mathrm{j}171.4\ \Omega$/phase. In Figure ***6-19***, the differential fault currents and the trip signal are shown. In this test, there is no effect of the inrush on the fault, because the fault happened long after the transformer was energized. The algorithm identified the fault and issued a trip signal in less than 3 msec. In addition, the proposed algorithm has never misidentified the three-phase fault. A few other samples of the results are provided in Figure ***6-20*** and Figure ***6-21***. The proposed dqWPT technique responded correctly again in all cases.

d) Secondary single line to ground fault, through resistance

This test was carried out by solidly connecting phase C to ground through resistance on the secondary side of the three-phase power transformer. Figure ***6-22*** shows clearly the experimental results of the differential fault currents and the trip signal. It is worth mentioning that, in this test, there is no inrush effect on the fault, because the fault happened long after the transformer was energized. The proposed dqWPT algorithm again made the right decision against the faulted condition and issued a trip signal in just 4 msec, as is obvious in the figure. In addition, the proposed algorithm has been tested several times under faulted conditions, for which the dqWPT-based protection algorithm has never misidentified any fault. Similar results were obtained by performing this test on the other two Phases A and B. A few other samples of the results are provided in Figure ***6-23***, Figure ***6-24***, Figure ***6-25***, Figure ***6-26***, and Figure ***6-27***. The proposed technique responded correctly again in all cases and most of them were within 3 msec of the fault inception.

e) Secondary side Turn to Turn fault

This test procedure was done by solidly short-circuiting the 550 and 600V taps in phase A. Figure ***6-28*** show the proposed dqWPT technique responses and the differential currents in three-phase fault currents, and the fault occurred later after energizing the transformer. It should be noted that the fault current magnitude is relatively low in this type of fault. However, the proposed dqWPT technique recognized the fault and issued the trip signal within 3 msec. Similar result is provided for the same fault on the phase B in Figure ***6-29***.

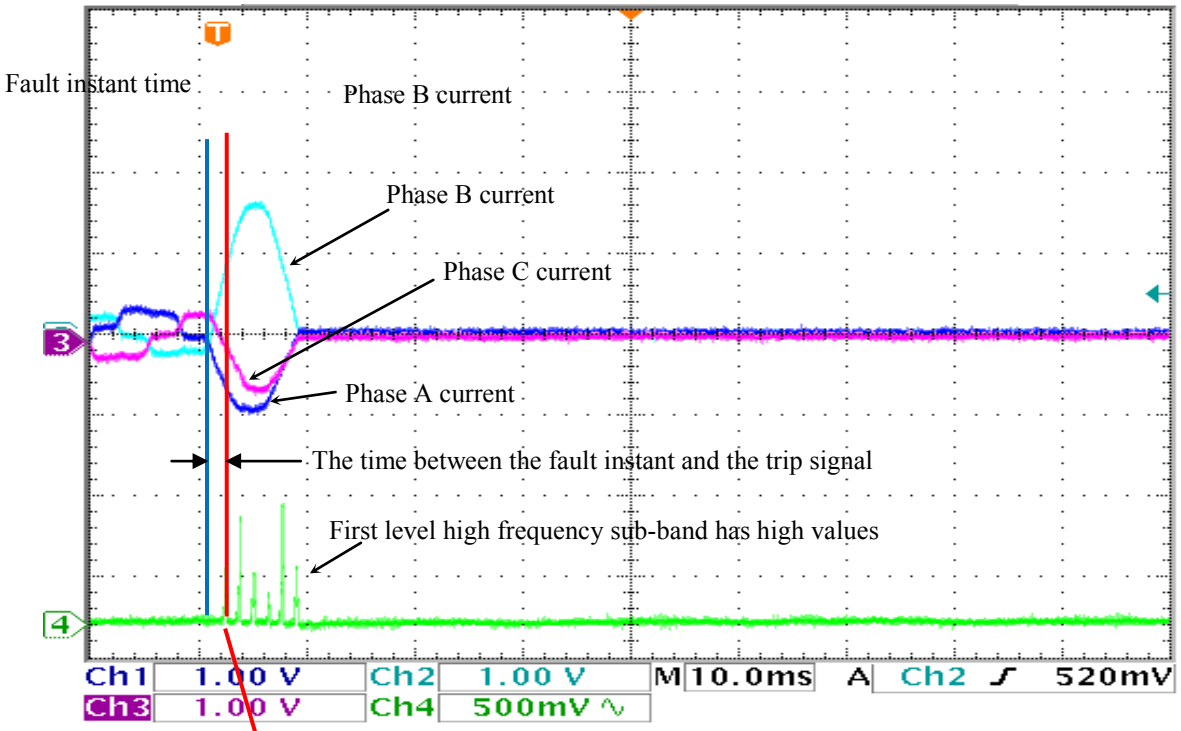

(a)

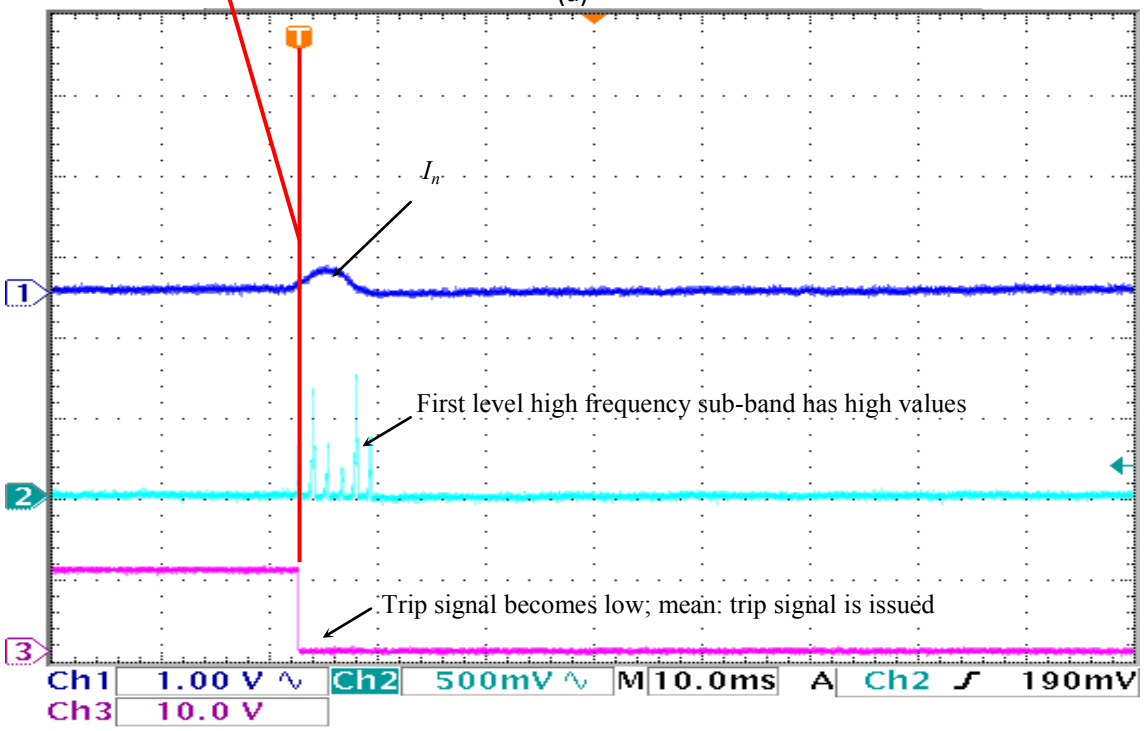

(b)

Figure 6-11 The experimental testing case of primary single line B to ground fault at non-linear load a) the three-phase transformer currents the 1st level high frequency sub-band b) $I_n = I_d^2 + I_q^2$ current components and the 1st level high frequency sub-band: the trip signal becomes low means the trip signal is issued.

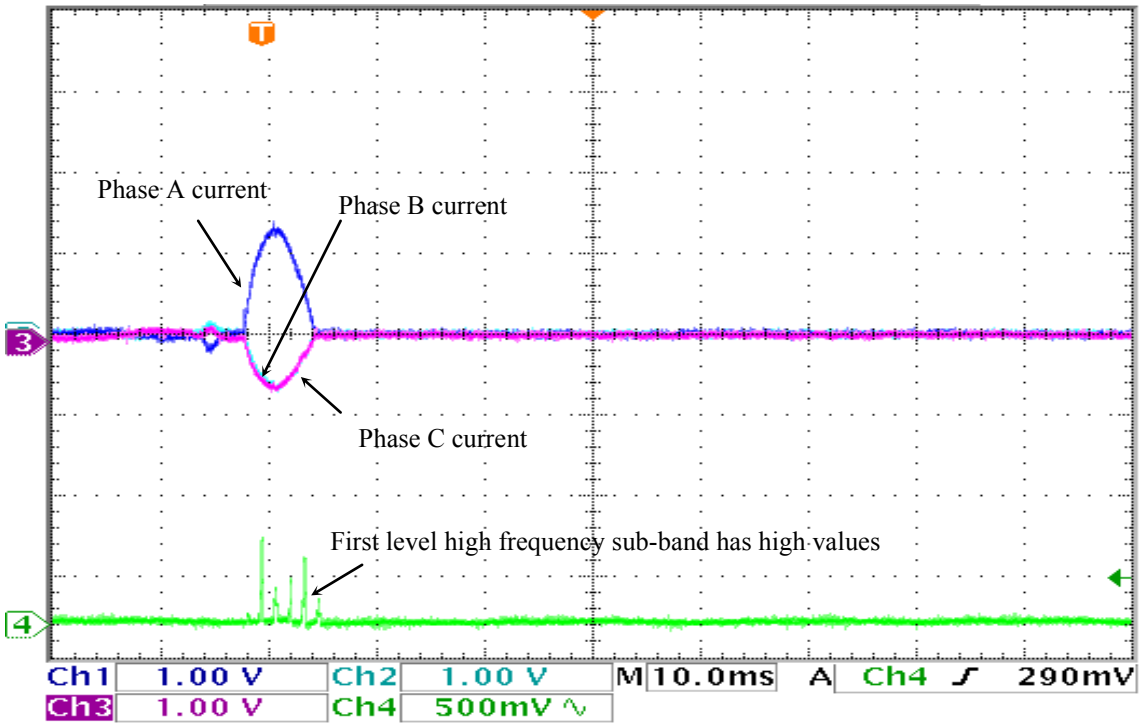

(a)

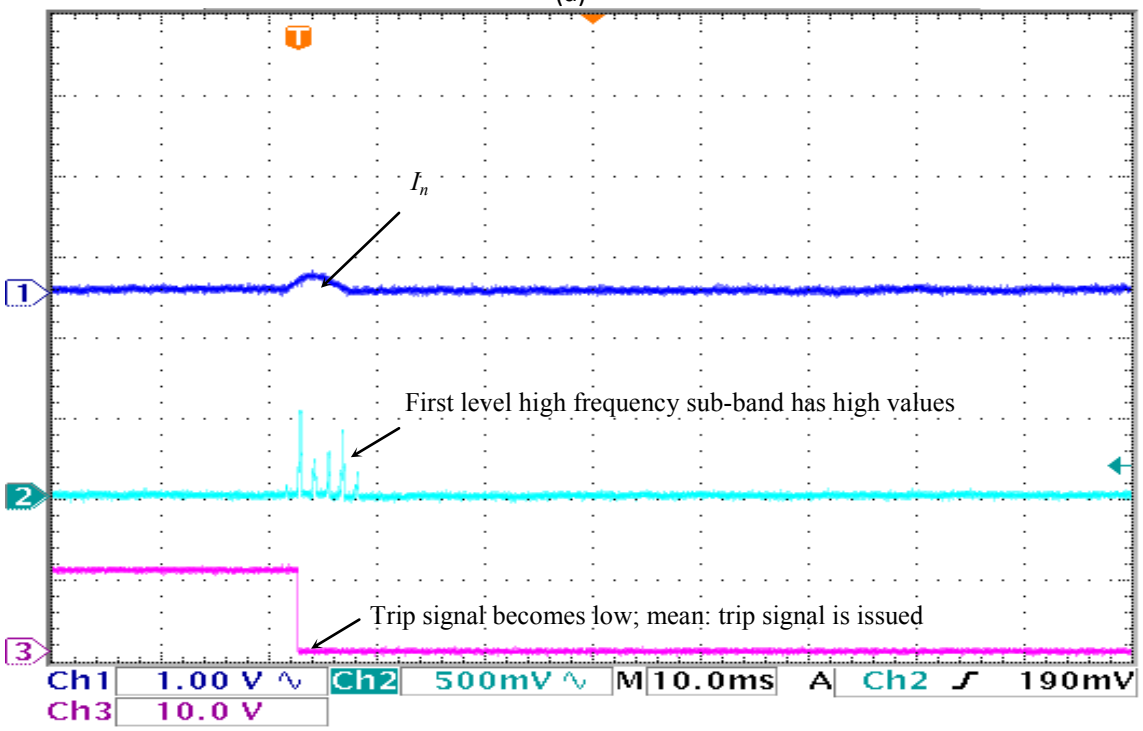

(b)

Figure 6-12 The experimental testing case of unloaded primary single line A to ground fault a) the three-phase transformer currents the 1st level high frequency sub-band b) dq current components and the 1st level high frequency sub-band: the trip signal becomes low means the trip signal is issued.

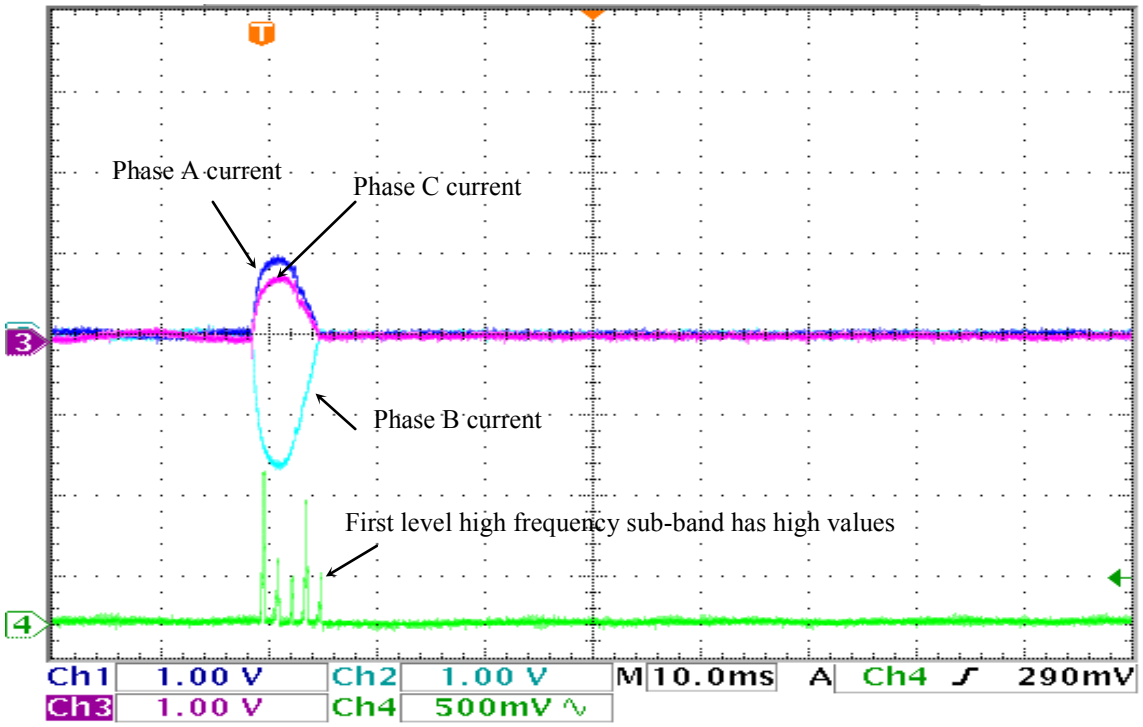

(a)

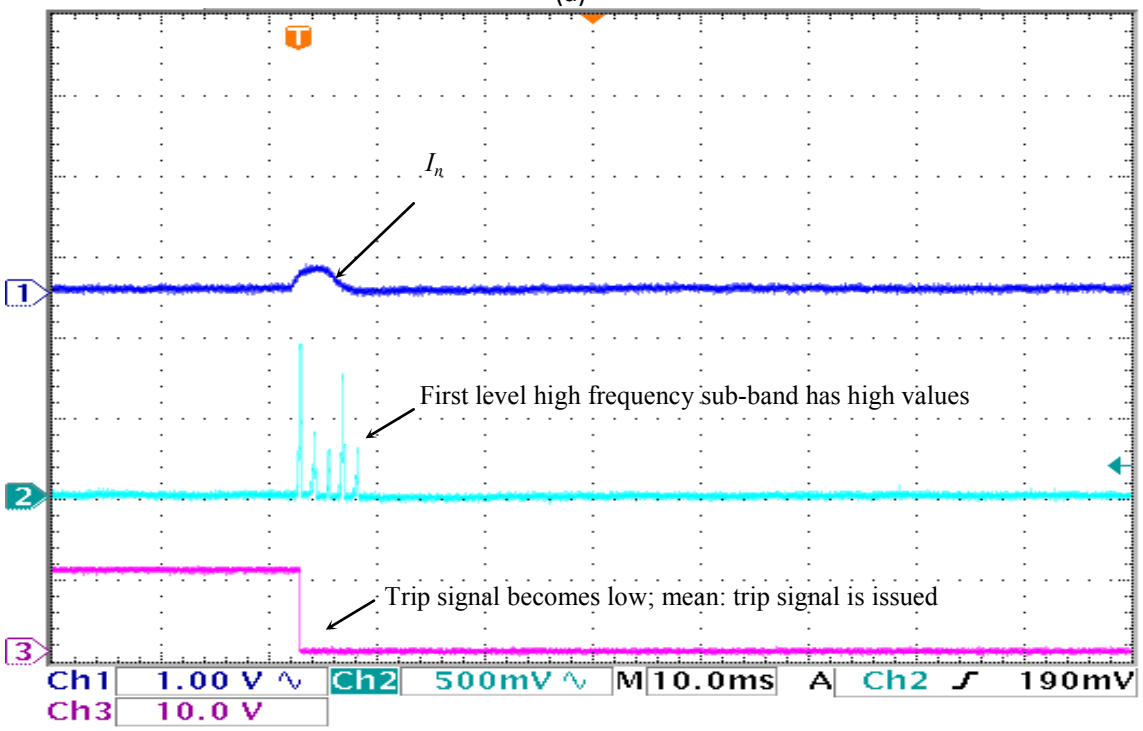

(b)

Figure 6-13 The experimental testing case of unloaded primary single line B to ground fault a) the three-phase transformer currents the 1st level high frequency sub-band b) $I_n = I_d^2+I_q^2$ current components and the 1st level high frequency sub-band: the trip signal becomes low means the trip signal is issued.

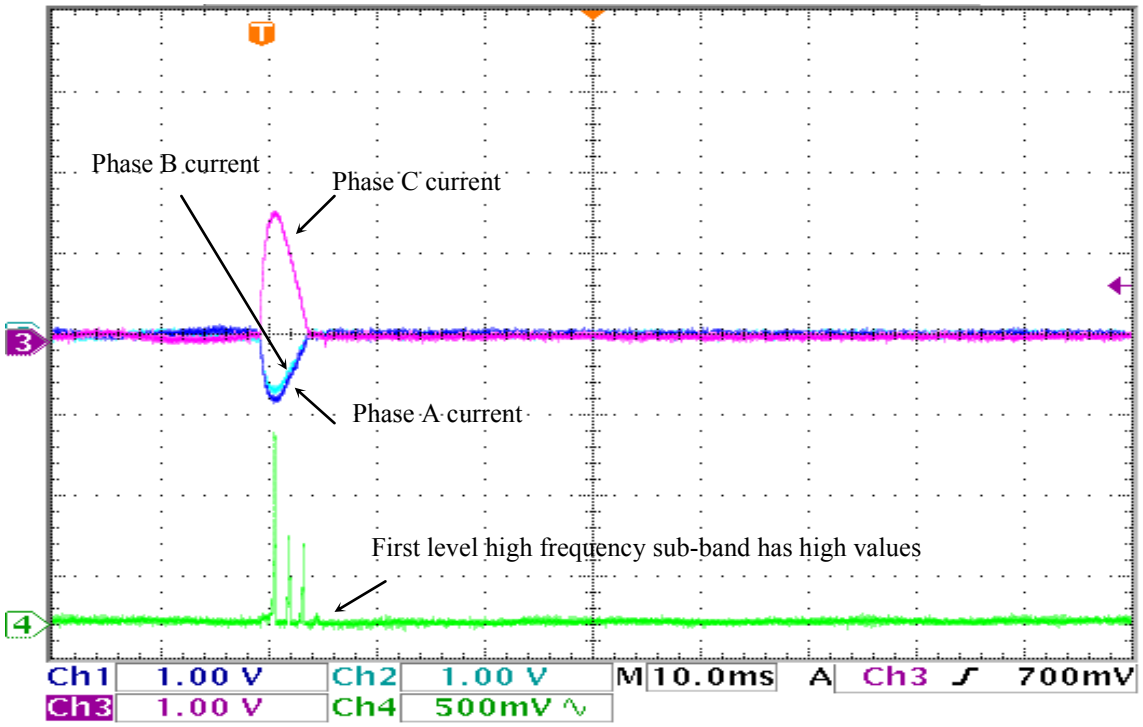

(a)

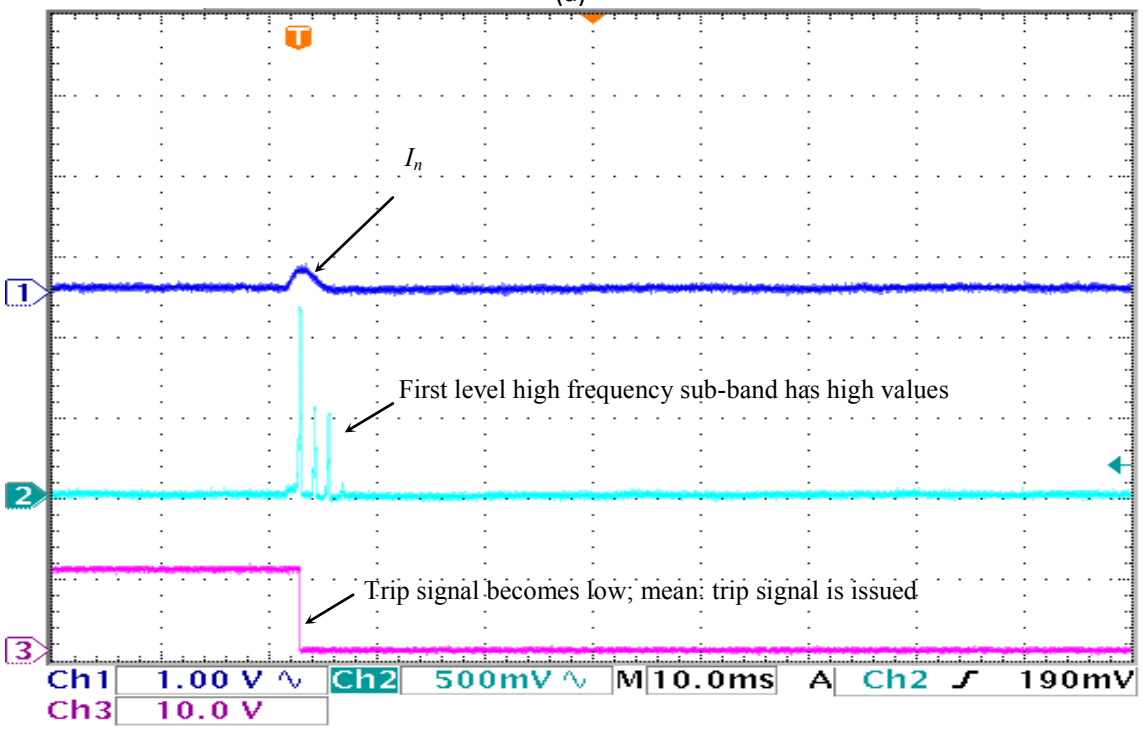

(b)

Figure 6-14 The experimental testing case of unloaded primary single line C to ground fault a) the three-phase transformer currents the 1st level high frequency sub-band b) $I_n = I_d^2+I_q^2$ current components and the 1st level high frequency sub-band: the trip signal becomes low means the trip signal is issued.

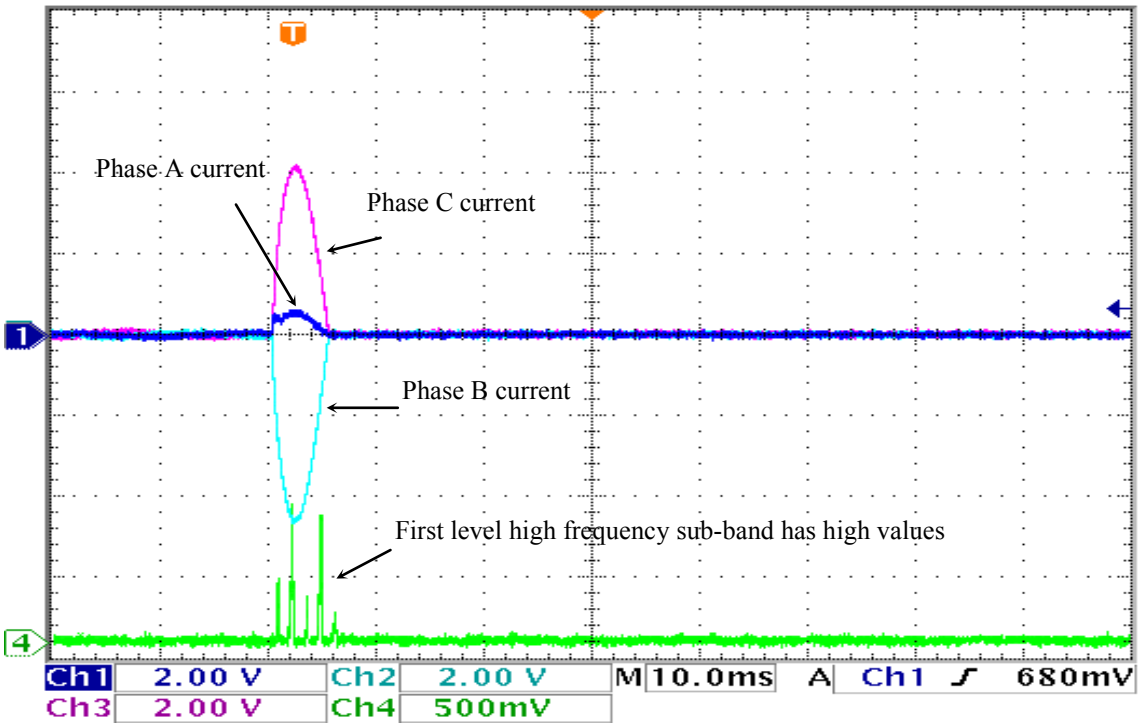

(a)

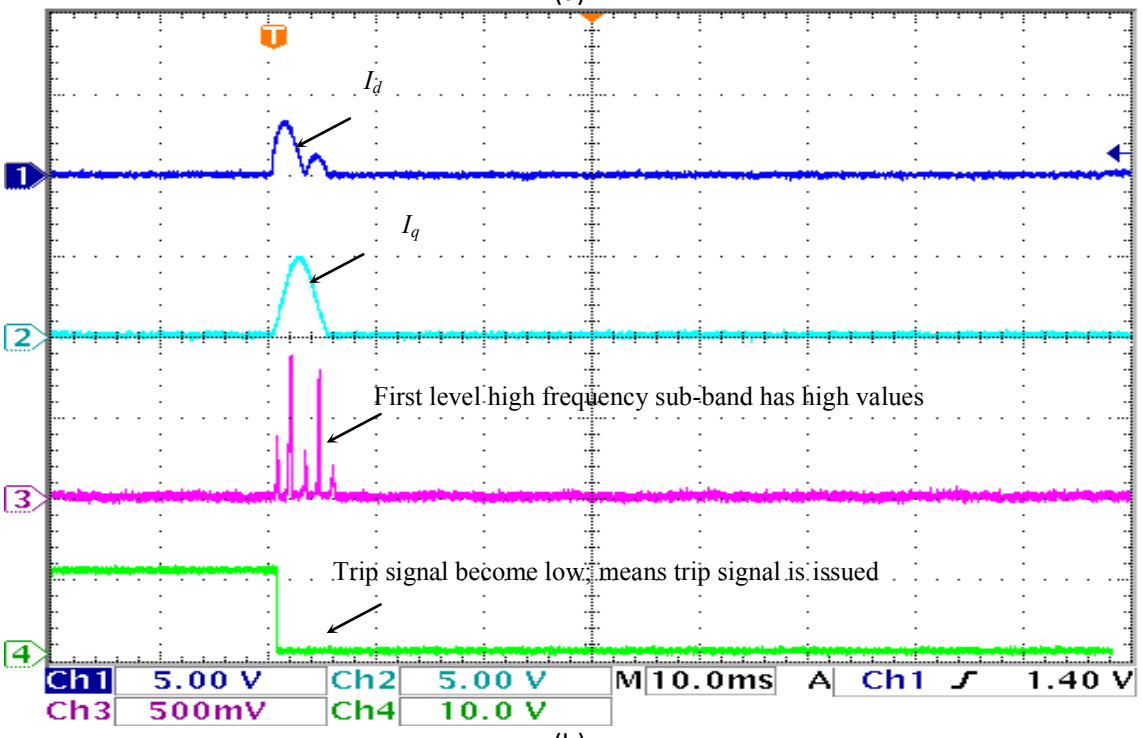

(b)

Figure 6-15 The experimental testing case of unloaded secondary phase C to B fault a) the three-phase unloaded transformer currents and the 1st level high sub-band frequencies b) dq current components and the 1st level high sub-band frequencies (high value): the trip signal becomes low means the trip signal is issued.

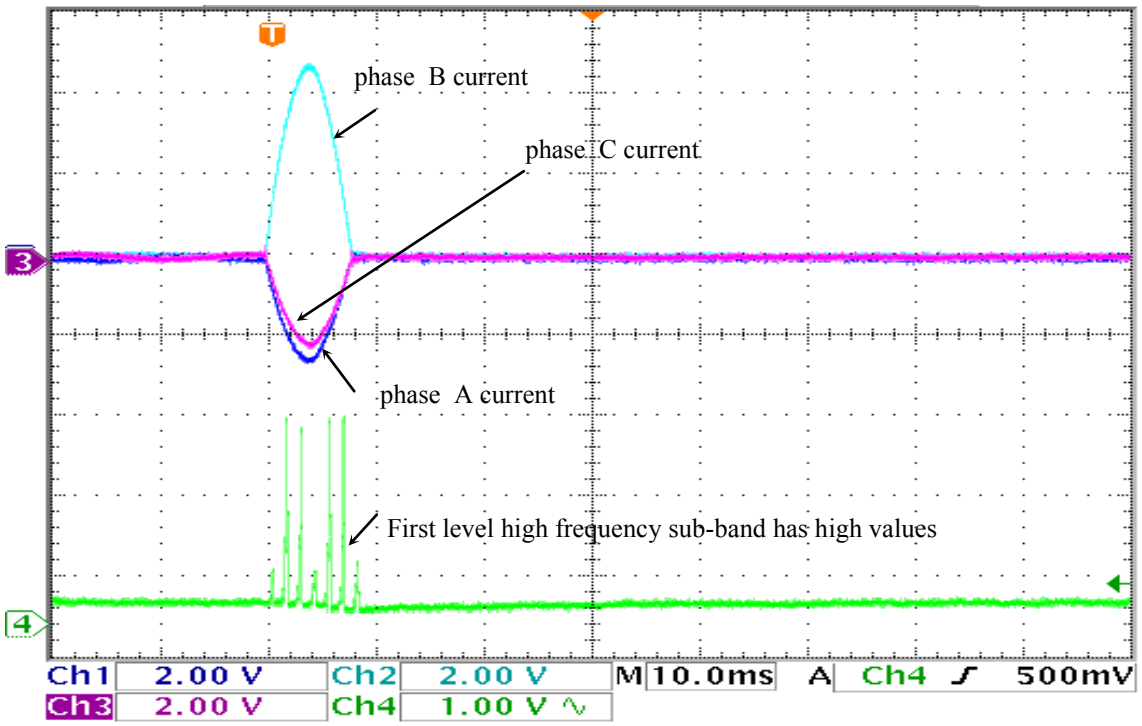

(a)

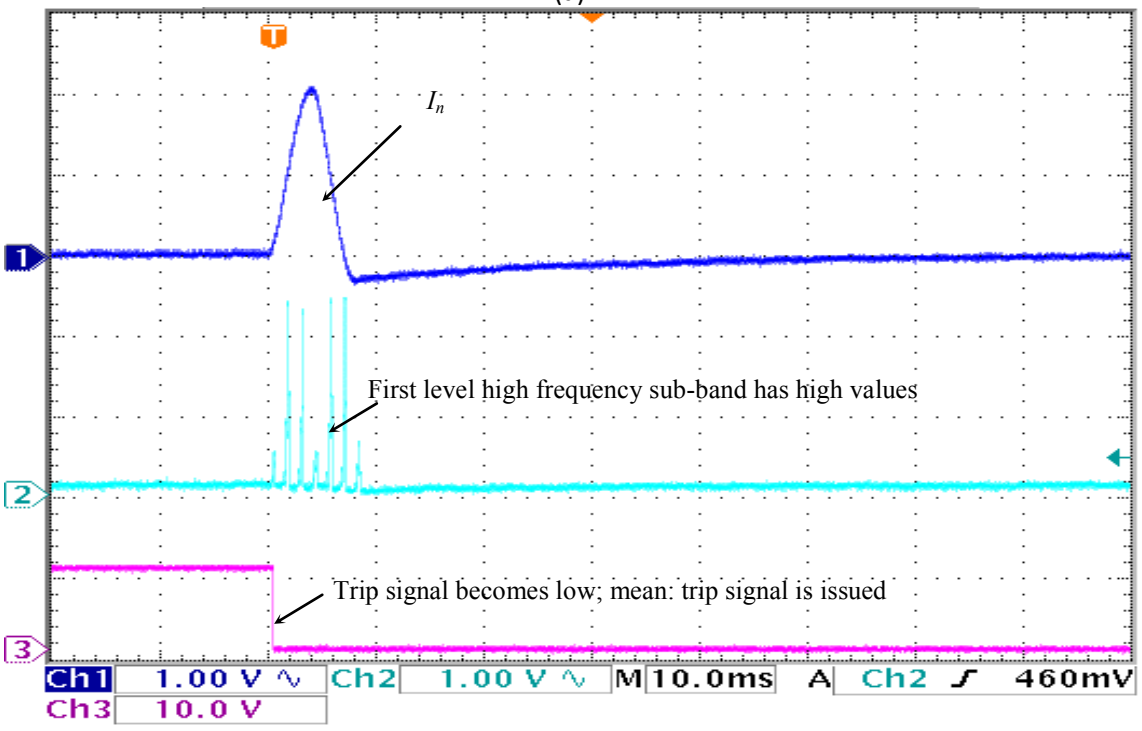

(b)

Figure 6-16 The experimental testing case of unloaded secondary phase B to C to ground fault a) the three-phase transformer currents the 1st level high frequency sub-band b) $I_n = I_d^2+I_q^2$ current components and the 1^{st} level high frequency sub-band: the trip signal becomes low means the trip signal is issued.

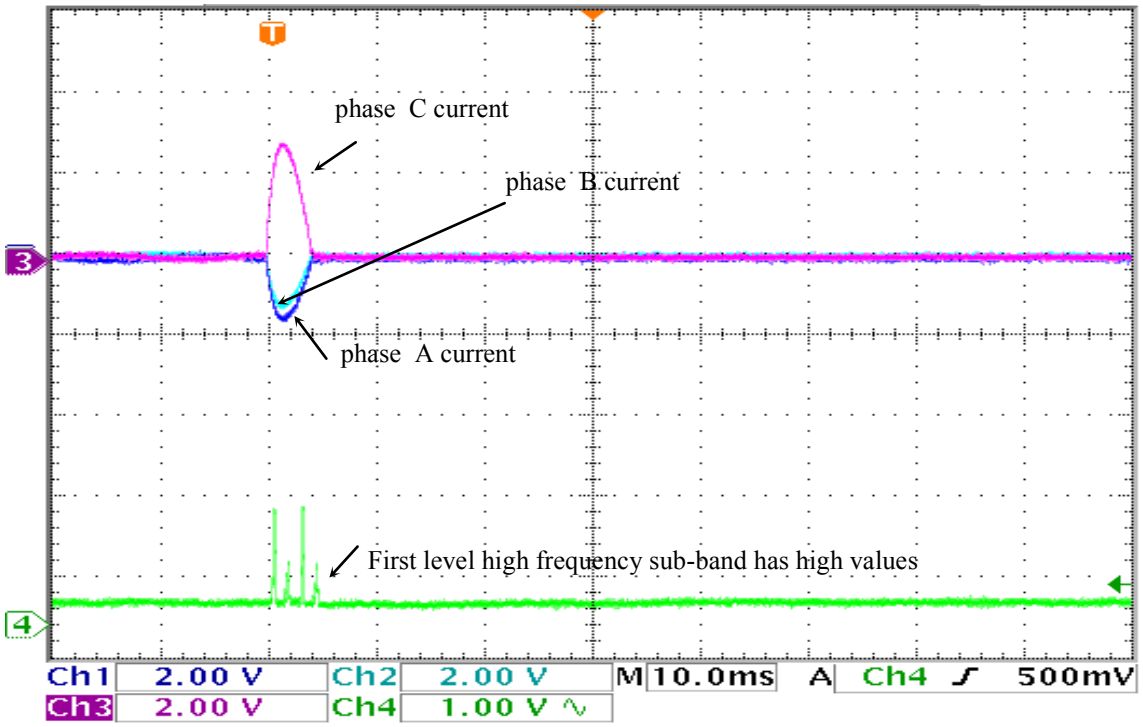

(a)

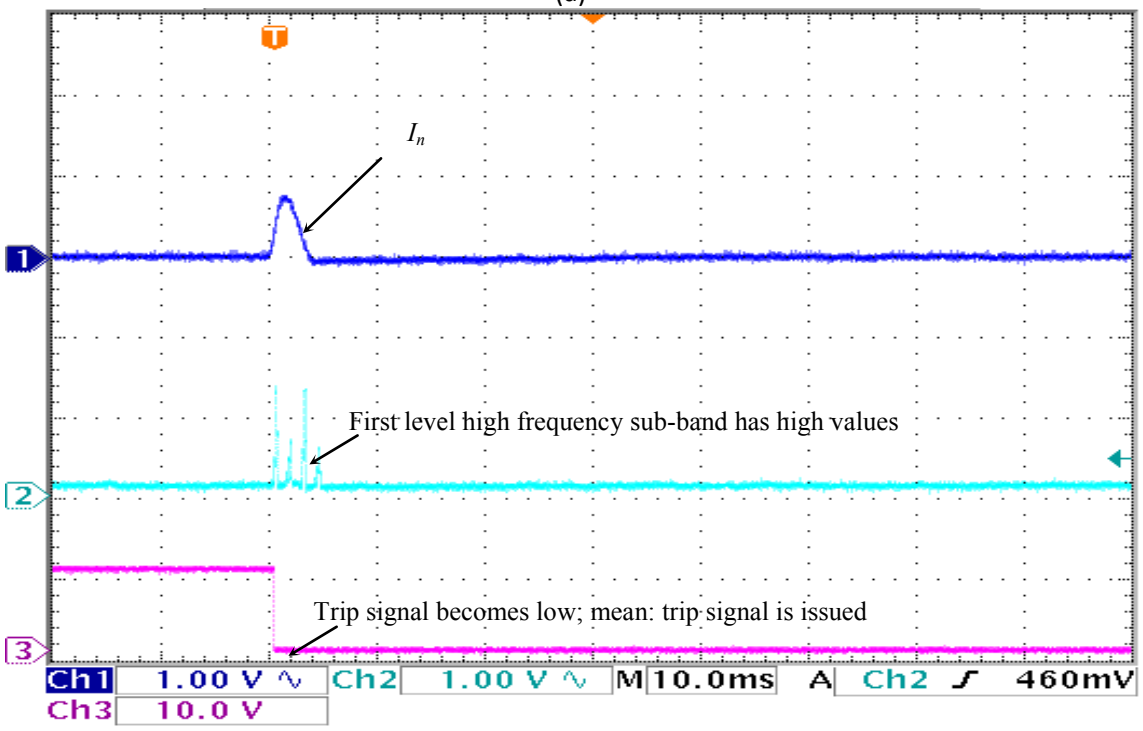

(b)

Figure 6-17 The experimental testing case of unloaded secondary phase C to A to ground fault a) the three-phase transformer currents the 1st level high frequency sub-band b) $I_n = I_d^2+I_q^2$ current components and the 1st level high frequency sub-band: the trip signal becomes low means the trip signal is issued.

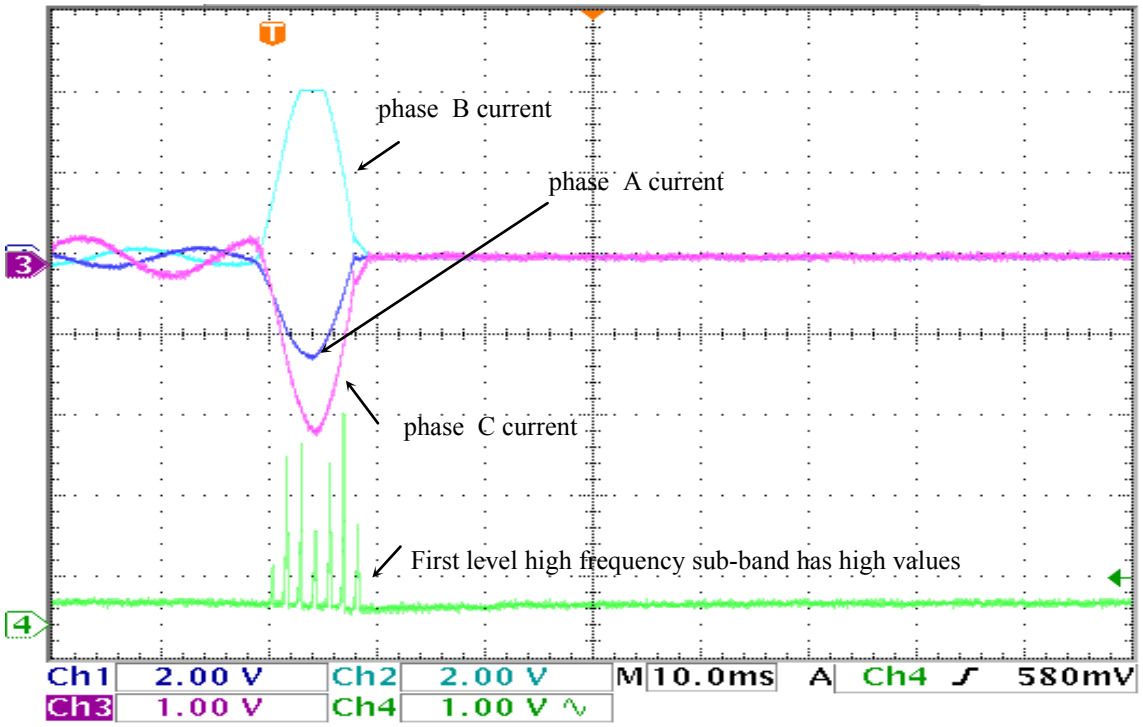

(a)

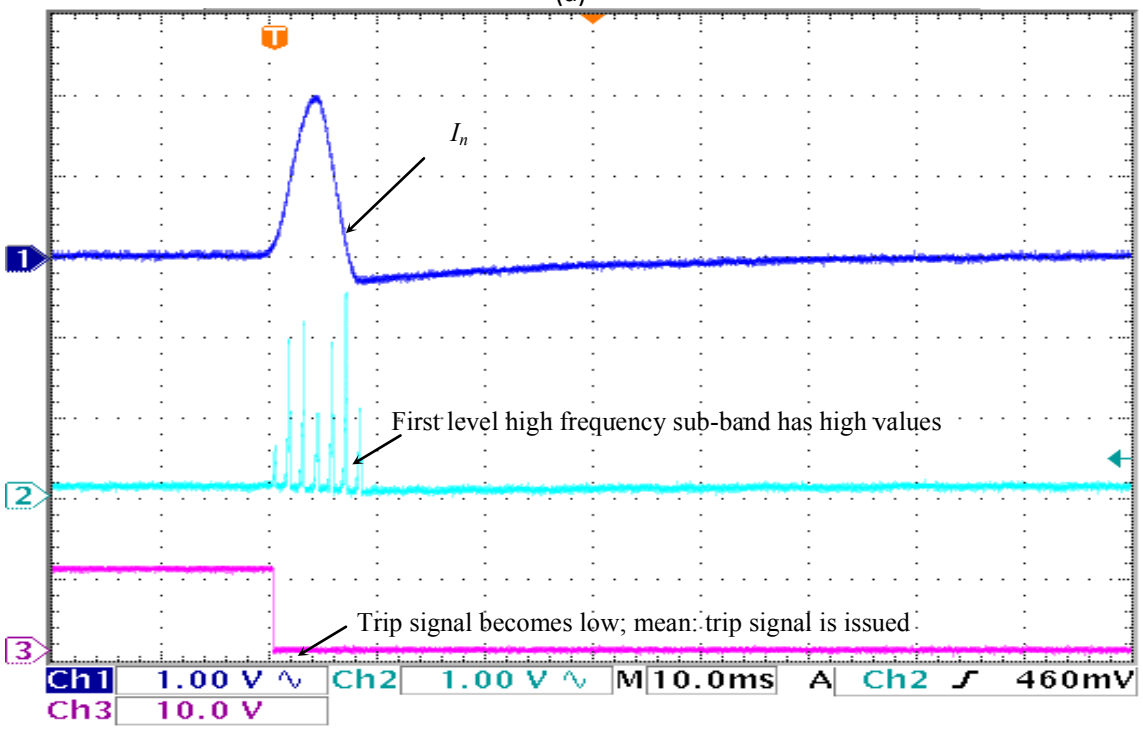

(b)

Figure 6-18 The experimental testing case of secondary phase C to B to ground fault at unbalanced R-L load a) the three-phase transformer currents the 1st level high frequency sub-band b) $I_n = I_d^2 + I_q^2$ current components and the 1st level high frequency sub-band: the trip signal becomes low means the trip signal is issued.

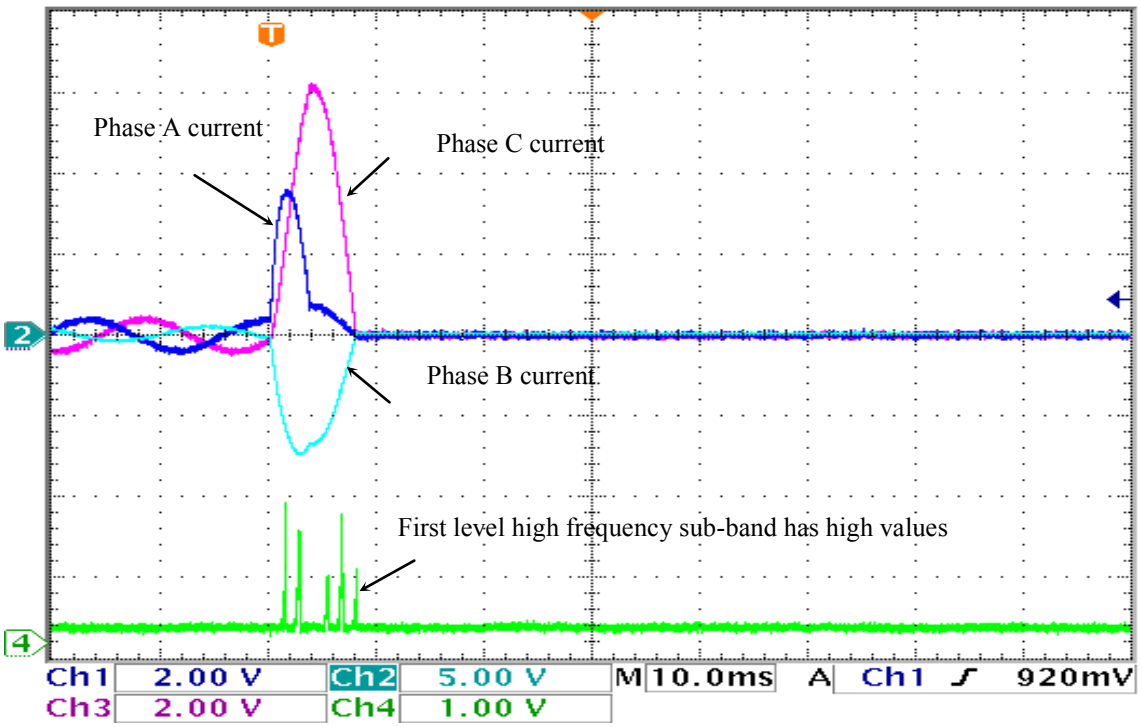

(a)

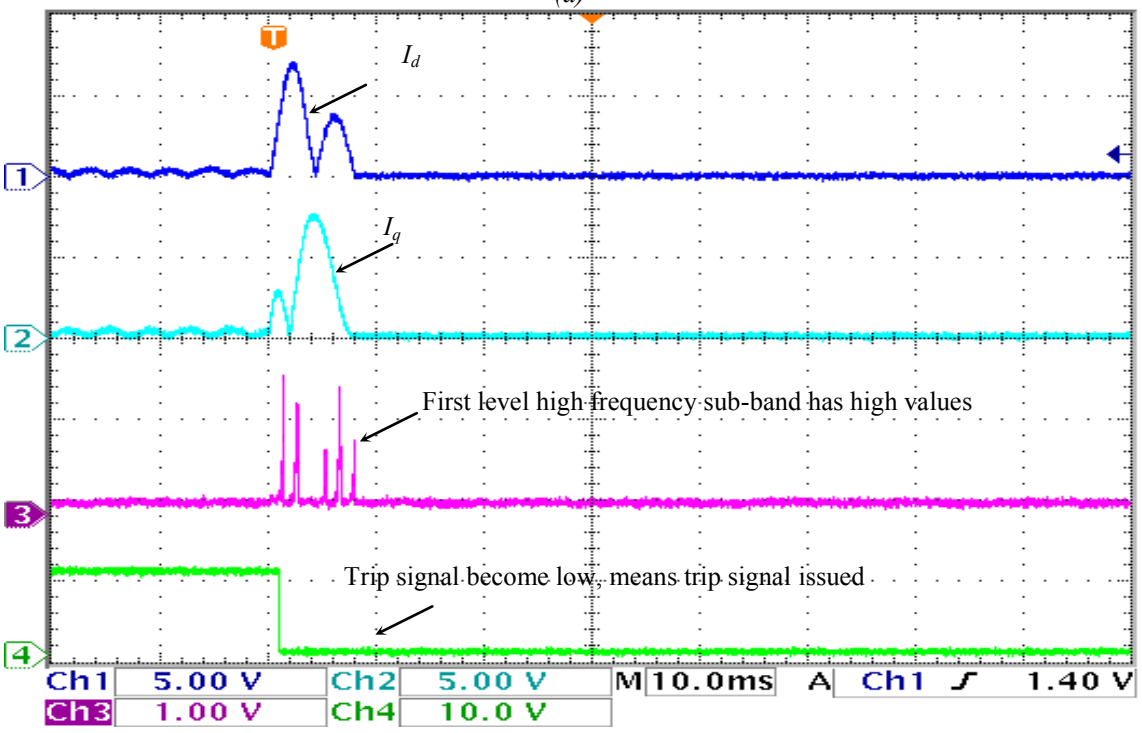

(b)

Figure 6-19 The experimental testing case of secondary three-phase fault at balanced load a) the three-phase unloaded transformer currents and the 1st level high frequency sub-band b) dq current components and the 1st level high frequency sub-band: the trip signal went low, means the trip signal is issued.

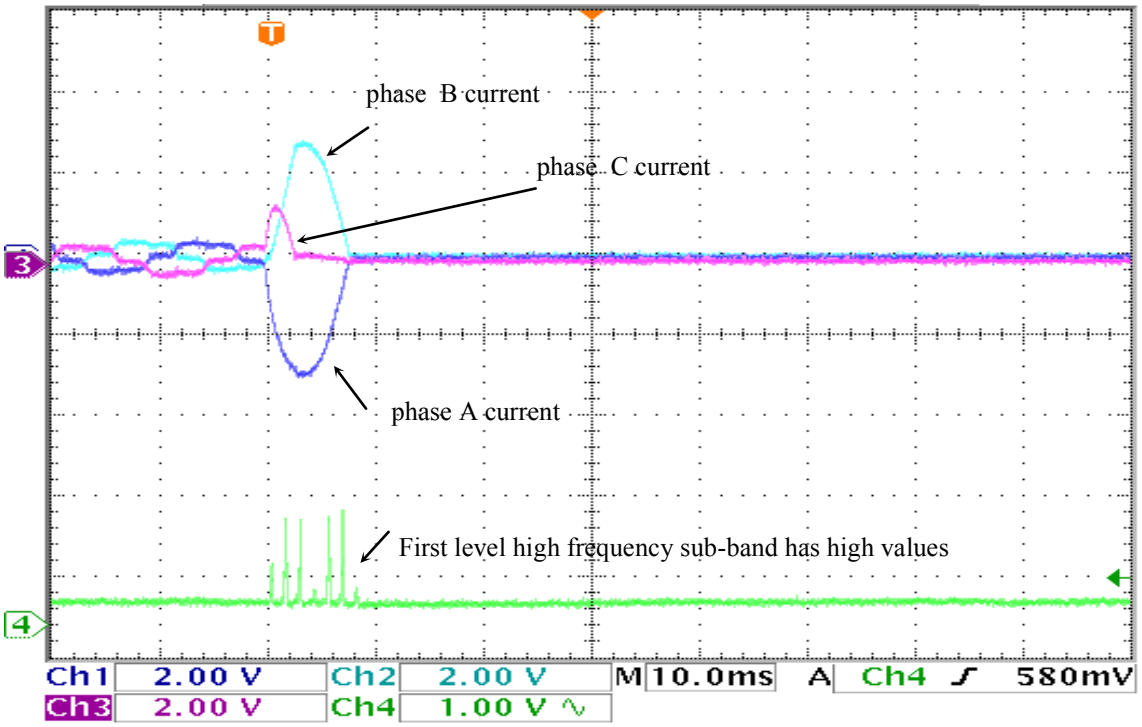

(a)

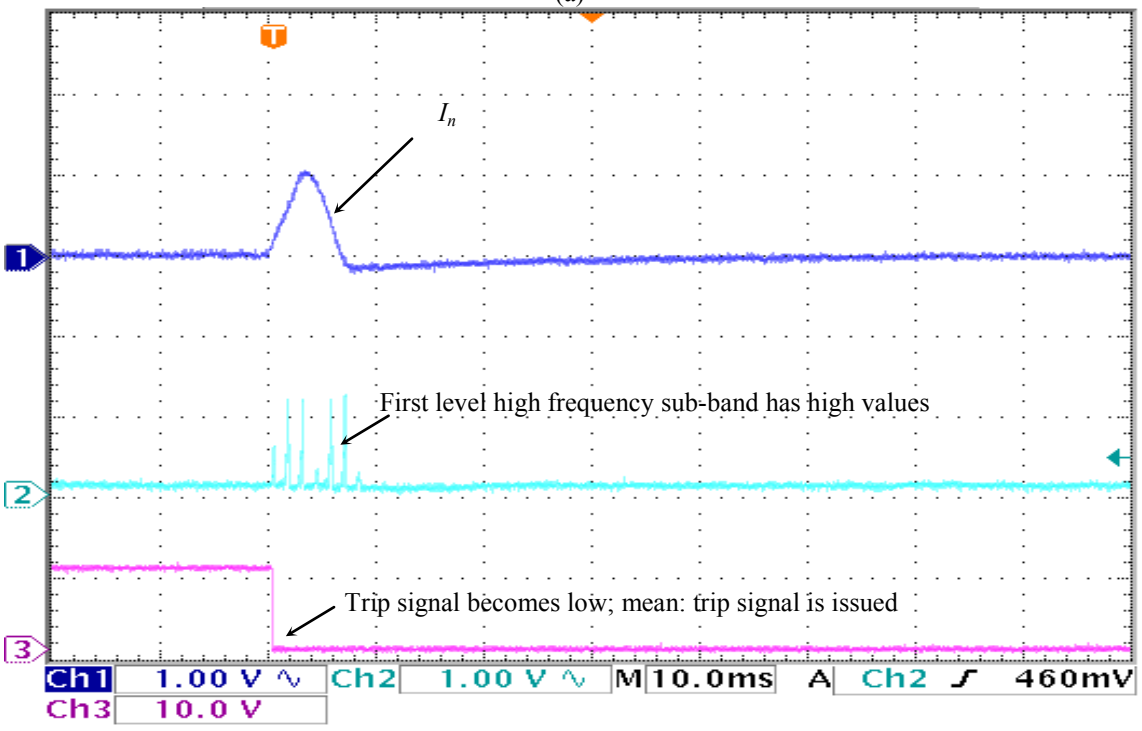

(b)

Figure 6-20 The experimental testing case of the secondary side three-phase Fault at non-linear load a) the three-phase transformer currents the 1st level high frequency sub-band b) $I_n = I_d^2+I_q^2$ current components and the 1st level high frequency sub-band: the trip signal becomes low means the trip signal is issued.

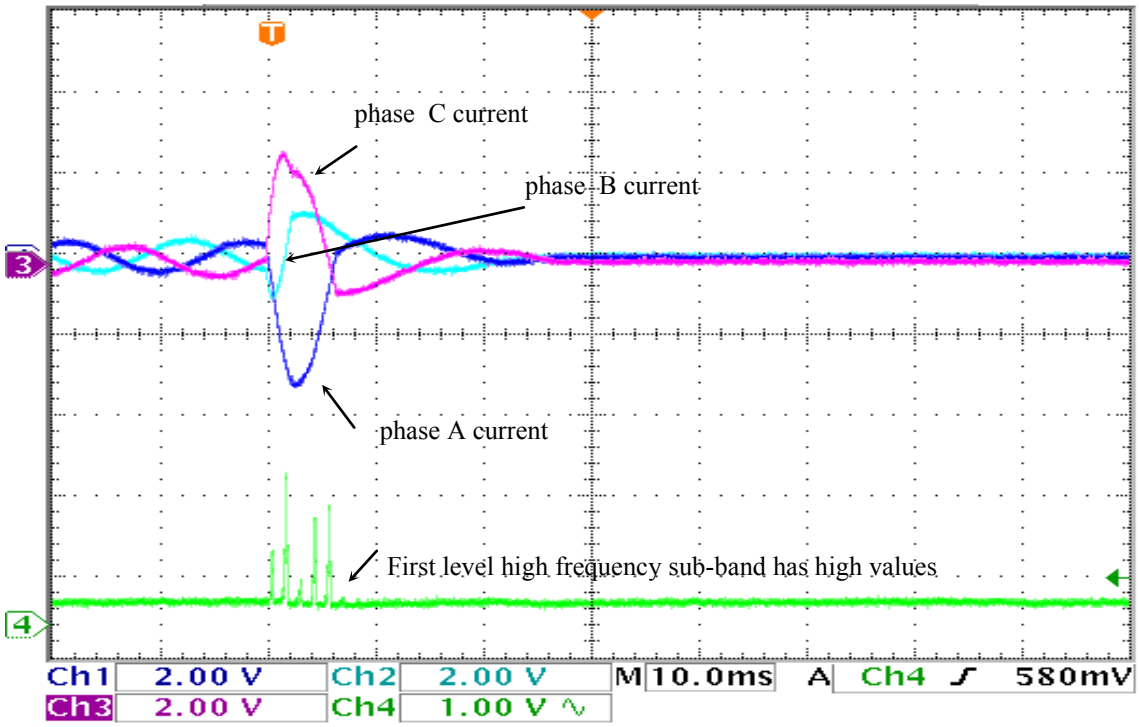

(a)

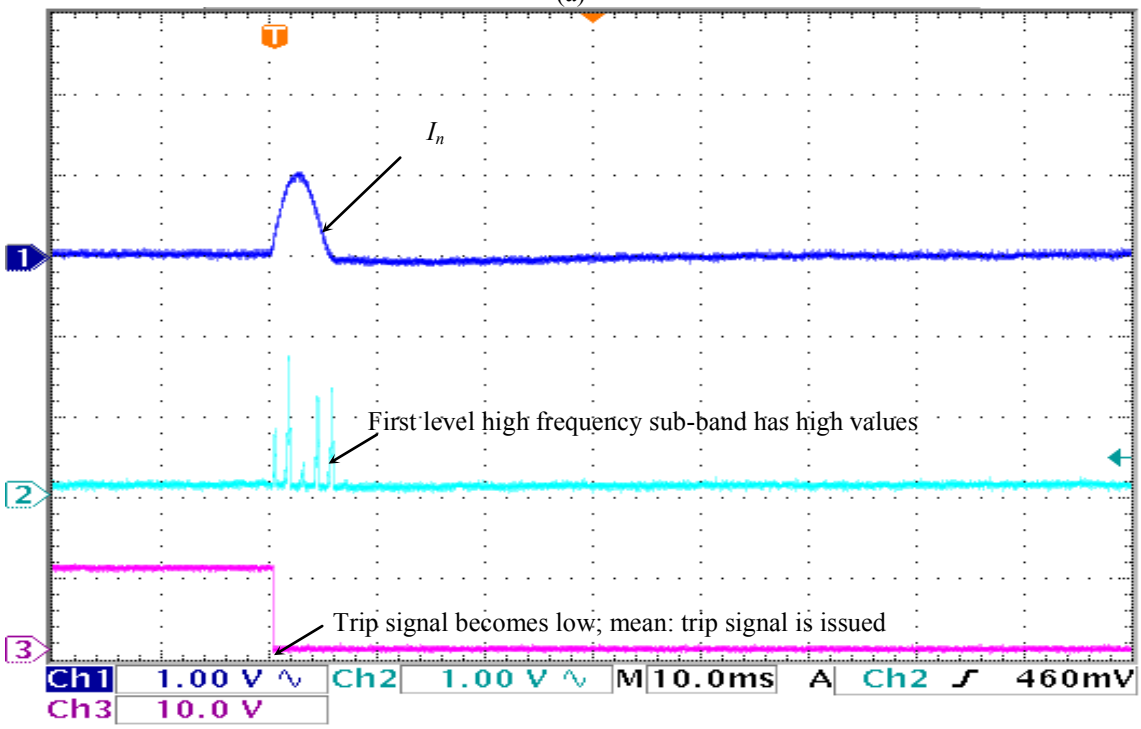

(b)

Figure 6-21 The experimental testing case of the secondary side three-phase Fault at induction motor load a) the three-phase transformer currents the 1st level high frequency sub-band b) $I_n = I_d^2+I_q^2$ current components and the 1st level high frequency sub-band: the trip signal becomes low means the trip signal is issued.

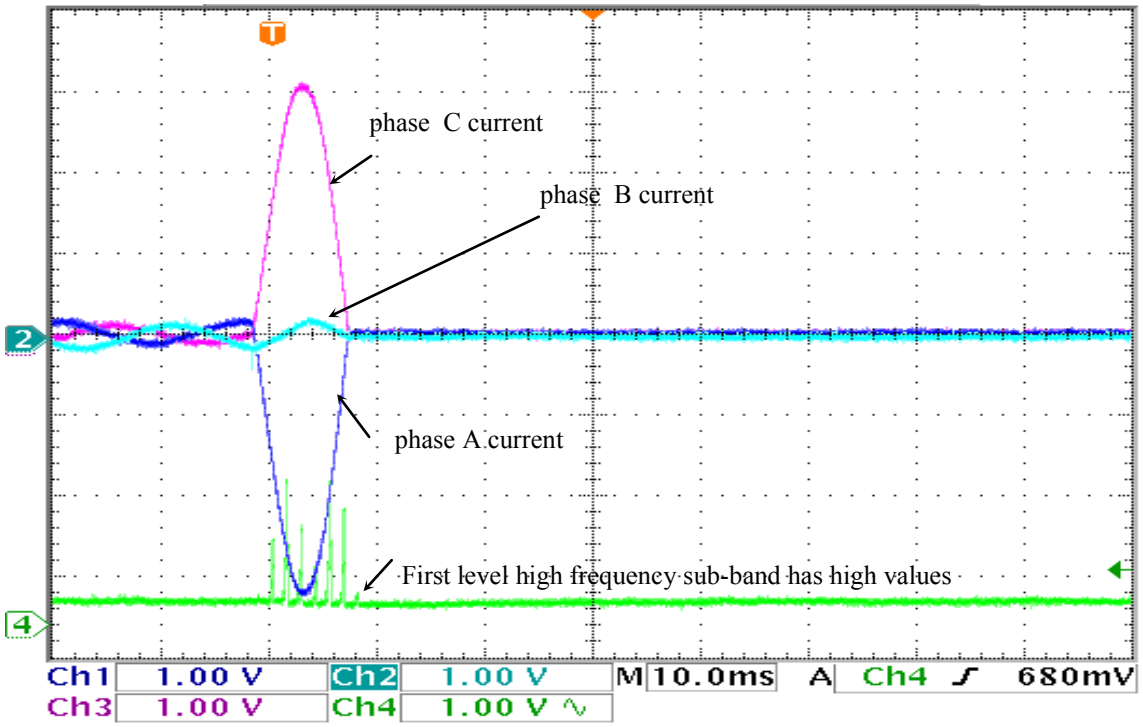

(a)

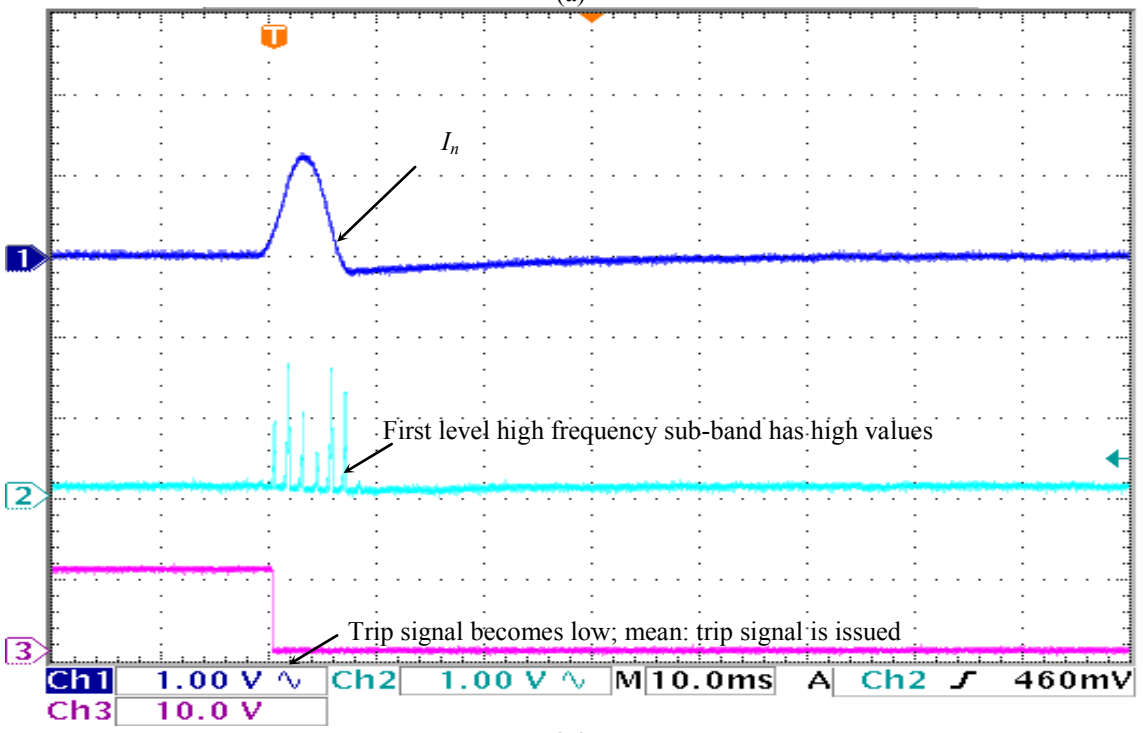

(b)

Figure 6-22 The experimental testing case of secondary Single Line A to Ground Fault at unbalanced load a) the three-phase transformer currents the 1st level high frequency sub-band b) $I_n = I_d^2+I_q^2$ current components and the 1st level high frequency sub-band: the trip signal becomes low means the trip signal is issued.

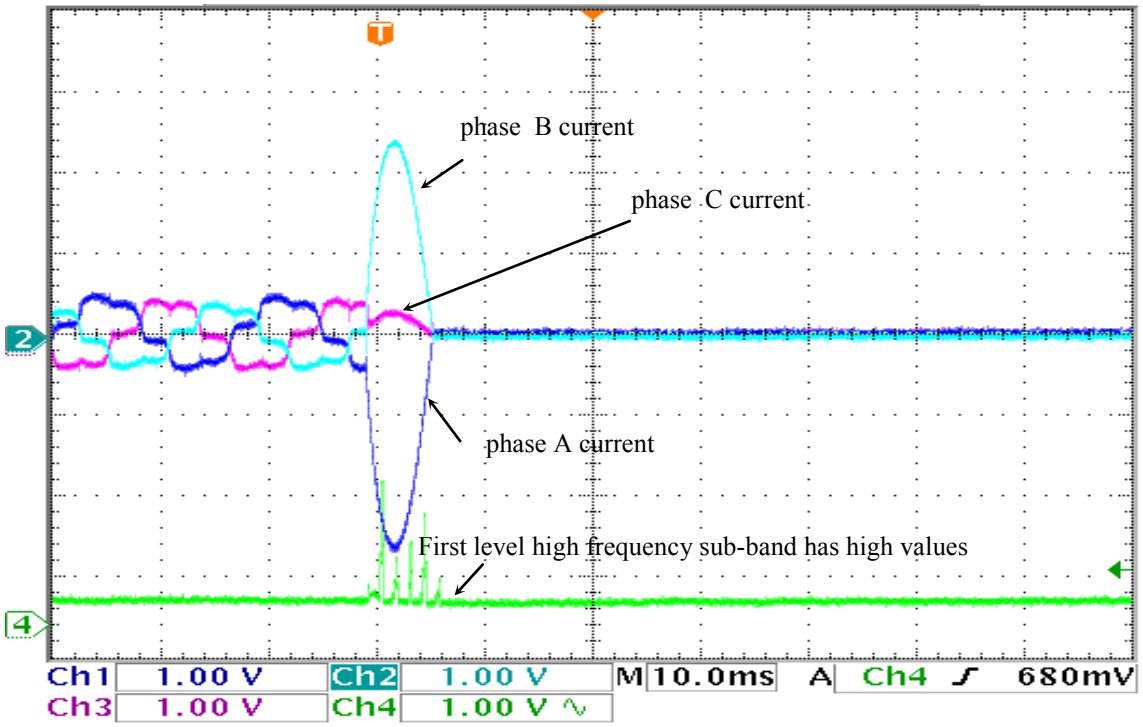

(a)

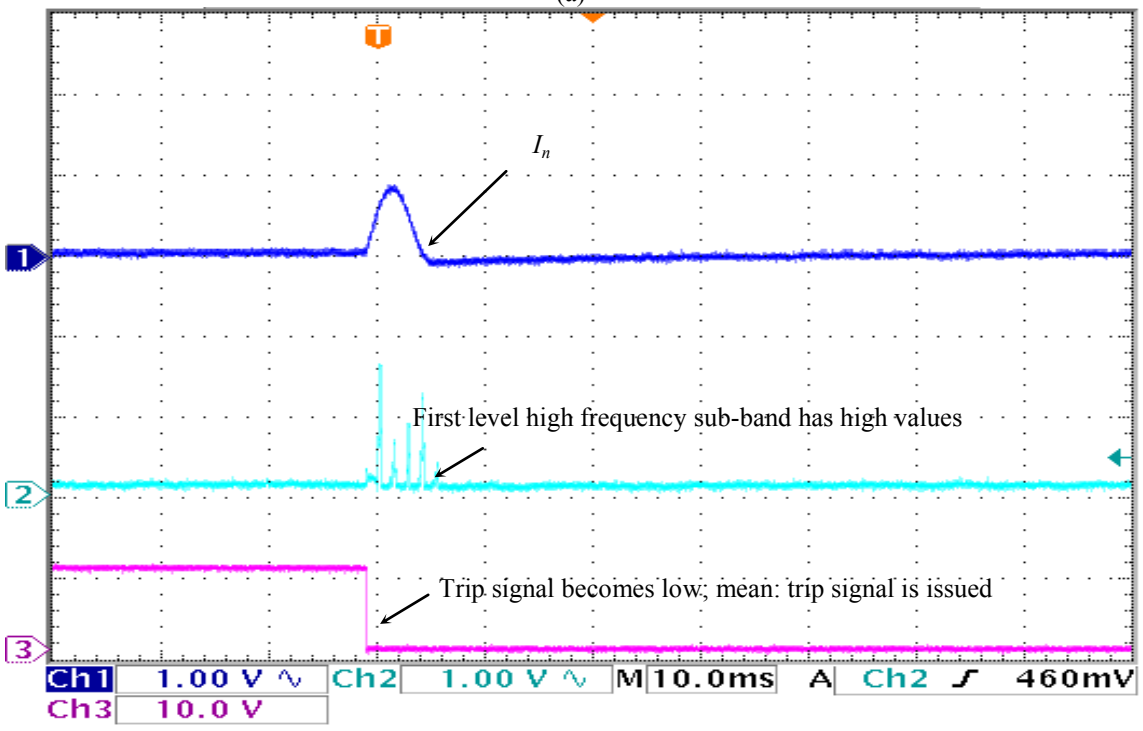

(b)

Figure 6-23 The experimental testing case of secondary Single Line B to ground fault at non-linear load a) the three-phase transformer currents the 1st level high frequency sub-band b) $I_n = I_d^2+I_q^2$ current components and the 1st level high frequency sub-band: the trip signal becomes low means the trip signal is issued.

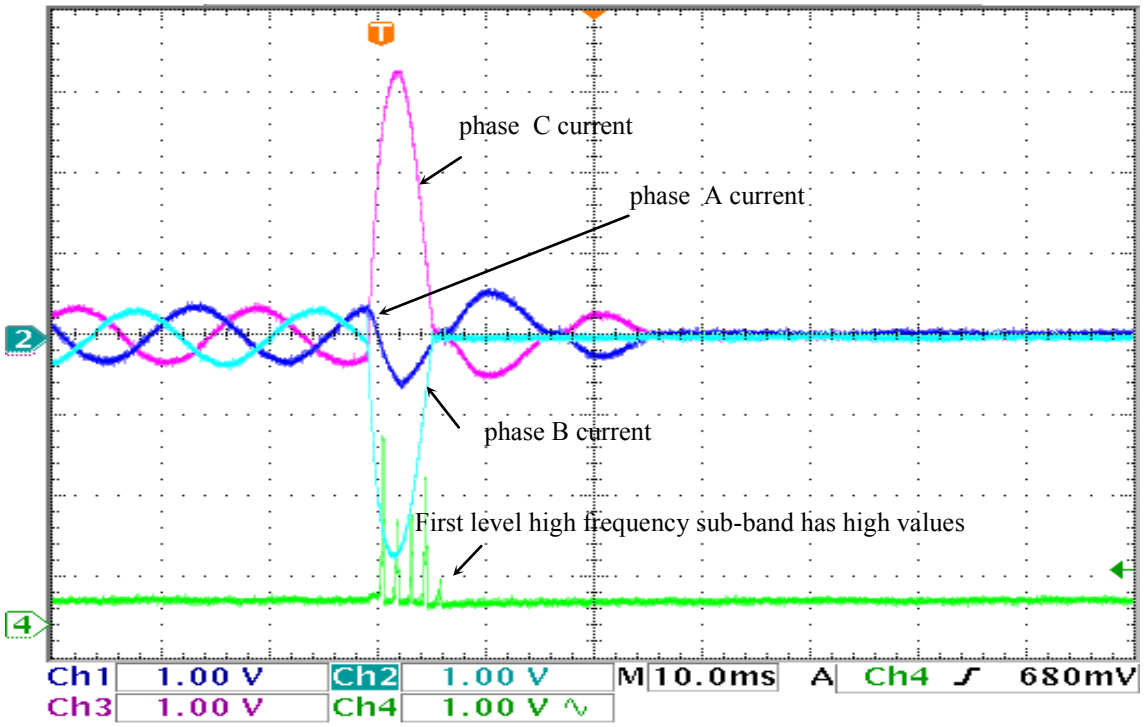

(a)

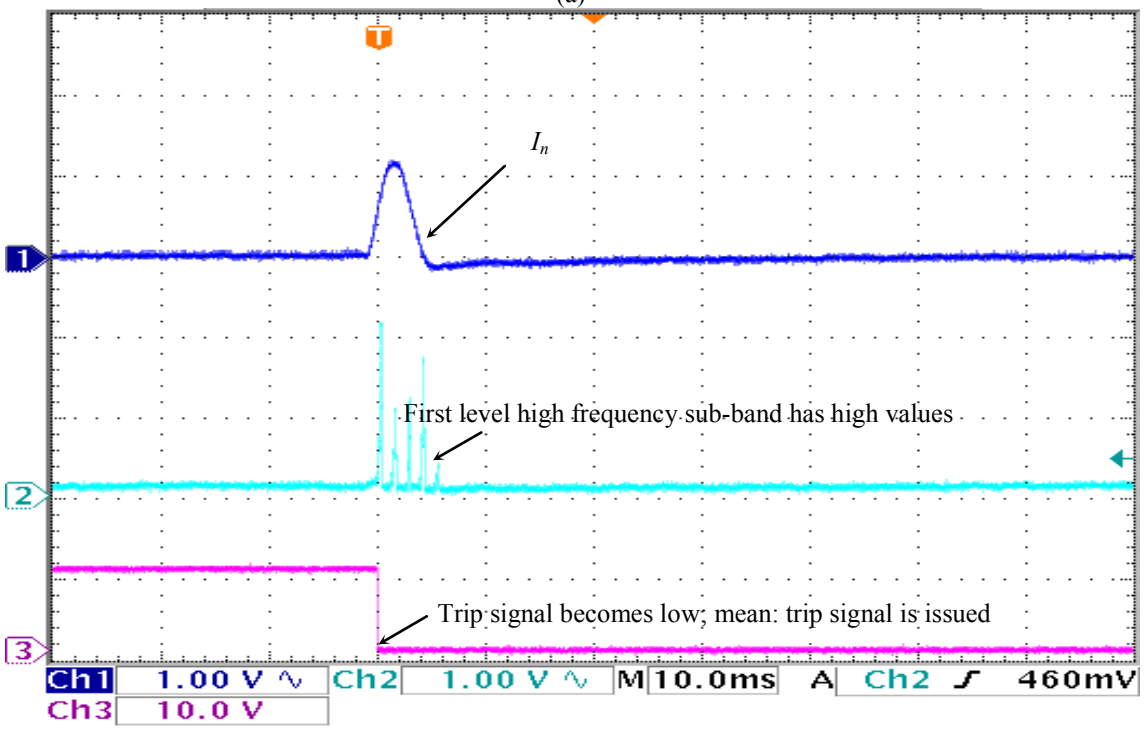

(b)

Figure 6-24 The experimental testing case of secondary single line C to ground fault at induction motor load a) the three-phase transformer currents the 1st level high frequency sub-band b) $I_n = I_d^2+I_q^2$ current components and the 1^{st} level high frequency sub-band: the trip signal becomes low means the trip signal is issued.

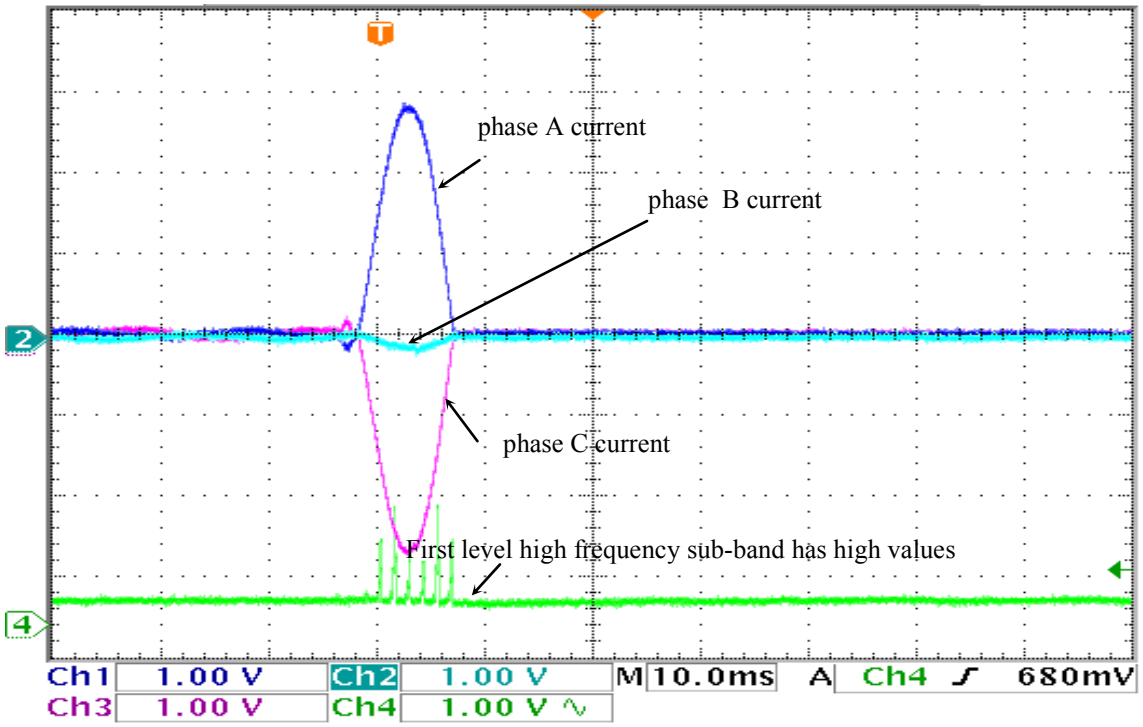

(a)

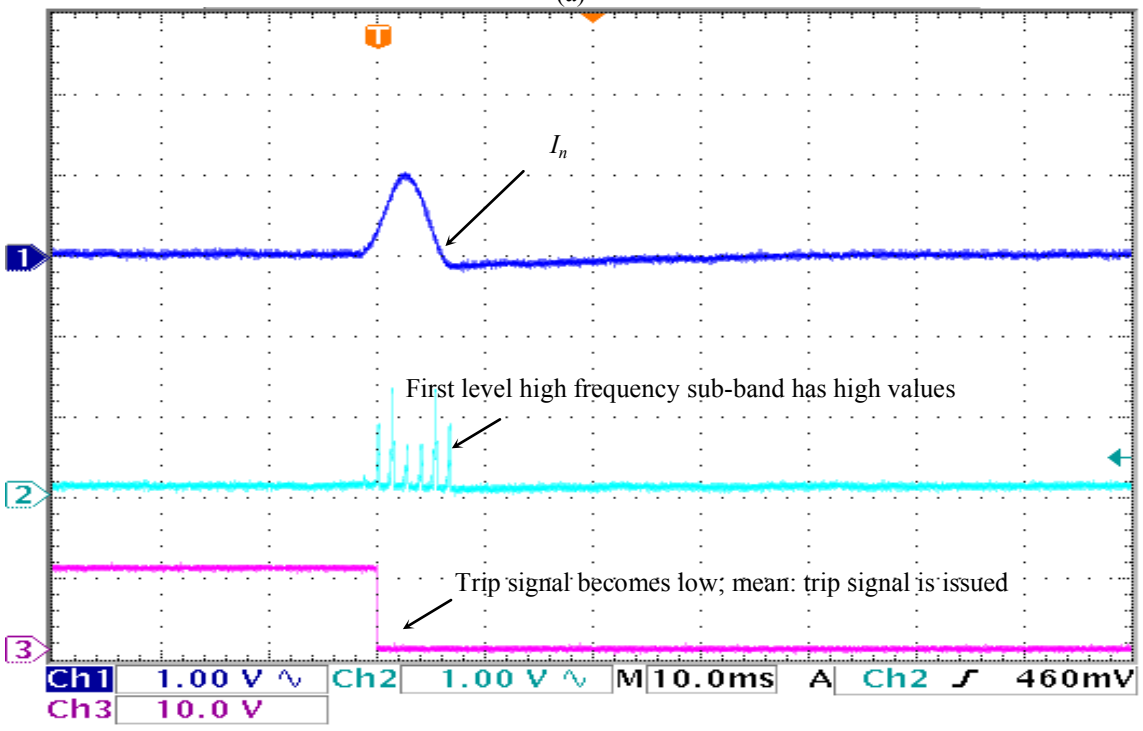

(b)

Figure 6-25 The experimental testing case of unloaded secondary single line A to ground fault a) the three-phase transformer currents the 1st level high frequency sub-band b) dq current components and the 1st level high frequency sub-band: the trip signal becomes low means the trip signal is issued.

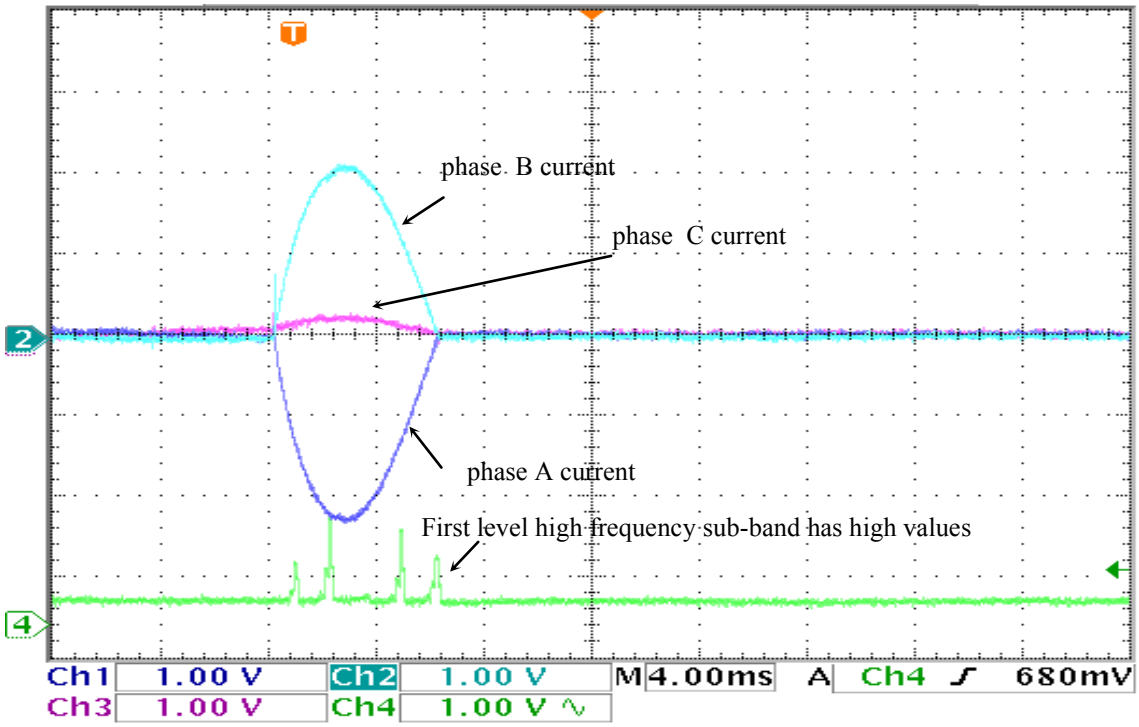

(a)

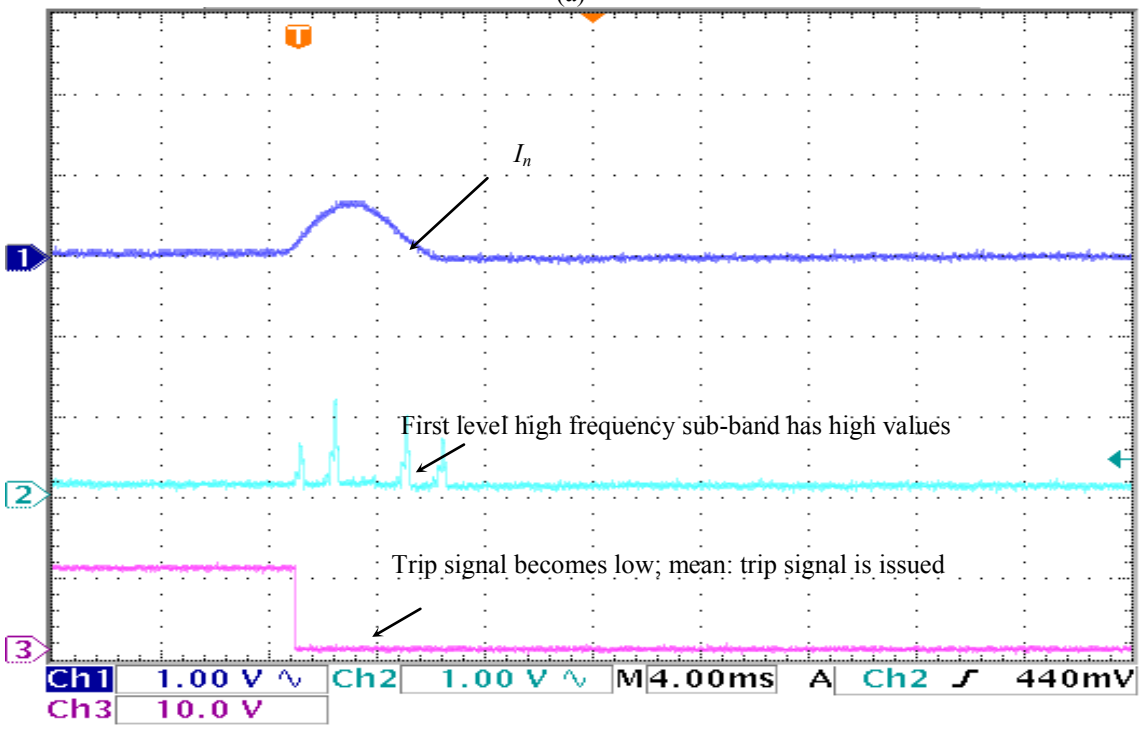

(b)

Figure 6-26 The experimental testing case of unloaded secondary single line B to ground fault a) the three-phase transformer currents the 1st level high frequency sub-band b) $I_n = I_d^2+I_q^2$ current components and the 1st level high frequency sub-band: the trip signal becomes low means the trip signal is issued.

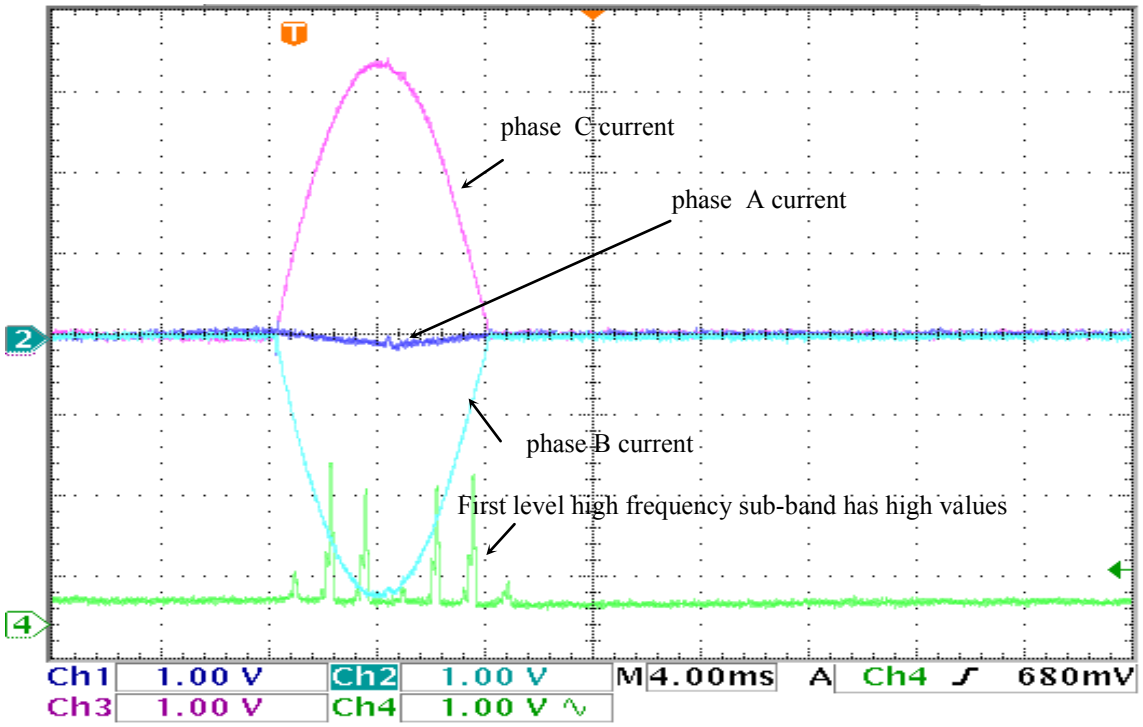

(a)

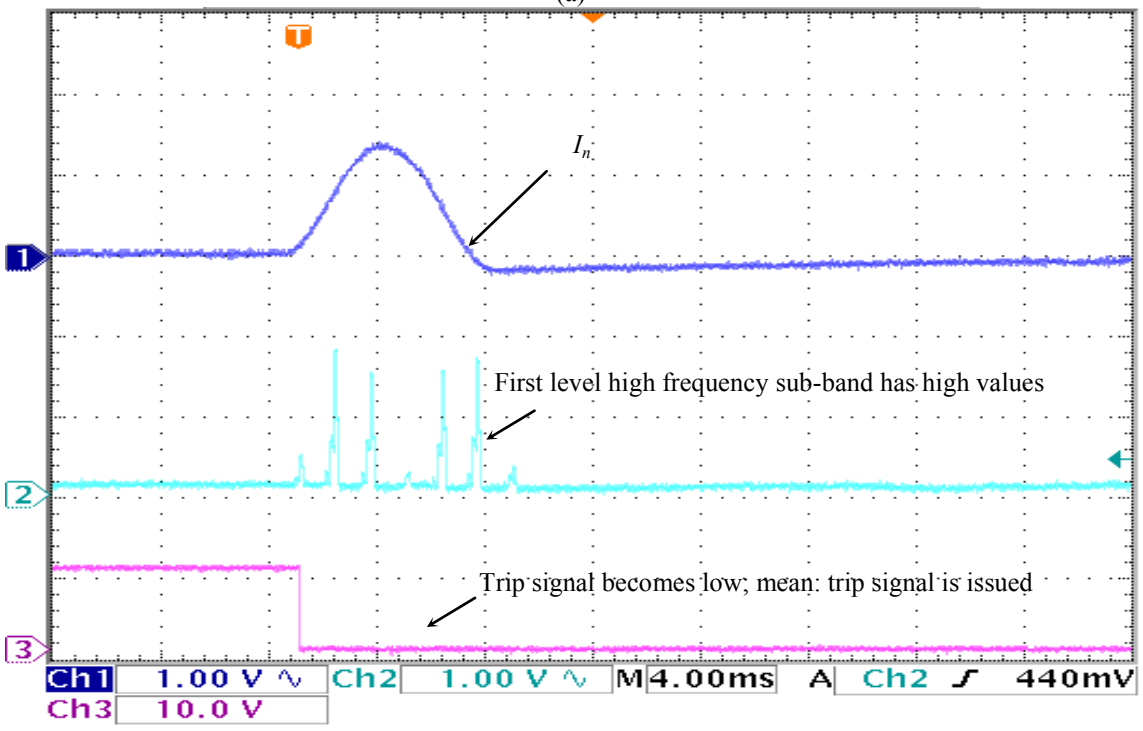

(b)

Figure 6-27 The experimental testing case of unloaded secondary single line C to ground fault a) the three-phase transformer currents the 1st level high frequency sub-band b) $I_n = I_d^2+I_q^2$ current components and the 1st level high frequency sub-band: the trip signal becomes low means the trip signal is issued.

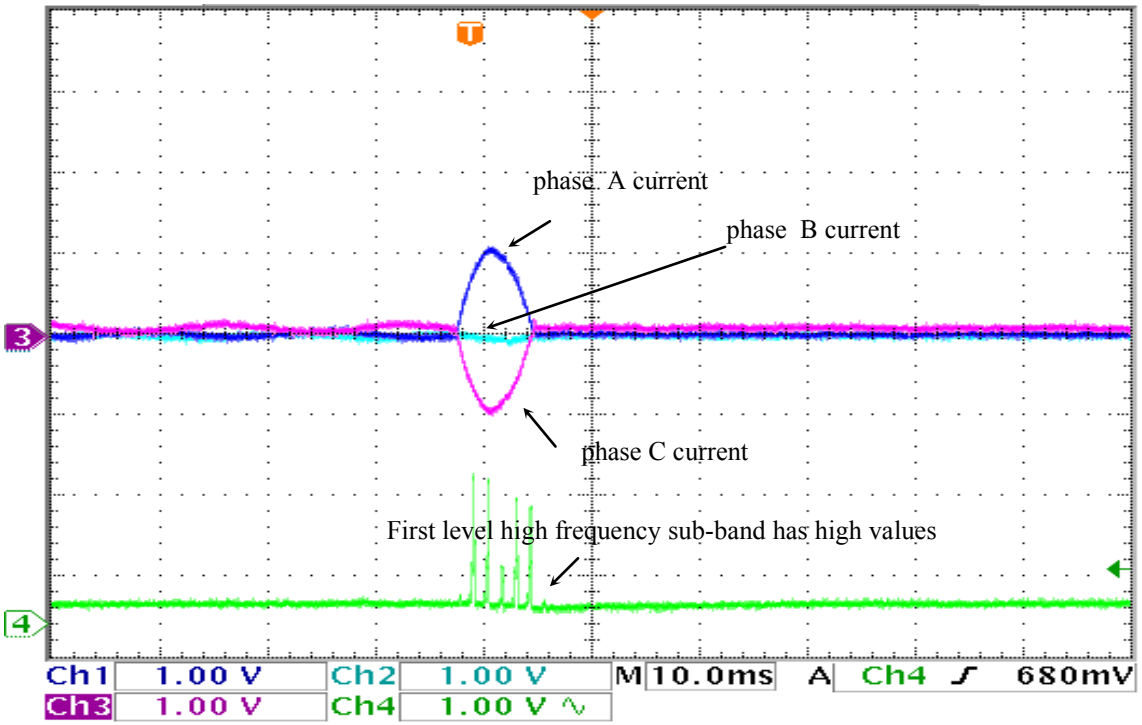

(a)

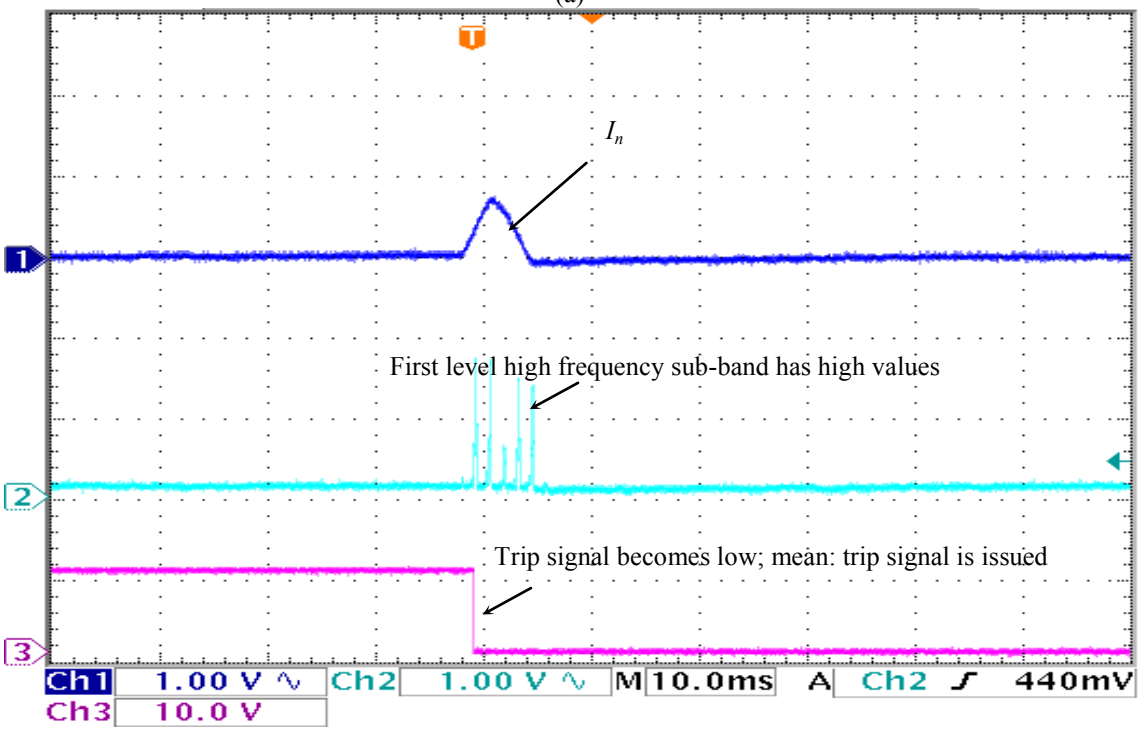

(b)

Figure 6-28 The experimental testing case of secondary phase A turn to turn fault a) the three-phase transformer currents the 1st level high frequency sub-band b) $I_n = I_d^2+I_q^2$ current components and the 1st level high frequency sub-band: the trip signal becomes low means the trip signal is issued.

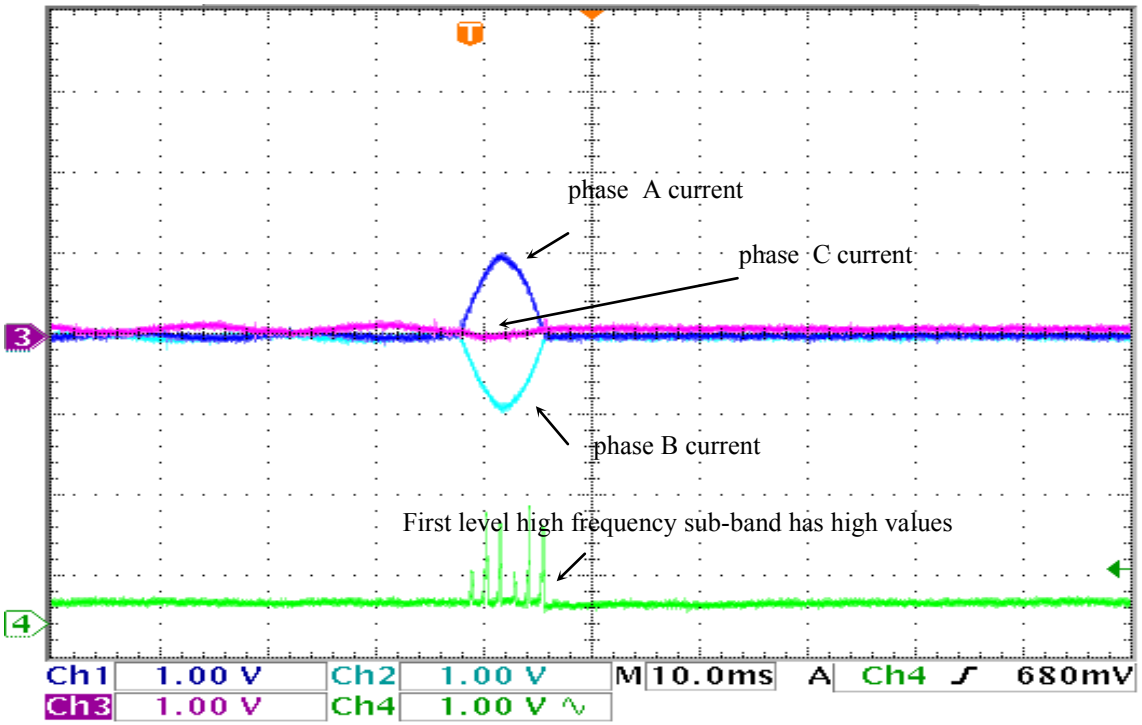

(a)

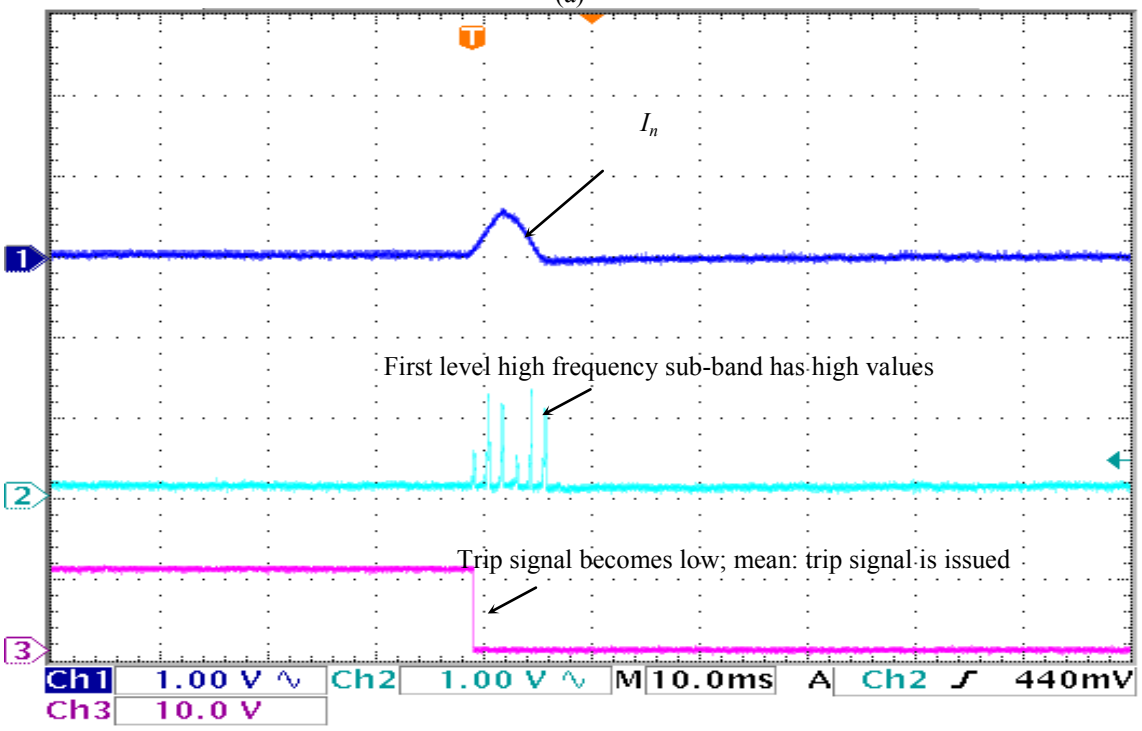

(b)

Figure 6-29 The experimental testing case of secondary phase B turn to turn Fault a) the three-phase transformer currents the 1st level high frequency sub-band b) $I_n = I_d^2+I_q^2$ current components and the 1st level high frequency sub-band: the trip signal becomes low means the trip signal is issued.

- **Experimental Testing Results for Other Disturbances:**

In order to make this work complete, a few critical tests have to be carried out to prove the efficacy of the proposed technique. These tests include some disturbances that may activate the differential relay and trip the power transformer if it is not designed to recognize such cases. The tests included in this part are the CTs mismatch and saturation, over-excitation, and external through-faults.

a) CTs Mismatch Currents

This experimental test was carried out to test the immunity of the proposed dqWPT algorithm against the CTs mismatch. These currents appear in the differential currents only if there is a CTs mismatch. To make this experimental test more difficult, the balanced inductive load of $Z = 343 + j171.4\ \Omega$/phase as shown in Figure ***6-30***, and unbalanced three-phase R-L load of $Z_a = 800 + j400$, $Z_b = 480 + j240$, $Z_c = 400 + j200$ as shown in Figure ***6-31*** were used. However, the algorithm did not consider this case as a fault, in which no change in the trip signal is indicated. The proposed dqWPT algorithm was tested several times for such balanced and unbalanced cases and it has never generated a trip signal to isolate the transformer, even with high differential current magnitudes or saturating cases.

b) CTs saturation,

Whenever the current transformers saturate, they cannot reproduce the primary current correctly at their secondary side according to their transformation ratio. Transformer core saturation takes place due to many reasons and the most important one is the excessive flow of high currents in their primary winding. The CTs saturation causes distortions in the output current of the CT, which leads to the disturbance of the protective relay. This experimental test was carried out to test the immunity and the stability of the proposed

dqWPT algorithm against CTs saturation that may occur due to excessive amounts of the magnetizing inrush currents or through faults. As shown in Figure ***6-32***, there is no change in the trip signal, which occurred, which indicates a non-faulted condition. The proposed algorithm was tested experimentally many times in such a case and it has never generated a trip signal, even with high differential current magnitudes or saturating cases.

c) Over-excitation,

This experimental over-excitation test was carried out to test the immunity of the proposed dqWPT algorithm against false tripping due to the over-excitation of the power transformer core. This test is carried out by increasing the supply voltage to about 130% of its rated voltage. Since the laboratory cannot supply more than 230V directly, the voltage was stepped up by another step-up transformer, which was connected in series with the test transformer. As can be seen from Figure ***6-33*** under loaded conditions, the current is quite distorted because of the presence of a strong fifth harmonic component. The figure shows no changes in the trip signal, indicating a non-faulted condition. The proposed dqWPT algorithm was tested experimentally many times in this case and it did not have any difficulty in keeping the trip signal high, even with high differential currents or saturating cases.

d) External or through faults,

This experimental test was carried out to test the immunity of the algorithm against the severe through faults. The through-current appears in the differential currents only for severe cases, which causes CTs saturation and, consequently, causes CTs mismatches. This case is considered as an extension of the CTs mismatches and saturations cases. Figure ***6-34***, depicts no changes in the trip signal, indicating a non-internal faulted condition. The proposed algorithm was tested in this case and it has never generated a trip signal.

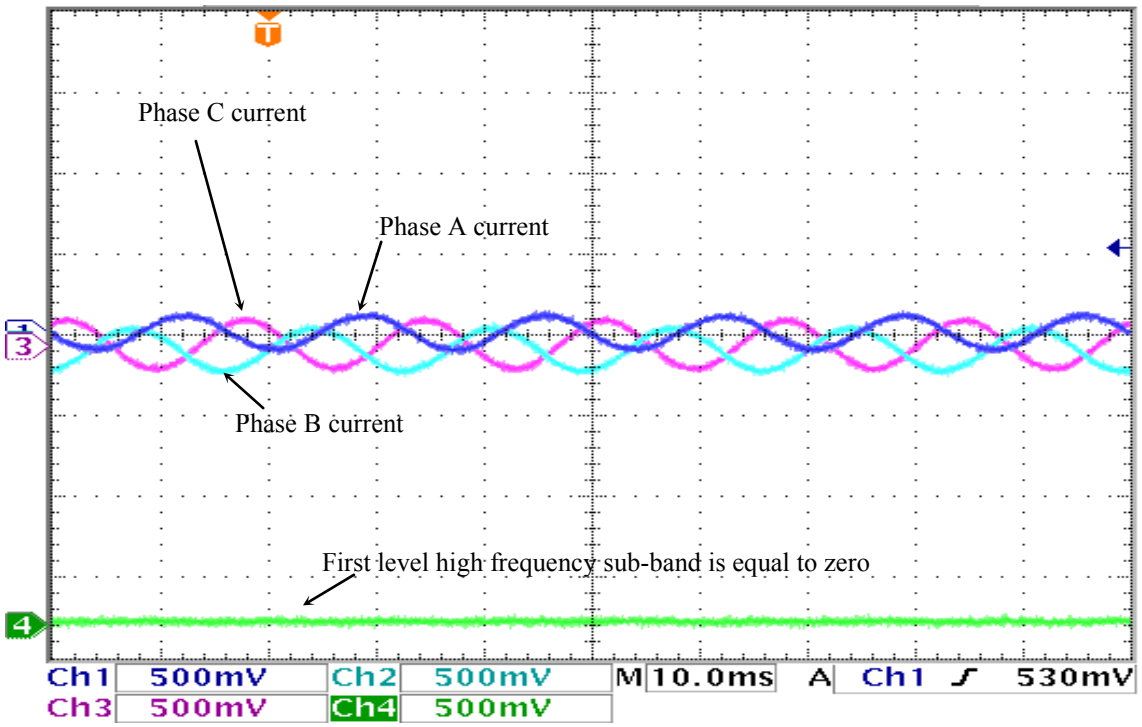

(a)

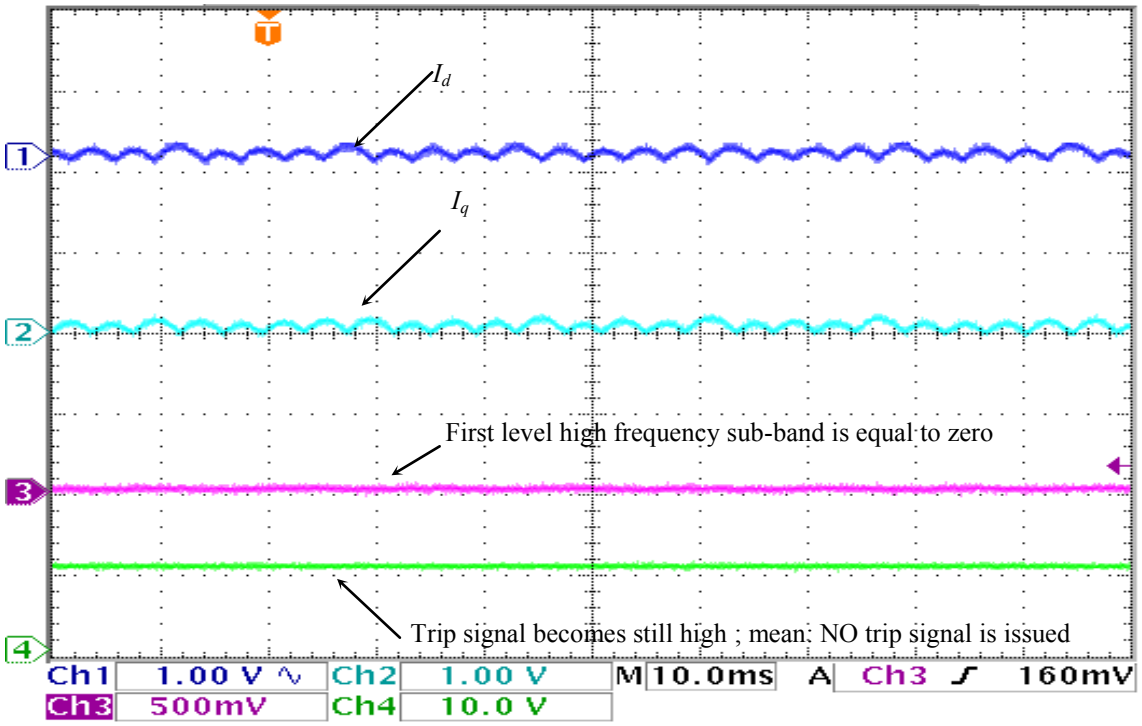

(b)

Figure 6-30 The experimental testing case of the CT mismatches at balanced load a) the three-phase loaded transformer currents and the 1st level high frequency sub-band b) dq current components and the 1st level high frequency sub-band and the trip signal is still high, means no trip signal is issued.

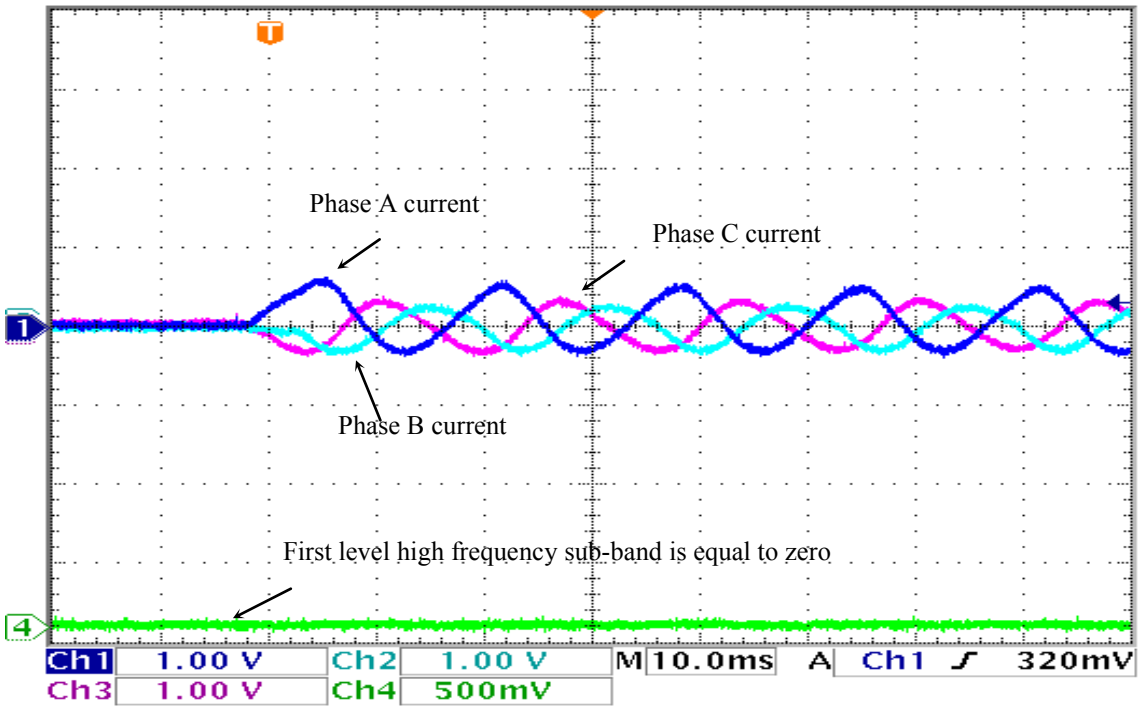

(a)

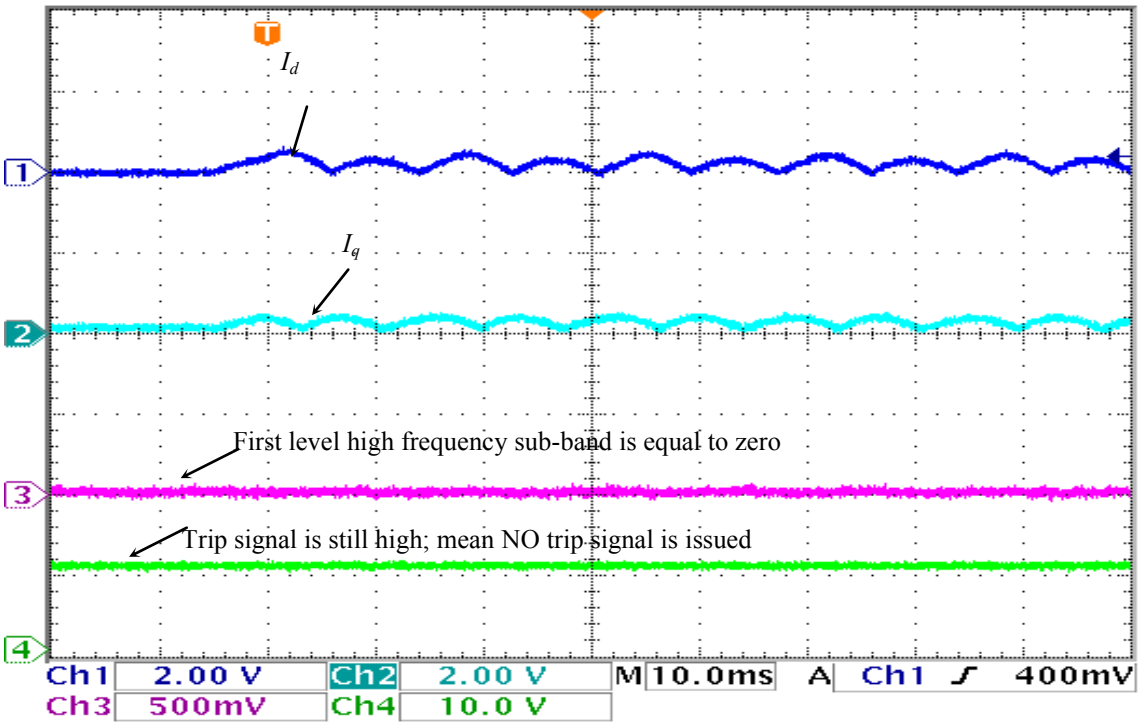

(b)

Figure 6-31 The experimental testing case of the CT mismatches at unbalanced load a) the three-phase loaded transformer currents and the 1st level high sub-band frequencies b) dq current components and the 1st level high sub-band frequencies (zero value): the trip signal is still high, means no trip signal is issued.

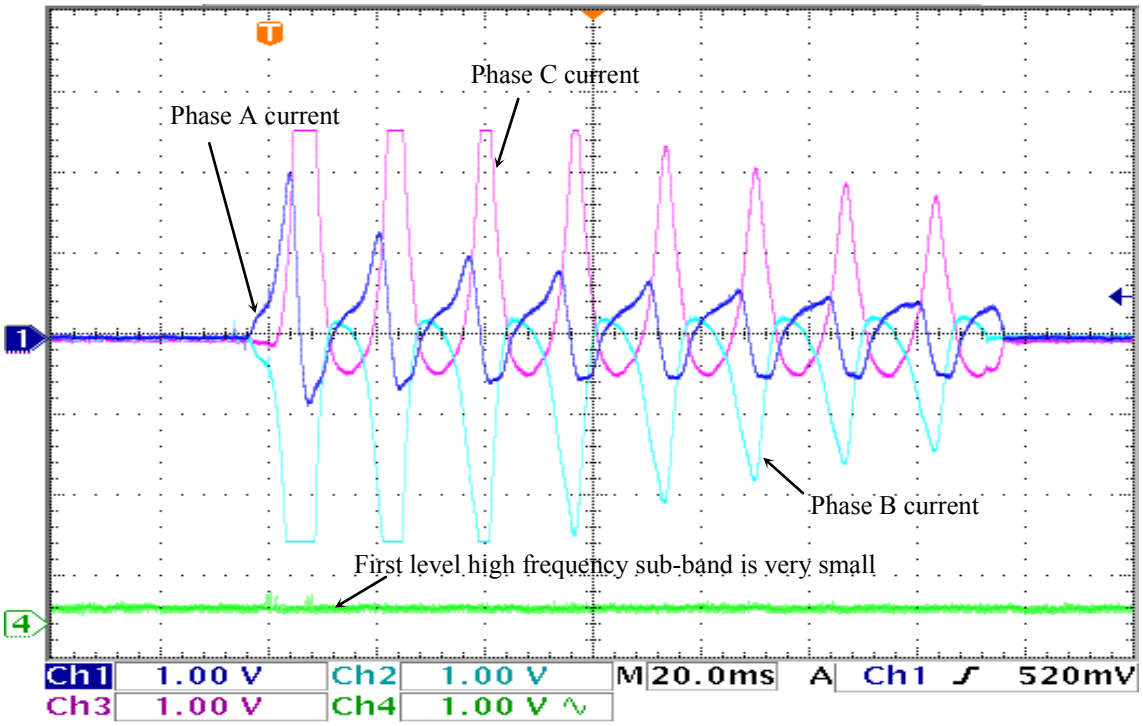

(a)

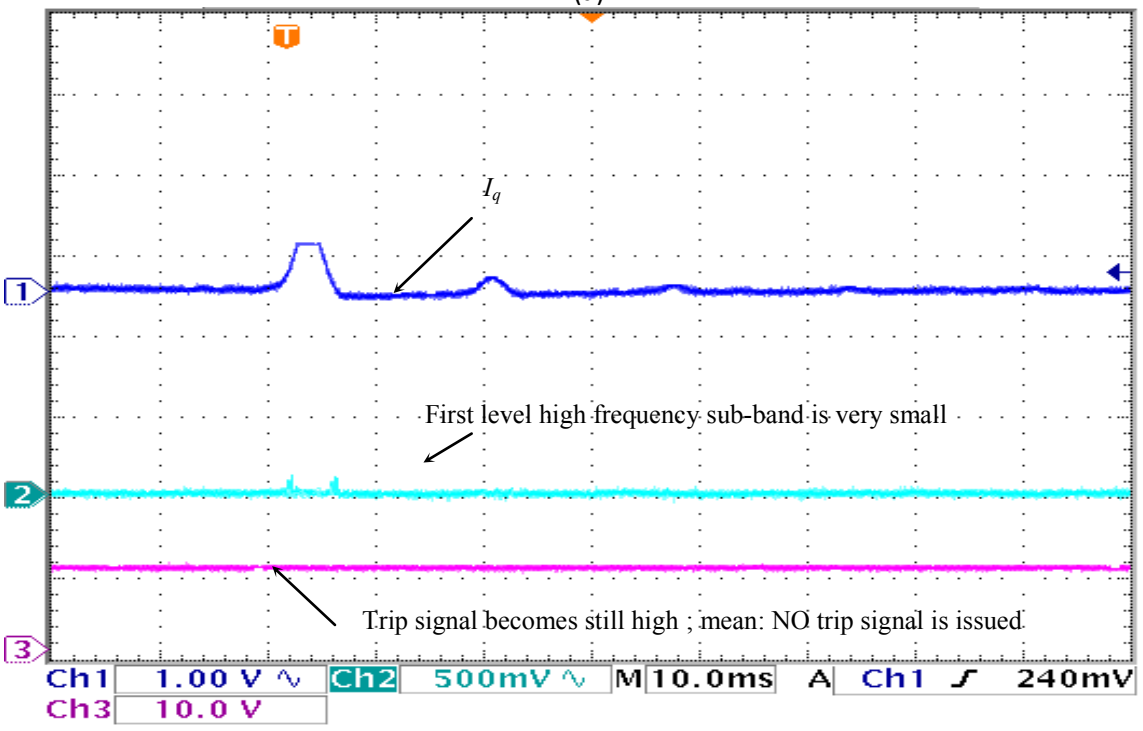

(b)

Figure 6-32 The experimental testing case of the CT Saturation a) the three-phase loaded transformer currents and the 1st level high sub-band frequencies b) $I_n = I_d^2+I_q^2$ current components and the 1st level high sub-band frequencies (zero value): the trip signal is still high, means no trip signal is issued.

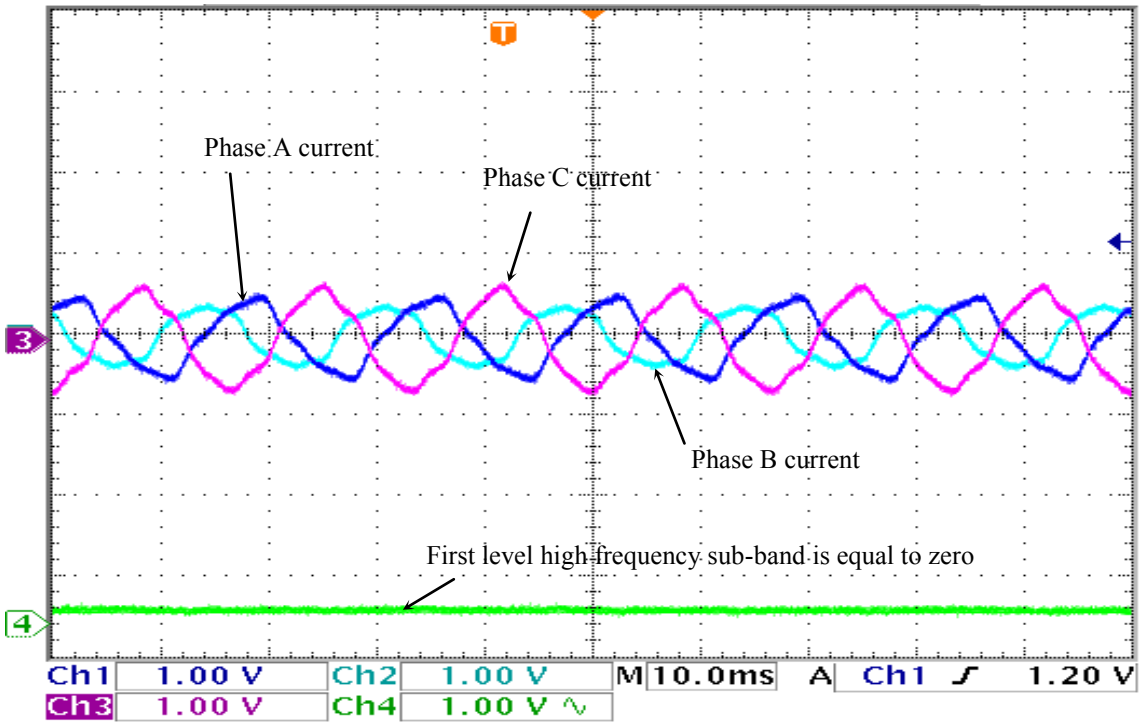

(a)

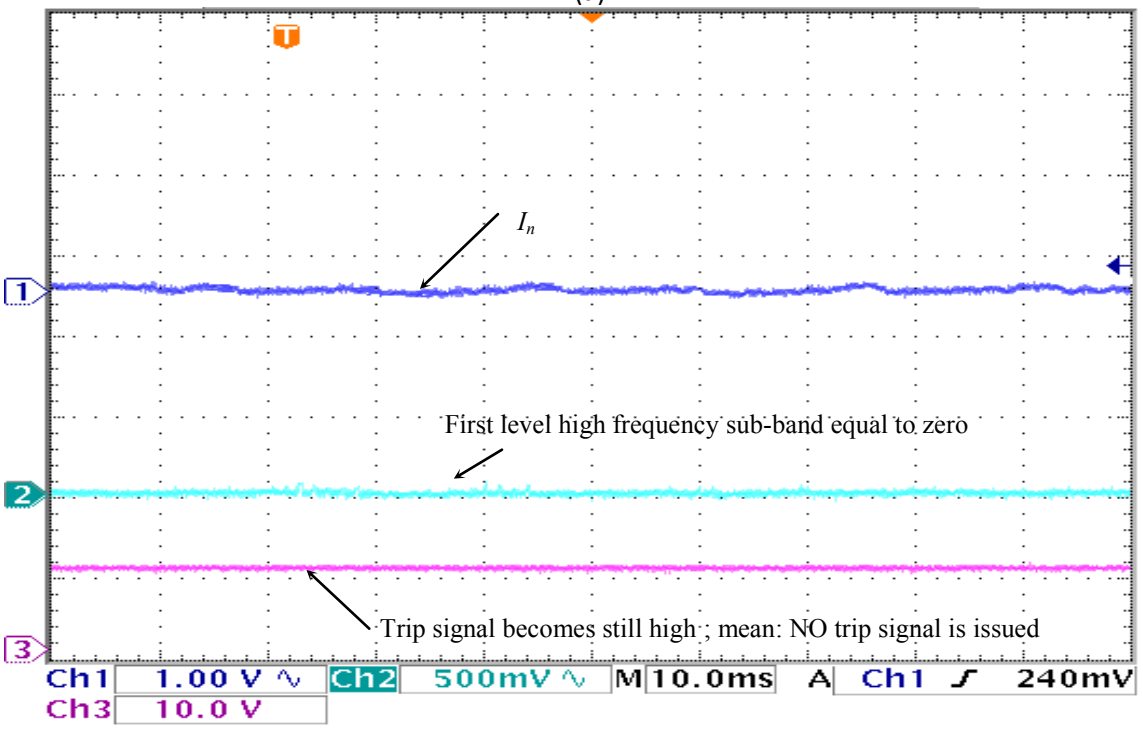

(b)

Figure 6-33 The experimental testing case of the over excitation at unbalanced load a) the three-phase loaded transformer currents and the 1st level high sub-band frequencies b) $I_n = I_d^2+I_q^2$ current components and the 1st level high sub-band frequencies (zero value): the trip signal is still high, means no trip signal is issued.

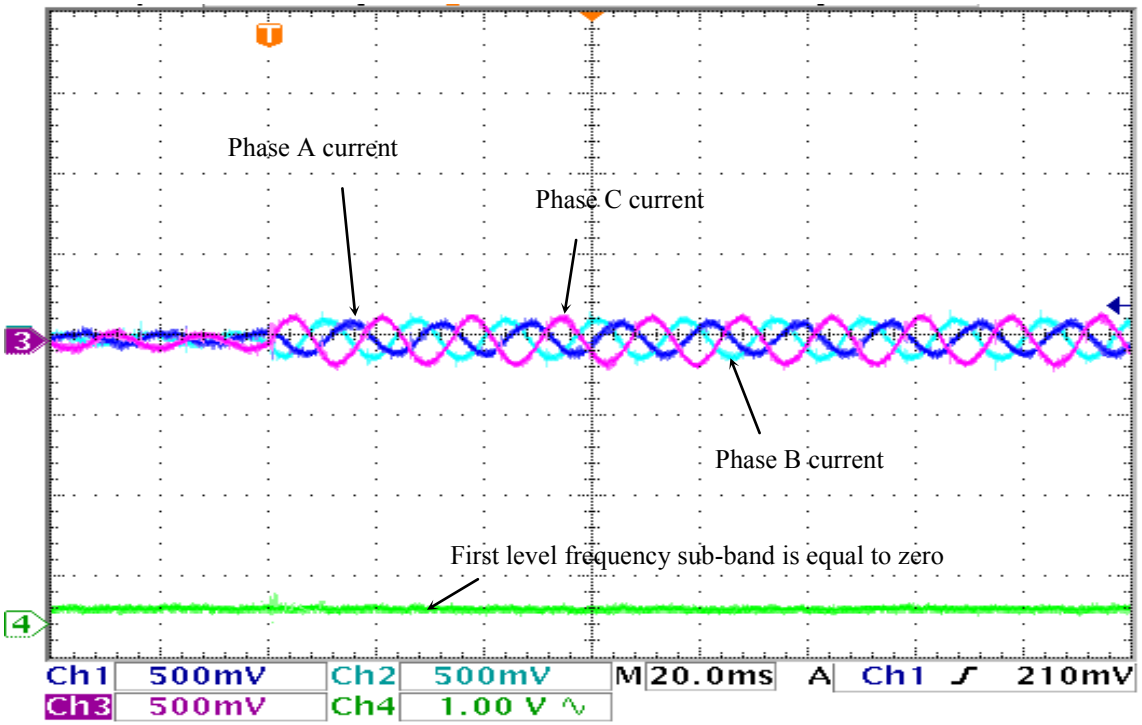

(a)

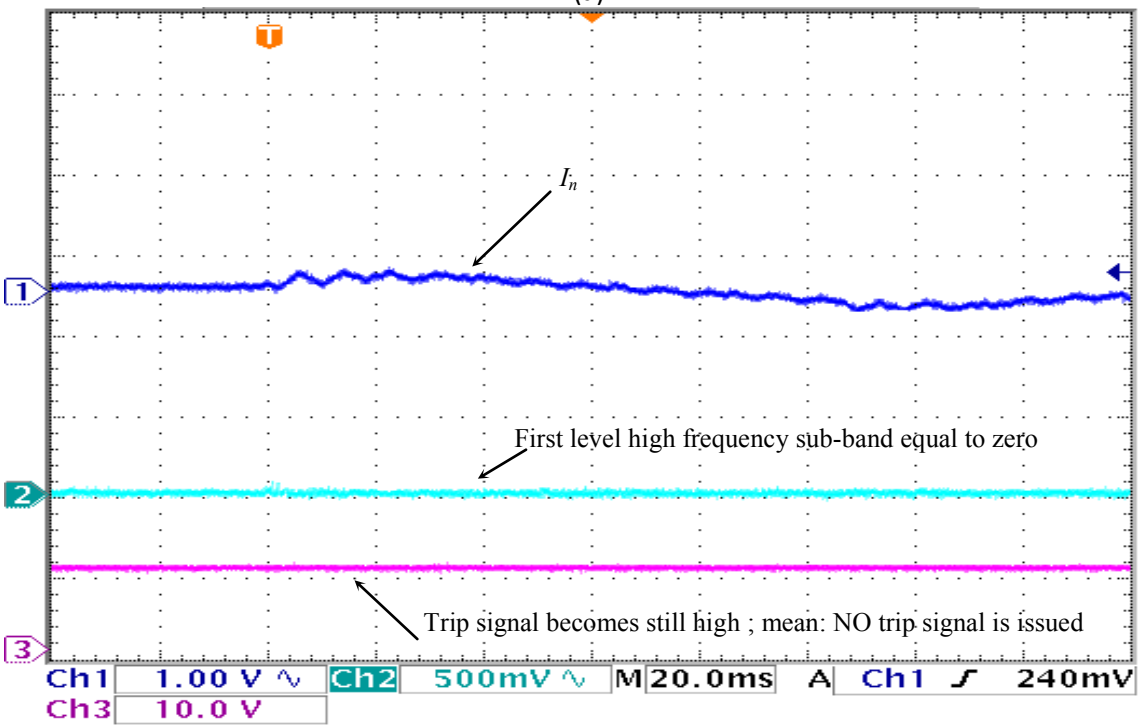

(b)

Figure 6-34 The experimental testing case of the external fault at unbalanced load a) the three-phase loaded transformer currents and the 1st level high sub-band frequencies b) $I_n = I_d^2+I_q^2$ current components and the 1st level high sub-band frequencies (zero value): the trip signal is still high, means no trip signal is issued.

B: Experimental Results for the Three-Phase 2kVA Laboratory Power Transformer:

In this part, extended results are provided to demonstrate the universal use of the proposed algorithm using a different power transformer and a modern DSP board (ds-1104). The transformer used in this part has different ratings and a different connection configuration. Its ratings are 2kVA, 127-220/2×(31.8-42-63.5)V, 50Hz, 3Φ, Δ-Y, step-down, core-type, three-winding, laboratory power transformer. It has an open access winding connection, so that any kind of connection can be made. In this setup, a Δ-Y connection was selected to perform the required tests. The testing of this transformer was carried out using the circuit connection shown in Figure *6-35* and a photograph of the experimental setup is shown in Figure *6-36*. This setup deffers from the setup in Figure ***6-1*** in the number of the inputs to the DSP board. The number of the input currents in the previous connection, shown in Figure ***6-1***, was three input currents only, using three current isolators. This is because of the limitation of the old DSP board (ds-1102), which accepts only four analog inputs and four analog outputs. However, the new DSP board (ds-1104) accepts eight analog inputs and eight analog outputs. This feature in the new DSP board gave us the ability to use six input currents, the three primary currents and the three secondary currents, using six current isolators. Then the differential currents are calculated from these inputs in the computer instead of performing those calculations on the hardware circuit using the current isolators.

On this three-phase multi-tap transformer, the Δ-Y, 220/127V, step-down configuration was chosen. The frequency rating of this transformer is 50Hz, and the supply frequency is 60Hz. This discrepancy in the frequency leads the core of the transformer to saturate easily. Moreover, the current transformers may also be saturated due to this discrepancy in the frequency. This core saturation makes the task more complicated for the proposed technique

to pass the test cases. The results of the test cases from the laboratory experiments, on this transformer, including the discussion and the figures, are provided in this part to prove the efficacy of the proposed technique.

- **Experimental Testing Results for Magnetizing Inrush Currents:**

The inrush current test was carried out several times and it has been observed that the proposed technique has never given a trip signal for such testing cases under different loading conditions. Some of the sample results are demonstrated in Figures (6.37-6.41). The figures provide clear evidence that the proposed technique has successfully detected this natural phenomenon and no trip signals were issued.

a) Unloaded Magnetizing Inrush Currents

This testing case was carried out several times when the transformer was not connected to any kind of loads. It has never generated a trip signal to isolate the transformer due to the inrush phenomenon, even with high differential current magnitudes. Some of the testing results are illustrated in Figure ***6-37***, Figure ***6-38*** and Figure ***6-39***. The results show that there are no trip signals issued due to the inrush phenomenon.

b) Loaded Magnetizing Inrush Current

The same tests were carried out again, several times when the transformer was connected to different types of loads. The testing results show that the proposed algorithm has never generated a trip signal in this case to trip the power transformer. A few cases are illustrated for different loading conditions in Figure ***6-40*** Figure ***6-41***. These results show that the proposed algorithm operated correctly and has never misidentified the inrush current as a faulted case.

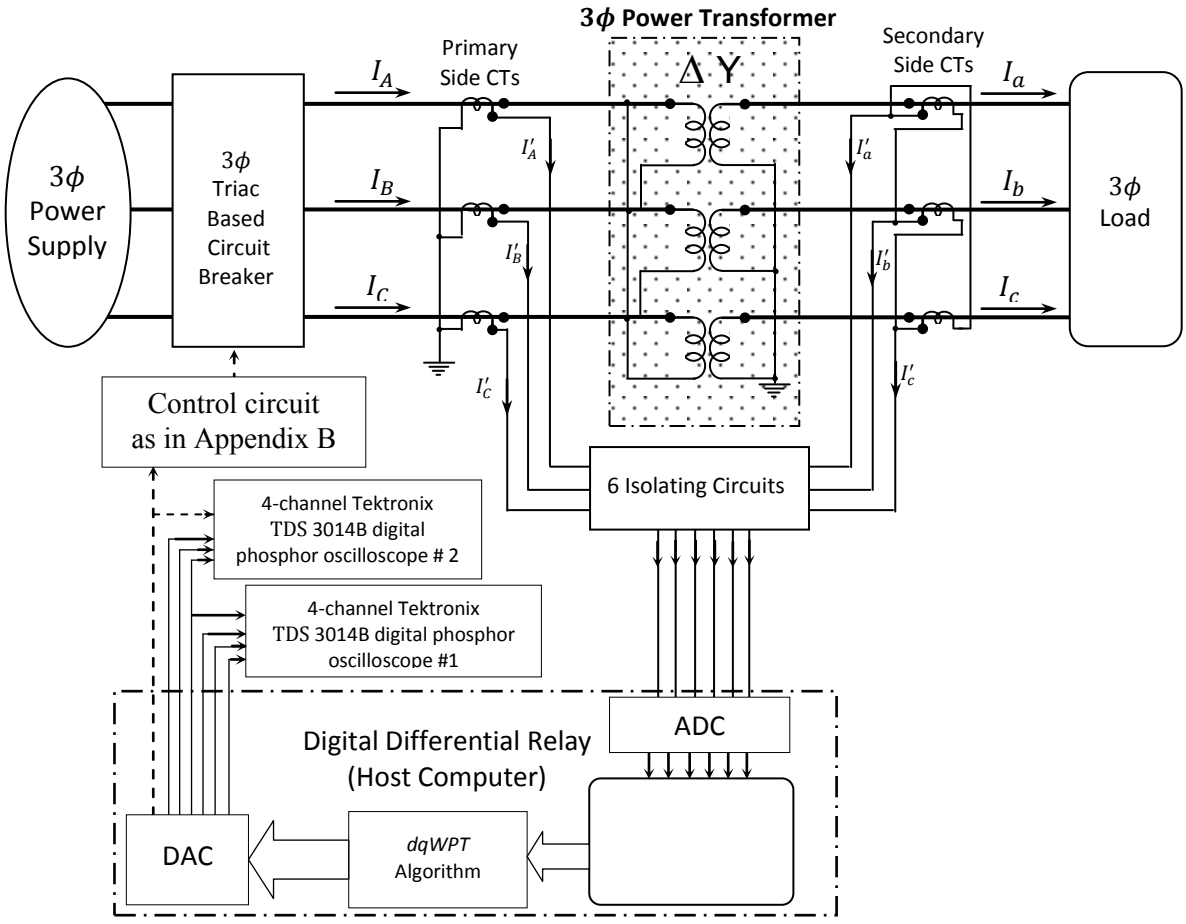

Figure 6-35 The circuit diagram of the experimental setup for the 2kVA transformer using ds-1104

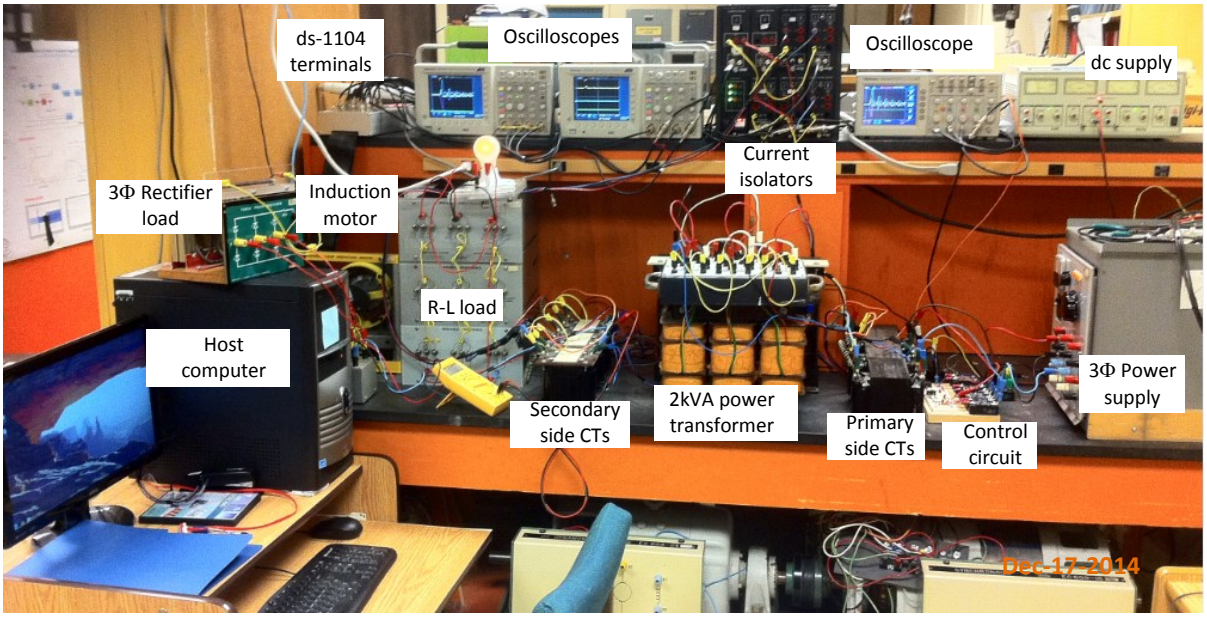

Figure 6-36 The experimental setup for 2kVA laboratory power transformer using ds-1104

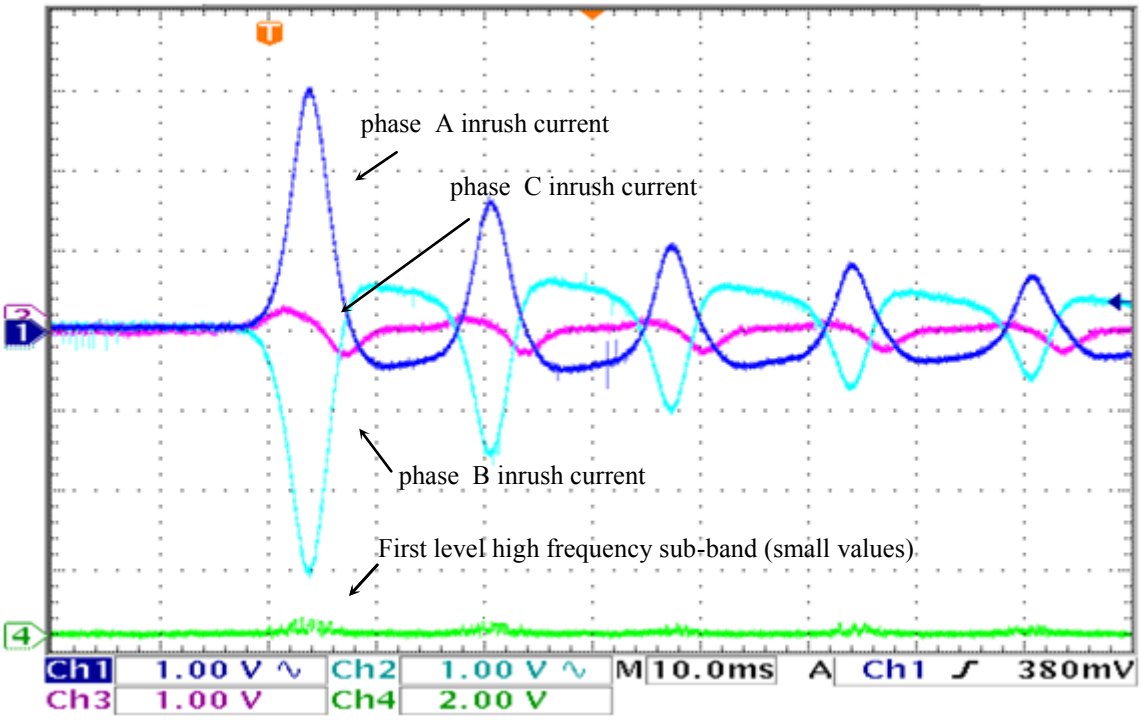

(a)

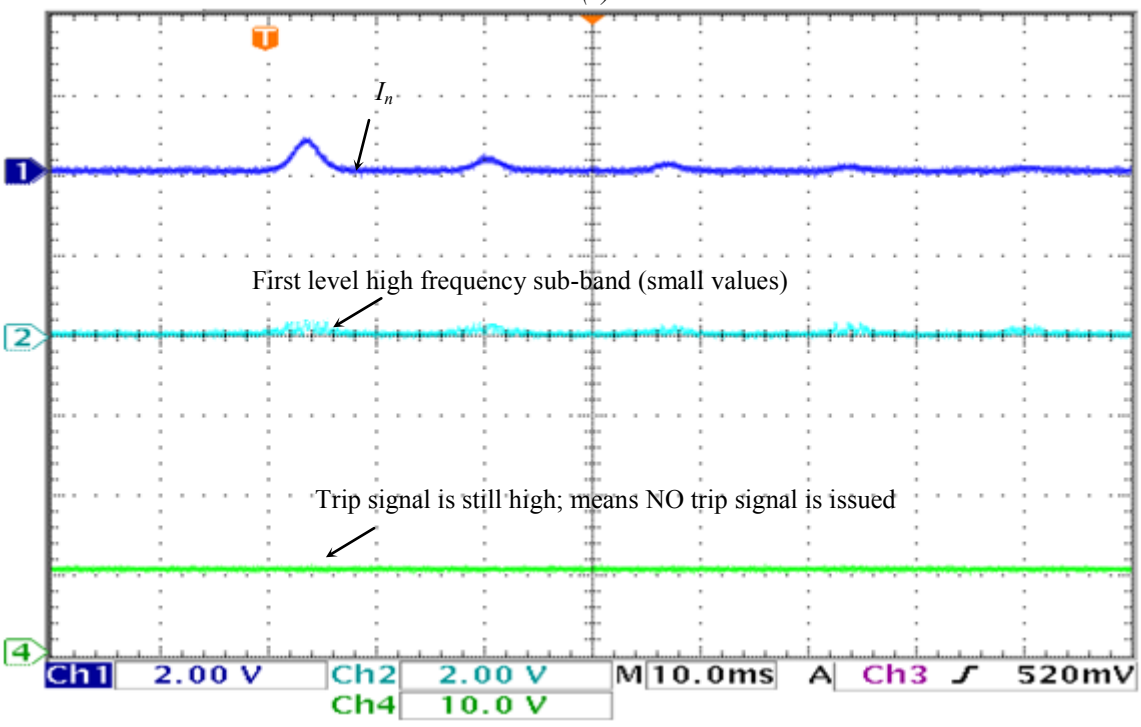

(b)

Figure 6-37 The experimental testing case of the unloaded magnetizing inrush current with phase A has positive peak and phase B has negative peak, a) the three-phase unloaded magnetizing inrush currents and the 1st level high frequency sub-band, b) dq current components and the 1st level high frequency sub-band: the trip signal is still high, means no trip signal is issued.

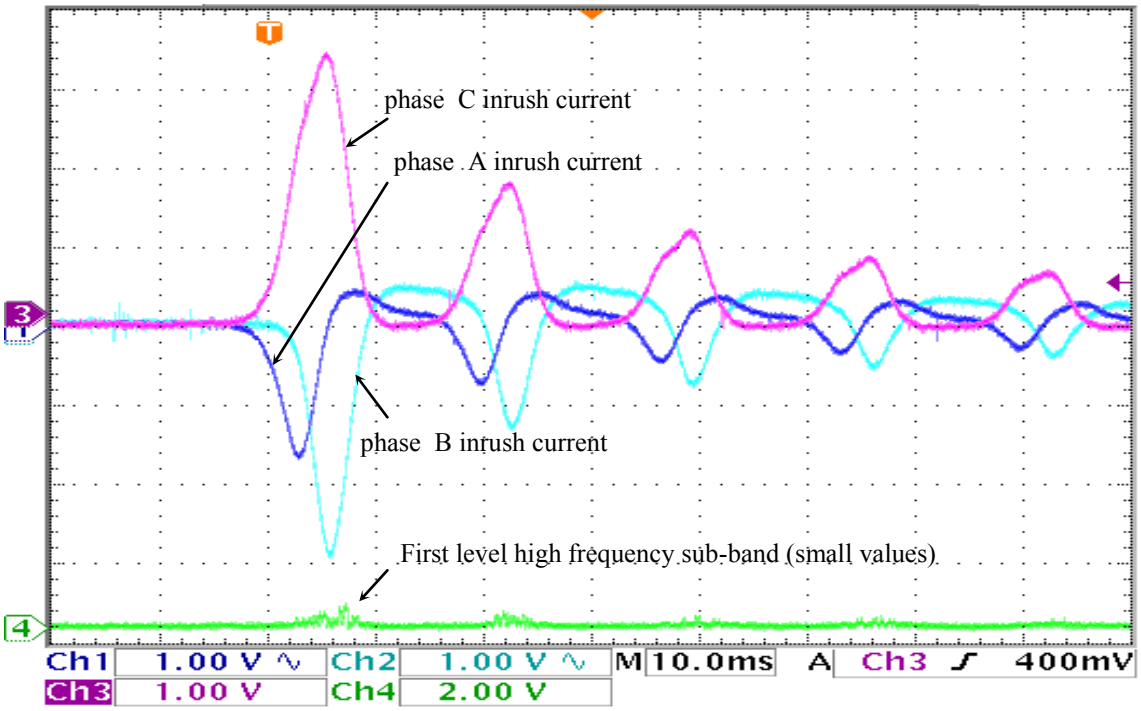

(a)

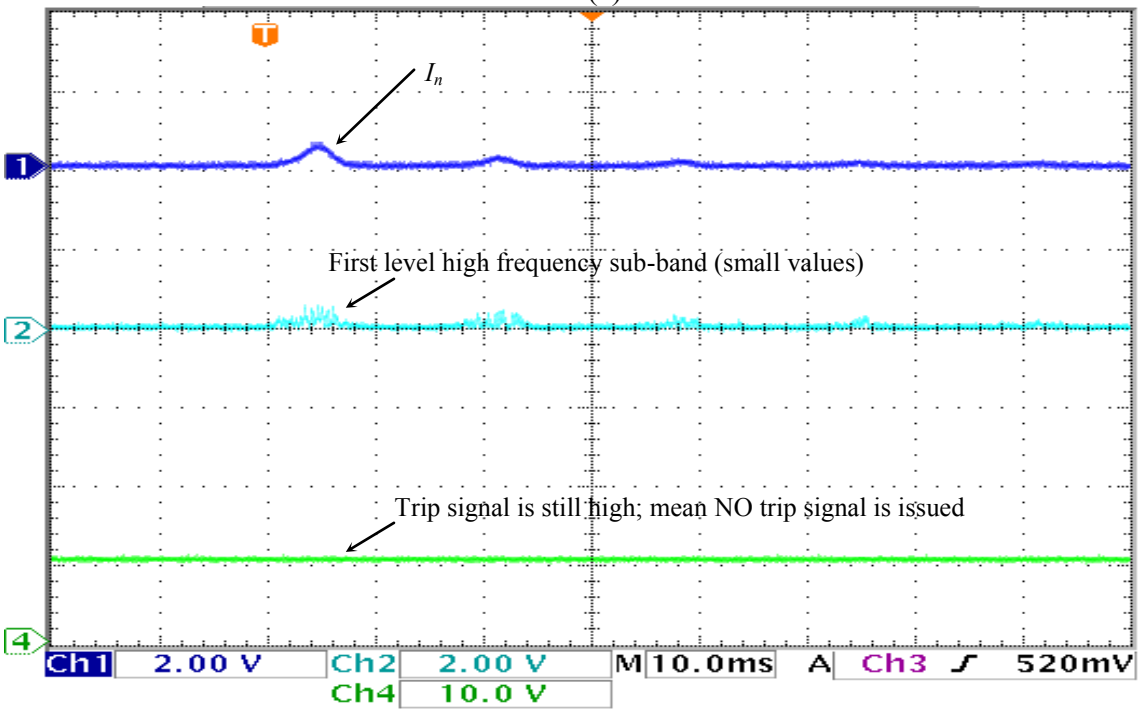

(b)

Figure 6-38 The experimental testing case of the unloaded magnetizing inrush current with phase C has positive peak and phases A& B have negative peaks, a) the three-phase magnetizing inrush currents and the 1st level high frequency sub-band, b) $I_n = I_d^2+I_q^2$ current component and the 1st level high frequency sub-band: the trip signal is still high, means no trip signal is issued.

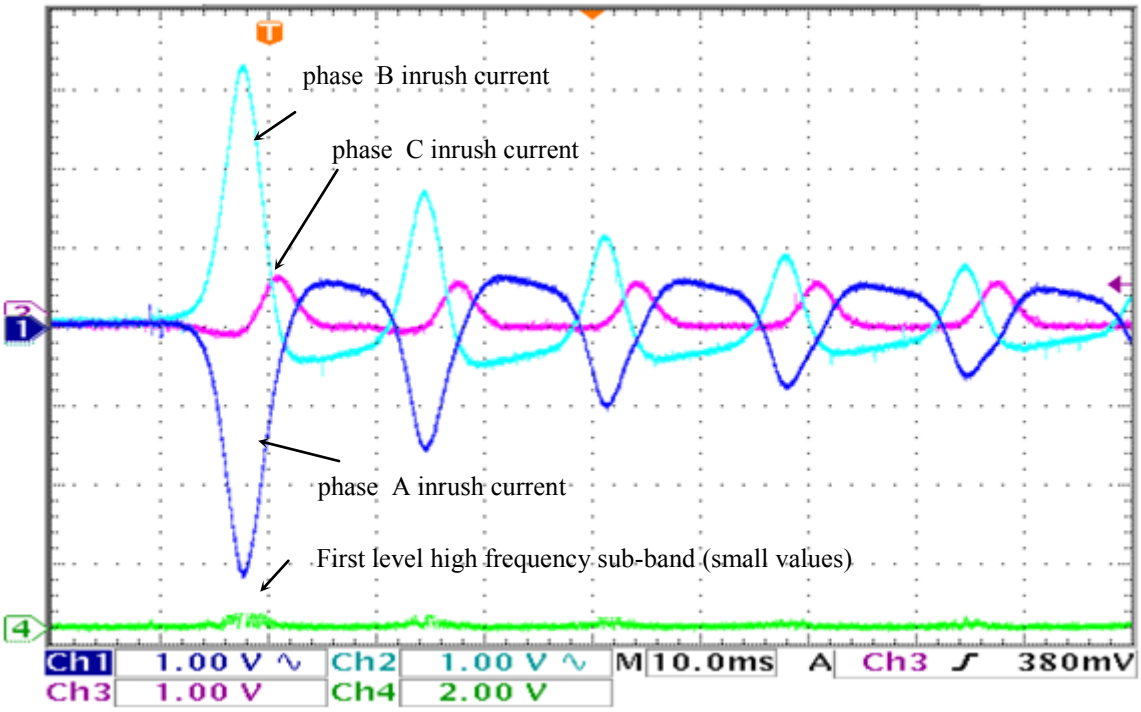

(a)

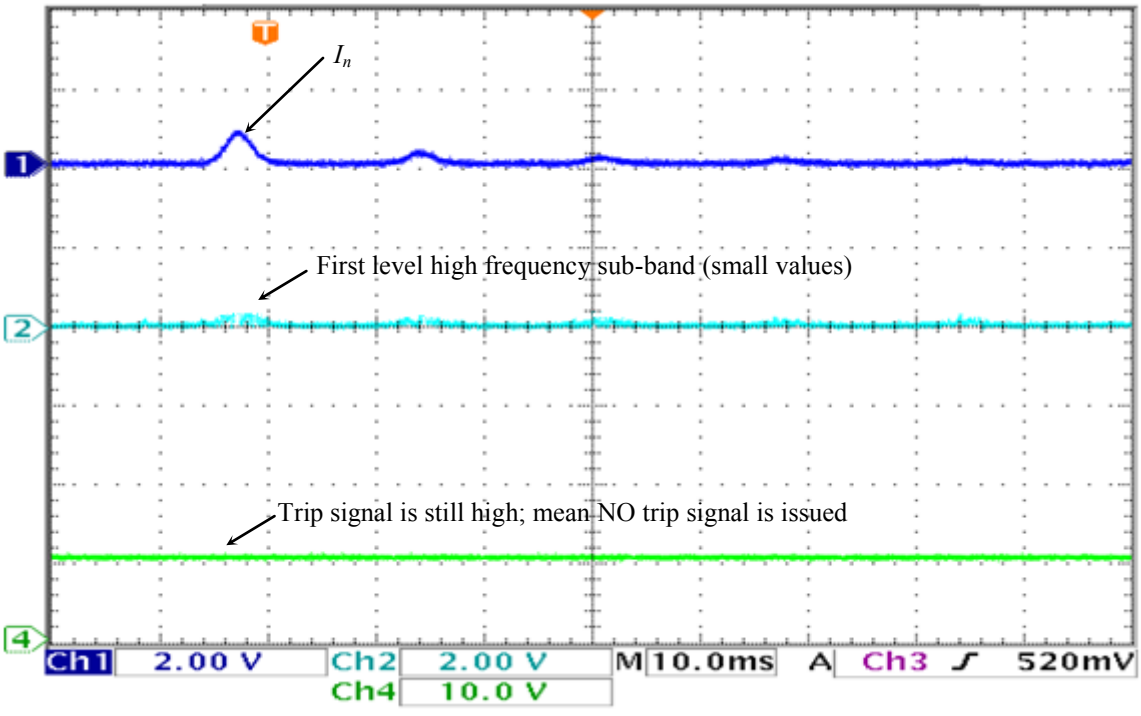

(b)

Figure 6-39 The experimental testing case of the unloaded magnetizing inrush current with phase B has positive peak and phases A has negative peak, a) the three-phase magnetizing inrush currents and the 1st level high frequency sub-band, b) $I_n = I_d^2+I_q^2$ current components and the 1st level high frequency sub-band: the trip signal is still high, means no trip signal is issued.

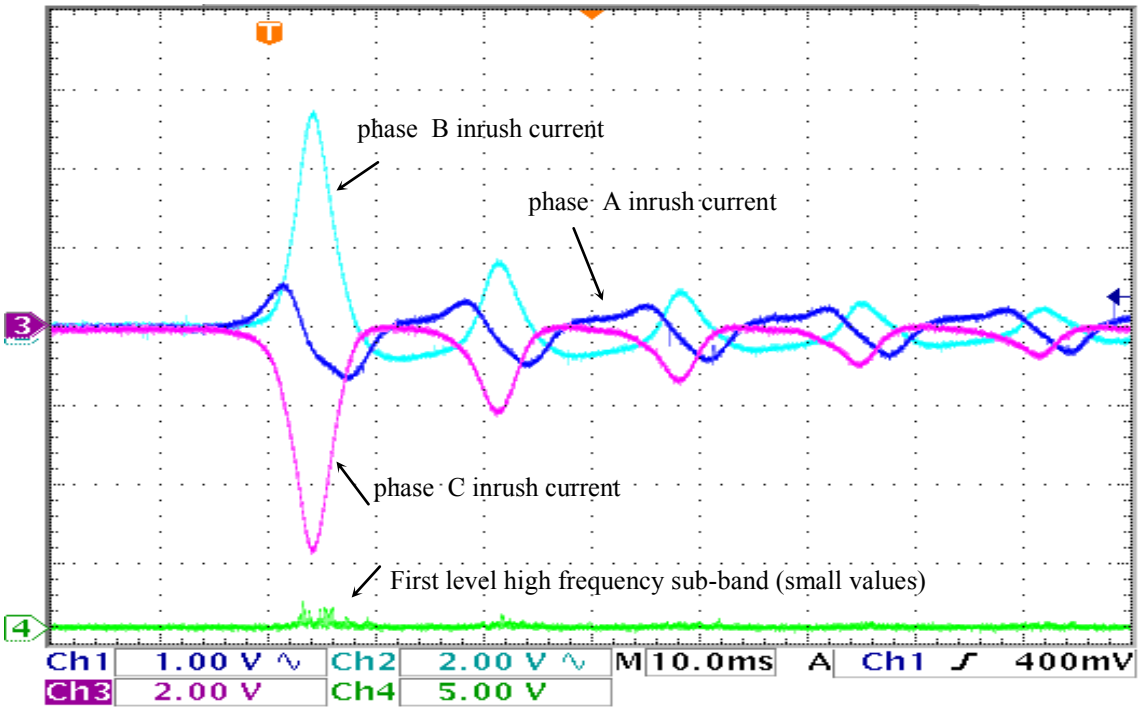

(a)

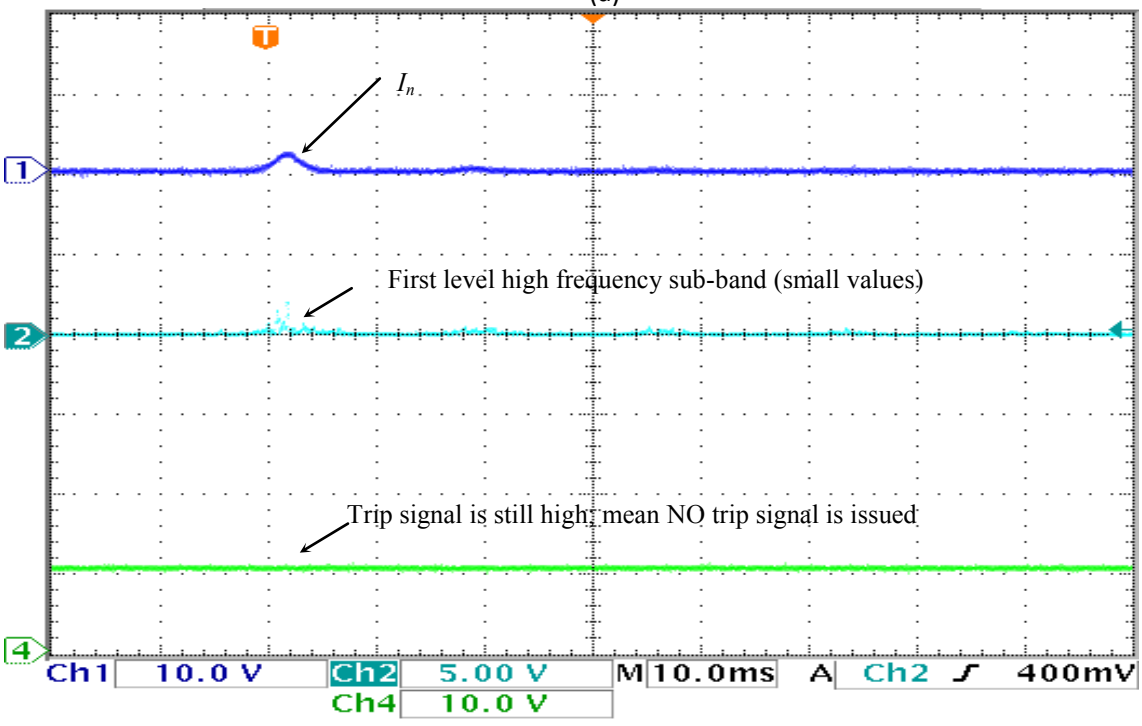

(b)

Figure 6-40 The experimental testing case of the magnetizing inrush current at unbalanced resistive-inductive load a) the three-phase magnetizing inrush currents and the 1st level high frequency sub-band b) $I_n = I_d^2+I_q^2$ current components and the 1st level high frequency sub-band: the trip signal is still high, means no trip signal is issued.

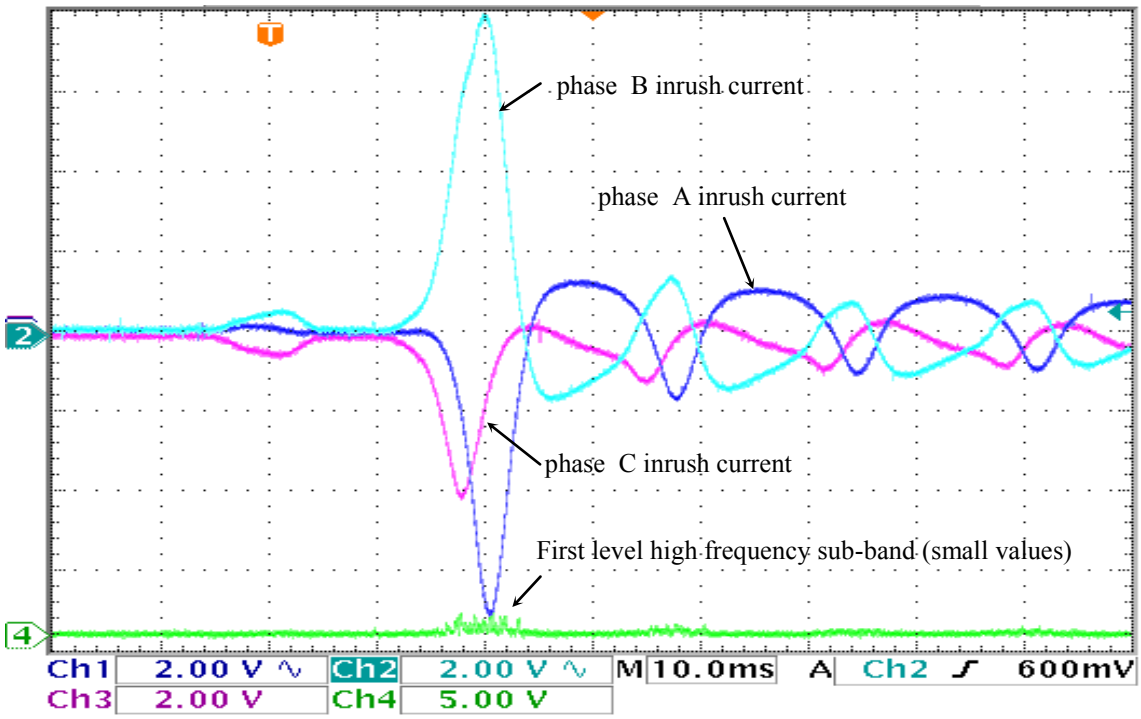

(a)

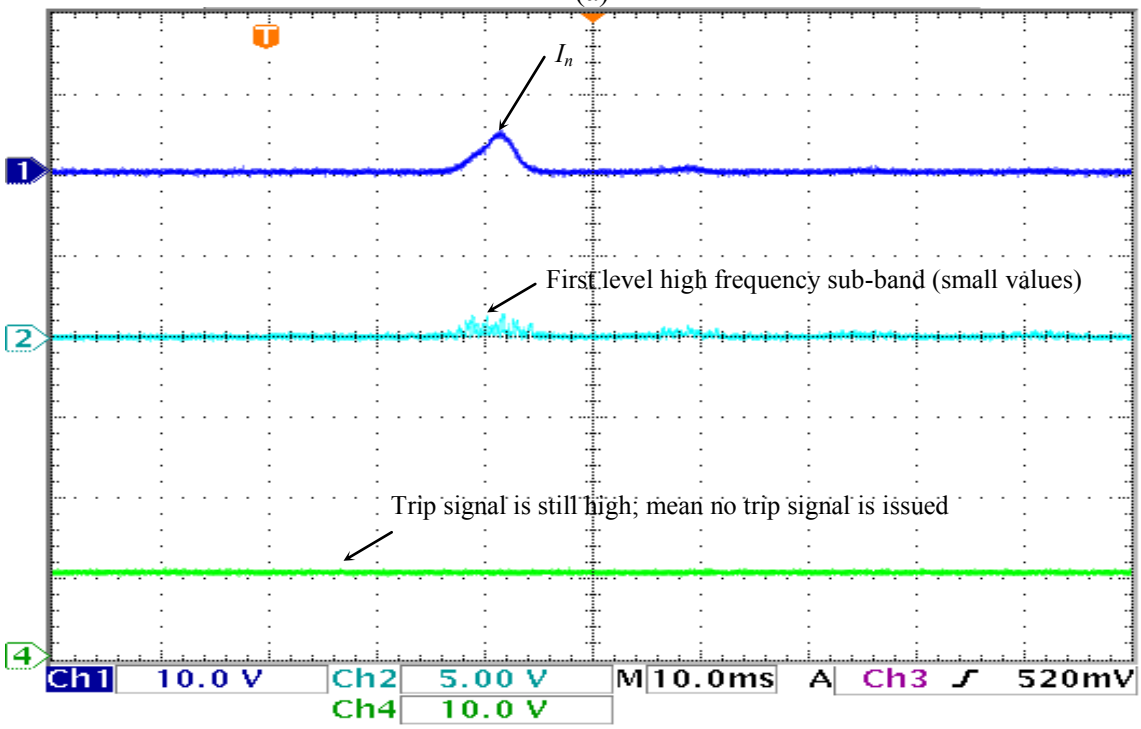

(b)

Figure 6-41 The experimental testing case of the magnetizing inrush current at induction motor load a) the three-phase magnetizing inrush currents and the 1st level high frequency sub-band b) $I_n = I_d^2+I_q^2$ current components the 1st level high frequency sub-band: the trip signal is still high, means no trip signal is issued.

- **Experimental Testing Results for Internal Faults:**

These experimental fault tests were carried out by connecting two phases of the transformer that are involved in the fault with and without the ground. A few samples of the results are provided as demonstrated in Figures 6.41 to 6.52 for different types of faults at different locations and loading conditions. The figures provide clear evidence that the proposed technique was able to detect the fault conditions and, hence, tripped the transformer within a few milliseconds. The proposed dqWPT technique provided a good performance in all the demonstrated cases, which proves its efficacy. Some of these cases are described in detail. It should be mentioned that all the faults were carried out when the source phase voltage was around 100V to avoid the high fault currents that could damage the equipment.

a) Primary Single Line to Ground Fault

This fault test was carried out by connecting the primary side phases to the ground. Figure ***6-42*** depicts the 3-phase differential currents of phase A to the ground fault when the transformer was connected to a unbalanced R-L load including the first level high frequency sub-band and the trip signal. This test was carried out several times under different loading conditions on the other two phases as shown in Figure ***6-43***, Figure ***6-44*** and Figure ***6-45***. The proposed technique responded correctly in all cases within the range of (2-4) msec of the fault inception.

b) Secondary Line to Line Faults

This fault test was carried out by short-circuiting two phases at a time on the secondary side of the power transformer. Figure ***6-46*** depicts a phase B to C to ground fault current, including the first level high frequency sub-band and the trip signal. The proposed technique has successfully produced the trip signal to is. The proposed technique was able to respond

to all of the faults within 4 msec of the fault inception.

c) Primary and Secondary Three-Phase Faults

This fault was carried out by connecting the three-phases together at the primary or secondary sides of the transformer at different loading conditions. Figure ***6-47***, Figure ***6-48*** and Figure ***6-49*** show the fault currents, including the first level high frequency sub-band components and the trip signal. The algorithm identified the fault easily and issued a trip signal within (2-4) msec. The proposed algorithm responded correctly again in all cases and has never misidentified the three-phase fault.

d) Secondary Single Line to Ground Fault

This test was carried out by connecting one phase at a time to ground on the secondary side. Figure ***6-50*** shows the experimental result of the phase B to ground fault including the first level high frequency sub-band components and the trip signal. As is obvious in the figure, the proposed algorithm issued a trip signal in just 3 msec. Several tests on the other two phases to ground, under different loading conditions were carried out.

e) Primary Line to Line Faults

This fault test was carried out by short-circuiting two phases at a time on the primary side of the transformer. Figure ***6-51*** and Figure ***6-52*** depict phase A to B and phase A to C faults respectively at different loading conditions, including the first level high frequency sub-band and the trip signal at no load. The proposed technique produced successfully the trip signal in about 2 msec after the beginning of the fault, which proves its efficacy.

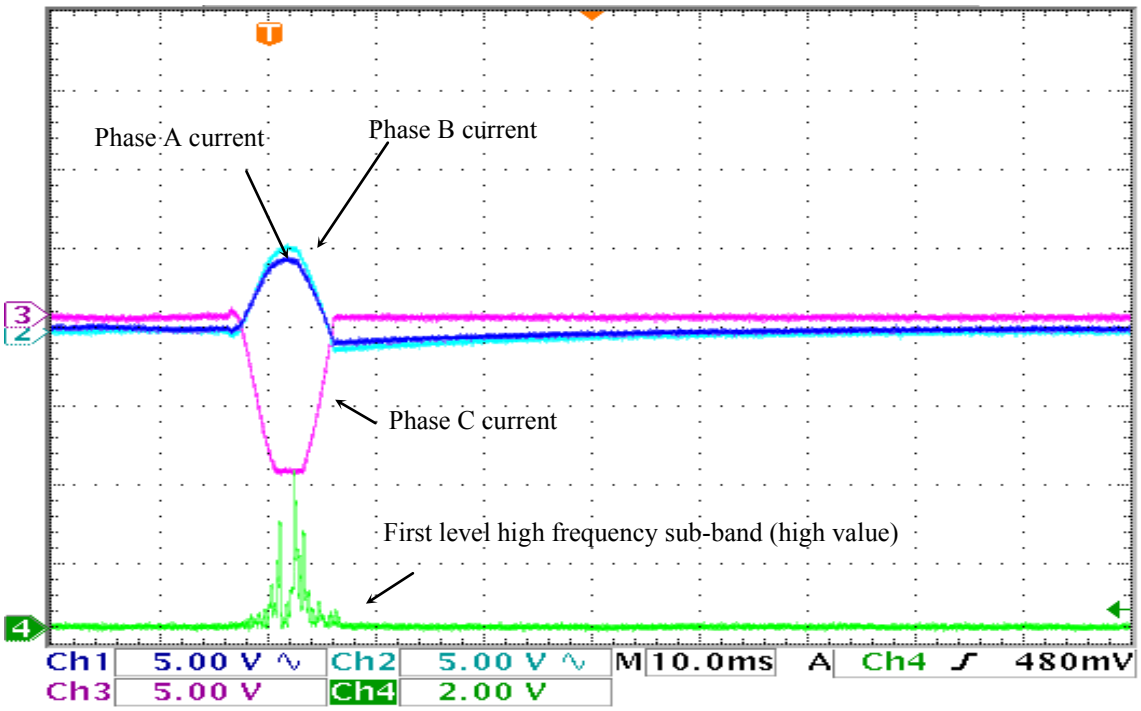

(a)

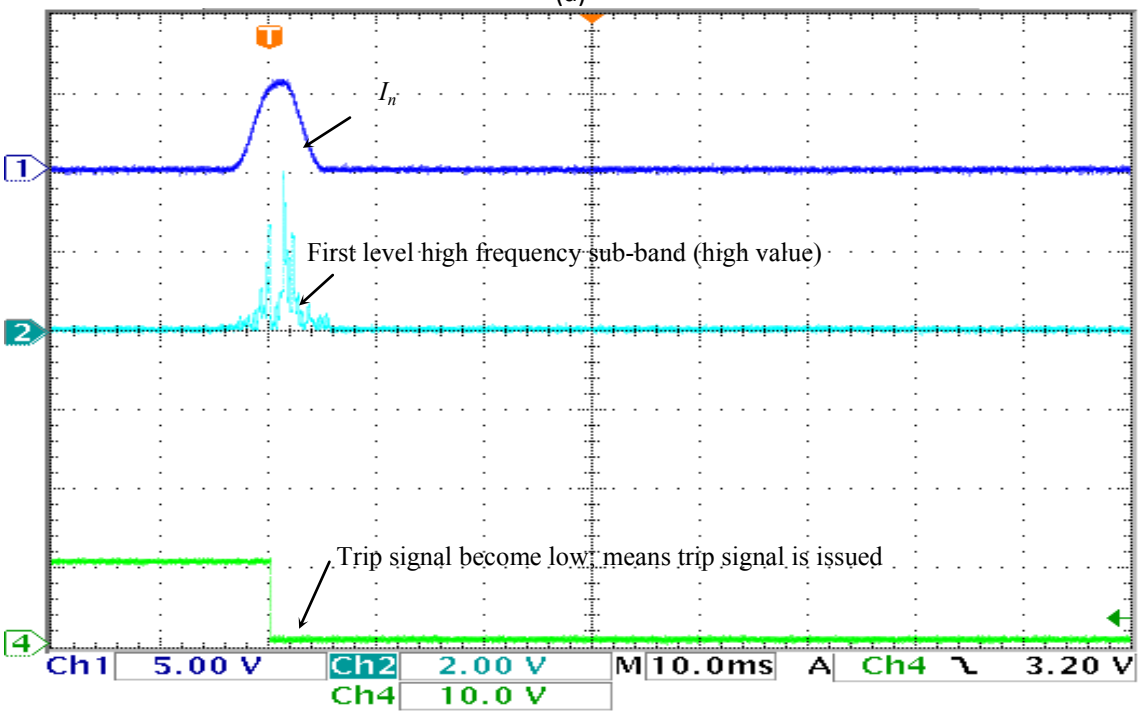

(b)

Figure 6-42 The experimental testing case of primary single line A to ground fault at unbalanced R-L load a) the three-phase transformer currents the 1st level high frequency sub-band b) $I_n = I_d^2+I_q^2$ current components the 1st level high frequency sub-band: the trip signal becomes low, means a trip signal is issued.

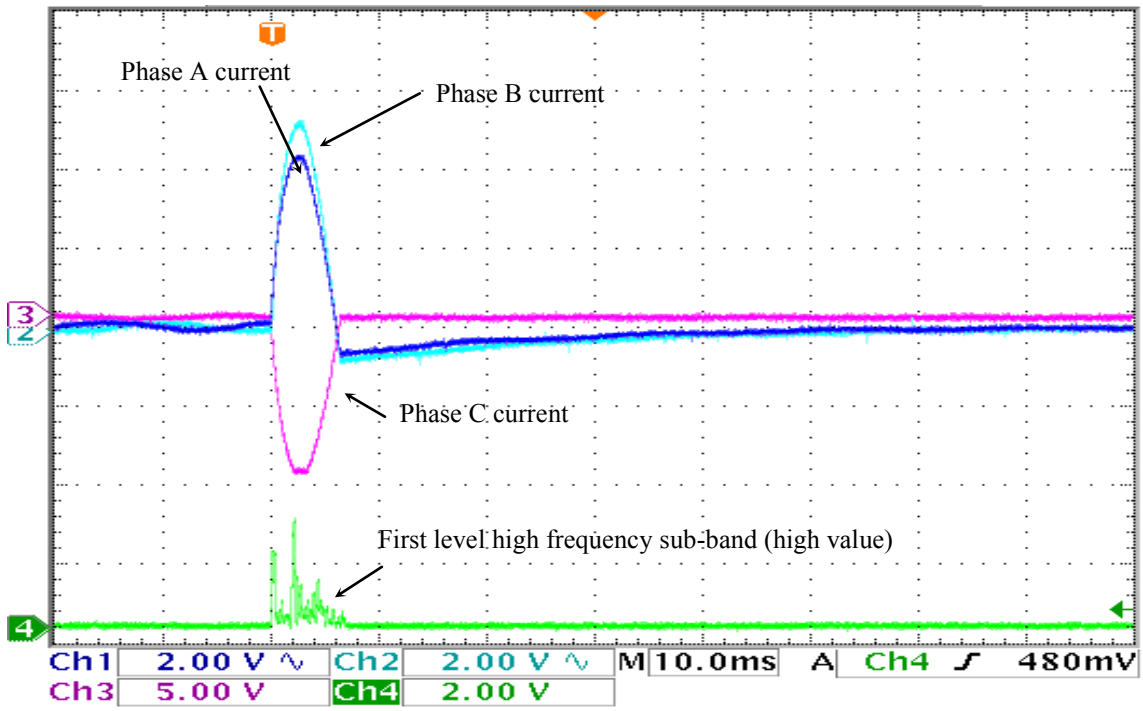

(a)

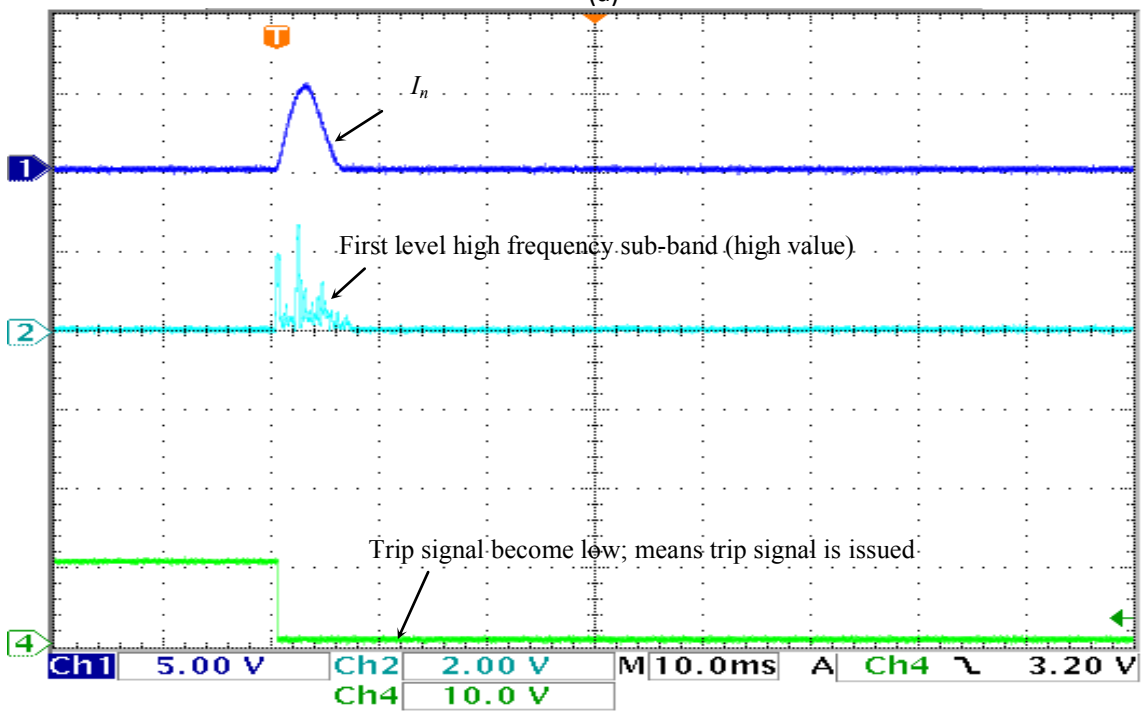

(b)

Figure 6-43 The experimental testing case of primary single line C to ground fault at induction motor load a) the three-phase transformer currents the 1st level high frequency sub-band b) $I_n = I_d^2+I_q^2$ current components and the 1st level high frequency sub-band: the trip signal becomes low, means a trip signal is issued.

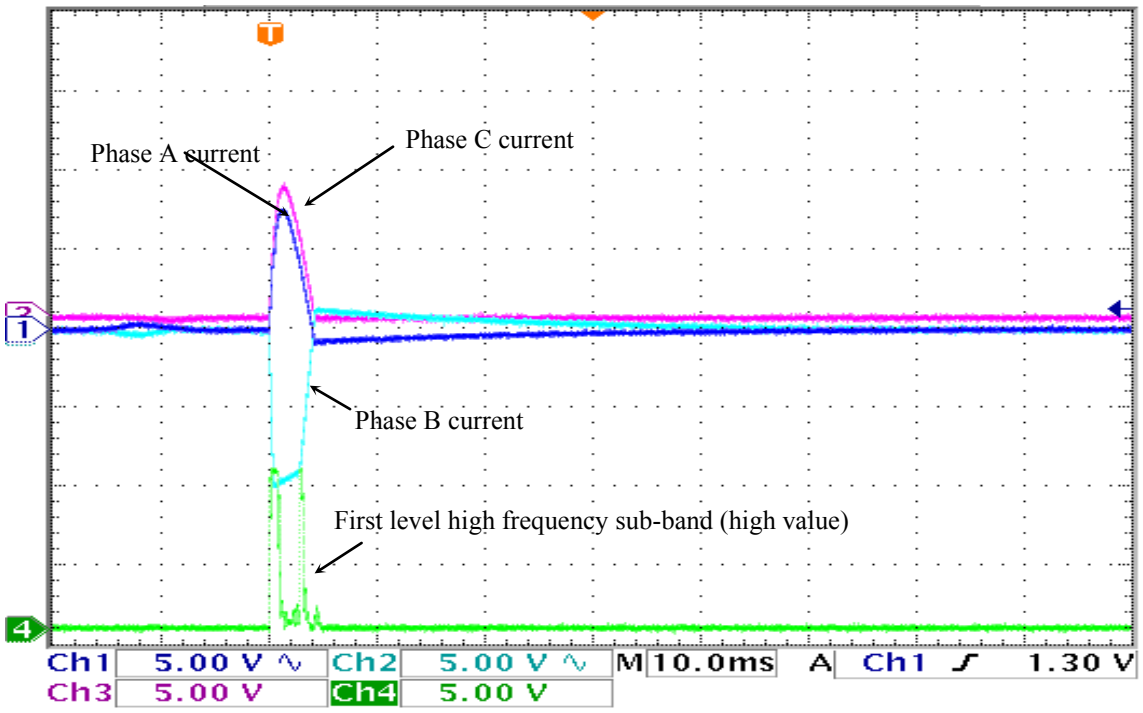

(a)

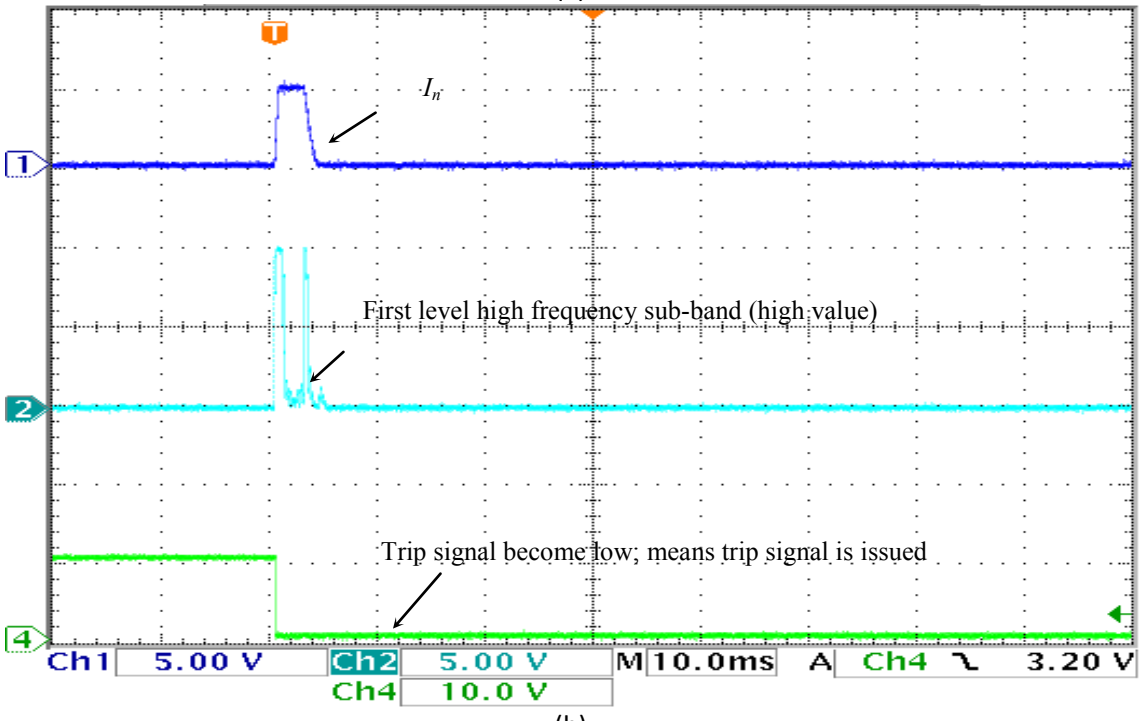

(b)

Figure 6-44 The experimental testing case of unloaded primary single line B to ground fault a) the three-phase transformer currents the 1st level high frequency sub-band b) $I_n = I_d^2+I_q^2$ current components and the 1^{st} level high frequency sub-band: the trip signal becomes low, means a trip signal is issued.

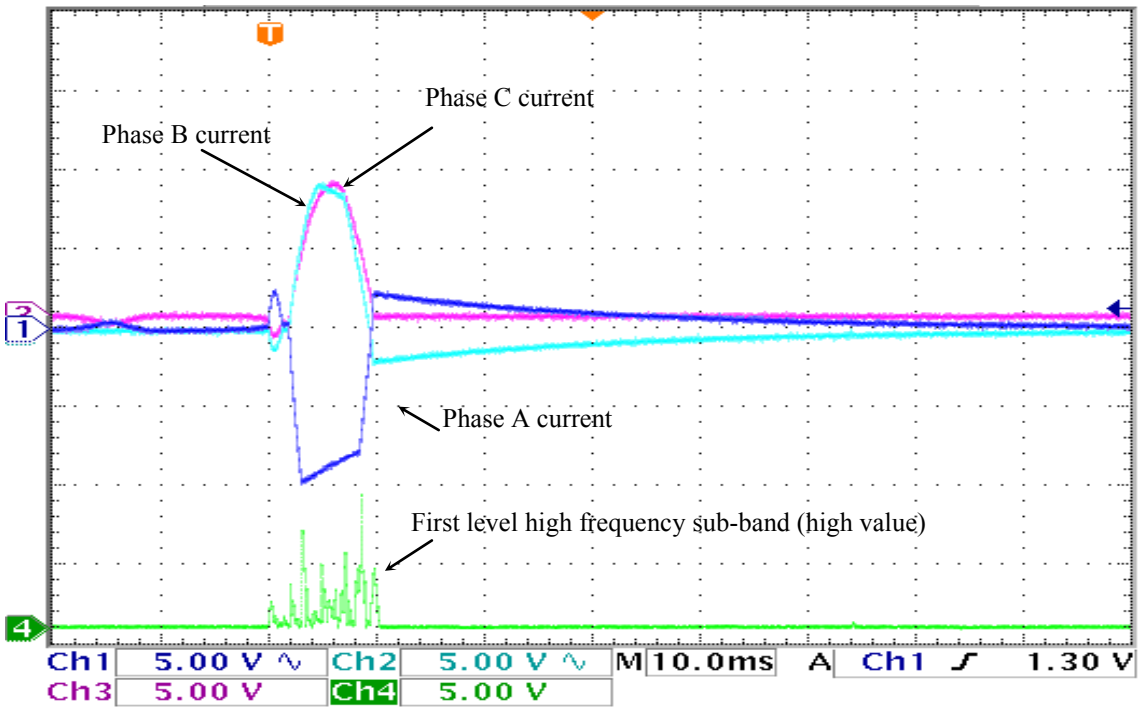

(a)

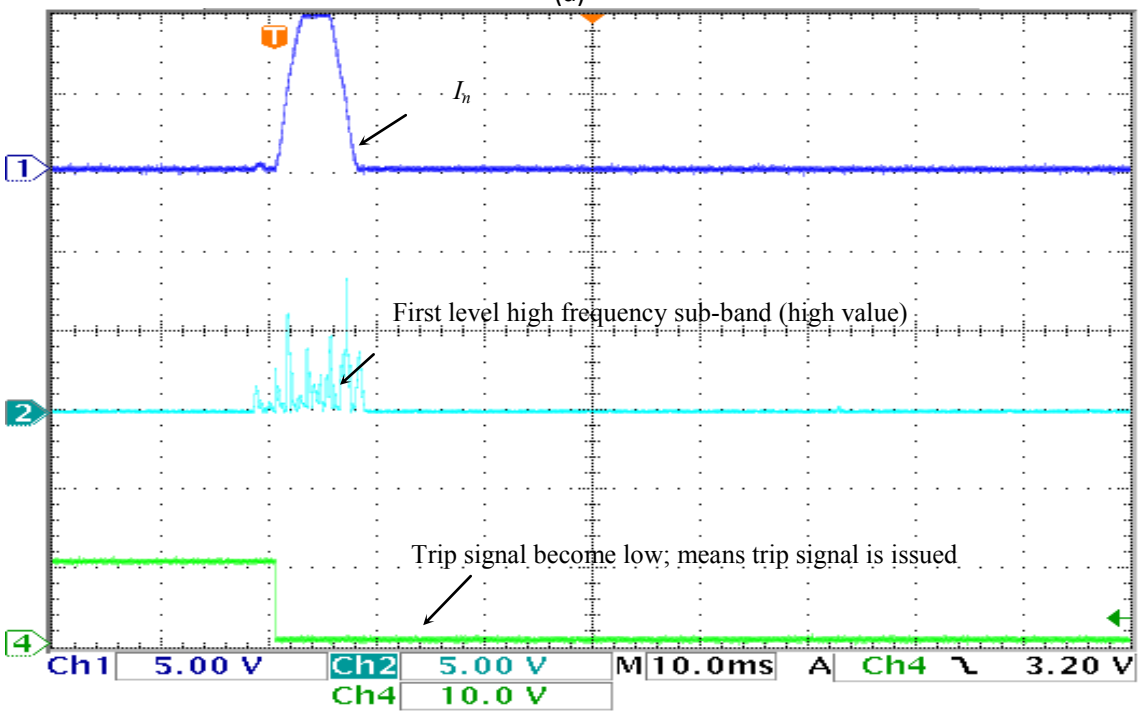

(b)

Figure 6-45 Another experimental testing case of unloaded primary single line B to ground fault a) the three-phase transformer currents the 1st level high frequency sub-band b) $I_n = I_d^2+I_q^2$ current components and the 1st level high frequency sub-band: the trip signal becomes low, means a trip signal is issued.

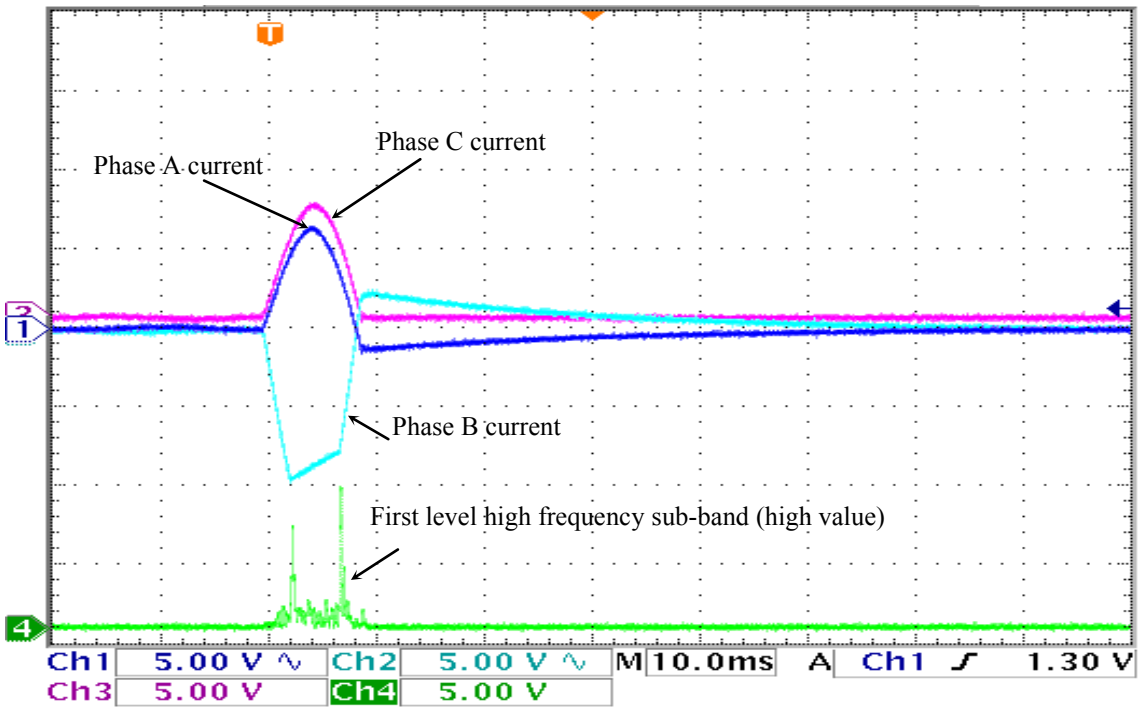

(a)

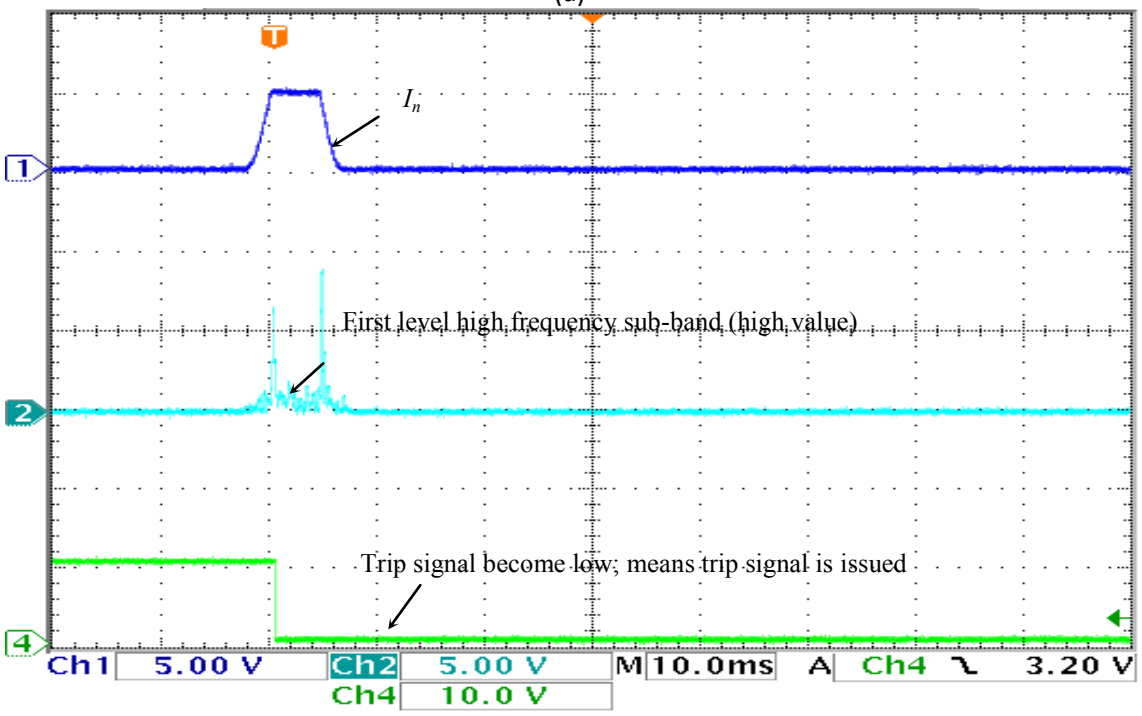

(b)

Figure 6-46 The experimental testing case of secondary phase B to C fault at balanced R-L load a) the three-phase transformer currents the 1st level high frequency sub-band b) $I_n = I_d^2+I_q^2$ current components and the 1^{st} level high frequency sub-band: the trip signal becomes low, means a trip signal is issued.

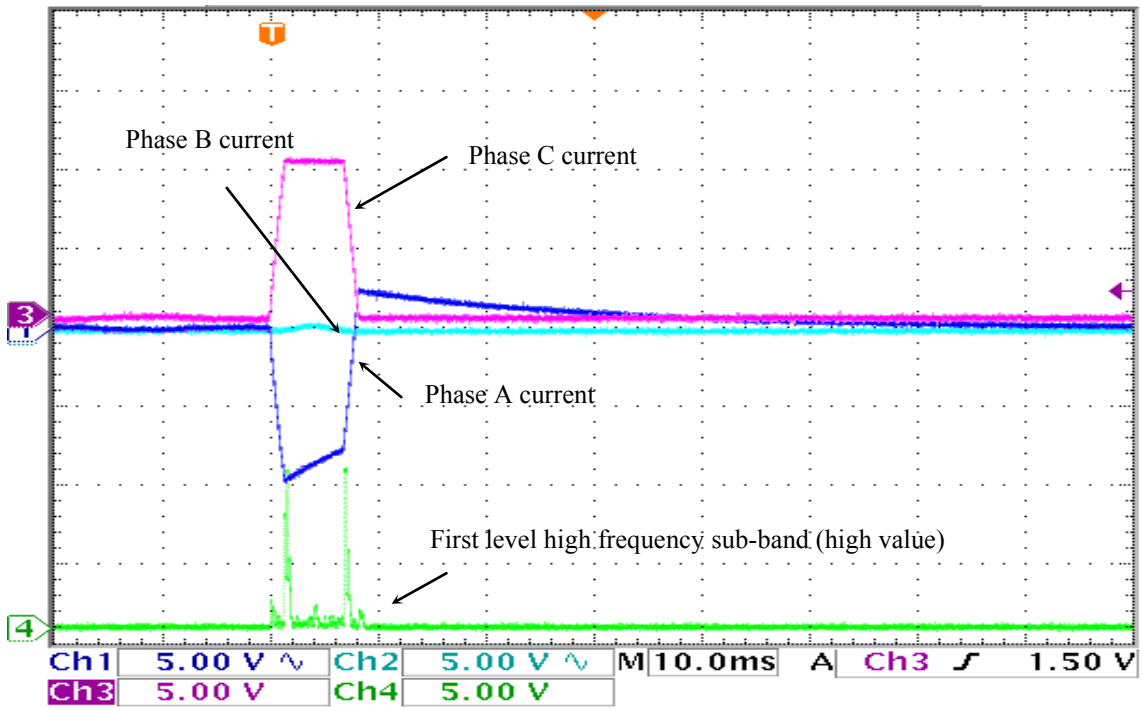

(a)

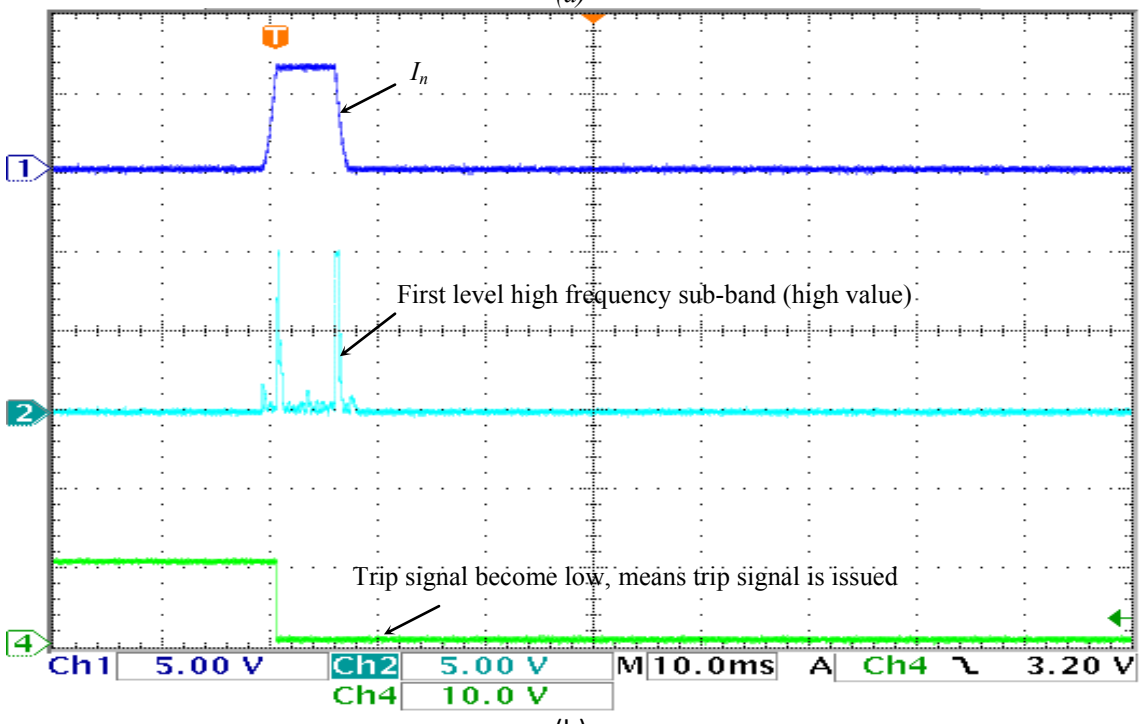

(b)

Figure 6-47 The experimental testing case of primary three-phase fault at balanced R-L load a) the three-phase unloaded transformer currents and the 1st level high frequency sub-band b) dq current components and the 1st level high frequency sub-band: the trip signal went low, means the trip signal is issued.

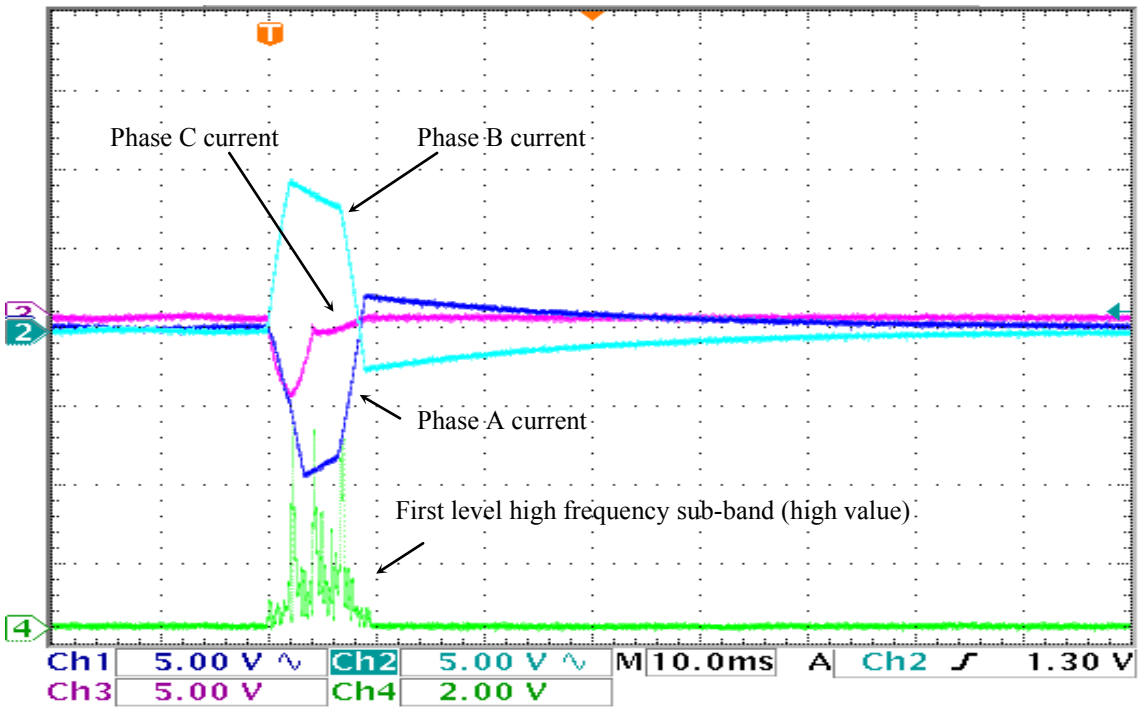

(a)

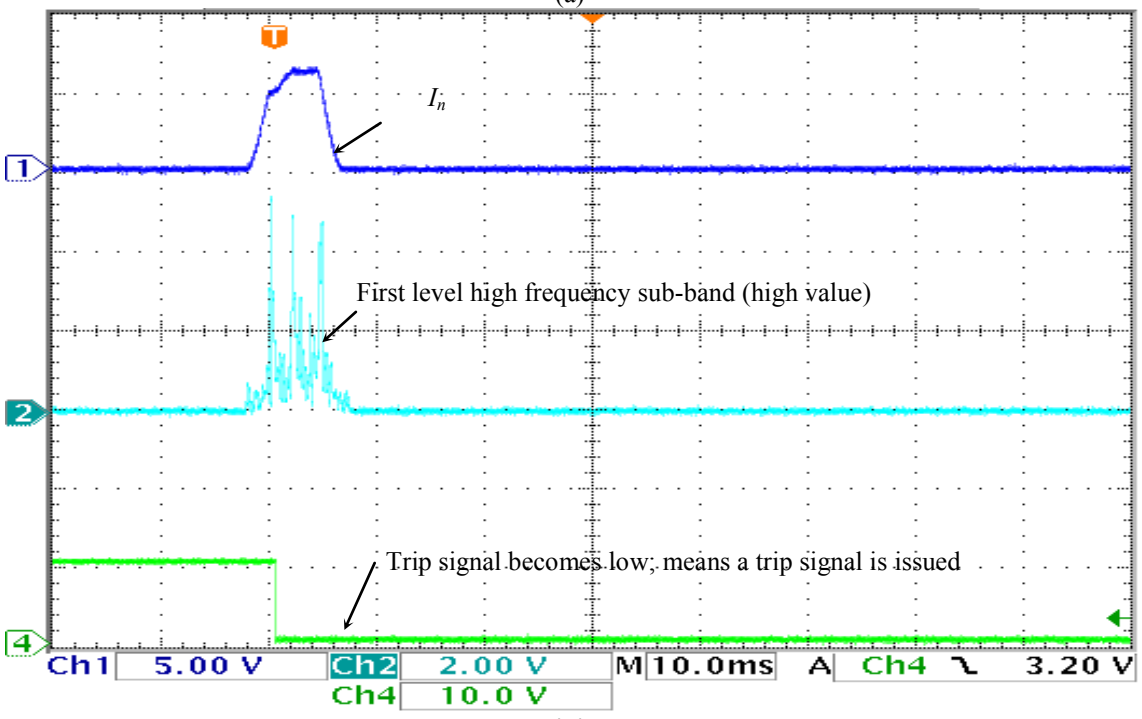

(b)

Figure 6-48 The experimental testing case of secondary side three-phase to ground fault at balanced R-L load a) the three-phase fault currents and the 1st level high frequency sub-band b) dq current components and the 1st level high frequency sub-band: the trip signal went low, means the trip signal is issued.

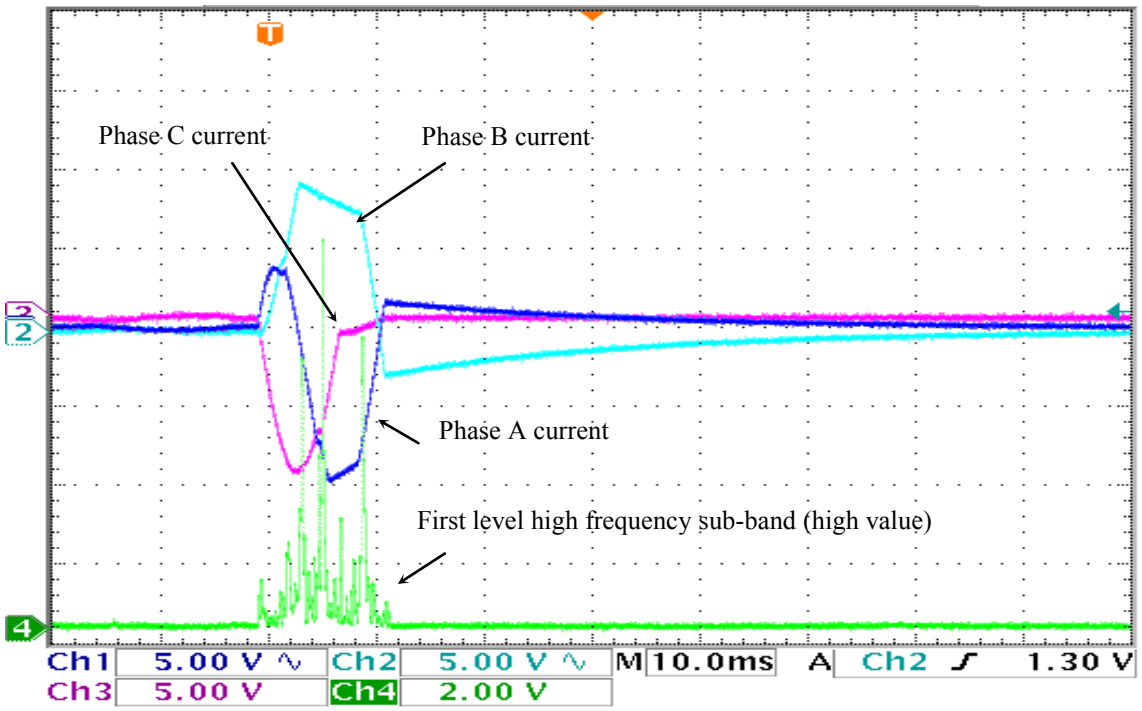

(a)

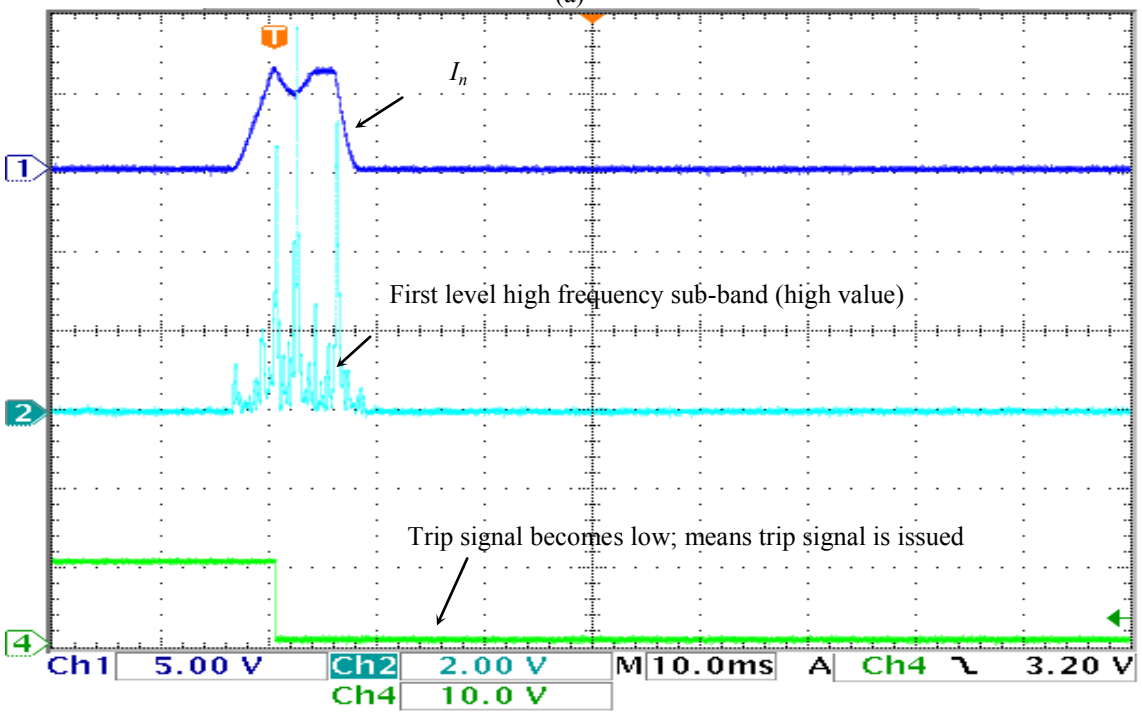

(b)

Figure 6-49 The experimental testing case of the secondary side three-phase fault at non-linear load a) the three-phase transformer currents the 1st level high frequency sub-band b) $I_n = I_d^2 + I_q^2$ current components and the 1^{st} level high frequency sub-band: the trip signal becomes low, means a trip signal is issued.

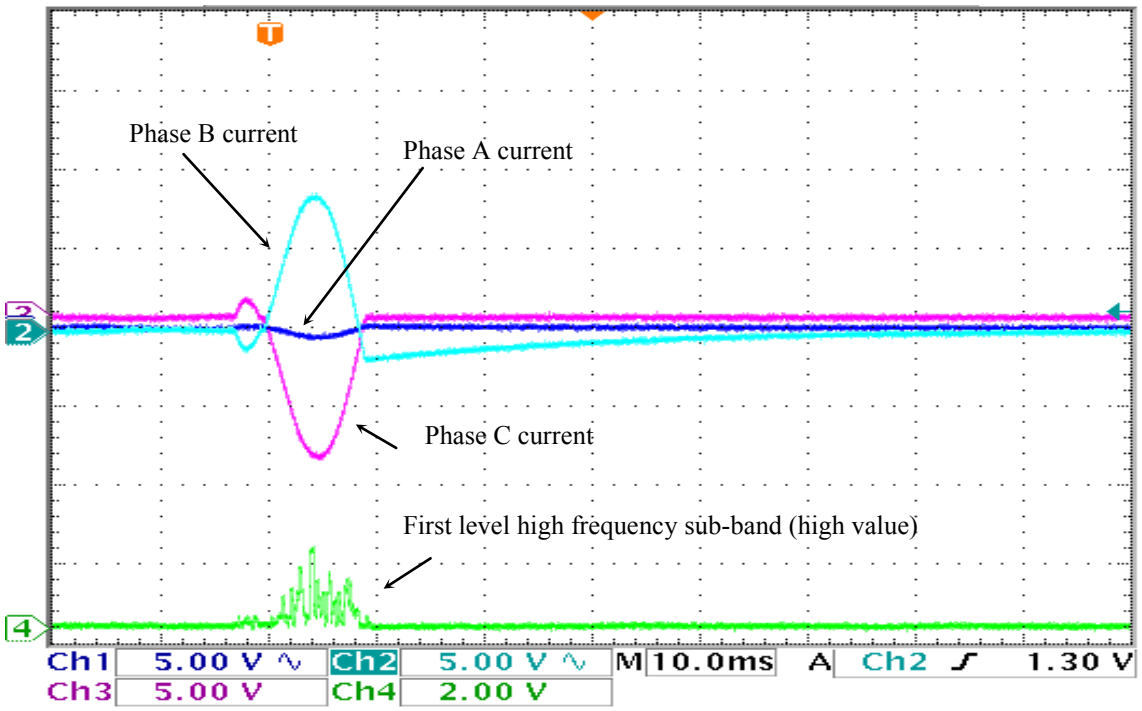

(a)

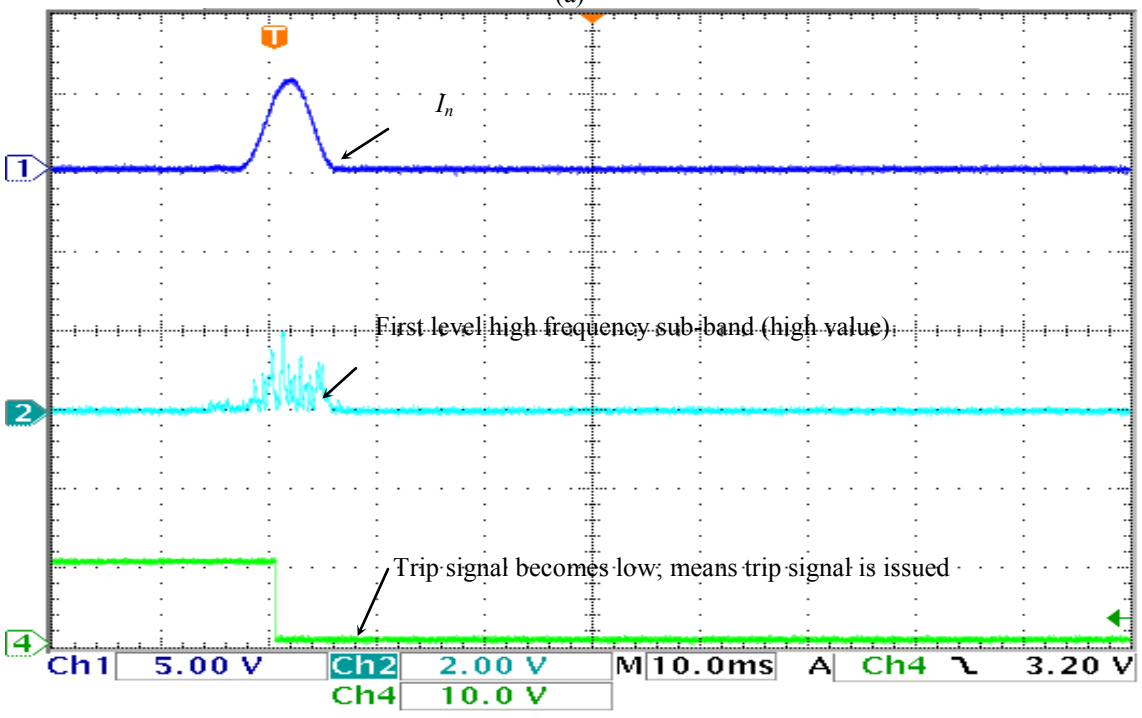

(b)

Figure 6-50 The experimental testing case of secondary single line B to ground fault at unbalanced load a) the three-phase transformer currents the 1st level high frequency sub-band b) $I_n = I_d^2+I_q^2$ current components and the 1st level high frequency sub-band: the trip signal becomes low, means a trip signal is issued.

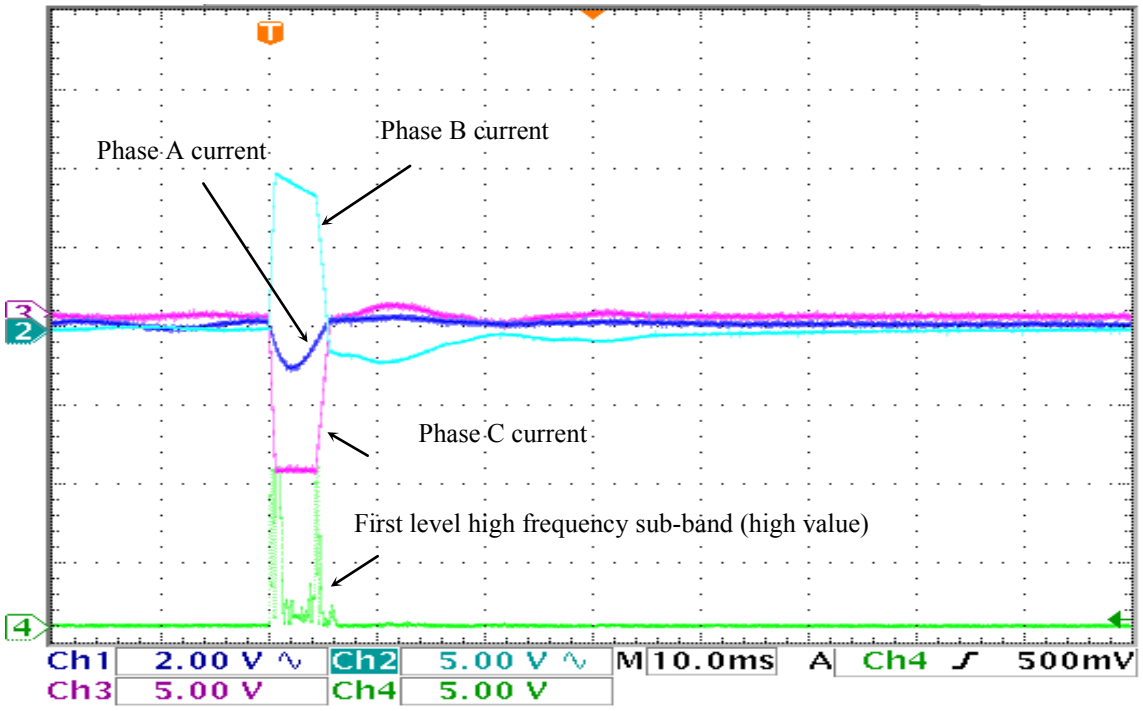

(a)

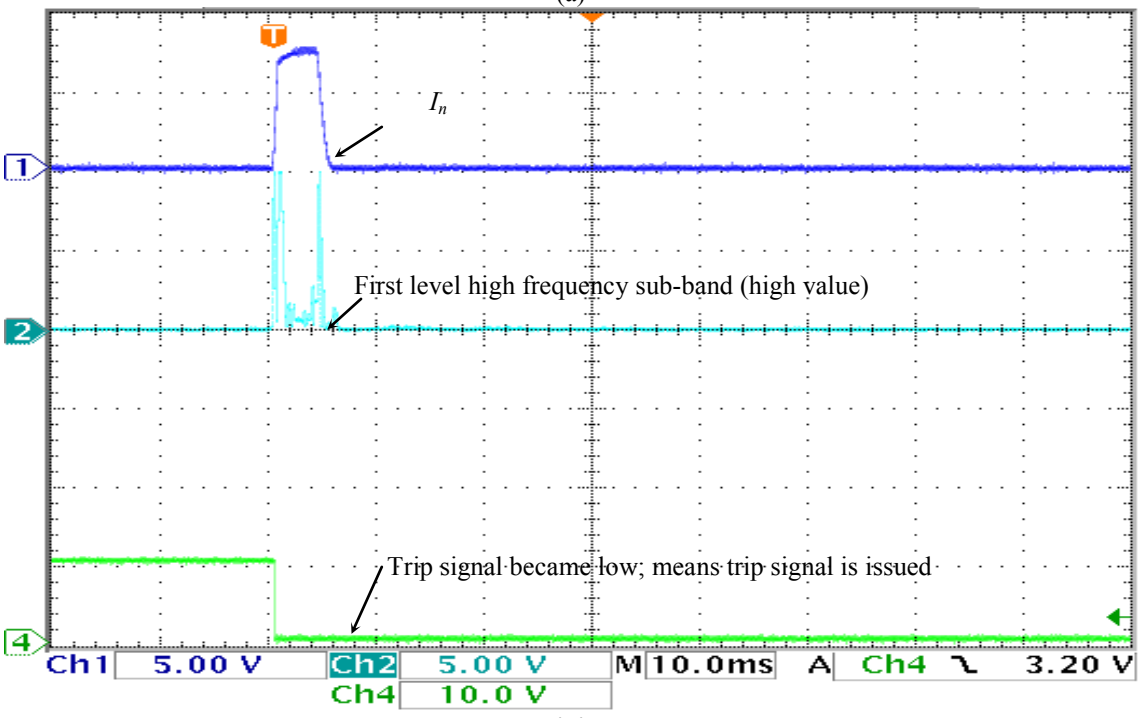

(b)

Figure 6-51 The experimental testing case of primary phase A to B fault at induction motor load a) the three-phase transformer currents the 1st level high frequency sub-band b) dq current components and the 1st level high frequency sub-band: the trip signal becomes low, means a trip signal is issued.

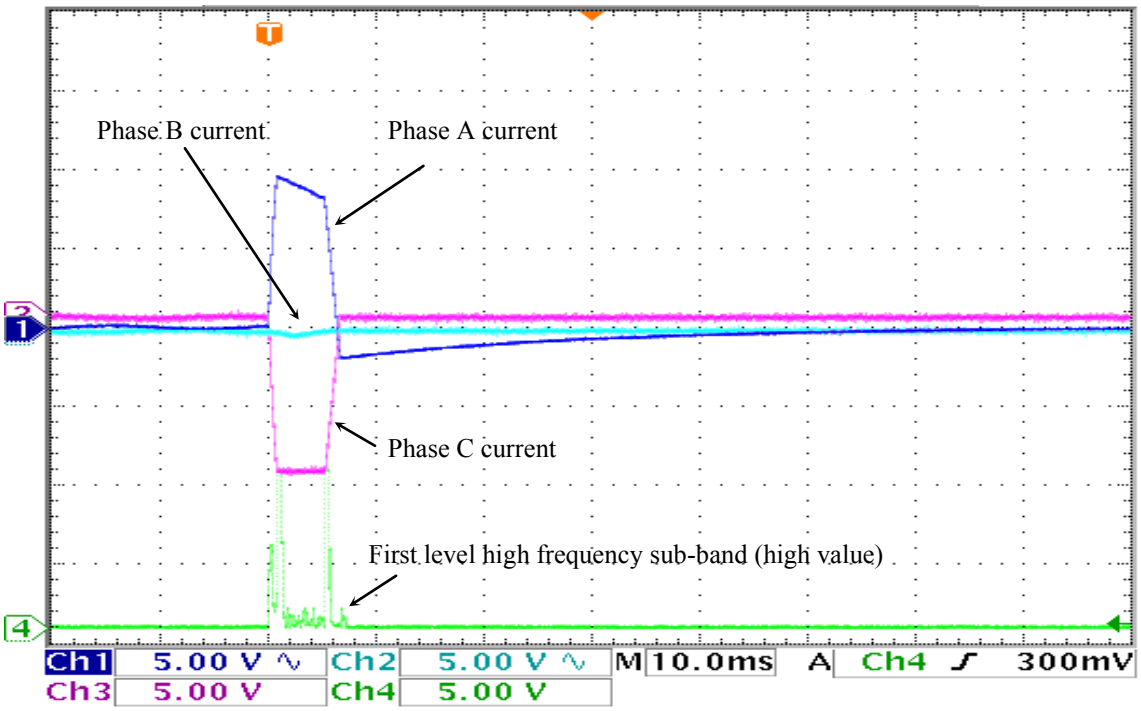

(a)

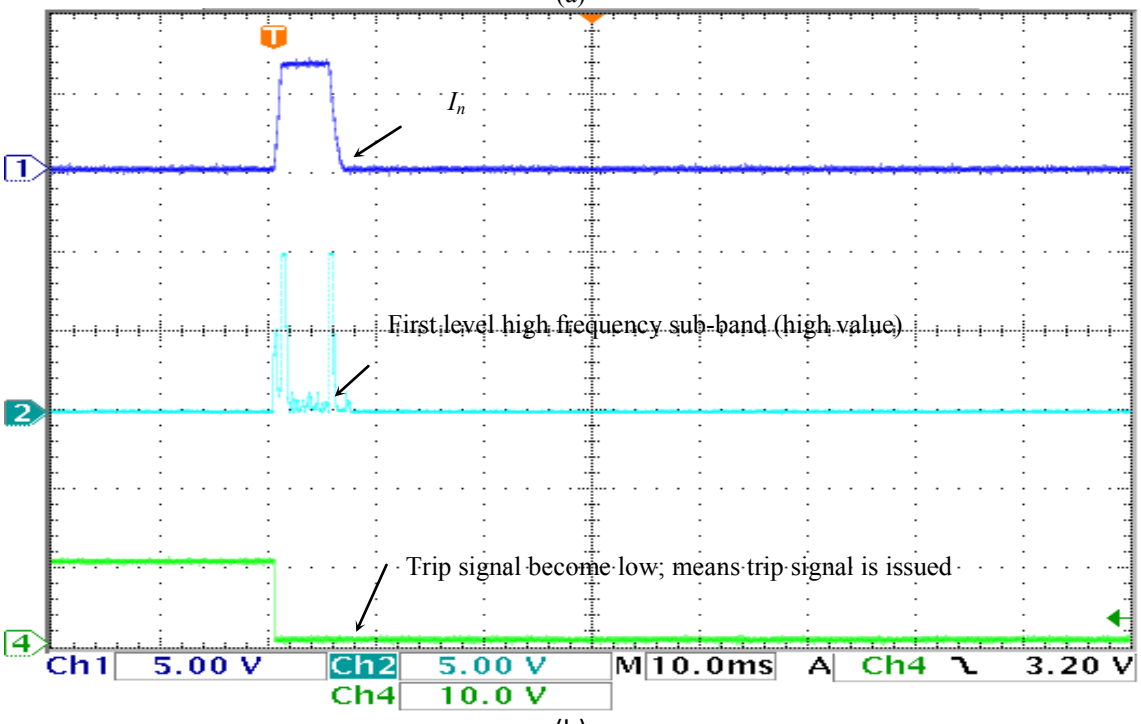

(b)

Figure 6-52 The experimental testing case of primary phase A to C fault at balanced R-L load a) the three-phase transformer currents the 1st level high frequency sub-band b) $I_n = I_d^2+I_q^2$ current components and the 1^{st} level high frequency sub-band: the trip signal becomes low, means a trip signal is issued.

- **Experimental Testing Results for Other Disturbances:**

This part completes the testing of the proposed technique, in which non-faulted disturbances as well as external faults outside the protected zone were made. These tests prove the accuracy and efficacy of the proposed technique. These kinds of disturbances may activate the differential relay and trip the power transformer if the relay is not designed to recognize such cases. The tests include the CTs mismatches and saturation, over-excitation, and external through faults.

e) CTs Mismatch Currents

These currents appear in the differential currents due to the discrepancies in the CTs used. These discrepancies create CTs mismatch. Figure ***6-53*** provides an example of the CTs mismatch at unloaded conditions. The proposed algorithm has successfully passed this test without creating any problems. It was also tested for other loading conditions successfully.

f) CT saturation,

This diagnostic test has to be carried out for differential protection relays, because CTs connect the protective relay with the hardware circuit of the power transformer. CT saturation may occur due to excessive amounts of magnetizing inrush currents or fault currents. CT saturation can obviously be noticed in many tests that were carried out for fault conditions such as Figure ***6-47***, Figure ***6-48***, Figure ***6-49***, Figure ***6-51***, Figure ***6-52*** and Figure ***6-54***. It is clear from the figures that the CTs saturated and could not pass the high currents, which distorts the signal. These figures show that the proposed technique has sent a trip signal to isolate the power transformer as if no any saturation took place.

g) Over-excitation,

This test is carried out by applying high voltage to the input of the power transformer, which was about 110% of the rated voltage. As can be seen from Figure ***6-55*** under an unbalanced load of $Z_a = 600 + j300$, $Z_b = 1200 + j600$, $Z_c = 2400 + j1200$, the current is relatively distorted because of the presence of a strong fifth harmonic component especially in phases B and C. The figure shows no change in the trip signal, which indicates a non-fault condition. This proves the efficacy of the proposed technique.

h) External or Through Faults,

External faults are one of the major problems that have to be considered in the design of the differential protection relay. This experimental test was carried out to test the immunity of the algorithm against through faults that may occur due to severe external faults outside of the protected zone. The through-current appears in the differential currents only for CT mismatches due to either mis-selection of the proper CTs or for severe cases of external faults, which causes CT saturation and, consequently, causes CTs mismatch. Figure ***6-56*** depicts that no trip signal was issued due to the occurrence of the external fault between phases B and C, which indicates a non-internal faulted condition. The proposed algorithm was tested many times in this case on the other two phases and it has never generated a trip signal.

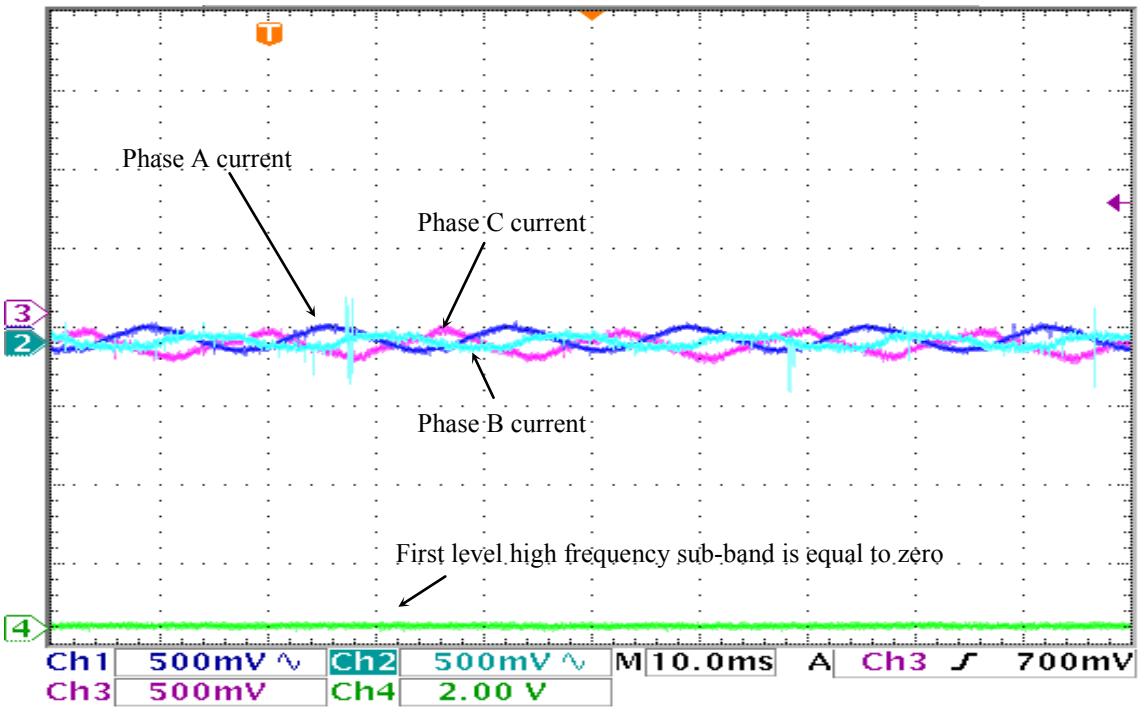

(a)

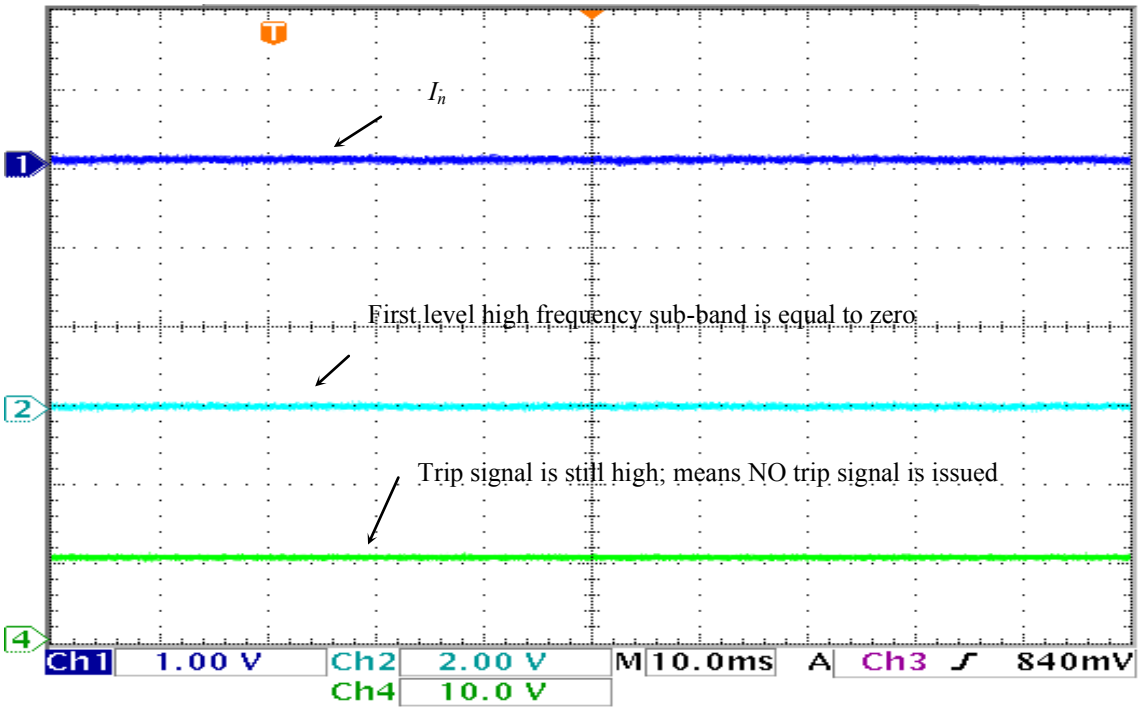

(b)

Figure 6-53 The experimental testing case of the CT mismatches at balanced load a) the three-phase loaded transformer currents and the 1st level high frequency sub-band b) dq current components and the 1st level high frequency sub-band and the trip signal is still high, means no trip signal is issued.

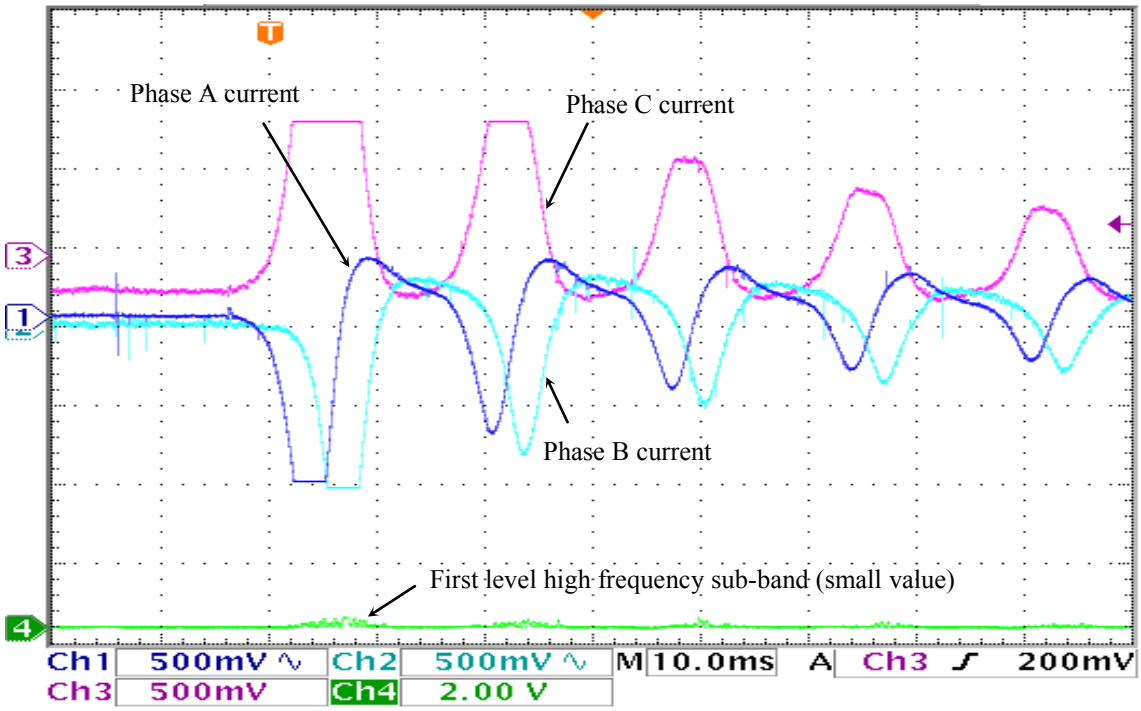

(a)

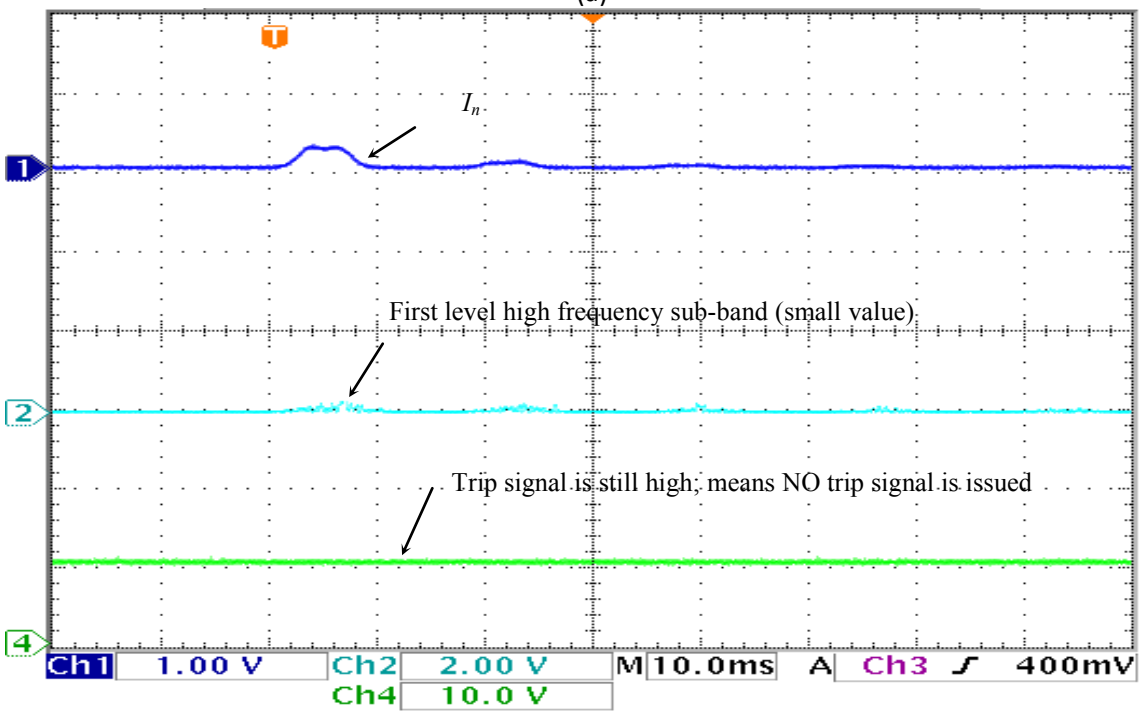

(b)

Figure 6-54 The experimental testing case of the CT Saturation a) the three-phase loaded transformer currents and the 1st level high sub-band frequencies b) $I_n = I_d^2+I_q^2$ current components and the 1st level high sub-band frequencies (zero value): the trip signal is still high, means no trip signal is issued.

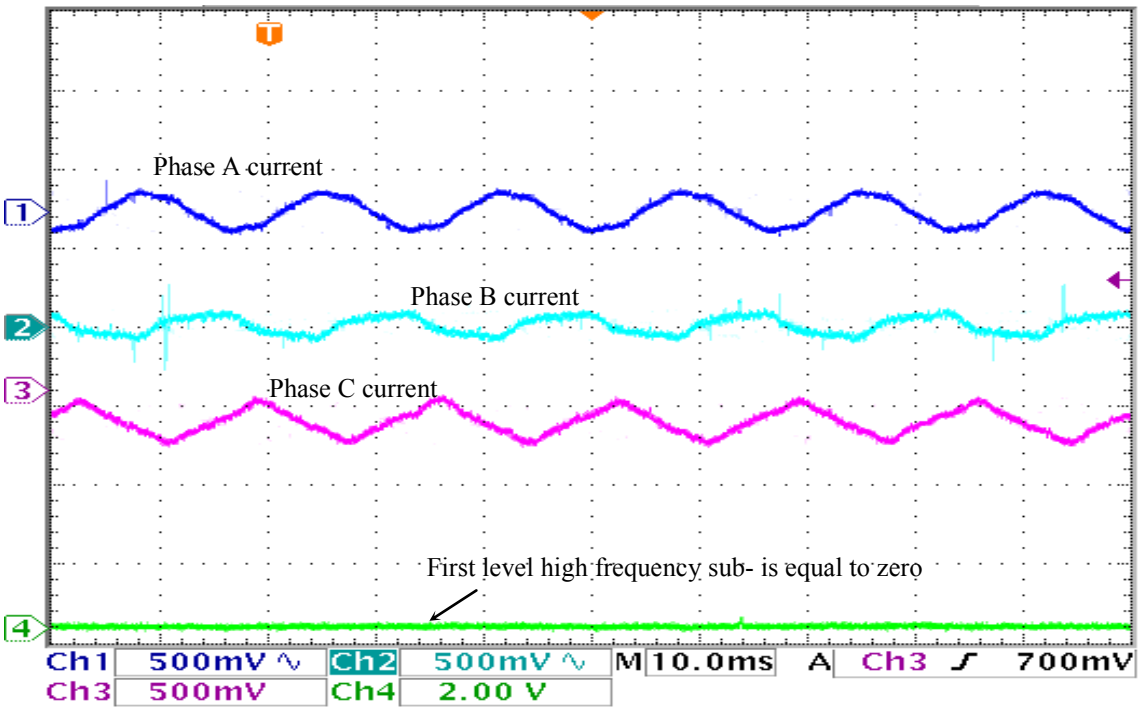

(a)

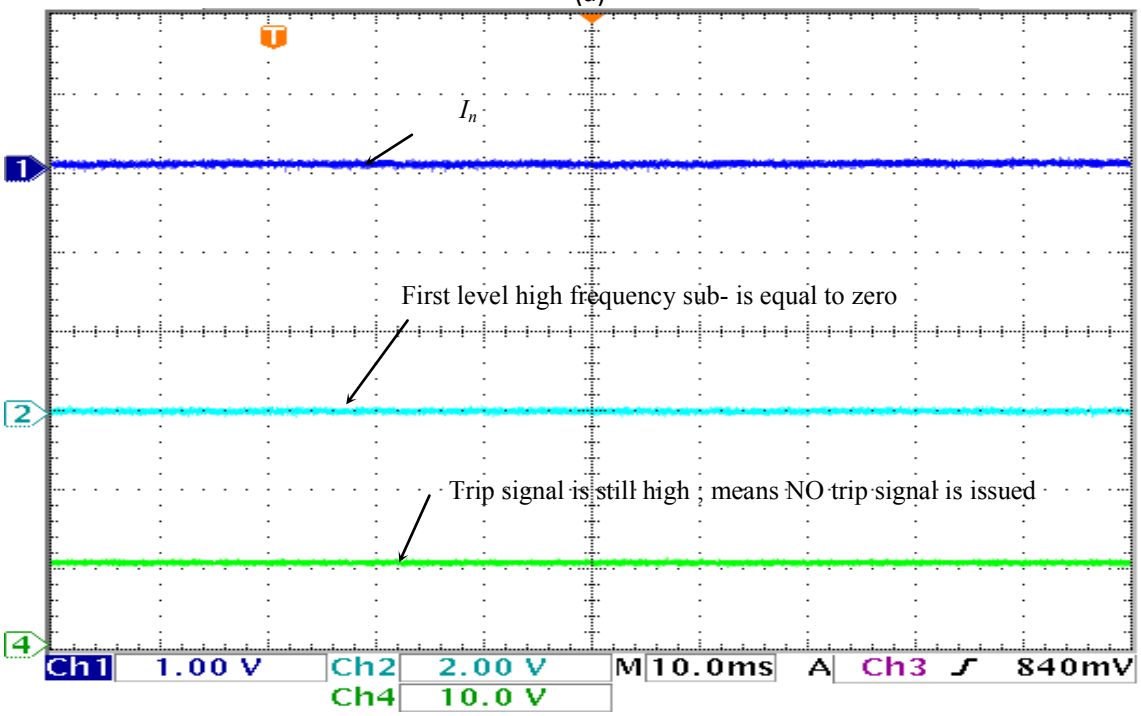

(b)

Figure 6-55 The experimental testing case of the over excitation at unbalanced load a) the three-phase loaded transformer currents and the 1st level high sub-band frequencies b) $I_n = I_d^2+I_q^2$ current components and the 1st level high sub-band frequencies (zero value): the trip signal is still high, means no trip signal is issued.

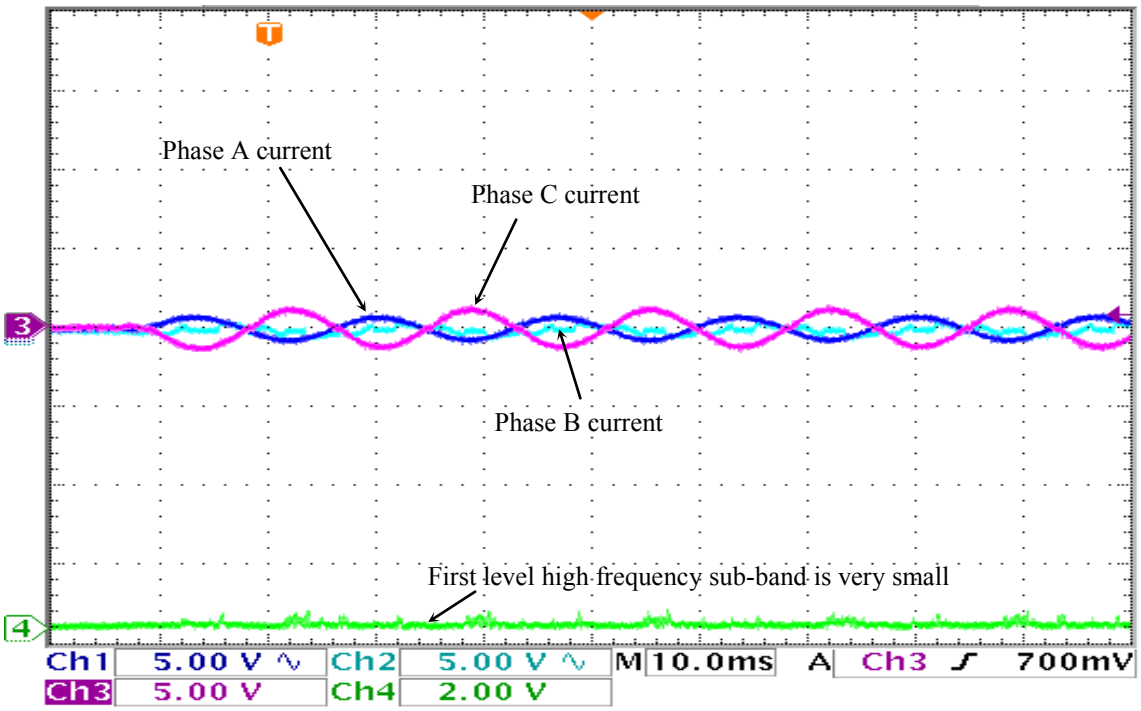

(a)

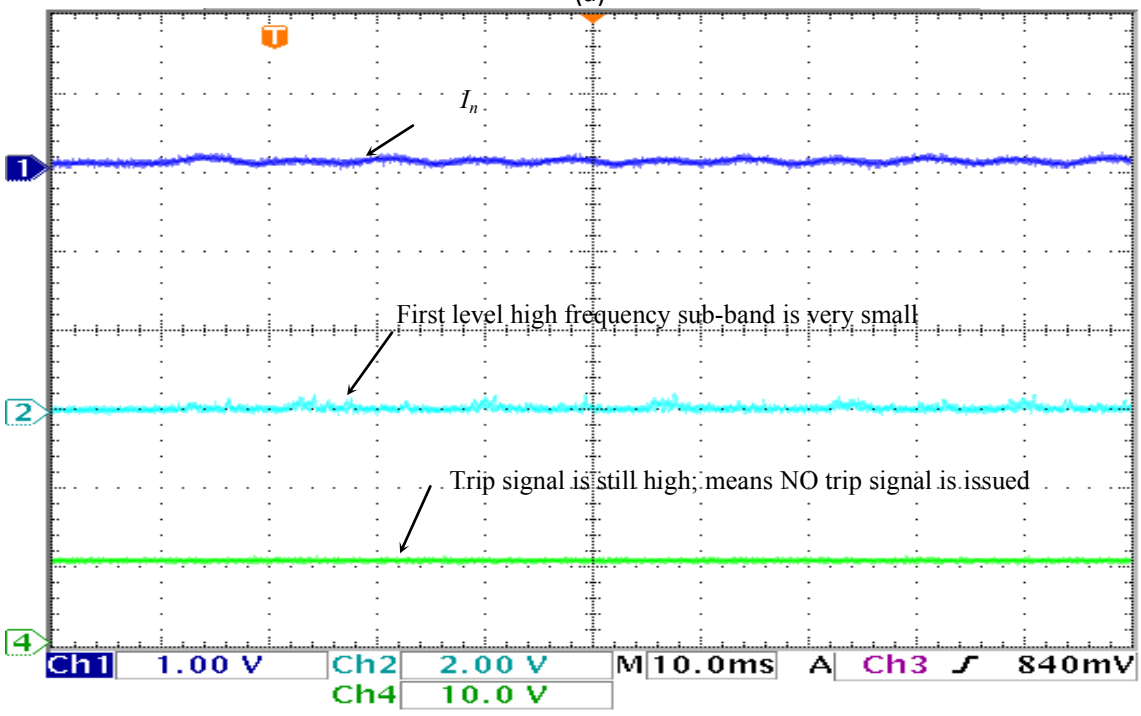

(b)

Figure 6-56 The experimental testing case of the external phase B to C fault at non-linear load a) the three-phase loaded transformer currents and the 1st level high frequency sub-band b) $I_n = I_d^2+I_q^2$ current components and the 1st level high frequency sub-band (zero value): the trip signal is still high, means no trip signal is issued.

The proposed dqWPT hybrid algorithm was successfully implemented and tested in a real time environment using the DSP board, ds-1102 and ds-1104 on two different power transformers. The experimental testing results are satisfactory and consistent. From the provided result, it is obvious that the response of the proposed hybrid technique is accurate and within a satisfactory period to detect the faults. In all the fault cases, the trip signal was issued in less than five milliseconds. Moreover, the measured CPU computational time, per time step is less than four μsec for different types of the test cases. The proposed dqWPT hybrid technique has proven its efficacy to detect and discriminate fault currents from inrush currents, even with the existence of some disturbances such as over-excitation and the CTs saturation and mismatches. The next chapter provides the conclusion of this work including the major contributions and suggested future works.

Chapter 7

Conclusions and Future Work

Protection for power transformers has improved significantly during the last three decades. Many different techniques for power transformer protection have been developed with different techniques and methodologies. However, due to the significant changes in modern power systems and the new design of power transformers, improvement of the protection systems is required to achieve the optimal functionality of the protection systems, in particular, the reliability, security and speed of response. The main challenges in the design of power transformer protection are avoiding false tripping due to magnetizing inrush currents and external faults. In addition, the designed technique has to detect all the internal faults and rapidly trip the power transformer to reduce the outage time and its consequences.

7.1 Conclusions

In this work, two different mathematical concepts are used to build the proposed hybrid technique. It consists of direct and quadrature axis (dq), and the wavelet packet transform (WPT). These two mathematical concepts are combined to provide a new hybrid technique $dqWPT$ for the digital differential protection of power transformers. This dqWPT hybrid technique is employed for detecting and classifying all types of disturbances that may occur within the power transformers. The development and implementation of off-line and real-time testing is carried out for the digital differential protection of three-phase transformers. The testing results of this technique show that it is able to distinguish successfully faults from inrush currents and associated transients for the protection of power transformers.

This proposed dqWPT hybrid technique was based on employing a single stage of WPT decomposition in order to extract the high frequency sub-band contents that are present in the dq axis components of the three-phase differential currents. Using the first level WPT details of the dq axis components of the differential current is found to provide the required information to diagnose the current flowing in the 3-phase power transformer. The extracted high frequency sub-band contents (details) of the dq axis components were parameterized using the WPT coefficients. These details components were employed to detect and classify disturbances in the 3-phase power transformer into faults and inrush currents. The WPT-based digital relay was carried out for two different 3-phase laboratory power transformers rated at 5kVA and 2kVA. Many cases of different faults and magnetizing inrush currents including CT saturation and mismatch, as well as, over-excitation and through-fault currents were considered for real-time testing of the $dqWPT$ based digital differential protection for the laboratory power transformers. The simulation and the experimental test results demonstrate a satisfactory performance in terms of speed and accuracy. These results show that the proposed technique has distinguished between the magnetizing inrush currents and all types of faults. Moreover, this proposed technique has provided fast and adequate security for tests such as CT saturation and mismatch, over-excitation, and external faults. In addition, the proposed hybrid technique has reduced the computational burden and the memory requirements for the real-time implementation of this digital relay without affecting the performance of the proposed technique. The results of these tests provide good support for employing the dqWPT-based hybrid digital relay for the digital differential protection of three-phase power transformers. The results show that the proposed technique can recognize any fault currents around four milliseconds. The trip signal is issued in all fault cases, in

spite of the existence of distortions due to CT saturation and DC offsets. The proposed technique has not misidentified any fault cases and successfully distinguished inrush currents from fault currents. The proposed hybrid technique has been found to be very suitable for the digital differential protection of modern power transformers through experimental investigations. It is worth mentioning that this hybrid technique constitutes a new contribution in the protection of power transformers.

The combination of the (dq) axis components with the WPT and its application in the real time protection of power transformers is a new contribution. This hybrid technique has a few advantages. For example, the specific sampling frequency constraint is removed by using the (dq axis) components of the currents. In addition, changing the abc to dq signals simplifies the implementation and reduces the computational time and memory requirements. It has been found that the technique insensitive to CTs mismatches and tap changers and not sensitive to the non-periodicity of the signal. Thus, the proposed hybrid technique is able to discriminate the high normal operating currents that occur due to CTs mismatch. The problem of the CTs mismatch in the differential protection algorithm does not usually allow the differential current to be zero. Applying the proposed hybrid technique to the periodic or non-periodic differential current signal produces the required frequency sub-bands for differential protection of power transformers. The major contributions include:

- A novel hybrid technique using the combination of the *dq*-axis components and the wavelet packet transform (*dqWPT*) has been developed for transformer protection, in which only a single stage of *WPT* decomposition is needed to extract the high frequency sub-band contents that are present in the *dq*-axis components of the differential currents.
- Original simple and elegant computer programing codes are developed in both

MATLAB m.file and C code in Turbo C (TC) language for the proposed technique.

- A short state-of-the-art review for differential protection of power transformers from 1880s until 2014 is provided. In addition, a survey for the use of wavelet analysis for power transformer protection is given.
- An experimental setup is implemented for acquiring the current data of different types of disturbances in order to performing the off-line data analysis.
- An efficient digital relaying algorithm based on the dqWPT hybrid technique is implemented in real-time for the protection of two different laboratory three-phase transformers using two different DSP boards ds-1102 and ds-1104.
- A critical discussion of the testing results of the dqWPT hybrid technique under various transients and distortions is presented.

7.2 Future Work:

It is suggested that the future researches should be directed to change and enhance this work. The researchers may find other ways to improve or extend the proposed work in this thesis. Some suggestions for how to make these improvements are given below:

- Over current and differential protection of synchronous generators,
- Transmission line differential protection,
- Power quality issues such as voltage sags, swells, under/over voltage, can be easily detected and classified by using this proposed technique. These kinds of transients affect the power quality factors of the power system, including smart grids.
- The combination of other mathematical tools may be considered to improve the performance of this technique, such as fuzzy logic, ANN and genetic algorithms.

Bibliography:

[1] The Canadian Electricity Association (CEA),, "Canada's Electricity Industry Survey 2151," Statistics Canada, May 5, 2013.

[2] M. Whelan and S. Normandin, "The History of The Transformer," Edison Tech Center, 2013.

[3] P. M. Anderson, Power System Protection, Piscataway, NJ: IEEE Press, 1999.

[4] Westinghouse, Applied Protective Relaying, Newark, N.J: Westinghouse Electric Coroporation, 1976.

[5] A. R. Van and C. Warrington, Protective Relays Their Theory and Practice, 3rd ed., vol. 1, Chapman Hall Press, 1985.

[6] C. Mardegan and D. Shipp, "Anatomy of a Complex Electrical Failure and its Forensics Analysis," *IEEE Transactions on Industry Applications,* vol. 50, no. 4, pp. 2910-2918, July-Aug. 2014.

[7] T. S. Sidhu, M. S. Sachdev and H. C. Wood, "Detecting Transformer Winding Faults Using Non-Linear Models of Transformers," in *Fourth International Conference on Developments in Power Protection*, 11-13 Apr. 1989.

[8] J. D. Glover, M. S. Sarma and T. Overbye, Power System Analysis & Design, 5th ed., Boston: PWS Publishing company, 2011.

[9] C. D. Hayward, "Harmonic-Current Restrained Relays for Transformer Differential Protection," *Transactions of the American Institute of Electrical Engineers,* vol. 60, no. 6, pp. 377-382, June 1941.

[10] R. Hamilton, "Analysis of Transformer Inrush Current and Comparison of Harmonic Restraint Methods in Transformer Protection," *IEEE Transactions on Industry Applications,* vol. 49, no. 4, pp. 1890-1899, July-Aug. 2013.

[11] M. Hegazy, "New Principle for Using Full-Wave Rectifiers In Differential Protection of Transformers," *Proceedings of the Institution of Electrical Engineers,* vol. 116, no. 3, pp. 425-428, March 1969.

[12] B. Jeyasurya and M. Rahman, "Application of Walsh Functions for Microprocessor-Based Transformer Protection," *IEEE Transactions on Electromagnetic Compatibility,* Vols. EMC-27, no. 4, pp. 221-225, Nov. 1985.

[13] L. F. Kennedy and C. D. Hayward, "Harmonic-Current-Restrained Relays for Differential Protection," *Transactions of the American Institute of Electrical Engineers,* vol. 57, no. 5, pp. 262-271, May 1938.

[14] M. A. Rahman and P. K. Dash, "Fast Algorithm for Digital Protection of Power Transformers," *IEE Proceedings in Generation, Transmission and Distribution,* vol. 129, no. 2, pp. 79-85, March 1982.

[15] Beckwith Electric Company, "M-3311A Transformer Protection," Beckwith Electric Co., Inc., Largo, Florida, USA, 2014.

[16] Schweitzer Engineering Laboratories, "SEL-487E Transformer Protection Relay," Schweitzer Engineering Laboratories, Inc. (SEL), Pullman, WA, USA, 2007-2014.

[17] M. S. Sachdev, T. S. Sidhu and H. C. Wood, "A Digital Relaying Algorithm for Detecting Transformer Winding Faults," *IEEE Transactions on Power Delivery,* vol. 4, no. 3, pp. 1638-1648, July 1989.

[18] Y. Wang, W. Xing, G. Zhang, W. Niu and D. Han, "Experimental Study of Testing Models for Low Noise Amorphous Alloy Core Power Transformers," in *International Conference on Electrical and Control Engineering (ICECE),* 25-27 June 2010.

[19] Y.-H. Chang, C.-H. Hsu, H.-L. Chu and C.-P. Tseng, "Magnetomechanical Vibrations of Three-Phase Three-Leg Transformer With Different Amorphous-Cored Structures," *IEEE Transactions on Magnetics,* vol. 47, no. 10, pp. 2780-2783, Oct. 2011.

[20] G. J. Wakileh, Power Systems Harmonics: Fundamentals, Analysis and Filter Design, Springer Berlin Heidelberg, 2001.

[21] B. C. Smith, J. Arrillaga and N. R. Watson, Power System Harmonic Analysis, John Wiley & Sons, 1997.

[22] H. Zheng and L. Zhou, "Rolling Element Bearing Fault Diagnosis Based on Support Vector Machine," in *2nd International Conference on Consumer Electronics, Communications and Networks (CECNet)*, 21-23 April 2012.

[23] S. A. Saleh and M. A. Rahman, "Real-time Testing of a WPT-Based Protection Algorithm for Three-phase Power Transformers," *IEEE Transactions on Industry Applications,* vol. 41, no. 4, pp. 1125-1132, July-Aug. 2005.

[24] S. A. Saleh, B. Scaplen and M. A. Rahman, "A New Implementation Method of Wavelet Packet Transform Differential Protection for Power Transformers," in *IEEE Industry Applications Society Annual Meeting (IAS)*, 3-7 Oct. 2010.

[25] S. A. Saleh, T. S. Radwan and M. A. Rahman, "Real-Time Testing of WPT-Based Protection of Three-Phase VS PWM Inverter-Fed Motors," *IEEE Transactions on Power Delivery,* vol. 22, no. 4, pp. 2108-2115, Oct. 2007.

[26] N. Li and R. Zhou, "Turbine Machine Fault Diagnosis Using Modified Redundant Second Generation Wavelet Packet Transform," in *10th World Congress on Intelligent Control and Automation (WCICA)*, 6-8 July 2012.

[27] F. Faggin, M. E. Hoff, S. Mazor and M. Shima, "The History of The 4004," *Micro, IEEE Computer Society,* vol. 16, no. 6, pp. 10-20, Dec 1996.

[28] B. Lundqvist, "100 years of relay protection, the Swedish ABB relay history," Sweden, 5 September 2011. [Online]. Available: https://www.kth.se/polopoly_fs/1.192745!/Menu/general/column-content/attachment/3_ABB_Jan-ErikFrey.pdf.

[29] A. Rahmati, "A directional current differential protection against CT saturation in two sides fed networks," in *Power Systems Conference and Exposition (PSCE)*, 20-23 March 2011.

[30] L. M. R. Oliveira and A. J. M. Cardoso, "Intermittent Turn-To-Turn Winding Faults Diagnosis In Power Transformers By The On-Load Exciting Current Park's Vector Approach," in *18th International Conf. on Electrical Machines (ICEM)*, 6-9 Sep. 2008.

[31] M. Kezunovic and Y. Guo, "Modeling and Simulation of The Power Transformer Faults and Related Protective Relay Behavior," *IEEE Transactions on Power Delivery,* vol. 15, no. 1, pp. 44-50, Jan 2000.

[32] K. Narendra, D. Fedirchuk, N. Zhang, R. Midence, N. Perera and V. Sood, "Phase Angle Comparison and Differential Rate of Change Methods Used For Differential Protection of Bus Bars and Transformers," in *Electrical Power and Energy Conference (EPEC)*, 3-5 Oct 2011.

[33] F. de Leon and A. Semlyen, "Efficient Calculation of Elementary Parameters of Transformers," *IEEE Trans. on Power Delivery,* vol. 7, no. 1, pp. 376-383, Jan 1992.

[34] A. Keyhani, S. W. Chua and S. Sebo, "Maximum Likelihood Estimation of Transformer High Frequency Parameters From Test Data," *IEEE Transactions on Power Delivery,* vol. 6, no. 2, pp. 858-865, Apr. 1991.

[35] F. de Leon and A. Semlyen, "Complete Transformer Model for Electromagnetic Transients," *IEEE Trans. on Power Delivery,* vol. 9, no. 1, pp. 231-239, Jan 1994.

[36] E. P. Dick and W. Watson, "Transformer Models for Transient Studies Based on Field Measurements," *IEEE Transactions on Power Apparatus and Systems,* Vols. PAS-100, no. 1, pp. 409-419, Jan. 1981.

[37] F. de Leon and A. Semlyen, "Reduced Order Model for Transformer Transients," *IEEE Transactions on Power Delivery,* vol. 7, no. 1, pp. 361-369, Jan. 1992.

[38] P. I. Fergestad and T. Henriksen, "Inductances for the Calculation of Transient Oscillations in Transformers," *IEEE Transactions on Power Apparatus and Systems,* Vols. PAS-93, no. 2, pp. 510-517, March 1974.

[39] A. Keyhani, S. M. Miri and S. Hao, "Parameter Estimation for Power Transformer Models from Time-Domain Data," *IEEE Transactions on Power Delivery,* vol. 1, no. 3, pp. 140-146, July 1986.

[40] Central Station Engineers, Electrical Transmission and Distribution Reference Book, East Pittsburgh, Pennsylvania : Westinghouse Electric Corporation , 1964.

[41] A. Aktaibi and M. A. Rahman, "A Software Design Technique for Differential Protection of Power Transformers," in *IEEE International Electric Machines & Drives Conference (IEMDC)*, Niagara Falls, 15-18 May 2011.

[42] C. D. Hayward, "Prolonged Inrush Currents With Parallel Transformers Affect Differential Relaying," *Electrical Eng.,* vol. 60, no. 12, pp. 1096-1101, Dec. 1941.

[43] K. Yabe, "Power Differential Method for Discrimination Between Fault and Magnetizing Inrush Current in Transformers," *IEEE Transactions on Power Delivery,* vol. 12, no. 3, pp. 1109-1118, July 1997.

[44] W. Schossig, "Introduction to the History of Differential Protection," in *PACWorld*

Magazine, Germany, PAC, SUMMER 2008, pp. 70-76.

[45] A. S. Fitzgerald, "The Design of Apparatus For The Protection of Alternating Current Circuits," *Journal of the Institution of Electrical Engineers,* vol. 62, no. 331, pp. 561-598, July 1924.

[46] R. E. Cordray, "Percentage Differential Transformer Protection," *IEEE, Electrical Engineering,* vol. 50, no. 5, pp. 361-363, May 1931.

[47] C. L. Lipman, "Some Recent Advances In The Design of Relays for The Protection of Alternating-Current Systems," *Journal of the Institution of Electrical Engineers,* vol. 70, no. 425, pp. 545-566, May 1932.

[48] E. C. Wentz and W. K. Sonnemann, "Current Transformers and Relays for High-Speed Differential Protection, With Particular Reference to Offset Transient Currents," *Transactions of the American Institute of Electrical Engineers,* vol. 59, no. 8, pp. 481-488, Aug 1940.

[49] L. F. Blume, G. Camilli, S. B. Farnham and H. A. Perterson, "Transformer Magnetizing Inrush Currents and Influence on System Operation," *Transactions of the American Institute of Electrical Engineers,* vol. 63, no. 6, pp. 366-375, June 1944.

[50] L. A. Finzi and W. H. Mutschler, "The Inrush of Magnetizing Current in Single-Phase Transformers," *Transactions of the American Institute of Electrical Engineers (AIEE),* vol. 70, no. 2, pp. 1436-1438, July 1951.

[51] E. L. Michelson, "Rectifier Relay for Transformer Protection," *Transactions of the American Institute of Electrical Engineers,* vol. 64, no. 5, pp. 252-254, May 1945.

[52] G. W. Mckenna, "Theory and Application of Transformer Differential Protection," *Transactions of the American Institute of Electrical Engineers,* vol. 69, no. 2, pp. 1197-1202, Jan. 1950.

[53] T. R. Specht, "Transformer Magnetizing Inrush Current," *Transactions of the American Institute of Electrical Engineers,* vol. 70, no. 1, pp. 323-328, July 1951.

[54] C. A. Mathews, "An Improved Transformer Differential Relay," *Electrical Engineering,* vol. 73, no. 7, pp. 648-648, July 1954.

[55] J. C. Neupauer, "Simultaneous Single-Line-to-Ground Faults on Opposite Sides of

Delta-Wye Transformer Banks," *Power Apparatus and Systems, Part III. Trans. of the American Institute of Electrical Engineers,* vol. 73, no. 2, pp. 1360-1366, Jan. 1954.

[56] R. L. Sharp and W. E. Glassburn, "A Transformer Differential Relay with Second-Harmonic Restraint," *Power Apparatus and Systems, Part III, Transactions of the American Institute of Electrical Engineers,* vol. 77, no. 3, pp. 913-918, April 1958.

[57] W. K. Sonnemann, C. L. Wagner and G. D. Rockefeller, "Magnetizing Inrush Phenomena in transformer Banks," *Power Apparatus and Systems, Part III. Transactions of the American Institute of Electrical Engineers,* vol. 77, no. 3, pp. 884-892, April 1958.

[58] J. E. Holcomb, "Distribution Transformer Magnetizing Inrush Current," *Power Apparatus and Systems, Part III. Transactions of the American Institute of Electrical Engineers,* vol. 80, no. 3, pp. 697-702, April 1961.

[59] T. R. Specht, "Transformer Inrush and Rectifier Transient Currents," *IEEE Transactions on Power Apparatus and Systems,* Vols. PAS-88, no. 4, pp. 269-276, April 1969.

[60] C. F. West and J. E. Deturk, "A Digital Computer for Scientific Applications," *Proceedings of the IRE,* vol. 36, no. 12, pp. 1452-1460, Dec. 1948.

[61] G. D. Rochfeller, "Fault Protection with a digital computer," *IEEE Transactions on Power Apparatus and systems,* Vols. PAS-88, no. 4, pp. 438-461, April 1969.

[62] A. G. Phadke and J. S. Thorp, Computer Relaying for Power Systems, 2nd ed., West Sussex: Research Studies Press, John Wiley and Sons, 2009.

[63] J. A. Sykes and I. F. Morrison, "A Proposed Method of Harmonic Restraint Differential Protection Relay for Power Transformers," *IEEE Transactions on Power Apparatus and Systems,* Vols. PAS-91, no. 3, pp. 1266-1272, April 1972.

[64] E. G. Schweitzer, R. R. Larson and A. J. Flecllsig, "An Efficient Inrush Current-Detection Algorithm for Digital Computer Relay Protection of Transformers," in *IEEE Power Engineering Summer Meeting, A77 510-1*, Mexico, 1977.

[65] R. R. Larson, A. J. Flechsig and E. O. I. Schweitzer, "The Design and Test of a Digital Relay for Transformer Protection," *IEEE Transactions on Power Apparatus and*

Systems, Vols. PAS-98, no. 3, pp. 795-804, May 1979.

[66] J. Thorp and A. Phadke, "A Microprocessor Based Three-Phase Transformer Differential Relay," *IEEE Transactions on Power Apparatus and Systems,* Vols. PAS-101, no. 2, pp. 426-432, February 1982.

[67] D. Barbosa, U. C. Netto, D. V. Coury and M. Oleskovicz, "Power Transformer Differential Protection Based on Clarke's Transform and Fuzzy Systems," *IEEE Transactions on Power Delivery,* vol. 26, no. 2, pp. 1212-1220, April 2011.

[68] H. P. S. Brian, "Experimental Testing of Stand – Alone Digital Relay for Power Transformer," M.sc dissertation, Faculty of Engineering and Applied Science, Memorial University of Newfoundland, St. John's, NL, Canada, 1993.

[69] E. Segatto and D. Coury, "A Differential Relay for Power Transformers Using Intelligent Tools," *IEEE Transactions on Power Systems,* vol. 21, no. 3, pp. 1154-1162, Aug. 2006.

[70] C. J. Mozina, "Improvements In Protection and Commissioning of Digital Transformer Relays at Medium Voltage Industrial Facilities," in *Industrial and Commercial Power Systems Technical Conference (I&CPS)*, 1-5 May 2011.

[71] Schweitzer Engineering Laboratories, "SEL-487E-3, -4 Transformer Differential Relay, Three-Phase Transformer Protection, Automation, and Control System," SCHWEITZER ENGINEERING LABORATORIES, INC., Pullman, WA, USA, 2007–2014.

[72] M. A. Rahman and B. Jeyasurya, "A State-of-The-Art Review of Transformer Protection Algorithms," *IEEE Transactions on Power Delivery,* vol. 3, no. 2, pp. 534-544, Apr 1988.

[73] Y. V. V. S. Murty and W. J. Smolinski, "Design and Implementation of a Digital Differential Relay for a 3-Phase Power Transformer Based on Kalman Filtering Theory," *IEEE Transactions on Power Delivery,* vol. 3, no. 2, pp. 525-533, Apr. 1988.

[74] W. Habib and M. A. Marin, "A Comparative Analysis Of Digital Relaying Algorithms For The Differential Protection Of Three Phase Transformers," *IEEE Transactions on Power Systems,* vol. 3, no. 3, pp. 1378-1384, Aug 1988.

[75] Y. V. V. S. Murty and W. J. Somlinski, "A Kalman Filter Based Digital Percentage Differential and Ground Fault Relay for 3-Phase Power Transformer," *IEEE Transactions on Power Delivery,* vol. 5, no. 3, pp. 1299-1308, Jul 1990.

[76] I. Hermanto, Y. V. V. S. Murty and M. Rahman, "A Stand-Along Digital Protective Relay for Power Transformers," *IEEE Transactions on Power Delivery,* vol. 6, no. 1, pp. 85-95, Jan 1991.

[77] A. Chaudhary, K. Tam and A. Phadke, "Modeling and validation of a transformer differential relay in EMTP," in *IEEE International Conference on Systems, Man and Cybernetics*, 18-21 Oct 1992.

[78] A. K. S. Chaudhary, Protection System Representation in the Electromagnetic Transients Program, Ph.D. dissertation, Virginia Tech, 1991.

[79] P. Liu, O. P. Mal, D. Chen, G. S. Hope and Y. Guo, "Improved Operation of Differential Protection of Power Transformers for Internal Faults," *IEEE Transactions on Power Delivery,* vol. 7, no. 4, pp. 1912-1919, Oct. 1992.

[80] M. R. Zaman and M. A. Rahman, "Experimental Testing of Artificial Neural Network Based Protection of Power Transformers," *IEEE Transactions on power Delivery,* vol. 13, no. 2, pp. 510-517, April 1998.

[81] A. L. Orille-Fernandez, N. K. I. Ghonaim and J. A. Valencia, "A FIRANN as a differential relay for three phase power transformer protection," *IEEE Transactions on Power Delivery,* vol. 16, no. 2, pp. 215-218, Apr 2001.

[82] M.-C. Shin, C.-W. Park and J.-H. Kim, "Fuzzy Logic-Based Relaying for Large Power Transformer Protection," *IEEE Transactions on Power Delivery,* vol. 18, no. 2, pp. 718-724, July 2003.

[83] G. Dıaz, P. Arboleya and J. Gomez-Aleixandre, "A New Transformer Differential Protection Approach on The Basis of Space-Vectors Examination," *Electrical Engineering (Archiv Fur Elektrotechnik),* vol. 87, no. 3, pp. 129-135, 2005.

[84] G. Dıaz, P. Arboleya, J. Gomez-Aleixandre and N. d. Abajo, "An Algorithm Using a Shape-Based Approach in Park's Plane for Transformer Differential Relaying on The Basis of Time-Dependent Symmetrical Components," *ScienceDirect - Electric Power*

Systems Research, vol. 73, no. 3, pp. 295-303, March 2005.

[85] M. Tripathy, R. P. Maheshwari and H. K. Verma, "Application of Probabilistic Neural Network for Differential Relaying of Power Transformer," *Generation, Transmission & Distribution, IET,* vol. 1, no. 2, pp. 218-222, March 2007.

[86] M. Tripathy, R. P. Maheshwari and H. K. Verma, "Probabilistic Neural Network Based Protection of Power Transformer," *Electric Power Applications, IET,* vol. 1, no. 5, pp. 793-798, Sept. 2007.

[87] M. Tripathy, R. P. Maheshwari and H. K. Verma, "Power Transformer Differential Protection Based On Optimal Probabilistic Neural Network," *Power Delivery, IEEE Transactions on,* vol. 25, no. 1, pp. 102-112, Jan. 2010.

[88] H. Abniki, M. Sanaye-Pasand, H. Dashti and S. Shishehchi, "A Novel and Fast Moving Window Based Technique for Transformer Differential Protection," in *North American Power Symposium (NAPS)*, 4-6 Aug. 2011.

[89] Z. Gajić, "Use of Standard 87T Differential Protection for Special Three-Phase Power Transformers-Part I: Theory," *IEEE Transactions on Power Delivery,* vol. 27, no. 3, pp. 1035-1040, July 2012.

[90] Z. Gajić, "Use of Standard 87T Differential Protection for Special Three-Phase Power Transformers-Part II: Application and Testing," *IEEE Transactions on Power Delivery,* vol. 27, no. 3, pp. 1041-1046, July 2012.

[91] B. Zheng and J. Zhang, "The Application and Analysis on Three Different Current Compensation Methods Used In Transformer Differential Protection," in *International Conference on New Technology of Agricultural Engineering (ICAE)*, 27-29 May 2011.

[92] D. Y. Shi, J. Buse, Q. H. Wu, L. Jiang and Y. S. Xue, "Fast Identification of Power Transformer Magnetizing Inrush Currents Based on Mathematical Morphology and ANN," in *Power and Energy Society General Meeting*, 24-29 July 2011.

[93] L. M. R. Oliveira and A. J. M. Cardoso, "Extended Park's Vector Approach-Based Differential Protection of Three-Phase Power Transformers," *Electric Power Applications, IET,* vol. 6, no. 8, pp. 463-472, September 2012.

[94] A. Hooshyar, M. Sanaye-Pasand, S. Afsharnia, M. Davarpanah and B. M. Ebrahimi,

"Time-Domain Analysis of Differential Power Signal to Detect Magnetizing Inrush in Power Transformers," *IEEE Transactions on Power Delivery,* vol. 27, no. 3, pp. 1394-1404, July 2012.

[95] D. Barbosa, D. V. Coury and M. Oleskovicz, "New Approach for Power Transformer Protection Based On Intelligent Hybrid Systems," *Generation, Transmission & Distribution, IET,* vol. 6, no. 10, pp. 1009-1018, Oct. 2012.

[96] W. Zhang, Q. Tan, S. Miao, L. Zhou and P. Liu, "Self-Adaptive Transformer Differential Protection," *Generation, Transmission & Distribution, IET,* vol. 7, no. 1, pp. 61-68, Jan. 2013.

[97] A. Hooshyar, M. Sanaye-Pasand and E. F. El-Saadany, "CT Saturation Detection Based on Waveshape Properties of Current Difference Functions," *IEEE Transactions on Power Delivery,* vol. 28, no. 4, pp. 2254-2263, Oct. 2013.

[98] L. A. Kojovic, M. T. Bishop and D. Sharma, "Innovative Differential Protection of Power Transformers Using Low-Energy Current Sensors," *IEEE Transactions on Industry Applications,* vol. 49, no. 5, pp. 1971-1978, Sept.-Oct. 2013.

[99] H. Dashti and M. Sanaye-Pasand, "Power Transformer Protection Using a Multiregion Adaptive Differential Relay," *IEEE Transactions on Power Delivery,* vol. 29, no. 2, pp. 777-785, April 2014.

[100] K. A. Tavares and K. M. Silva, "Evaluation of Power Transformer Differential Protection Using the ATP Software," *Latin America Transactions, IEEE (Revista IEEE America Latina),* vol. 12, no. 2, pp. 161-168, March 2014.

[101] S. A. Saleh and M. A. Rahman, "Testing of a Wavelet Packet Transform-Based Differential Protection for Resistance-Grounded Three-Phase Transformers," in *14th IAS Annual Meeting, Record of the Industry Applications Conference*, 2-6 Oct. 2005.

[102] C. H. Kim and R. Aggarwal, "Wavelet Transforms in Power Systems: Part I," *IEE Power Engineering Journal,* vol. 14, no. 2, pp. 81-87, 2000.

[103] O. A. S. Youssef, "A Wavelet-Based Technique for Discrimination Between Faults and Magnetizing Inrush Currents in Transformers," *IEEE Transactions on Power Delivery,* vol. 18, no. 1, pp. 170-176, Jan 2003.

[104] S. Saleh and M. Rahman, "Off-line testing of a wavelet packet-based algorithm for discriminating inrush current in three-phase power transformers," in *Large Engineering Systems Conference on Power Engineering*, 7-9 May 2003.

[105] S. A. Saleh and M. A. Rahman, "Modeling and Protection of a Three-Phase Power Transformer Using Wavelet Packet Transform," *IEEE Transactions on Power Delivery,* vol. 20, no. 2, pp. 1273-1282, April 2005.

[106] J. Faiz and S. Lotfi-Fard, "A Novel Wavelet-Based Algorithm for Discrimination of Internal Faults From Magnetizing Inrush Currents in Power Transformers," *IEEE Transactions on Power Delivery,* vol. 21, no. 4, pp. 1989-1996, Oct. 2006.

[107] S. A. Saleh and M. A. Rahman, "Testing of a Wavelet-Packet-Transform- Based Differential Protection for Resistance-Grounded 3ϕ Transformers," *IEEE Transactions on Industry Applications,* vol. 46, no. 3, pp. 1109-1117, May-June 2010.

[108] A. M. Gaouda and M. M. A. Salama, "DSP Wavelet-Based Tool for Monitoring Transformer Inrush Currents and Internal Faults," *IEEE Transactions on Power Delivery,* vol. 25, no. 3, pp. 1258-1267, July 2010.

[109] M. Jamali, M. Mirzaie, S. A. Gholamian and S. M. Cherati, "A Wavelet-Based Technique for Discrimination of Inrush Currents from Faults in Transformers Coupled with Finite Element Method," in *Applied Power Electronics Colloquium (IAPEC)*, 18-19 April 2011.

[110] S. A. Saleh, B. Scaplen and M. A. Rahman, "A New Implementation Method of Wavelet-Packet-Transform Differential Protection for Power Transformers," *IEEE Trans. on Industry Applications,* vol. 47, no. 2, pp. 1003-1012, March-April 2011.

[111] M. Gong, X. Zhang, Z. Gong, W. Xia, J. Wu and C. Lv, "Study on a New Method To Identify Inrush Current of Transformer Based on Wavelet Neural Network," in *International Conf. on Electrical and Control Engineering (ICECE)*, 16-18 Sep. 2011.

[112] Y. Long and N. Jingdong, "A Wavelet Transform Based Discrimination Between Internal Faults and Inrush Currents in Power Transformers," in *International Conf. on Electric Information and Control Engineering (ICEICE)*, 15-17 April 2011.

[113] Y. Long, "An Approach to Identify Magnetizing Inrush Currents and Its Simulation,"

in *International Conference on Electronic and Mechanical Engineering and Information Technology (EMEIT)*, 12-14 Aug. 2011.

[114] H. Abniki, H. Monsef, M. T. Nabavi-Razav and M. E. Gardeshi, "Differential Protection Improvement of Power Transformers Using Wavelet Analysis of Power System Frequency," in *16th International Conference on Intelligent System Application to Power Systems (ISAP)*, 25-28 Sep. 2011.

[115] B. S. Munir and J. J. Smit, "Evaluation of Various Transformations To Extract Characteristic Parameters From Vibration Signal Monitoring of Power Transformer," in *Electrical Insulation Conference (EIC)*, 5-8 June 2011.

[116] E. Gomez-Luna, G. Aponte Mayor, J. Pleite Guerra, D. F. Silva Salcedo and D. Hinestroza Gutierrez, "Application of Wavelet Transform to Obtain the Frequency Response of a Transformer From Transient Signals-Part 1: Theoretical Analysis," *IEEE transactions on Power Delivery,* vol. 28, no. 3, pp. 1709-1714, July 2013.

[117] M. S. A. Rahman, P. Rapisarda and P. L. Lewin, "Construction of Finite Impulse Wavelet Filter for Partial Discharge Localisation Inside a Transformer Winding," in *2013 IEEE Electrical Insulation Conference (EIC)*, 2-5 June 2013.

[118] R. A. Ghunem, R. El-Shatshat and O. Ozgonenel, "A Novel Selection Algorithm of a Wavelet-Based Transformer Differential Current Features," *IEEE Transactions on Power Delivery,* vol. 29, no. 3, pp. 1120-1126, June 2014.

[119] J. C. Gonzales Arispe and E. E. Mombello, "Detection of Failures Within Transformers by FRA Using Multiresolution Decomposition," *IEEE Transactions on Power Delivery,* vol. 29, no. 3, pp. 1127-1137, June 2014.

[120] ALSTOM, "Network Protection & Automation Guide," layout by Flash Montpeller France, printed by Cayfosa Barcelona, Spain, July 2002.

[121] S. H. Horowitz and A. G. Phadke, Power System Relaying, 3rd ed., West Sussex: Research Studies Press, John Wiley & Sons, 2008.

[122] Westinghouse Electrical Transmission and Distribution Reference Book, East Pittsburgh, Pennsylvania: Central Station Engineers of the Westinghouse Electric Corporation, 1964.

[123] B. H. P. So, experimental Testing of Stand-Alone Digital Relay for Power Transformers, St. John's, NL: Master of Engieering Thesis, Memorial University of Newfoundland, 1993.

[124] R. Yacamini, "Harmoincs Caused by Transformer Saturation," in *An International Conference of Harmoincs In Power Systems*, Manchester, England, 1981.

[125] S. A. Saleh, A. Aktaibi, R. Ahshan and M. A. Rahman, "The Development of a d – q Axis WPT-Based Digital Protection for Power Transformers," *IEEE Transactions on Power Delivery,* vol. 27, no. 4, pp. 2255-2269, Oct. 2012.

[126] IEEE Std C57.116-1989, "IEEE Guide for Transformers Directly Connected to Generators," IEEE Service Center, New York, 1989.

[127] M. A. Rahman, B. So, M. R. Zaman and M. A. Hoque, "Testing of Algorithms for a Stand-Alone Digital Relay for Power Transformes," *IEEE Transations on Power Delivery,* vol. 13, no. 2, pp. 374-385, Apr 1998.

[128] A. Degens, "Algorithm for a Digital Transformer Differential Protection Based on a Least-Squares Curve-Fitting," *Generation, Transmission and Distribution, IEE Proceedings C,* vol. 128, no. 3, pp. 155-161, May 1981.

[129] Y. Wang, Y. Lu and C. Cai, "A Variable Data-Window Phaselet Transformer Differential Protection Algorithm Based on Recursive Least Square Theory," in *IEEE 2011 4th International Conference on Electric Utility Deregulation and Restructuring and Power Technologies (DRPT)*, 6-9 July 2011.

[130] F. El-Sousy, "Hybrid H-Based Wavelet-Neural-Network Tracking Control for Permanent-Magnet Synchronous Motor Servo Drives," *IEEE Transactions on Industrial Electronics,* vol. 57, no. 9, pp. 3157-3166, Sept. 2010.

[131] O. A. S. Youssef, "Online Applications of Wavelet Transforms to Power System Relaying - Part II," in *Power Engineering Society General Meeting, 2007. IEEE*, 24-28 June 2007.

[132] A. Boggess and F. J. Narcowich, A First Course in Wavelets with Fourier Analysis, Hoboken, New Jersey: John Wiley & Sons, Inc., 2009.

[133] S. Mallat, A Wavelet Tour of Signal Processing, IEEE SP. Magazine 14-38, Oct. 1991.

[134] D. Esteban and C. Galand, "Application of Quadrature Mirror Filters to Split Band Voice Coding Schemes," in *IEEE International Conference on Acoustics, Speech, and Signal Processing, ICASSP '77*, May 1977.

[135] M. J. T. Smith and T. I. Barnwell, "Exact Reconstruction Techniques for Tree-structured Subband Coders," *IEEE Transactions on Acoustics, Speech and Signal Processing,* vol. 34, no. 3, pp. 434-441, Jun 1986.

[136] L. A. Monzon, Constructive Multiresolution Analysis and The Structure of Quadrature Mirror Filters, Yale University: PhD thesis, May 1994.

[137] D. K. Ruch and P. J. V. Fleet, Wavelet Theory, An Elementary Approach With Applications, A John Wiley & Sons, Inc., Publication, 2009.

[138] Y. Meyer, Wavelets and Operators, Advanced Mathematics, Cambridge University Press, 1992.

[139] S. Mallat, "Multiresolution Approximations and Wavelet Orthonromal Bases of L^2(R)," *Transactions of the American Mathematical Society,* vol. 315, no. 1, pp. 69-87, Sep. 1989.

[140] A. E. Age, A Survey of The Development of Daubechies Scaling, Master of Arts Thesis, Department of Mathematics and Statistics: University of South Florida, July 6th, 2010.

[141] R. R. Coifman and M. V. Wickerhauser, "Entropy-Based Algorithms For Best Basis Selection," *IEEE Transactions on Information Theory,* vol. 38, no. 2, pp. 713-718, March 1992.

[142] S. Sheng, K. K. Li, W. L. Chan, X. Zeng, D. Shi and X. Duan, "Adaptive Agent-Based Wide-Area Current Differential Protection System," *IEEE Transactions on Industry Applications,* vol. 46, no. 5, pp. 2111-2117, Sept.-Oct. 2010.

[143] A. Aktaibi and M. A. Rahman, "Wavelet Packet Transform Algorithm Based Differential Protection of Three phase Power Transformers," in *the 20th Annual Newfoundland Electrical and Computer Engineering Conf. (NECEC)*, Nov. 1, 2011.

[144] A. Aktaibi and M. A. Rahman, "A Novel Technique for Differential Protection of Power Transformers," in *XXth International Conference on Electrical Machines*

(ICEM), Marseille, France, 2-5 Sept. 2012.

[145] Wickerhauser and M. Vicror, Adapted Wavelet Analysis, from Theory to Software, IEEE Press, A K Peters, 1994.

[146] A. Ferrero and G. Superti-Furga, "A New Approach to The Definition of Power Components in Three-Phase Systems Under Nonsinusoidal Conditions," *IEEE Trans. on Instrumentation and Measurement,* vol. 40, no. 3, pp. 568-577, Jun 1991.

[147] R. H. Park, "Two-Reaction Theory of Synchronous Machines-Generalized Method of Analysis," *Transactions of the American Institute of Electrical Engineers,* vol. 48, no. I, pp. 716-727, July 1929.

[148] A. Ferrero, A. P. Morando, R. Ottobon and G. Superti-Furga, "On the Meaning of the Park Power Componenets in Three-Phase Systems under Non-Sinusoidal Conditions," *European Transactions on Electrical Power,* vol. 3, no. 1, pp. 33-43, Sept. 2007.

[149] P. C. Krause, O. Wasynczuk and S. D. Sudhoff, Analysis of Electric Machinery and Drive Systems, 2nd ed., Wiley-IEEE Press , 2002.

[150] P. C. Krause and C. H. Thomas, "Simulation of Symmetrical Induction Machinery," *IEEE Transaction on Power Apparatus and Systems,* vol. 84, no. 11, pp. 1038-1053, Nov. 1965.

[151] T. S. Sidhu and M. S. Sachdev, "Online Identification of Magnetizing Inrush and Internal Faults in Three-Phase Transformers," *IEEE Transactions on Power Delivery,* vol. 7, no. 4, pp. 1885-1891, Oct. 2005.

Appendices

Appendix A: The Matlab Code and the Simulink Model

The code of the proposed algorithm in the Off-Line simulation process and the Real-Time experimental setup is shown below in a brief encrypted way.

```
Load the input data x[i]
Defining the variables
Perform the circular counter [n]
Read_the_input_data y[n] = x[i]
Calculate Id & Iq according to the equations (5.1)
Calculate I_D according to the equation (5.2)
For j=1 to w
d=d+I[j]*h[w+1-j]
If |d| > threshold
Trip
Else No Trip
```

A simplified Matlab/Simulink Model (MDL) of the proposed algorithm in the off-line simulation process is shown below in figure (A.1).

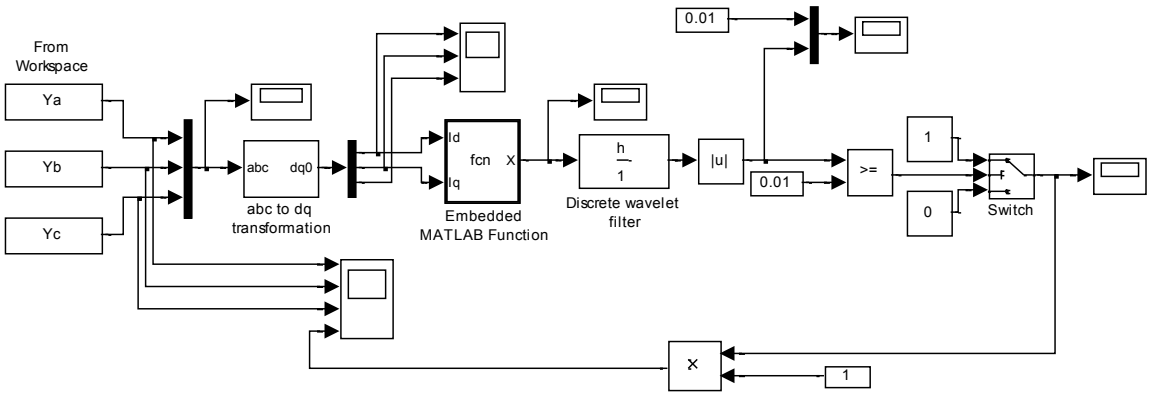

Figure A-1 the Matlab/Simulink model of the proposed algorithm

Appendix B: Circuit Breaker Control Circuit

Isolating the faulted power system device from the grid requires three main systems, the protection system, circuit breakers and control circuit. In this work, the control circuit is used to turn ON or turn OFF the three-phase circuit breakers according to the control command provided by the protection system. The three-phase circuit breakers used in this research are mainly solid state relays, which are basically Triac circuit breakers (CBs). The internal structure of these solid-state relays is provided in appendix (G). As shown in Figure 0-1, the circuit topology of this control scheme is based on the $\mathrm{NPN}-\mathrm{2N2222}$ transistor switch. This transistor control circuit receives control signals from the DSP-board's analog output terminal, namely high ($10V\ dc$) or low ($0V$) signals, through the base of the transistor. The high-level control signal makes the transistor work in the saturation region, and makes it turn to the ON state. This action closes the circuit of the $10V\ dc$ supply, which in turn causes the Triac circuit breakers to turn to the ON state. On the other hand, if the control signal is (0V), then the transistor operates in the cut off region. This action opens the circuit of the $10V\ dc$ supply, which in turn causes the 3ϕTriac circuit breakers to turn to the OFF state. To energize the power transformer a control signal of the high level is sent to the control circuit from the computer relay. This means that the initial value of the control signal is set to the high level. Accordingly, if any fault has occurred in the protected area, the control signal will be changed from the high level to low level in order to isolate the power transformer. Therefore, whenever the trip signal becomes low in the figures, the CBs are changed to the OFF state.

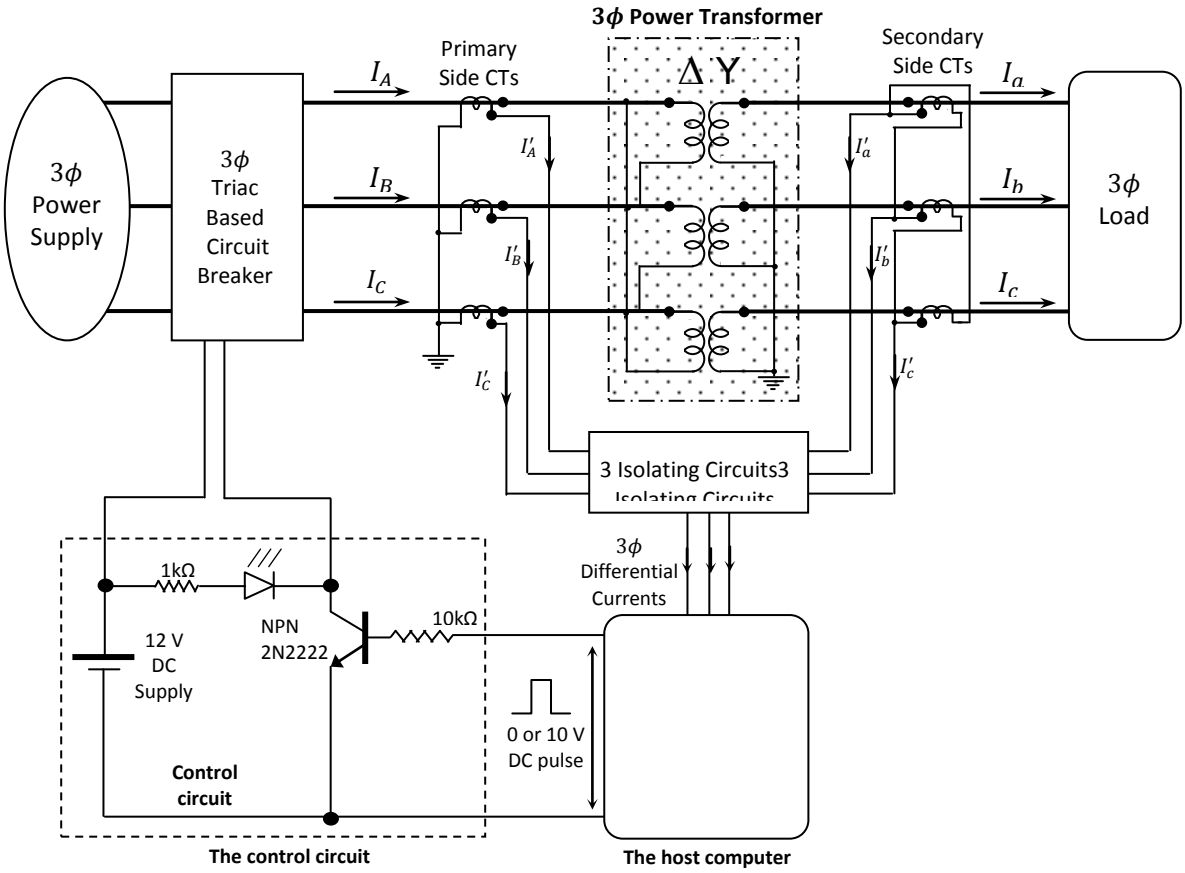

Figure B-1 The experimental control circuit layout

Appendix C: The Experimental Setup Photographs

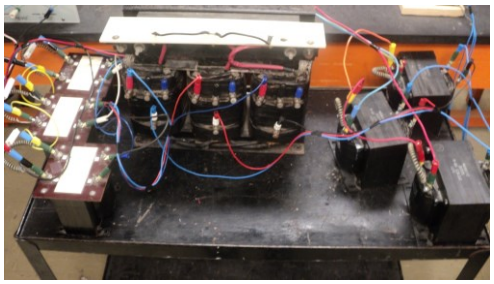

Figure (C.1) The experimental setup of the proposed work in the laboratory

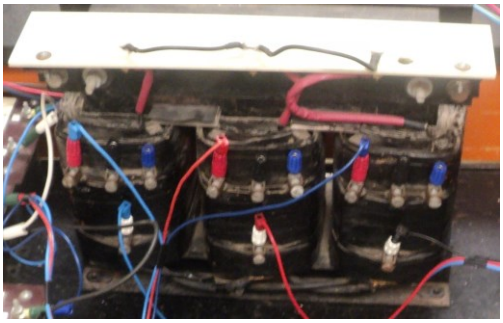

Figure (C.2) the $3\emptyset$, $5\ kVA$, $60\ Hz$, *core-type,* $230/550-575-600$, Δ-Y *Laboratory power transformer*

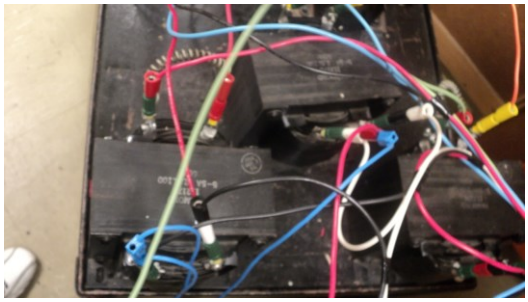

Figure (C.3) the primary side current transformers

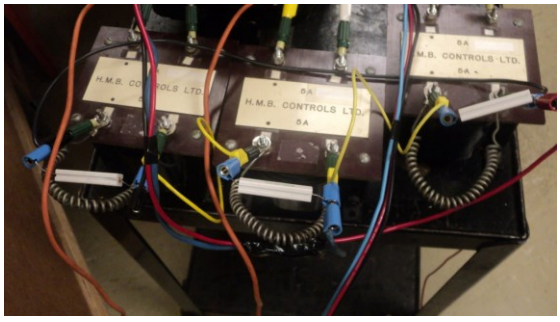

Figure (C.4) the secondary side current transformers